EXPERIMENTAL INVESTIGATION OF OIL-WATER TWO-PHASE FLOW ACROSS A LARGE DIAMETER SLIGHTLY INCLINED PIPE

JOHN NDAA SAMSON, M.Eng.

Thesis submitted to the University of Nottingham for the Degree of Doctor of Philosophy

March, 2024

ABSTRACT

The production and transportation of oil and water safely and economically across process equipment and pipeline networks have been a major challenge in the process and petroleum industry. In order to properly design the oil-water separator and transportation system, the hydrodynamic behaviour such as the spatial distribution (flow pattern), holdup and pressure drop of the oil–water two-phase flow needs to be well understood. This study aims to experimentally investigate the flow development and interfacial behaviour of oil-water two-phase flow across a large diameter inclined pipe. The pipe geometry used is a 127 mm ID of length 8.4 m with inclination +1º to +5º to the horizontal. The test fluids are tap water ($\rho = 998$ kg/m^3, $\mu = 1$ mPa.s) and silicone oil ($\rho = 916$ kg/m^3, $\mu = 4.7$ mPa.s). Three (3) different configurations of fluid inlet devices were used in order to investigate how the phase distributions are affected by the design of the fluid inlet device. The inlet devices are the T-type (first inlet device), Y-type (second inlet device) and Y-type with a separator plate (third inlet device). Four (4) flushed-mounted conductance probes (CP) located at 9.6D (CP1), 19.2D (CP2), 28.8D (CP3) and 56.6D (CP4) from the fluid inlet device (D is the internal diameter of the test pipe) were used to measure the Oil Volume Fraction (OVF) which gives an indication of the region within the pipe cross-section occupied by the oil phase. A double parallel wire probe (DPWP) was fabricated and mounted on the test-pipe to measure the instantaneous height of the water layer which upon analysis will give an indication of the interfacial wave amplitude for a given flow condition. In addition, Phantom V12.1 high-speed camera was used to capture flow images through a viewing box filled with water to avoid image distortion due to the curvature of the pipe.

Based on experimental observations and inspection of some of the flow images, different flow patterns were identified depending on the fluid inlet device and pipe inclination used. For the T-type fluid inlet device, four (4) distinct flow patterns were observed at +1º pipe inclination

and they include stratified wavy with mixing at the interface (SW&MI), dispersed oil in water and water (Do/w&w), dispersed water in oil and oil (Dw/o&o) and dispersed oil in water (Do/w). Upon using the Y-type fluid inlet device, five (5) flow patterns were identified including stratified smooth (ST), stratified smooth with mixing at the interface (ST&MI), dispersed oil in water and water (Do/w&w), dispersed water in oil and oil (Dw/o&o) and dispersed water in oil (Dw/o) and finally, using the Y-type fluid inlet device with a separator plate, only three (3) flow patterns were identified including stratified smooth (ST), stratified wavy (SW) and stratified wavy with mixing at the interface (SW&MI). Increase in pipe inclination from +1° to +5° had a remarkable effect on the spatial distribution of the phases and also from the flow pattern maps across all the three fluid inlet devices, an increase in the region occupied by the water-dominant flow patterns (Do/w&w and Do/w) was observed due to the effect of the axial component of the gravitational force on the denser water phase.

The distribution of OVF in the axial direction was determined and was found to be a function of the water-cut (WC), mixture velocity (U_m) and pipe inclination. The slippage characteristics, which indicate the relative speed between two phases, were also determined. It was found that these characteristics are influenced by both the mixture velocity (Um) and the inclination of the pipe.

From the analysis of the instantaneous height of the water layer measured by the Double Parallel Wire Probe (DPWP) and the flow images obtained from the high-speed camera, the interfacial wave characteristics such as the wave amplitude, wavelength and wave speed were determined and their responses to changes in the input flow conditions such as the WC, U_m and pipe inclination were examined. The wave aspect ratio which characterises the geometrical structure of the oil-water wavy interface was also determined and was found to be a function of the modified Froude number. An empirical correlation for the wave aspect ratio was

proposed and tested on the current experimental data and data from Castro et al., (2012) and Premanadhan et al., (2019) and similar trend was observed across all the data tested.

Stability analysis based on the Inviscid Kelvin-Helmholtz (IKH) stability criteria was used to test the stability of the interface as a result of the competition between the destabilizing effect of the inertial force and the stabilizing effect of the gravitational force and the surface tension force. For all the flow conditions tested, the relative velocities fell below the stability limit line which suggests that the system is stable and by implication, it means any disturbance introduced at the inlet will decay with time as the flow traverses in the axial direction.

ACKNOWLEDGEMENT

Words may not be sufficient for me to appreciate my lovely parents; late Mr. Samson Abah and Mrs. Theresa Samson for the love and encouragement they provided most especially my Dad (Mr. Samson Abah) who never lived to see the end of this journey but I am so sure he will be so proud and he will forever live in my heart. To all my siblings (Mrs. Roseline, Mrs. Lovina, Mrs. Bridget, Mrs Augustina, Miss Blessing and Miss Cynthia), I want to sincerely thank you all for the love. Never to forget also the wonderful love and support I received from my parent-in-law, Prof. Michael. U. Adikwu and Dr. Victoria Adikwu. I really appreciate.

Finally, to my partner in this journey from the very beginning, the only person who knows, feels and experience both the highs and the lows, the peaks and the troughs with me, my lovely **wife**, Mrs. Jacinta Samson. You have truly been a pillar of support in my moments of despair. I would never have come this far without you always by my side. I am forever grateful for your care and unadulterated love you always showed to me. To my lovely kids- Aniela, Makayla and Kaniel, thanks for your love and understanding even when dad is not always around to take you all to the playground.

All Glory to God for the gift of the Holy Spirit in providing all the inspiration, wisdom, guidance and strength to do this work. Without Him, I am nothing. Praise be to His name forever.

TABLE OF CONTENTS

x

LIST OF FIGURES

CHAPTER 4

CHAPTER 5

LIST OF TABLES

NOMENCLATURE

Roman letters

Symbol	Description	Dimension
A	Cross-sectional area of the pipe	(m^2)
A_O, A_1	Cross-sectional area occupied by oil	(m^2)
A_w, A_2	Cross-sectional area occupied by water	(m^2)
A_{w1}, A_{o1}	Area occupied by the water and oil respectively at the crest side of the solitary wave	(m^2)
A_{w2}, A_{o2}	Area occupied by the water and oil respectively at the trough side of the solitary wave	(m^2)
B	Magnetic flux density	(T)
C_i	Correction factor	(-)
c_s	Interfacial wave speed	(m/s)
C_w	Conductance when the test assembly is full of water	(Ω^{-1})
C_m	Conductance when the test assembly is full of oil-water mixture	(Ω^{-1})
C_v	Critical wave velocity	(m/s)
C_{iv}	Critical wave velocity at the inception of instability For inviscid flow	(m/s)
C	Complex wave velocity	(m/s)
C_{rn}	Neutral stability wave speed	(m/s)
C_s	Sheltering effect	(-)
D	Internal diameter of the pipe (ID)	(m)
D_o	Hydraulic diameter of the pipe containing oil	(m)
D_w	Hydraulic diameter of the pipe containing water	(m)
De	Spacing between electrodes	(m)
d	Pipe internal diameter (ID)	(m)
E	Potential impedance	(Ω)
EOR	Enhanced Oil Recovery	(-)
E_o	$E\ddot{o}tv\ddot{o}s$ (Bond) number	(-)
f_i	Interfacial friction factor of a wavy surface	(-)
fg	Interfacial friction factor of a smooth surface	(-)
f_k	Wall friction factor	(-)
f_o	Friction factor of the oil phase	(-)
f_w	Friction factor of the water phase	(-)
f_m	Friction factor of the mixture	(-)

Fr_M	Modified Froude number	(-)
Fr_{SG}	Froude number based on superficial gas velocity	(-)
Fr_{SL}	Froude number based on superficial liquid velocity	(-)
g	Acceleration due to gravity	$\left(m/_{s^2}\right)$
G^*, Ge^*	Dimensionless conductance	(-)
G	Actual conductance	(Ω^{-1})
G_m	Conductance of the fluid mixture	(Ω^{-1})
G_o	Conductance when the pipe is full of the conductive fluid	(Ω^{-1})
H_w	Water holdup	(-)
H_O	void fraction	(-)
h_w	Oil-water interface height	(m)
h	Height of film thickness	(m)
h^+	Dimensionless liquid film thickness	(-)
h_l	Equivalent thickness of the liquid layer	(m)
H_l	Fraction of the total volume occupied by the liquid phase	(-)
I	Electric current	(A)
k	Real wave number	(m^{-1})
K_{TD}	Constant to account for the presence of finite waves	(-)
k_n	Neutral stability wave number	(m^{-1})
L	Diameter of the pipe (Length)	(m)
$\dot{m}_G$	Mass flow rate of the gas phase	$\left(Kg/_s\right)$
$\dot{m}_L$	Mass flow rate of the liquid phase	$\left(Kg/_s\right)$
OC	Oil Cut	(-)
OVF	Oil Volume Fraction	(-)
P_{io}	Pressure in the oil phase	$\left(N/_{m^2}\right)$
P_{iw}	Pressure in the water phase	$\left(N/_{m^2}\right)$
P_L	Wetted perimeter of the electrodes	(m)
Q_o	Oil volumetric flow rate	$\left(m^3/_s\right)$
Q_w	Water volumetric flow rate	$\left(m^3/_s\right)$
$R_1(h_w)$	Radius of curvature of the interface along the axial direction	(m)
$R_2(h_w)$	Radius of curvature of the interface along the cross-sectional direction	(m)

Re_G	Gas Reynolds Number	(-)
Re_L	Liquid Reynolds Number	(-)
R_x	Variable resistor	(Ω)
R_{ref}	Reference resistor	(Ω)
R_a	Resistor of resistance on the Wheatstone bridge	(Ω)
r_c	Radius of curvature	(m)
r	Ratio between the oil superficial velocity to water superficial velocity	(-)
s	Width of the electrode	(m)
S	Slip ratio	(-)
S_1, S_o	Length of the pipe section occupied by oil	(m)
S_2, S_w	Length of the pipe section occupied by water	(m)
S_i	Interfacial length	(m)
T_{ai}	Time the probe indicates phase (a)	(s)
T	Total time of the experiment	(s)
U_m	Mixture velocity	(m/s)
u_1	Mean velocity in the oil phase	(m/s)
u_2	Mean velocity in the water phase	(m/s)
$U_o, U_{io,}$	Oil *in-situ* (phase) velocity	(m/s)
U_{so}	Oil superficial velocity	(m/s)
U_w, U_{iw}	Water *in-situ* (phase) velocity	(m/s)
U_{sw}	Water superficial velocity	(m/s)
V_{SG}	Gas superficial velocity	(m/s)
V_{SL}	Liquid superficial velocity	(m/s)
V	Voltage	(V)
V_{in}	Input voltage	(V)
V_{out}	Output voltage	(V)
WC	Water Cut	(-)
We	Weber number	(-)
$\bar{x}$	Mean	
X*	Modified Lockhart-Martinelli parameter	(-)

Greek symbols

α_b	The local volume fraction of a phase (a) at a point (b)	(-)
α, a	Average wave amplitude	(m)
α_o	Oil holdup	(-)

α_w	water holdup	(-)
β_o	Oil input volumetric fraction	(-)
β_w	Water input volumetric fraction	(-)
ε_w	Water in-situ volumetric fraction	(-)
η	Interface location from the centre plane	(m)
ρ_G	Density of the gas phase	(m^3)
ρ_L	Density of the liquid phase	(m^3)
ρ_m	Density of the mixture	(m^3)
$\Delta\rho$	Density difference	(m^3)
λ	Wavelength	(m)
λ_m	Apparent conductivity of the two-phase mixture	$(\Omega^{-1}\mathrm{m}^{-1})$
λ_o	Electrical conductivity of the liquid	$(\Omega^{-1}\mathrm{m}^{-1})$
σ	Interfacial Tension	$\left(N/m\right)$
σ	Electrical conductivity	$(\Omega^{-1}\mathrm{m}^{-1})$
$\psi_1,\psi_2,$ ψ_3,ψ_4	Coefficients of the equation for radius of curvature	(-)
θ	Contact angle	(radian)
τ_i	Shear stress provided by the gas phase	$\left(N/m^2\right)$
τ_{iL}	Interfacial shear stress needed for a steady state flow	$\left(N/m^2\right)$
μ_o	Oil viscosity	$\left(N.s/m^2\right)$
μ_w	Water viscosity	$\left(N.s/m^2\right)$
θ,α	Pipe inclination angle	(radian)
ω	Angular frequency	(s^{-1})

`CHAPTER 1

1.0   INTRODUCTION

The simultaneous flow of two or more phases (solid, liquid or gas) otherwise known as multiphase flow differ considerably in terms of hydrodynamic behaviour compared with the single phase flow owing to the presence of deformable interface between the phases. As a result of the presence of the deformable interface, the different fluid phases are able to redistribute themselves in a number of flow configurations known as flow patterns. These flow patterns are fundamentally different from each other due to the differences in the spatial distribution of the interface, hence the hydrodynamic behaviours such as the holdup distribution, pressure drop, heat and mass coefficients and velocity profiles are different. The evolution of these flow patterns is dependent on several variables such as the fluid flow rates, fluid physical properties (viscosity, density and interfacial tension), pipe geometry and pipe inclination.

In the study of multiphase flow systems, extensive research had been conducted with a particular focus on co-current gas-liquid and liquid-liquid two-phase flow across pipelines and other conduits. Although several research efforts had been done on other types of multiphase flow systems such as gas-solids (Wang et al., 2017; Zhao et al., 2022; Varaksin and Ryzhkov, 2023), liquid-solids two-phase flows (Liu et al., 2021; Hong et al., 2023) and also the gas-liquid-solid three phase flows (Rahman et al., 2013; Hu et al., 2022; Khan et al., 2022), consideration will not be given to them because they fall outside the scope of this work.

In spite of the numerous importance of the liquid-liquid flow in industrial applications, yet they had not been studied to the same extent as the gas-liquid flow. Also, the mechanistic models formulated for the gas-liquid two-phase flows cannot be used directly in predicting the hydrodynamic behaviour of the liquid-liquid system as a result of the fundamental differences that exist between the gas-liquid and liquid-liquid two-phase flow.

Shi et al., (2003) stated that significant differences exist between the hydrodynamic behaviour observed in gas-liquid flow and liquid-liquid flow and this is due to the differences in the physical properties that characterizes the constituent phases. Torres et al., (2016) also stated that the fundamental difference between the gas-liquid and liquid-liquid flow behaviour is caused mainly by the large momentum transfer capacity and the small buoyancy effects that occur in the liquid-liquid flow systems. Also, to compare the properties between the liquid-liquid flow and gas-liquid flow systems, it will be noted that the density ratio in gas-liquid flow is of the order 10^{-3} which is significantly lower than that of the liquid-liquid flow system which varies between 0.7 and 1.1. Similarly, the viscosity ratio for the gas-liquid flow system is of the order 10^{-2} which is also significantly lower than that of the liquid-liquid flow system which varies between 0.3 and 10^4 (Torres et al., 2016). Another interesting difference is that for gas-liquid flow, only the liquid phase is favoured to wet the internal wall of the pipe or conduit unlike the liquid-liquid flow where both liquids have the potential to wet the internal wall of the pipe or conduit depending on the wettability characteristics of the pipe or conduit material (Izwan et al., 2015).

The systematic study of liquid-liquid flow system particularly the oil-water two-phase flow started over half a century ago (Russell et al., 1959, Charles et al., 1961) and since then, there had been a continuous research effort in that direction due to its numerous importance in industrial applications including the petroleum industry. In the petroleum industry, quite a number of the fields are maturing and as such large quantity of water is produced along with the crude oil and transported across long distances to surface processing facilities located onshore or offshore. Also, for wells with depleted reservoir pressure, several enhanced oil recovery techniques are used to maximize crude oil production and one of such technique is the water injection method which adds significant quantity of water to the crude oil. The presence of large quantities of water in the crude oil is a major challenge in the efficient

transportation, separation and processing of the crude oil in a safe and economic manner (Izwan et al., 2015). In spite of the challenges in producing oil wells with significant water content, Pouraria et al., (2016) stated that the operation of such wells can still be reasonable even for water-cut as high as 90% and to corroborate that, Ngan (2010) also stated that oil wells can still be in operation even with a production stream containing 98% water or more.

The initial thrust in the study of the oil-water two-phase flow was to device method of transporting crude oil across pipelines with minimum pressure drop and improved pumping efficiency with the addition of small quantity of water (Russell et al., 1959, Charles et al., 1961, Charles and Lilleleht, 1966) particularly for high viscous oils. However, over the years, there had been significant impetus in investigating further the behaviour of the oil and water mixtures with particular focus on their co-current transportation across pipelines. Hence the scope in the study of oil-water flow system had expanded which includes flow pattern identification and characterization, measurement and modelling of pressure gradients, holdup distribution and the understanding of interfacial phenomena over a wide range of flow conditions, fluid properties and pipe configuration such as pipe geometry and pipe inclination (Ibarra et al., 2015).

The study of the interfacial phenomena in oil-water two-phase flow with emphasis on the growth and propagation of interfacial wave structures is particularly important because they have a significant effect on the heat and mass transfer of a two-phase flow (Guo et al., 2001, Li et al., 1997 and Bontozoglou and Hanratty 1989), and also in the accurate prediction of the pressure drop characteristics and in-depth understanding of the flow pattern transition (Al-Wahaibi et al., 2011).

In the study of flow development and interfacial wave phenomena in oil-water two-phase flow, the bulk of the research efforts in the literature used test pipes of small to medium size internal diameter (25 mm to 56.3 mm ID) (Chakrabarti et al., 2005; Marcelo et al., 2012; Barral and

Angeli, 2013; Huang et al., 2012; Elseth, 2001 and Perera et al., 2019) with $E\ddot{o}tv\ddot{o}s$ number (E_o) ranging between 7 to 37.6. In small diameter pipes, it had been established that the interfacial tension is usually higher than the force due to buoyancy, hence it controls the shape of the interface and other hydrodynamic parameters. However, similar studies on inclined large diameter pipes (pipe ID greater than 100 mm) where the interfacial tension is less than the buoyancy force (larger $E\ddot{o}tv\ddot{o}s$ number) have not been undertaken to the same extent as that of the small diameter pipes, hence there is a scarcity of data in the literature to effectively develop mechanistic models to predict interfacial behaviour and other hydrodynamic parameters in large diameter inclined pipes.

On this basis, it becomes necessary to investigate the flow development and interfacial wave behaviour of oil-water two-phase flow across a large diameter slightly inclined pipe whose geometry is similar to that used in oil and gas and other industrial processes and generate sufficient data so that empirical models can be developed that can accurately predict the behaviour of these fluids as they flow simultaneously through the pipe.

1.1 AIM OF THE RESEARCH

The aim of the research is to experimentally investigate the flow development and the interfacial wave behaviour in oil-water two-phase flow across a large diameter slightly inclined pipe.

1.2 RESEARCH OBJECTIVES

The objectives of this research include the following:

- To identify and categorise the different flow patterns in oil-water two-phase flow for specific values of mixture velocity, U_m (0.08 m/s to 0.4 m/s), Water-Cut, WC (10% -

70%) and pipe inclination (+1º to +5º) and also to compare the flow patterns with those obtained in the relevant literature.

- To investigate the effect of change in the inclination angle (+1º to +5º), Water-Cut, WC (10% - 70%) and mixture velocity, U_m (0.08 m/s to 0.4 m/s) on the distribution of the Oil Volume fraction (OVF) and water holdup for the oil-water two-phase.

- To investigate the effect of Water-Cut, WC (10% - 70%), mixture velocity, U_m (0.08 m/s to 0.4 m/s), and pipe inclination (+1º to +5º) on the slippage characteristics between the oil and water phases.

- To measure the properties of the interfacial waves (wave amplitude, wavelength and wave speed), characterize the interfacial waves and develop a relationship between the wave aspect ratio and Froude number.

- To perform the stability analysis of the interface based on the Kelvin-Helmholtz stability criterion.

- To investigate the effect of the fluid inlet devices (T-type, Y-type and Y-type with split plate inlet mixers) on the hydrodynamic behaviour of the oil-water mixture (flow patterns, holdup and slippage.

1.3 JUSTIFICATION

The in-depth study of the flow development and propagation of interfacial wave across a large diameter pipe will find numerous applications in the process industry and particularly in the oil and gas. As the oil, water and gas flow together through pipes from the production wells to the processing facilities, they tend to form different geometrical configurations as a result of the presence of multiple deformable interfaces. These geometrical configurations otherwise known as flow patterns is dependent on so many variables such as the flow velocities of the different phases, pipe diameter, physical properties of the phases and pipe inclination. Apart from the fact that the flow patterns determines the values of other hydrodynamic parameters such as the

void fraction, liquid holdup, pressure drop and heat transfer coefficients, it equally determines which of the phases will be in direct contact with the pipe wall and in turn it defines the range of pressure drop experienced in the flow and hence the pumping capacity required, the rate of corrosion experienced by the pipe and eventually the distribution of the corrosion inhibitors within the flow system. The careful study of how the flow develop particularly the growth and propagation of interfacial waves within the flow system will bring a greater understanding to phenomena such as the phase inversion and flow regime transitions which will eventually guide the design and optimization of the pipelines and processing equipment for the oil-water two-phase flow systems.

1.4   SUMMARY

A brief description of liquid-liquid flow was provided in this chapter, along with a comparison between single-phase flows and multiphase flow systems in terms of the presence of multiple deformable interfaces. Various hydrodynamic parameters, such as liquid holdup, pressure drop, heat and mass transfer coefficients, and velocity profiles, were stated to be directly influenced by the presence of these deformable interfaces. The lack of research on liquid-liquid flow systems was highlighted in contrast to the extensive studies conducted on gas-liquid systems. Additionally, fundamental differences between gas-liquid and liquid-liquid flows, particularly regarding their physical properties as noted by various studies, were discussed. A systematic review of liquid-liquid flow in its historical context was also provided, along with the rationale for the current study. Finally, the aim, research objectives, and justification for this study were established.

CHAPTER TWO

2.0   LITERATURE REVIEW

The simultaneous flow of two immiscible liquids is encountered in various important fields such as the chemical, food and the petroleum industries. In spite of the wide industrial applications of the liquid-liquid flow systems, extensive research has not been done on this field compared to myriad of researches done on the gas-liquid flow systems (Brauner, 2003, Xu et al., 2008). The systematic study of liquid-liquid flow started relatively late compared to the gas-liquid system and the primary objective then was to enhance the transportation of heavy crude oil across pipelines with minimal pressure drop and pumping power requirement. (Russell et al., 1959, Charlse et al., 1961 and Valle, 1998).

In petroleum industry the oil, water and gas are known to co-exist in the formation rock. Extracting the oil from the reservoir is usually accompanied by water and the extracted oil/water mixture will be pumped through several lengths of surface/subsea pipelines to either onshore or offshore processing facilities. Also, to boost the recovery of more oil from matured oil wells where the formation pressure had depleted, several Enhanced Oil Recovery (EOR) methods have been used. One example of the EOR method is the water injection method where water is pumped into the reservoir to improve the reservoir pressure and as a result, substantial amount of water will be present in the oil/water mixture that will be pumped either to the onshore or offshore processing facilities. Pouraria et al., (2016) stated that in contrast to the early days of offshore oil industry when the amount of produced water is negligible, these days many wells are matured and are producing large amount of water and the operation of such wells might be reasonable even for water cuts as high as 90%.

In order to efficiently transport the oil and water mixture through the array of pipelines in both the surface and sub-surface locations, a thorough understanding of the hydrodynamic behavior

of the oil-water two-phase flow such as the flow regime, interfacial wave characterization, distribution of liquid holdup and the pressure drop are vitally important. Also, the knowledge obtained from the study of the hydrodynamic behavior of oil-water two-phase flow will be required for the optimum design of the processing equipment and also to serve as a basis to study other complex systems such as the oil-water-gas three-phase systems.

The study of liquid-liquid flow across a pipe often include the accurate measurement of the regions of the pipe cross-section occupied by the phases (holdups), the pressure drop, in-situ velocities of the phases and the spatial distribution of the phases otherwise known as the flow patterns. The following section will give a brief description of these concepts used in the study of the liquid-liquid system.

2.1 BASIC CONCEPTS IN LIQUID-LIQUID FLOW

In order to properly understand the complex nature of the liquid-liquid flow system, some basic concepts needs to be defined to serve as a basis for further knowledge to be built on. Some of these concepts includes:

2.1.1 Input Volumetric Fractions

The input volumetric fractions for the water and oil phase is also known as the Water Cut (WC) or Oil Cut (OC). It can be defined as the ratio of the volumetric flow of either the water or oil phase to the total volumetric flow at the inlet section. Given the input volumetric flow rate for the water and oil phase as Q_w and Q_o, the input volumetric fractions can be given below:

$$\text{Water Cut (WC)} = \beta_w = \frac{Q_w}{Q_w + Q_O} \tag{2.1}$$

$$\text{Oil Cut (OC)} = \beta_o = \frac{Q_O}{Q_w + Q_O} \tag{2.2}$$

But for a pipe of constant cross-sectional area,

$$U_{sw} = \frac{Q_w}{A} \, , U_{so} = \frac{Q_o}{A} \tag{2.3}$$

Where U_{sw}, U_{so} are the superficial velocities of the water and oil phase.

Therefore, WC $= \beta_w = \frac{U_{sw}}{U_{sw} + U_{so}}$, OC $= \beta_o = \frac{U_{so}}{U_{sw} + U_{so}}$ $\tag{2.4}$

Where $U_{sw} + U_{so} = U_m$ is the mixture velocity.

2.2.2 Oil Volume Fraction

Oil Volume Fraction (OVF) is an in-situ measurement which indicates the fraction of the pipe cross-section occupied by the oil phase. It is a ratio of the actual cross-sectional area occupied by the oil phase to the total pipe cross-sectional area. The OVF is one of the main parameters used in characterizing the liquid-liquid flow system. It is a dimensionless quantity with values ranging between 0 and 1 which represents two extremes with no oil in the pipe and with the pipe full of oil respectively. Several methods are used to measure this quantity which will be discussed extensively in subsequent section.

Given that the actual area occupied by the oil phase is A_O and the total area of the pipe sross-section is A, then

$$OVF = \frac{A_O}{A} \tag{2.5}$$

The water holdup can also be obtained as:

$$H_w = \frac{A_w}{A} \tag{2.6}$$

$$OVF + H_w = \frac{A_O}{A} + \frac{A_w}{A} = \frac{A_O + A_w}{A} = 1 \text{ (since } A_O + A_w = A) \tag{2.7}$$

The cross-sectional area occupied by the water and oil phase (A_w and A_O) can be seen in the sketch represented in Figure 2.1.
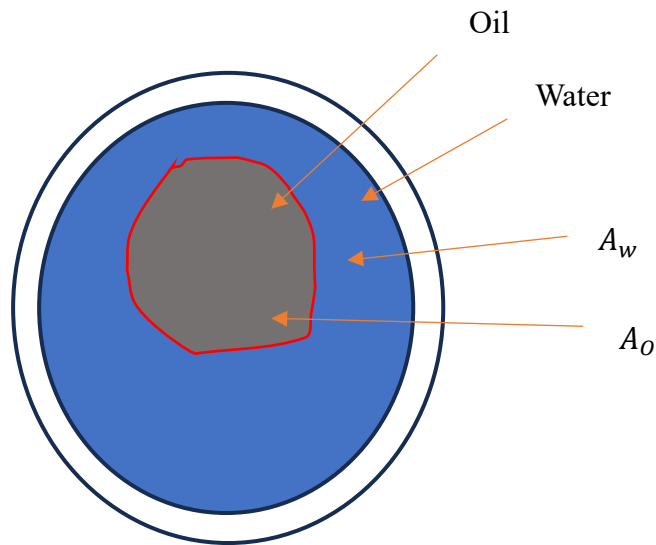
Figure 2.1: A sketch of the pipe cross-section showing the area occupied by the water phase (A_w) and oil phase (A_O)

2.2.3 In-Situ Velocity (Phase Velocity)

The in-situ (phase) velocity of the oil or water phase is the actual velocity of the phase as it moves across any given cross-section in a pipe. As a result of the slip between the phases where one phase flow faster than the other phase due to several factors such as buoyancy effects, gravitational effects, pipe wettability and pipe inclination, it was observed that the actual velocities of the phases are different from the inlet or superficial velocities and it is a function of the holdup of the phase.

$$U_o = \frac{U_{so}}{OVF} \qquad\qquad U_w = \frac{U_{sw}}{H_w} \qquad\qquad (2.8)$$

Where U_o, U_w are the the in-situ (phase) velocity of the oil and water.

2.2.4 Slip Velocity

The slip velocity can be determined as the difference between the in-situ velocities of the less dense phase and that of the denser phase. Alternatively, the slip ratio can be quantitatively determined as the ratio of the in-situ velocity of the less dense phase to the in-situ velocity of the denser phase (Colombo et al., 2013). For a specific case of oil/water two-phase flow, the slip ratio can be expressed as the ratio of the in-situ oil velocity (U_o) to in-situ water velocity (U_w) since the density of the oil phase is less than that of the water phase.

$$S = \frac{U_o}{U_w} = \frac{U_{so}/H_o}{U_{sw}/H_w} \qquad (2.9)$$

where U_{so} and U_{sw} are the oil and water superficial velocities while H_o and H_w are the holdups for oil and water respectively. $\beta_w = \frac{U_{sw}}{U_{sw} + U_{so}}$, OC $= \beta_o = \frac{U_{so}}{U_{sw} + U_{so}}$

From equation 2.4,

Then $U_{sw} = \beta_w(U_{sw} + U_{so})$, $U_{so} = \beta_o(U_{sw} + U_{so})$ $\qquad (2.10)$

$\frac{U_{so}}{U_{sw}} = \frac{\beta_o(U_{sw} + U_{so})}{\beta_w(U_{sw} + U_{so})} = \frac{\beta_o}{\beta_w}$ (since the mixture velocity $(U_{sw} + U_{so})$ is constant $\qquad (2.11)$

Since the ratio of the superficial velocities of the oil to that of water is equal to the ratio of the input volume fraction of oil (β_o) to that of water (β_w), equation (2.9) can then be expressed as:

$$S = \frac{\beta_o/H_o}{\beta_w/H_w} = \frac{\beta_o/\beta_w}{H_o/H_w} \qquad (2.12)$$

The value of the slip ratio S can give an indication on which of the phases is moving faster than the other. If $S > 1$, it means that $U_o > U_w$ and the oil phase is moving faster than the water phase whereas if $S < 1$, it means that $U_w > U_o$ and the water phase is moving faster than the oil phase. However, if $S = 1$, it means that $U_o = U_w$ and both phases are moving at the same

velocity and this usually occur in a fully dispersed flow where the dispersed droplets are moving at the mean velocity of the continuous phase.

2.3   FLOW PATTERNS AND FLOW PATTERN MAPS IN LIQUID-LIQUID FLOW SYSTEMS.

Liquid-liquid two-phase flow can be described as the simultaneous flow of the two immiscible liquids through a given conduit. As the flow progresses, there is a redistribution of the interface between the liquids as a result of changes in flow conditions such as the flow rates, fluid properties, flow geometry and pipe inclination. These spatial geometrical distributions of the interface are termed the flow patterns and they are used to characterize the liquid-liquid two-phase flow systems because they determined the holdup distribution, velocity profiles and the pressure drop in such systems. The 2D representation of these flow patterns with specific boundaries that delineates the transition region of one flow pattern to another is termed the flow pattern map.

In studying liquid-liquid systems, there are inherent complexities which arises due to the nature of the phases involve. These complexities arises due to low density difference between the phases, very large differences in viscosity ratio which can vary from less than one to more than a million, complex interfacial chemistry, potential to form oil-water emulsions and the possibility of either of the phases to wet the pipe (Ismail et al., 2015). Thus, it becomes very difficult to identify the flow patterns in liquid-liquid systems with the same consistency as was the case in the gas-liquid system. For instance, the pioneering work of Russell et al., (1959) and that of Charles et al., (1961) were able to identify 3 to 4 flow patterns whereas Oglesby (1979) reported 14 flow patterns.

In the same manner, several other researchers such as Oliemans et al., (1987), Arirachakaran et al., (1989), Amey et al., (1993) and Kurban et al., (1995) made great attempt in classifying the

flow patterns based on their experimental observations but it turns out that the naming of these flow patterns are quite subjective and do not sometimes describe adequately the features of these flow patterns

However, with advances in instrument design and improved measuring techniques, flow patterns have been identified more accurately as evidenced in the work of Trallero (1997), Nadler and Mewes (1997), Angeli and Hewitt (1998) and Shi (2001), Edomwonyi-otu and Angeli (2015) and Ahmed and John (2021) among others where more detailed flow patterns were identified and objectively analyzed.

Table 1.0: Summary of experimental works on flow patterns for oil-water flow in horizontal pipes

Author(s)	Internal pipe diameter (mm) / Pipe material	Oil/water density ratio	Oil/water viscosity ratio	Measurement Techniques	Flow patterns observed
Russell et al., (1959)	20.3 Acetate Butyrate	0.84	20.1	Visual observation	SM,Bo,Do/w
Charles et al., (1961)	26.4 Acetate Butyrate	1.0	6.3,16.8.65.0	Visual observation	W/O, ANNU,, O/W&W,Oil-slugs-in-water, O/W
Guzhov et al., (1973)	39.4 Steel	0.89	21.8	Visual observations	ST&MI, W/O, O/W,O/W&W, W/O&O/W
Arirachakaran et al., (1989)	38.1 & 26.4 Steel	0.89,0.87 & 0.86	4.7,58,84,115,237 & 2116	Visual observation	O/W,W/O, W/O & O/W
Fujii et al., (1994)	25.0 Transparent acrylic	1.0	55.0	High speed photography	O/W,W/O, W/O & O/W, plug flow
Kurban et al., (1995)	24.3 & 24.0 Glass acrylic	0.8	1.6	Conductivity probe High speed photography	ST, ST&MI, W/O
Trallero et al., (1997)	50.8 Acrylic resin	0.85	29.7	Visual observation Video images Holdup/pressure fluctuation data	ST,ST&MI,W/O,O/W, Do/w&w, W/O&O/W
Nadler and Mewes (1997)	59.0 Perspex	0.84	18.0 & 35.0	Visual observation	ST, ST&MI, W/O,O/W, W/O&O/W,O/W&W
Vedapuri et al., (1997)	100.0 Plexiglass	-	2.0	-	ST&MI, W/O&O/W
Angeli and Hewitt (1998)	24.3 & 24.0 Steel and acrylic resin	0.8	1.6	Conductivity needle probe	ST,O/W, O/W, W/O&O, O/W&W, W/O&O/W
Soleimani (1999)	26.4 Stainless steel	0.8	1.6	Gamma densitometer, High frequency impedance probe	ST, W/O&O,W/O, O/W, O/W&W, W/O &O/W
Angeli and Hewitt (2000a)	24.0 & 24.3 Acrylic resin and steel	0.8	1.6	Conductivity needle probe, Photography	ST,O/W,W/O,W/O&O,O/W&W,W/O&O/W
Elseth (2001)	58.0 Plexiglass	0.79	1.6	Laser Doppler Anemometry, Gamma Densitometer	SS,SW,SM,Do-DP,Dw-DP,Do-I,Dw-I,Do-H,Dw-H
Vielma et al.,(2003)	40.0 Plexiglass & Stainless steel	0.89	428.0	Visual observation	ST,ST&MI,W/O,O/W,O/W&W,W/O&O/W,Slug
Lovick and Angeli (2004)	38.0 Stainless steel	0.82	6.0	Impedance probe	ST,W/O,O/W,O/W&W W/O&O/W
Mandal et al.,(2007)	12.0 & 25.0 Polymethyl-Methacrylate (PMMA)	0.79	1.2	Visual observation & Digital photography	WW,SW,Slug,Plug,O/W, Rivulet, Dual Continuous.
Al-Wahaibi and Angeli (2007)	38.0 Stainless steel	0.82	6.5	Conductivity probe & High speed camera	ST, SW, DC
Vielma et al., (2007)	50.8 Transparent pipe	0.85	15.0	High speed camera & Conductivity probe	ST,ST&MI,W/O,O/W,O/W&W,W/O&O/W
Kumara et al.,(2010)	56.0 Stainless steel	0.79	1.64	Visual observation, Gamma densitometer, Particle image Velocimetry (PIV)	ST,ST&MI,W/O,O/W,O/W&W,W/O&O/W
Barral (2014)	38.0 Acrylic	0.83	6.5	Conductance probes & High speed camera	ST,SW,DC
Ismail et al., (2015)	50.8 Stainless steel	0.818	1.75	Visual observation & Photography	STW,STSD&O, SDSE&TO,DWE,DO
Edomwonyi-otu and Angeli (2015)	14.0 Acrylic	0.828	6.5	High speed camera	ST,SW,Rivulet flow,DC,Do/w, Dw/o
Ahmed and John (2021)	16.9 Stainless steel	0.901 & 0.919	202 & 630	High speed camera	ST, SW,Plug,Stratified wavy droplets,Droplets at the interface,

In Table 1.0, it is observed that the researchers gave different names to the flow patterns observed in their experimental campaigns. However, there are quite a lot of similarities in terms of the flow structures and the interface configuration of the phases albeit the names of the flow patterns might be different. For instance, Angeli and Hewitt (2000a) identified flow patterns called the Stratified wavy with drops (SWD) and the Three layers (3L) and based on the description of these flow patterns by the researchers, it corresponds directly with the Stratified wavy with mixing at the interface (SW&MI) flow pattern identified by several researchers such as Trallero et al., (1997), Nadler and Mewes (1997), Liu et al.,(2003) and Kumara et al.,(2010) among others. Similarly, the Mixed flow pattern (M) identified by Angeli and Hewitt (2000a) have a similar description to the dispersed flow (Do/w or Dw/o) flow patterns identified by other researchers such as Kumara et al., (2009), Perera et al., (2017) and Tan et al., (2018)

In other to categorize all the flow patterns observed in the horizontal oil-water flow, the work of Trallero et al (1997) will be used as a basis since most of the flow patterns observed by other researchers will fall within these categorization with probably very few exceptions such as the Rivulet flow patter observed by Mandal et al., (2007) and Edomwonyi-Itu and Angeli (2015).

2.4   CLASSIFICATION OF FLOW PATTERNS FOR HORIZONTAL OIL-WATER FLOW.

Several research efforts to classify flow patterns observed in oil-water horizontal flow have been undertaken by different researchers in the past, but the work of Trallero (1995) was quite classic in that, an attempt was made to give a detail classification of these flow patterns. Trallero (1995) used a 16.54 m long acrylic test pipe of 50.8 mm ID in carrying out the experimental campaigns. The test fluids used are 28.8 ± 6.2 cP oil with density 884 ± 3 kg/m^3 and water with density 1037 ± 3 kg/m^3 and viscosity of 0.97 ± 0.08 cP. Trallero (1995) used a combination of techniques to identify the flow patterns which includes visual/video

observations, characteristics of the differential pressure fluctuations, detailed examination of the pressure loss, local average phase continuity and finally the examination of the holdup data. Six flow patterns were identified after careful examination of the experimental data and they include: stratified flow (ST), stratified flow with mixing at the interface (ST&MI), dispersed oil in water and water (Do/w&w), oil in water emulsion (o/w), water in oil emulsion (w/o) and finally dispersed water in oil and dispersed oil in water (Dw/o & Do/w). The description of these flow patterns will be given below:

2.4.1 Stratified Flow (ST)

Stratified flow (ST) is the flow pattern observed at very low superficial velocity of the oil and water phase. In such a flow configuration, the gravitational force acts on the phases and as a result of density difference, the flow separates into two layers where the low density fluid occupies the upper layer and the denser fluid occupies the lower layer with a clear and stable interface between them. Both phases maintain their continuity at the top and bottom of the pipe. In most cases, this is the first flow pattern identified by most of the researchers as can be seen in Table 1.0. However, in some cases, due to the disturbance along the interface as a result of the differences in the relative velocity between the phases, waves begin to appear along the interface and such flow pattern is termed Stratified wavy (SW).
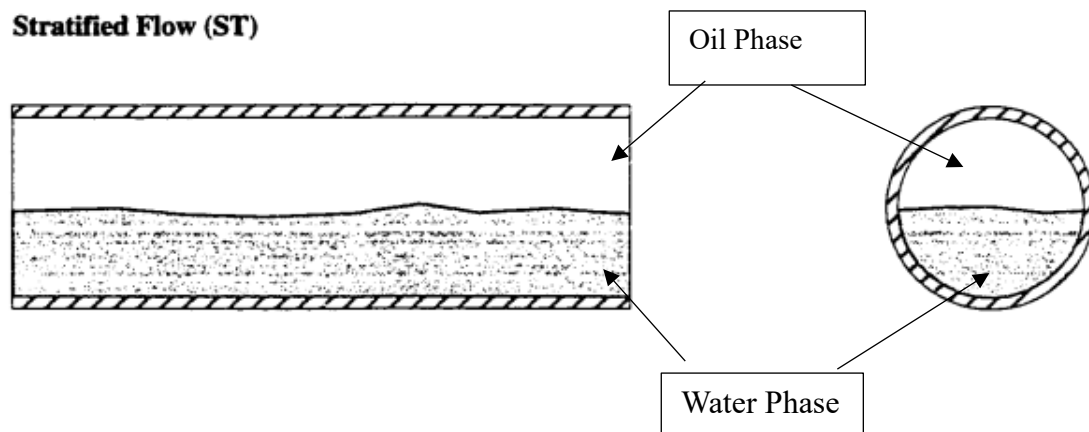
Figure 2.2: Sketch of the Stratified (ST) flow pattern (Trallero et al., 1997)

2.4.2 Stratified flow with mixing at the interface (ST&MI)

The ST&MI flow pattern occur when there is an increase in the mixture velocity and drops begin to evolve along the interface due to the shearing effect. According to Kumara et al., (2009), the existence of the droplets close to the interface is due to the competition between the dynamic forces and the buoyant forces acting on the droplets. The buoyant force which enhances the settling of the droplets is stronger than the dynamic force which tends to spread the droplets across the pipe cross-section, hence the droplets remain close to the interface. Both phases still maintain their continuity at the top and bottom of the pipe, however the region close to the interface are dominated by droplets of either of the phases. Several researchers identify this flow pattern but some researchers gave it a different name such as Three layer (3L) flow pattern by (Angeli and Hewitt, 2000a).
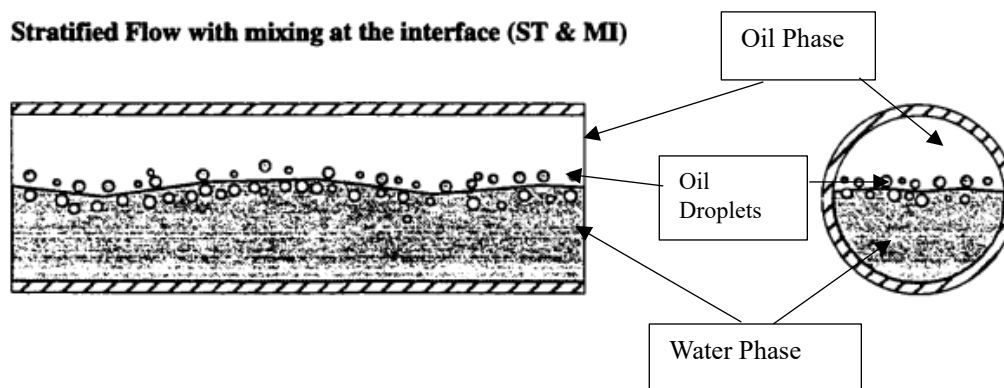
Figure 2.3 Sketch of the Stratified flow with mixing at the interface (ST&MI) flow pattern (Trallero et al., 1997)

2.4.3 Dispersion of oil in water and water (Do/w&w)

The Do/w&w flow pattern is classified as a water-dominated flow pattern. This type of flow pattern occur in an oil-water flow system where the water superficial velocity and water-cut are high. The turbulent kinetic energy of the water phase is also high which eventually disrupts the continuity of the oil phase, hence a dispersion of the oil phase in water is formed over a

continuous water layer (Trallero et al., 1997). Several researchers identified this flow pattern as can be seen in Table 1.0.
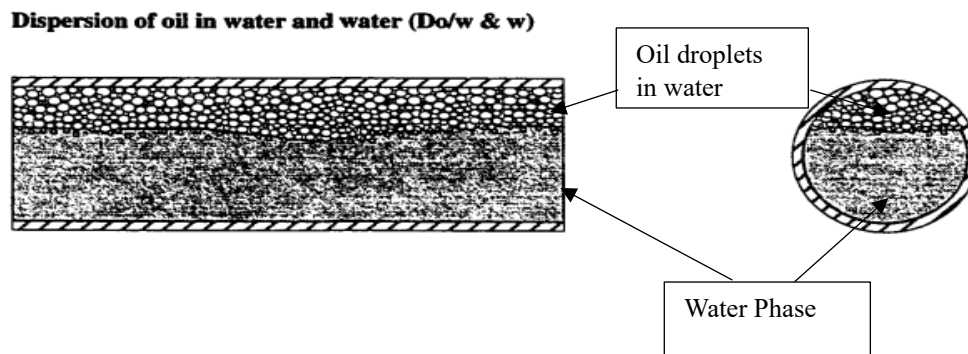
Figure 2.4 Sketch of the Dispersion of oil in water and water (Do/w&w) flow pattern
(Trallero et al., 1997)

2.4.4 Dispersion of water in oil and oil in water (Dw/o & Do/w)

The Dw/o & Do/w flow pattern occur when there is an interdispersion of one phase into the other. The increase in the superficial velocity of both the oil and water phase results in the growth of the mixing region and as a result, two types of dispersions coexist (Dw/o & Do/w) where the water layer is occupied by the oil droplets while the oil layer is occupied by the water droplets. Some researchers such as Al-Wahaibi and Angeli (2007) and Barral (2014) identified this flow pattern as Dual continuous (DC) flow.
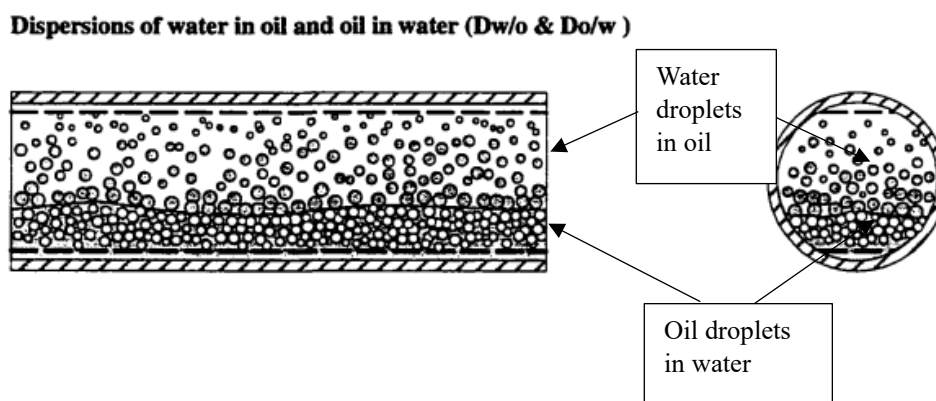
Figure 2.5 Sketch of the Dispersion of oil in water and water in oil(Do/w&w/o) flow pattern
(Trallero et al., 1997)

2.4.5 Oil in water emulsion (O/W)

The O/W flow pattern occur at a very high water superficial velocity and low oil superficial velocity. In this flow configuration, the dispersive turbulent energy of the water phase is sufficient to distribute the oil droplets uniformly across the pipe section formimg an O/W emulsion.

Oil in water emulsion (o/w)

Oil droplets

Water phase
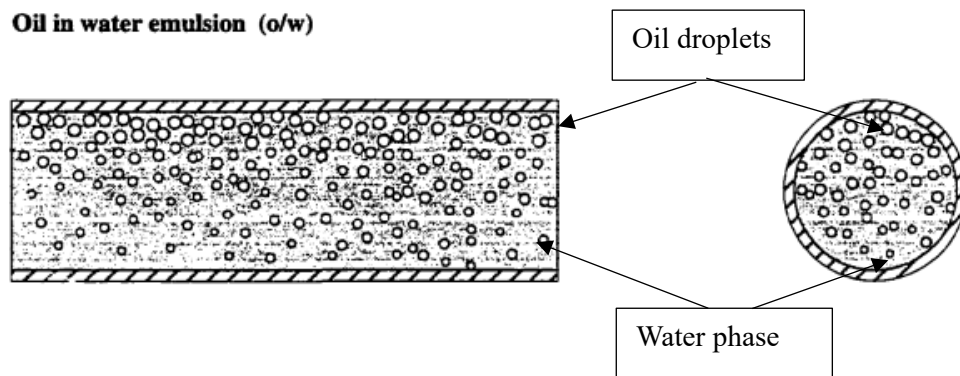
Figure 2.6: Sketch of the Oil in water emulsion (O/W) flow pattern (Trallero et al., 1997)

2.4.6 Water in oil emulsion (W/O)

The W/O flow pattern is an oil dominated flow pattern which occur at a vey high oil superficial velocity and low water superficial velocity. In this flow pattern the oil phase is the continuous phase and the water is homogeneously dispersed in the oil phase to form an emulsion.

Water in oil emulsion (w/o)

Oil Phase

Water droplets
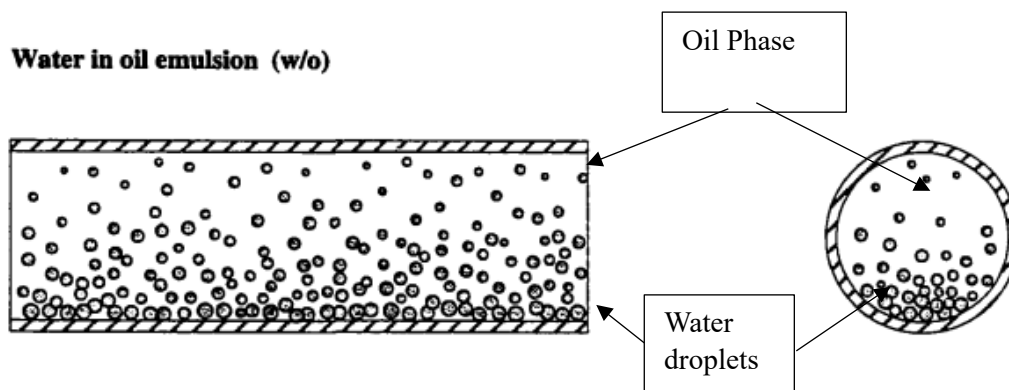
Figure 2.7 Sketch of the water in oil emulsion (W/O) flow pattern (Trallero et al., 1997)

2.5 FLOW PATTERN MAPS FOR OIL-WATER TWO-PHASE FLOW

The different flow patterns and their corresponding transitional boundaries are usually represented on a 2D plot known as a flow pattern map. The axis system by most researchers in presenting the flow pattern maps was to use the superficial velocities of the phases as seen in the Figure 2.7.
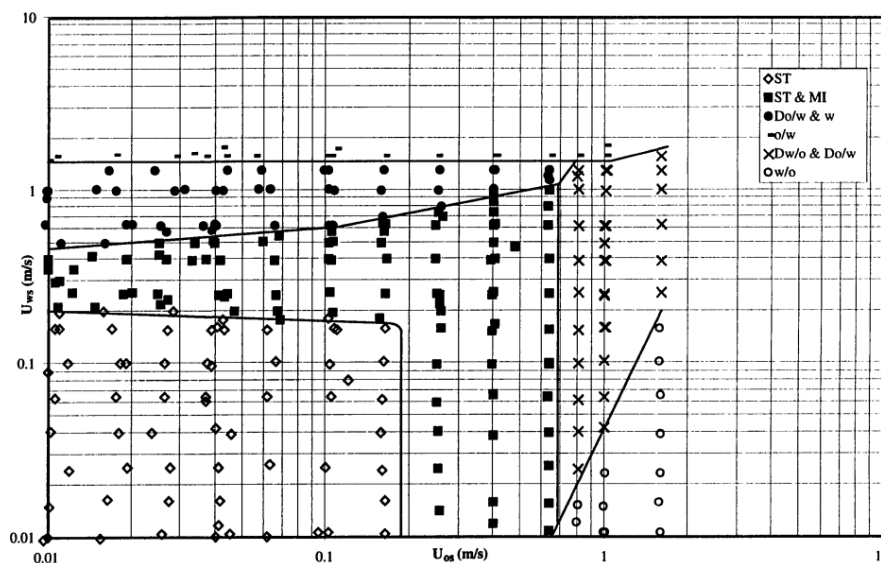
Figure 47. Experimental flow pattern map, horizontal, present study,
(D = 5.01 cm, μ_o/μ_w = 29.60, ρ_o/ρ_w = 0.85, σ = 36 dynes/cm).

Figure 2.8: Flow pattern map showing the regions of the different flow regimes and their corresponding transition boundaries. (Trallero, 1997).

However, a number of researchers such as Soleimani (1999), Angeli and Hewitt (2000), Lovick and Angeli (2004), Kumara et al., (2009), and J.Tan et al., (2018) among others used the mixture velocity (U_m) and the water-cut (WC) as the axes for the flow pattern maps as seen in Figure 2.8. As a result of these differences in the coordinate systems used by different researchers and the fundamental differences in parameters such as the pipe geometry, fluid types, and flow conditions used by these researchers, it becomes very difficult to compare and interpret the flow pattern maps.

Consequently, efforts to develop a flow pattern map with wider applicability were undertaken by researcher such as Osundare et al., (2020) where ratios of different dimensionless numbers

20

which adequately describes the physics of the system are used as the coordinates of the flow pattern map which can be seen in Figure 2.9. Similarly, Hapanowicz (2010) used the mass flux of the oil and water phase while Ahmed and John (2021) used the momentum of the phases as coordinates in the flow pattern maps as seen in Figure 2.10.
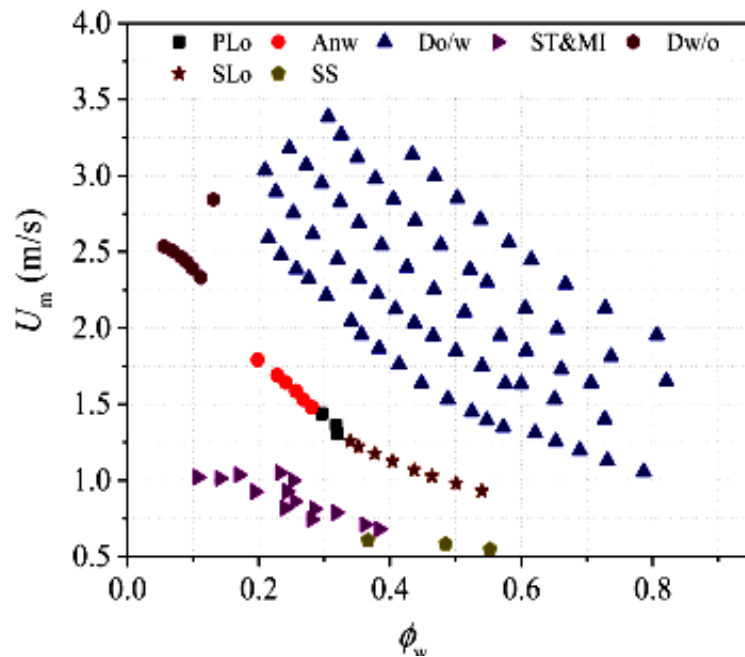
Figure 2.9: Flow pattern map for a viscous oil-water flow across a horizontal pipe.

(J. Tan et al., 2018)
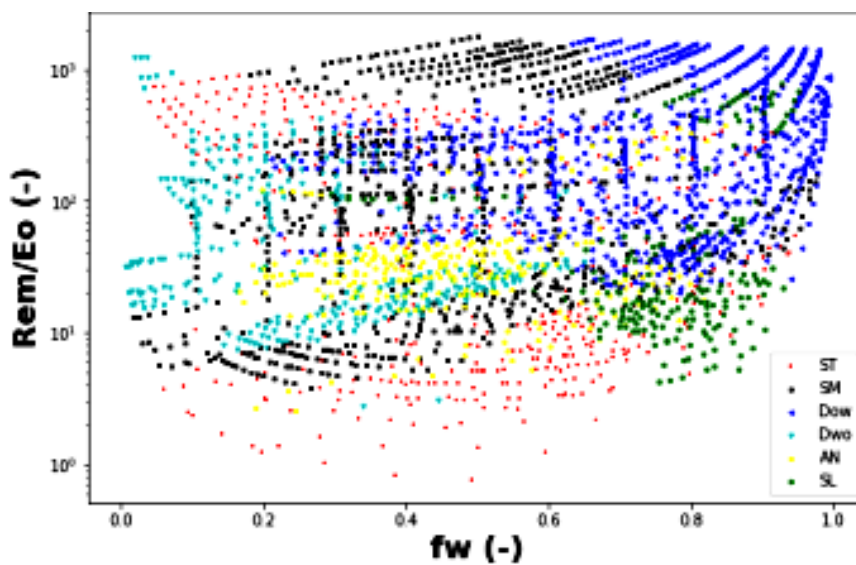
Figure 2.11: A flow pattern map using the momentum of the oil and water as the coordinate. (Ahmed and John, 2018)

2.6 FLOW PATTERNS AND FLOW PATTERN MAPS FOR OIL-WATER FLOW ACROSS AN INCLINED PIPE.

There are few studies in the literature that focuses on the simultaneous flow of oil and water across an inclined pipe compared to large number of studies for the flow across horizontal pipes. The flow of oil and water across an inclined pipe is fundamentally different from that of the horizontal pipe with regards to the action of the gravitational force on the fluids. Both the horizontal and inclined pipes experience the action of the normal component of the gravitational force which enhances segregation between phases. However, only flows across the inclined pipes experience the action of the axial component of the gravitational force which could either retard or enhance the flow depending on the pipe orientation and the flow direction. For upward inclined pipes, the axial component of the gravitational force retards the flow while for downward inclined pipes, the axial component of the gravitational force enhances the flow.

Several researchers such as Flores et al., (1999), Lum et al.,(2006), Rodriguez and Oliemans(2006), Atmaca et al., (2009), Kumara et al., (2009),Rodriguez et al., (2012) and Xu et al., (2012) have made great attempts in studying oil-water flow across inclined pipes with inclination angles ranging from $\pm 1^o$ to $\pm 90^o$. The flow patterns commonly observed by these researchers are similar to those observed by Trallero et al (1997) for flow across a horizontal pipe which were discussed in the previous sections and a schematic diagram of the flow patterns identified by Flores et al., (1999) can be seen in Figure 2.11. However, some new flow patterns were observed such as the plug flow identified by Kumara et al., (2009) for +5º inclination angle and at high input water fraction and Lum et al., (2006) for +10º inclination angle while Hanafizadeh et al., (2015) identified slug and annular flow. Also, it was equally observed that the degree of mixing increased at the interface for the inclined pipes as a result of the disturbance introduced due to the pipe inclination (Kumara et al., 2009). For the flow pattern maps, it was observed also that the pipe inclination affects the transitional boundaries for the different flow patterns. For instance, Hanafizadeh et al., (2015) stated that on increasing the pipe inclination to +5º, the transition boundary between slug and bubbly flow moved to the right towards higher oil superficial velocities. The same observation was made for the transition boundary between the slug and annular flow.

Similarly, Kumara et al., (2009) argued that increasing the pipe inclination from +1º to +5º ensures that the region on the flow pattern map occupied by Dw/o flow pattern decreases in size while an expansion in the size of the region occupied by Do/w pattern was also observed due to the effect of the axial component of the gravitational force on the denser water phase as seen in Figure 2.12. A summary of the experimental work for the oil-water flow across an inclined pipe can be seen in Table 2.0.

Table 2.0: Relevant experimental studies of oil-water flow across inclined pipes.

Author(s)	Internal pipe diameter (mm)	Oil Density (Kg/m³)	Oil Viscosity (mPa.s)	Inclination Angle (degrees)	Flow patterns observed
Flores et al.,(1998)	50.8	850	1.68	45,60,75,90	Do/w,VFDw/o, o/wCF,w/oCF,Dw/o,VFDw/o.
Abduvayt et al., (2006)	106.4	800	1.88±0.19	±0.5,±3	Segregated, semi-segregated, semi-dispersed
Lum et al., (2006)	38	828	6.0	±5,+10	ST,Dw/o,Do/w,DC,Plug flow
Rodriguez and Oliemans (2006)	76.2	830	100	±5	ST&MI,Do/w&w,Do/w,Do/w&Dw/o
Grassi et al., (2008)	21	886	533,653,799	±10, +15	ST,Do/w,Core annular flow (CAF),Plug/slug flow,ST&Do/w,CAF & Do/w,Slug & Do/w
Atmaca et al., (2009)	50.8	859	1.6	±2	ST, ST&MI,Do/w&w, Dw/o&o, Do/w&Dw/o,O/W,W/O
Kumara et al., (2009)	56	790	1.64	±5	ST,ST&MI,Do/w&w,Do/w&Dw/o,Do/w,Dw/o, Plug flow
Perera et al., (2018)	56	788	1.6	±5,+6	ST,ST&MI,Do/w&w,Do/w&Dw/o,Dw/o,Do/w,Plug flow
Zhang et al., (2020)	20	841	11.98	+1,+5,+15	ST, ANNU.
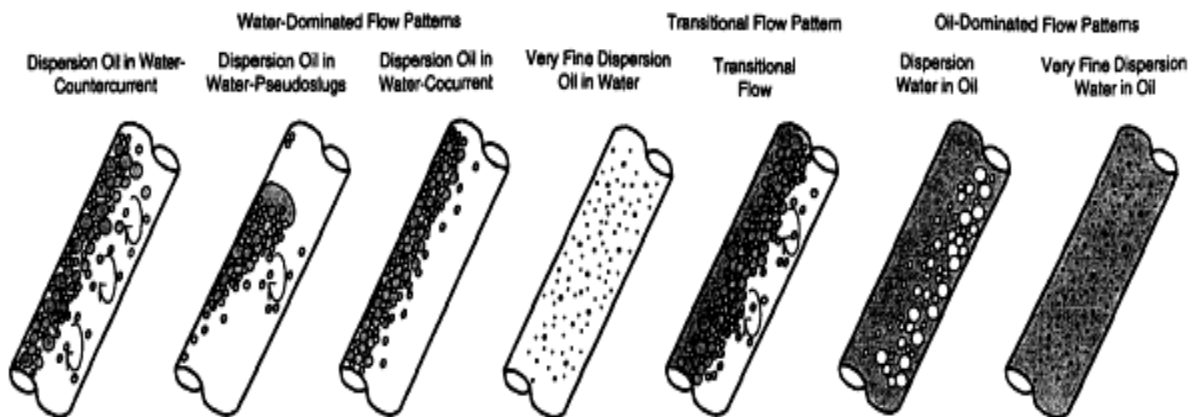
Figure 2.12: Schematic diagram of some flow patterns across an inclined pipe. (Flores et al., 1999)

24
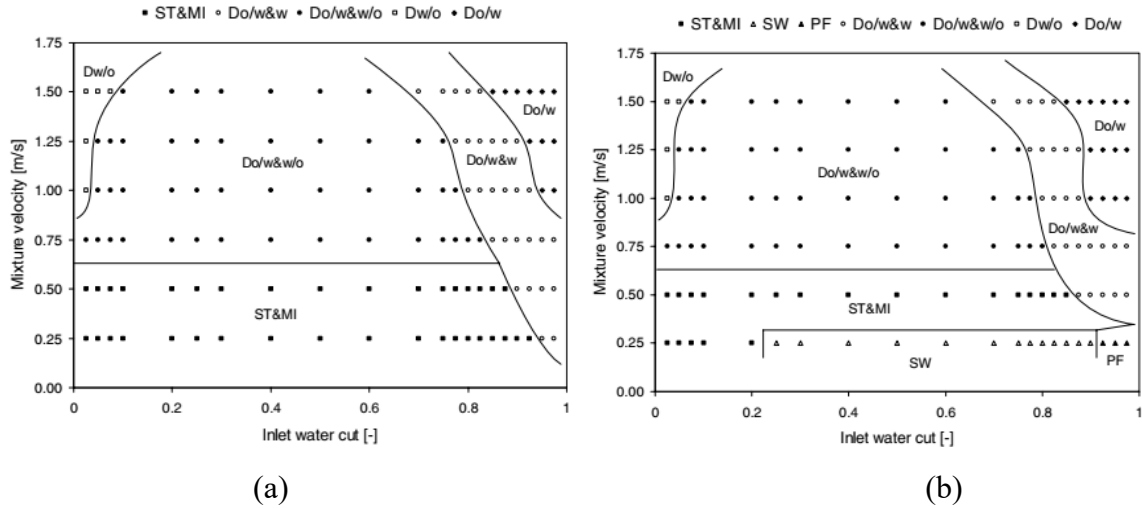
Figure 2.13: Flow pattern maps showing the transition boundaries for oil-water flow across an inclined pipe (a) +1º (b) +5º (Kumara et al., 2009).

2.7   LIQUID HOLDUP MEASURING TECHNIQUES.

The liquid holdup can be defined as the ratio of the cross-sectional area occupied by a given liquid to the total area of the cross-section. The liquid holdup plays a pivotal role in understanding the flow distribution and is widely used in mechanistic models for the prediction of the flow patterns, pressure drops and mixture properties. Also, for the petroleum industry, the prediction of the volume fraction is needed in the effective design and operation of the oil-water transport system including the design of the surface production facilities (Abubakar et al., 2018).

The liquid holdup cannot be determined analytically except through empirical correlations resulting from experiments. In the literature, there are three different techniques used in the measurement of the volume fraction. They are the shut-in method, probe method and the nuclear method. Brief discussion on these methods will be done in the subsequent sections but great consideration will be given to the conductance method which is a component of the probe method used in this work both in this chapter and the next.

2.7.1 Shut-in method

The shut-in method of measuring the volume fraction utilizes quick-closing valves and a measuring cylinder. The quick-closing valves uses a solenoid to quickly isolate a section of the test pipe containing the two-phase fluid mixture and the measuring cylinder used to collect and measure the total volume of the fluids, the volume of the particular phase of interest and finally the volume fraction of the phase can be determined. This method of measuring the volume fraction is particularly suitable for steady state measurements on non-intermittent streams and also for validating the value of the volume fraction with those obtained from other techniques.

In measuring the liquid holdup for an oil-water flow systems, a number of researchers such as Atmaca et al., (2008), Colombo et al., (2015), Ismail et al., (2015) and el have used the quick-closing valve method mainly because of its relative simplicity and reliability compared to other methods. However, the drawbacks in using this method are its inability to measure local void fraction distribution, its effect on the flow system when the valves are shut-in suddenly and inability to completely drain fluids of high viscosity (Gardenghi et al., 2020). A schematic showing how the shut-in method is used in measuring the liquid holdup can be seen in Figure 2.13.
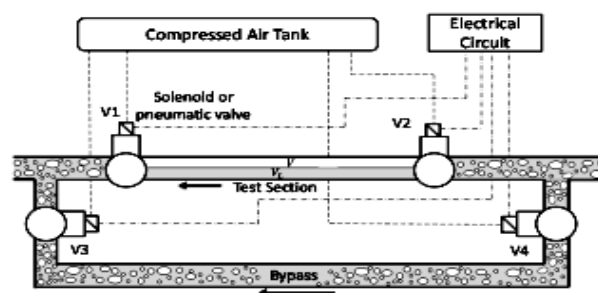
Figure 2.14: Measurement of volume fraction using the quick-closing valve method (Gardenghi et al., 2020).

2.7.2 The Probe method

The probe method is widely used in determining the volume fraction. It encompasses several other methods which includes the electrical method, optical method and ultrasound method. The probes could either be intrusive if they directly interfere with the flow of the fluids or non-intrusive if they do not interfere with the flow of the fluids.

The electrical method utilizes the differences in the electrical properties of the fluids such as the electrical resistivity or conductance (for conductive fluids) and electrical capacitance or impedance (for non-conductive fluids) to identify and quantify the phases present in the fluid mixture. The electrical probes can either be in the form of a single probe, multiple probes, wire-mesh or ring of electrodes that flushes with the internal wall of the pipe. The high frequency impedance probes used by Vigneaux et al., (1998) and Angeli and Hewitt (2000a) to measure the local volume fraction are examples of the multiple probe method used for the oil-water flow system. Since the probe is a point sensor, the local volume fraction of a phase can be determined if the fraction of the time the probe resides in a given phase is known (Angeli and Hewitt 2000a). The local volume fraction of a phase (a) at a point (b) inside the pipe can be given as:

$$\alpha_b = \lim_{T \to \infty} \sum_i \frac{T_{ai}}{T} \qquad (2.13)$$

Where T_a is the time the probe indicates phase (a) while T is the total time of the experiment.
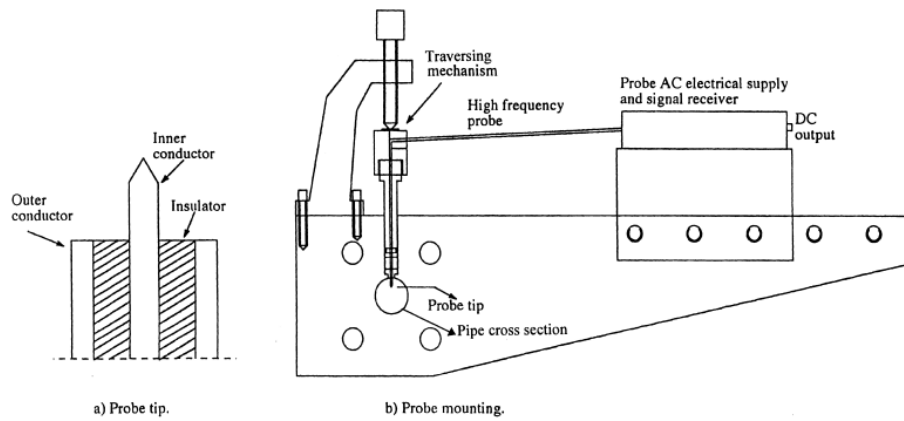
Figure 2.15: A high frequency impedance probe showing the tip and the probe mounting (Angeli and Hewitt 2000a).

Electrical Capacitance Tomography (ECT) and Electrical Resistance Tomography (ERT) are methods used to visualize the permittivity and conductivity distribution inside a pipe by measuring a set of capacitance and resistance between the electrodes surrounding the pipe. Based on the distribution of the permittivity and conductivity around a given pipe cross-section, the images showing the distribution of the phases can be constructed. ECT and ERT have been widely used in measuring the void fraction in gas-liquid (Elkow and Rezkallah, (1996), Gamio et al., (2004), Li et al., (2013), and Al-Mutairi et al., (2020)) but for the liquid-liquid flow system, only very few applications can be found in the literature (Hasan and Azzopardi (2007),Yang et al., (2012), Mohamad et al., (2016), Liu et al., (2017) and Perera et al., (2018)).
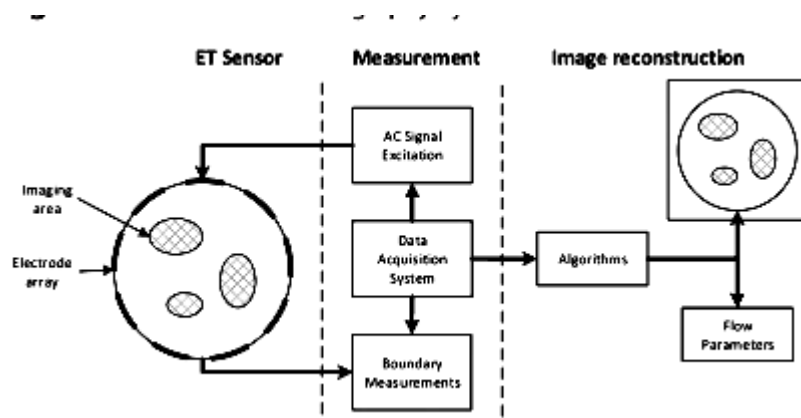
Figure 2.16: Schematic diagram of a typical ECT system. (Cui et al., 2016)

The ECT/ERT techniques are useful in providing the cross-sectional images of the fluid distribution which gives a real-time picture of the flow patterns and volume fraction in the two-phase flow system. However, the disadvantages in using this system includes the need for a fast data acquisition system, the distortions often affecting the reconstructed tomograms, and the simultaneous iterative techniques that must be employed to reconstruct an image from permittivity signals (Al-Mutairi et al., 2020).

The optical method of measuring void fraction is based on the differences in the optical properties of the multiphase system as a result of the passage of light through the multiphase media. The principle of operation of the optical probe technique is based on the differences in the refractive index between the two-phase mixture and it uses optical fibre for transmitting the beam of light. The process involves the transmission of light through the optical fibre to the tip of the probe in contact with the two-phase mixture and the re-transmission of the light signal back through the tip of the probe and the optical fibre to the surface electronics that processes the signal which is dependent on the refractive index of the two-phase media. For liquid-liquid system, Fordham et al., (1999), Hamad et al., (1997,2000), Jana et al., (2007), Mena et al., (2008) and Hao et al., (2023) had successfully used the optical method in determining the volume fraction because of the inherent advantages this method presents such as the ability to measure local (instantaneous) void fraction, high spatial and temporal resolution, small probe dimensions and high probe sensitivity. However, there are quite a number of disadvantages in using this method such as the additional flow disturbances created by the optical probes and bubble or droplets deformation which results in measuring errors (Gui et al., 2019), the necessity of drilling holes in the test section to place the optical fibres and finally the probes are quite expensive.

2.7.3 The nuclear method

The use of the nuclear method which includes x-ray and gamma ray in the determination of volume fraction in a two-phase system is based on the attenuation of the radiation ray or beam (gamma ray, neutron beam or x-ray) as it traverses through the two-phase system. The attenuation coefficient is dependent on the density of the material and the strength of the radiation source for example, solids have higher density and therefore have a higher attenuation coefficient than liquids, and liquids have a higher attenuation coefficient than gases. Similarly, higher energy radiation source will produce rays with lower attenuation coefficient while lower energy radiation source will produce rays with higher attenuation coefficients (Kwon & Kim, 2020). Based on the attenuation coefficient, the volume fraction can be determined using the Beer-Lambert's law. For liquid-liquid system, Elseth (2001), Rodriguez and Oliemans (2006) and Kumara et al., (2010) are some of the few researchers who successfully deployed this method in measuring the volume fraction because the x-ray densitometer has a high spatial resolution and both methods are non intrusive. However, the gamma-ray densitometer has low temporal and spatial resolution but cheaper to setup while the x-ray densitometer has low temporal resolution and quite expensive to setup. Also, instantaneous measurement of volume fraction is difficult to be determined using both methods because the radiation detectors measures the radiation intensity by counting the number of particles received in a given time interval.

2.8   CONDUCTANCE METHOD OF MEASURING THE VOLUME FRACTION

The conductance method is one of the methods used in measuring the volume fraction of a fluid mixture in which the continuous phase is electrically conductive and there is a conductivity contrast between the phases in the fluid mixture. Generally, conductance sensors

can determine the volume fraction by either measuring the electrical conductance (conductivity) or resistance (resistivity) of the fluid mixture. The fundamental working principle of the conductance sensor is based on the Ohm's law because once an electrical current of a given magnitude is applied to the fluid mixture through the electrodes and the voltage between the electrodes is measured, then the resistance or conductance can be determined. The use of the conductance techniques in measuring the volume fraction can broadly be classified into intrusive and non-intrusive method based on the design of the sensor. The intrusive method includes all the methods where the sensing electrodes are designed to protrude into the flow and make direct contact with the flow structures and in some cases, this could distort the velocity profile thereby increase the pressure drop. Examples of such probes are the needle-contact probes and parallel-wire probes. On the other hand, the non-intrusive method includes all the methods where the sensing electrodes are designed to flush with the internal wall of the pipe without obstructing the flow and a typical example of this method is the ring electrode design. In the following section, a summary of the relevant experimental work on the use of the conductance probes in measuring the liquid holdup will be given while the detail theoretical description will be given in the next chapter.

The conductance probes have been used extensively in gas-liquid two-phase flow by several researchers to measure the liquid film thickness particularly in the annular flow regime. Coney (1972) propounded the theory for the parallel rectangular conductance probes used in the measurement of the liquid film thickness. The theory allows the prediction of the electrical conductance as a function of the film thickness and it also includes the effect of a step change in the film thickness so that accurate prediction of the probe resolution can be made.

Asali et al., (1985) was the first to use the ring probe to measure the liquid film height in a vertical annular flow based on the work of Coney (1972). The researchers performed experiments for vertical flow of air and liquid across two pipes of diameter 2.29 and 4.2 cm

respectively. Measurements of the local liquid film thickness were made using the ring electrodes which consist of a pair of circular electrodes and on the basis of their results, improved methods were developed to predict the height of the liquid film and pressure drop.

Fossa (1998) investigated the performance of the ring-shaped and the plate electrodes in measuring the conductance of gas-liquid mixture in pipes. In conducting the experiment, a 70 mm ID test pipe with 3 flushed ring electrodes located 14 mm and 24 mm apart were used. The test section was divided into two with the first part designed to study the electrode response to annular flow while the other part was designed to study the response of the probe under stratified, bubbly and annular flow regimes. The response of the ring electrodes was compared to the theoretical solution of Coney (1972) and there was a good agreement.

Andreussi et al., (2015) developed a novel test section containing circumferential array of conductance probes to measure the liquid film distribution around a pipe wall of a liquid layer flowing in a near-horizontal pipe. The conductance probes made up of three parallel, rigid stainless steel wires 0.3 mm in diameter and aligned along the flow direction with a spacing of 12 mm between the wires were used in measuring the liquid holdup. The three-electrode geometry was adopted by the researchers to minimize current losses towards the earth and they equally operate the probes simultaneously without multiplexing which results in good circumferential resolution of the film thickness and a substantial reduction of the current dispersion. Analytical or numerical integration of the Laplace equation was used by the researchers to determine the probe conductance and optimize the geometry of the test section. Based on their findings, the researchers concluded that the theoretical predictions are quite accurate and agree well with the static calibration of the probes and also the conductance probes provide fairly accurate readings of the circumferential film distribution.

Several other researchers such as Andritsos and Hanratty (1987), Bontozoglou et al., (1989), Al-Sarkhi et al., (2011) and Ayati (2018 have successfully deployed the conductance probe in measuring liquid film thickness in a gas-liquid flow system. Interestingly, the theory that underpins the operation of the conductance probes including the calibration method was centered on the study of the liquid film thickness which was the primary focus of most of the researches in the gas-liquid flow system. But for the liquid-liquid system, the bulk of the researches carried out using the conductance probes particularly the parallel wire probes were aimed at studying interfacial wave phenomena. However, other parameters such as the liquid holdup and flow patterns have been determined using the conductance probe most especially the ring or multiple pins type.

Al-Wahaibi and Angeli (2011) experimentally studied the interfacial waves in a stratified horizontal oil-water flow using the parallel wires conductance probes and high speed camera.The parallel wire probes were made from 0.5 mm thick stainless steel wires placed 5 mm apart along the central plane of the pipe cross-section. Voltage measurements from the parallel wire probe showed a direct relationship with the interfacial height. Wave amplitudes and lengths were obtained from the time series of the interfacial height and the behavior of these interfacial wave parameters as flow condition changes were thoroughly investigated by these researchers.

Barral and Angeli (2013) used the double-wire conductance probe to study the interfacial characteristics of stratified liquid-liquid flow. The probe was made from stainless steel wires of thickness 0.5 mm and are placed 2 mm apart. The wires are tensioned and placed at the central plane of the pipe and for stratified oil-water flow, the voltage signals from the probe gave an indication of the interfacial height variations over time. Based on their results, the researchers were able to obtain time-averaged flow parameters and power spectrum from the measurements of the interfacial height. From the result of the power spectrum analysis, the

researchers were able to identify range of high frequencies which reflect the fluctuating nature of the oil-water interface.

Zhai et al., (2020) designed two conductance parallel wire probes (CPAP) to reconstruct the liquid-liquid interfaces at $\pm 3^o$ pipe inclination. The researchers used a glycerol/water combination with silicon oil across a 20 mm ID pipe. The CPAP was made up of eight pairs of parallel wire-type electrodes placed at equal distance at the pipe cross-section. The diameter of the electrodes was 0.2 mm with a 2.5 mm separating distance between the electrodes. Based on their experimental results, the researchers were able to reconstruct the interface between the aqueous solution and the silicone oil within the stratified flow (ST) and stratified with mixing at the interface (ST&MI) flow regimes. The reconstructed interface from CPAP was compared with that obtained from Planar Laser induced Flourescence (PLIF) method and there was close agreement. Other researchers who successfully used the conductance probes in measuring interfacial phenomena includes Park et al., (2016), Chinaud et al., (2017) and Zhang et al., (2020) among others.

Conductance probes have equally been applied in the liquid-liquid system for the determination of liquid holdup, wave velocity and the identification of flow patterns. For the measurement of liquid holdup, several research efforts have been made and a few will be highlighted for instance a method was developed by Zhai et al., (2012) of using the mini-conductance probes to measure liquid holdup in horizontal oil-water two-phase flow where the researchers designed and optimized the geometry of the ring conductance probes. The sensitivity and linearity of the measurement response with the variation of the oil holdup was determined by the researchers and they concluded that these parameters are dependent on the flow pattern. Similarly, Zhou et al., (2020) used the parallel-wire conductance probes to measure water holdup in near-horizontal pipes and compared the results with the values obtained using the quick-closing valves (QCV) and there was good agreement. Other researchers who applied the conductance

probes in determining the holdup includes Xinghe et al., (2012), Xu et al., (2016), Kong et al., (2016), Liu et al., (2016) and Han et al., (2018) among others.

In identifying the flow patterns using the conductance probes, Du et al., (2012) used the signals obtained from mini-conductance probes to identify the flow patterns in small diameter vertical upward two-phase flow. Similarly, Zhai et al., (2015) were able to detect in great detail the local flow structures of horizontal oil-water two-phase flow using mini-conductance probes and based on the fluctuating characteristics of these flow structures as flow condition changes, different flow patterns were identified and the flow pattern map was constructed with the experimental transitional boundaries compared with predictions from theoretical models in literature. Other researchers who identified different flow patterns using the conductance probes includes Zong et al., (2010), Chen et al., (2015) and Desamala et al., (2015) among others.

2.8.1   THEORY OF THE CONDUCTANCE PROBE

The use of the flush-mounted Conductance Probe (CP) immersed in the oil-water two-phase mixture is based on the potential field theory. When electrolytes are exposed to alternating current excitation, their electrical behavior is resistive provided the frequency of the applied signal is sufficiently high. The electric field can be modeled as time invariant as long as the regions have small dimensions compared to the wavelength of the electric field. Laplace equation for the electrical potential can be used to describe the problem with the proper boundary conditions.

$$\nabla^2 V = 0 \qquad\qquad\qquad (2.14)$$

The solution of the Laplace equation above can be obtained analytically or numerically depending of the probe geometry and the form of the interface between the phases.

According to Coney (1973), the conductance of the probe can be conveniently expressed in terms of a dimensionless parameter (dimensionless conductance) G^* where

$$G^* = \frac{G}{\sigma L} \qquad (2.15)$$

G is the actual conductance (Ω^{-1}), σ is the electrical conductivity of the liquid ($\Omega^{-1}m^{-1}$) and L (m) is the length of the electrode segment conducting the measured current.

Fossa (1998) equally stated that the dimensionless conductance, G^* can also be expressed in terms of a complete elliptical integral of the first kind as

$$G^* = \frac{K(m_1)}{K(1-m_1)} \qquad (2.16)$$

$k(m)$ can be defined as :

$$k(m) = \int_0^{\frac{\pi}{2}} (1 - m sin^2\theta)^{-\frac{1}{2}} d\theta \qquad (2.17)$$

where

$$m = \frac{Sinh^2\left(\frac{\pi s}{2h}\right)}{Sinh^2\left(\frac{\pi(s + D_e)}{2h}\right)} \qquad (2.18)$$

D_e(m) is the spacing between the electrodes, s (m) is the width of the electrode and h is the film height (m)

Andreussi et al., (1988) built on the work of Coney (1973) and showed that their solution holds for cylindrical geometry. For a specific case of annular and stratified flow configurations where the ring electrodes are covered by the conductive phase (the liquid layer), equation (3.3) will still be valid if the length *l* of the electrodes are replaced by the wetted length of the electrodes, P_L. The equivalent thickness of the liquid layer, h_l will then be given as:

$$h_l = AH_l/P_L \qquad (2.19)$$

Where A is the cross-sectional area (m^2), P_L is the wetted perimeter of the electrodes (m) and H_l is the fraction of the total volume occupied by the liquid phase.

In order to compare the theory with relevant experimental data, Andreussi et al., (1988) suggested using the normalized conductance, Ge^* which is the conductance obtained when the pipe is full of the conductive liquid (water).

For uniformly dispersed two-phase system (e.g. bubbly flow), the normalized conductance, Ge^* is found to be proportional to the apparent conductivity of the two-phase mixture, λ_m when ring electrodes are used to measure the liquid holdup. Several models have been developed to determine λ_m as a function of the average liquid holdup and the liquid conductivity including the models of Maxwell (1882) and Bruggeman (1935) which can be given as:

$$\text{Maxwell's Model} \qquad Ge^* = \frac{G_m}{G_o} = \frac{\lambda_m}{\lambda_o} = \frac{2H_l}{3 - H_l} \qquad (2.20)$$

$$\text{Bruggeman's Model} \quad Ge^* = \frac{G_m}{G_o} = \frac{\lambda_m}{\lambda_o} = H_l^{3/2}$$

(3.9)

Where

G_m and G_o are the conductance of the fluid mixture and the conductance when the pipe is full of the conductive fluid respectively.

λ_m and λ_o are the electrical conductivity of the fluid mixture and that of the liquid respectively.

H_l is the liquid holdup.
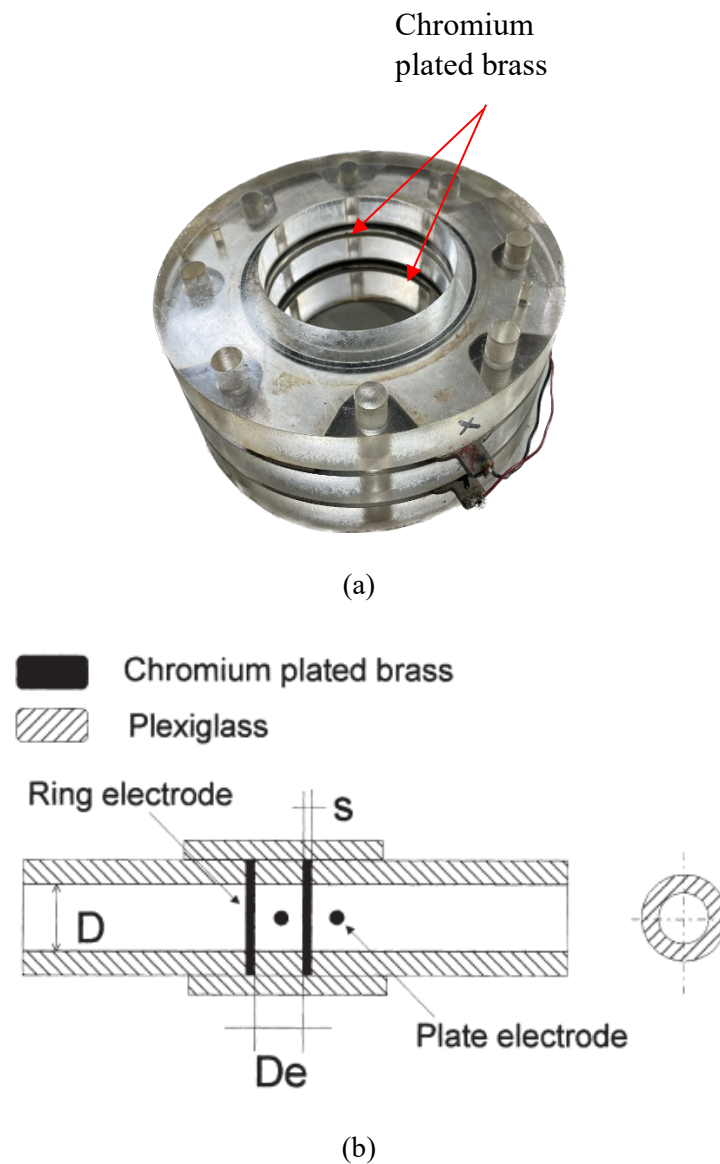
Figure 2.16a: (a) Pictorial representation of the conductance probe showing the Chromium plated brass electrodes (b) Cut-out section of the probe assembly showing the geometrical dimension.

The composition of the probe assembly includes two (2) circular chromium plated brass and four (4) acrylic plates having the same internal diameter (ID = 127 mm) as the pipe in the test section. The width of the chromium plated brass is 2 mm while the probe aspect ratio, D_e/D is 0.34.

2.9   INTERFACIAL CHARACTERISTICS IN A STRATIFIED TWO-PHASE FLOW

Stratified flow with smooth interface is the basic flow pattern observed in the simultaneous flow of gas-liquid or liquid-liquid flow across pipes at low superficial velocities of the phases

where the less dense phase (oil or gas) occupies the top layer and the denser water phase occupies the bottom layer. On increasing the flow rate of the either of the phases, the morphology of the interface begins to change as a result of the growth and development of waves along the interface. These waves develop as a result of several factors one of which is hydrodynamic instabilities (Kelvin-Helmholtz instability) at the interface caused by the turbulent flow of the faster flowing phase (Ayati, 2018). The appearance of these interfacial waves play a very important role in determining the flow pattern transition, liquid holdup distribution and the pressure drop encountered in such system.

Prior to the study of interfacial waves in liquid-liquid system, a lot of similar studies had been conducted on the gas-liquid flow particularly for the annular flow regime and it will be of immense interest if a brief consideration is given to it to establish the foundation in understanding the interfacial wave phenomena in liquid-liquid system.

2.9.1 Studies of interfacial behavior in gas-liquid stratified flow

There are a number of studies that focuses on the interfacial waves in gas-liquid system. The initial thrust in undertaking such studies was to establish theoretical basis for the flow pattern transition taking into cognizance the physics of the flow. On that note, Wallis (1969) and Taitel and Dukler (1976) carried out extensive theoretical studies on the propagation of interfacial waves in order to understand the physics of the flow pattern transition. The researchers successfully developed flow pattern transition models which are dependent on void fraction, pressure drop and fluid velocities. Further studies were subsequently carried out to understand the types of wave occurring at the interface and to identify which of the wave type are responsible for interfacial instability. One of such studies was carried out by Andritsos and Harantty (1987a,b) who conducted an experiment to determine the interfacial stress using horizontal pipes of diameters 2.52 and 9.53 cm with liquid of viscosities ranging from 1 to 80

mPa.s. Based on their results, they identify regular 2D waves and large amplitude irregular waves associated with K-H instabilities. The researchers found that the increase in the interfacial stress were closely associated with the large amplitude waves. Also, the researchers showed in their findings that the ratio of the interfacial friction factor (f_i) in a wavy surface to the value for a smooth surface (f_g) is strongly related to the ratio of wave height to the wave length otherwise known as wave steepness. In fact, while comparing the friction factor for the wavy stratified and stratified smooth flow patterns, Bontozoglou and Hanratty (1989) stated that in a two-phase gas-liquid system, the friction factor in a wavy stratified flow can be about 50 times that of the stratified smooth flow pattern.

In order to apply these findings in designing physical systems, there is need to relate the characteristics of these interfacial waves such as the wave amplitude, wavelength and wave speed to their corresponding input parameters (input flow rates, fluid properties and pipe geometry) through appropriate empirical relationships for design and optimization purposes. As a result, several experimental campaigns were undertaken and among which are:

Paras and Karabelas (1991) studied the evolution of interfacial waves in a gas-liquid flow across a pipe of 50.8 mm ID. The researchers used the parallel-wire conductance probes to obtain the time domain signals from which interfacial wave propagation speed was determined. The dimensionless film thickness defined as the roughness of the interface was used with the gas superficial velocity to correlate the wave speed and based on their findings, the researchers proposed the following correlation for the wave speed.

$$c_s = 0.75 + 0.002\left(V_{GS}^2 \frac{h}{D}\right)^{0.5} \tag{2.21}$$

Where c_s, V_{GS}, h, D represents the interfacial wave speed (m/s), gas superficial velocity (m/s), height of film thickness (m) and the pipe diameter (m)

Tzotzi and Andritsos (2013) made an attempt to understand the evolution of the wave structures along the interface and they developed a model to predict the onset of 2D waves. The researchers equally used the modified Kelvin-Helmholtz stability criterion to successfully predict the transition to large amplitude 3D waves at low liquid flow rates.

Gawas et al., (2014) investigated the wave characteristics in gas-oil two-phase flow across a horizontal and slightly inclined pipe of 152.4 mm ID. The researchers used a double-wire capacitance probes to determine the wave characteristics such as the wave amplitude, wave celerity and wave frequency along the interface. Gawas et al., (2014) found that the wave celerity increases almost linearly with the gas velocity but increases only slightly with increase in the liquid velocity. Also, while investigating the effect of the wave celerity on some dimensionless numbers, the researchers found that the wave celerity is a strong function of the modified Lockhart-Martinelli parameter, X* or the ratio of the Froude number based on the superficial liquid and gas velocities.

$$X^* = \sqrt{\frac{\rho_G}{\rho_L}} \frac{\dot{m}_L}{\dot{m}_G} = \sqrt{\frac{\rho_L}{\rho_G}} \frac{V_{SL}}{V_{SG}} = \frac{Fr_{SL}}{Fr_{SG}} \qquad (2.22)$$

Where X* is the modified Lockhart-Martinelli parameter

$$Fr_{SL} = \sqrt{\frac{\rho_L V_{SL}^2}{(\rho_L - \rho_G)gDcos(\theta)}} \qquad Fr_{SG} = \sqrt{\frac{\rho_G V_{SG}^2}{(\rho_L - \rho_G)gDcos(\theta)}} \qquad (2.23)$$

$\rho_G, \rho_L, V_{SG}, V_{SL}, \dot{m}_G, \dot{m}_L, D, \theta$ represents the density of the gas (kg/m^3), density of the liquid (kg/m^3), superficial velocity of the gas (m/s), superficial velocity of the liquid (m/s), mass flow rate of the gas (kg/s), mass flow rate of the liquid (kg/s), diameter of the pipe (m) and the pipe inclination (degree) respectively.

$$\frac{C}{V_{SL}} = 3.51 \, X^{*-0.81} \quad \text{for} \quad X^* < 0.305 \qquad (2.24)$$

And $\quad \dfrac{C}{V_{SL}} = 6.102 \, X^{*-0.495} \quad \text{for} \quad X^* > 0.305 \qquad (2.25)$

In the stratified-atomization and annular flow regimes, the researchers equally developed an empirical relationship between the wave amplitude and the modified Lockhart-Martinelli parameter and also the base film thickness. On comparing the predictions from these empirical models with mechanistic model in literature (Watson 1989), there was agreement.

Wang et al., (2020) performed an experimental and theoretical study on the interfacial characteristics of a gas-liquid horizontal flow at high pressure. The researchers used a high speed camera to capture the structure of the interface as the mixture flow through a 50 mm pipe ID. Dimensionless liquid film thickness at different gas pressure was determined and an empirical relationship with the liquid Reynolds number was proposed as:

$$h^+ = 0.215 Re_L^{0.781} \left(1 - \frac{h}{D}\right)^{-0.382} \tag{2.26}$$

Where h^+, h, D and Re_L are the dimensionless liquid thickness, liquid thickness, pipe internal diameter and the liquid phase Reynolds number respectively.

Similarly empirical relationships were developed for the wave amplitude, frequency and wave speed.

Saini et al., (2022) carried out an analysis of interfacial dynamics for stratified and stratified wavy flow using Laser Doppler Velocimetry (LDV) method synchronized with a computerized 3-dimensional traverse system to measure the interface level or liquid height. The researchers used a $25\pm0.15\ mm$ ID pipe where the air/water fluid mixture passes through. Reynolds number for both the gas and liquid phases (Re_{SL} and Re_{SG}) were calculated based on their corresponding superficial velocities within the stable stratified flow region. The relationship between the dimensionless liquid height ($\frac{h}{D}$) and the Reynolds numbers were determined. Based on their experimental findings, an empirical relationship that could predict the

dimensionless liquid height based on the input parameters presented in form of the Reynolds numbers was obtained as:

$$\frac{h_L}{D} = 0.0697(Re_{SL})^{0.365}(Re_{SG})^{-0.086} \tag{2.27}$$

Where h_L, D, Re_{SL}, Re_{SG} represents the height of the liquid layer (m), pipe diameter (m), liquid Reynolds number and gas Reynolds number respectively.

The researchers compared the predictions from the empirical model with that of Taitel and Dukler (1976) and there was a Mean Absolute Relative Deviation (MARD) of about 18.79% due to approximations used in deriving the analytical expression proposed by Taitel and Dukler (1976).

2.9.2 Studies of interfacial behavior in liquid-liquid stratified flow

Liquid-liquid flow systems and particularly the oil-water flow is fundamentally different from the gas-liquid flow system. The latter is characterized by high viscosity and density differences while the former is characterized by low density difference between the phases. As a result of the extremely high density difference in the gas-liquid system, they are usually gravity dominated in the horizontal stratified flow, therefore the interface separating the gas and liquid phase can reasonably be assumed to be planar. However, in oil-water flow system, the density difference between both phases is small and either of the phase have the potential of wetting the pipe, therefore the assumption of a flat interface may not be accurate except for systems with large Bond number.

$$\text{Bond number (Bo)} = \frac{\Delta\rho g d^2}{\sigma} \tag{2.28}$$

Where $\Delta\rho$, d, g and σ represents the density difference between the liquid (Kg/m^3), the pipe internal diameter (m), acceleration due to gravity (m/s^2) and interfacial tension (N/m).

Oil-water flow systems with large Bond number could either mean that the density difference between the phases is extremely large, the pipe diameter is very large or the interfacial tension between the liquid is very small, therefore the characteristics of such a system could approximate to that of a gas-liquid system, hence the assumption of a flat interface is valid. However, for oil-water flow systems with small Bond number (capillary systems, reduced gravity systems or small density differential systems) (Gorelik and Brauner, 1999) where the surface forces predominate over the inertia forces, the liquid that wets the pipe tends to climb over the pipe wall resulting in a curved interface as experimentally observed by researchers such as Valle and Kvandel (1995) and Angeli et al., (2002) to mention just a few.

The study of the interfacial behavior in liquid-liquid systems had initially been driven by the need to understand the relationship between the cross-sectional interface curvature and the input parameters so that closure models can be developed and incorporated into the Two-Fluid model for better prediction of pressure drop and liquid holdup.

Brauner (1996) attempted to model theoretically the location and shape of the oil-water interface.
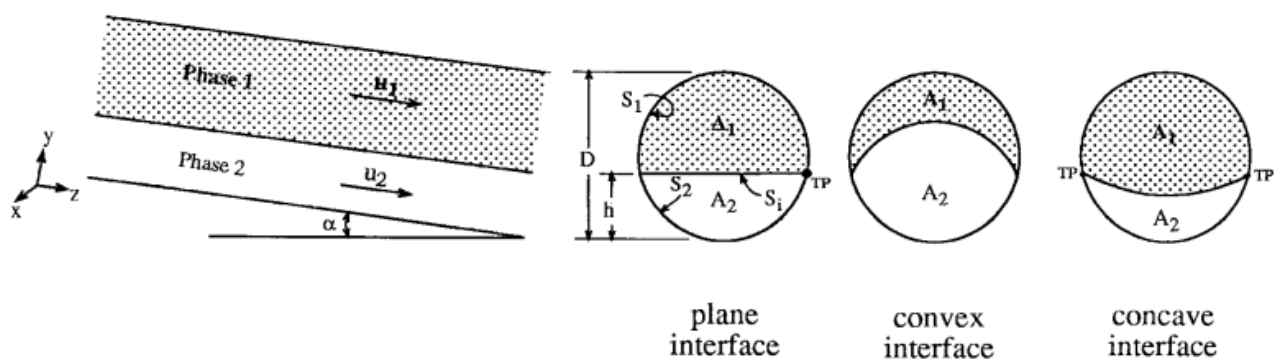
Figure 2.17: Schematic diagram of a stratified flow showing the interfacial configurations and parameters. (Gorelik and Brauner, 1999).

The location of the interface was obtained using the stress balance in the x and y direction. The condition of the equilibrium between the pressure jump across the interface taking into

cognizance the surface tension force and the local radius of the interface curvature with the assumption that the interface curvature in the axial direction is infinite were used to develop the expression for the location of the interface given as:

$$\sigma \frac{d}{dx}\left\{\frac{d\eta/dx}{[1+ (d\eta/dx)^2]^{\frac{3}{2}}}\right\} - (\rho_1 - \rho_2)\eta g cos\beta = \text{const} = \lambda \qquad (2.29)$$

Where $\sigma, \rho_1, \rho_2, \eta, g, \beta$ represents the interfacial tension (N/m), density of the denser phase (Kg/m^3), density of the less dense phase (Kg/m^3), interface location from the centre plane (m), acceleration due to gravity (m/s^2) and the pipe inclination (in radians) respectively. It should be noted that the first term in equation (2.22) represents the normal stress acting on the interface while the second term is the gravitational pull to flatten the interface.

On solving for the quasi-static condition using the variational problem of minimizing the total energy, the location of the interface $\eta(x)$ can be obtained taking into consideration the wettability condition at the pipe wall and its symmetry with the y-axis and also the fluid in-situ holdup. In fact, Brauner (1996) observed a strong dependence of the interface shape with the liquid holdup where for fluids with equal wettability and for a given Bond number, the interface was convex for a low holdup of the lower phase, concave for higher holdup and planer for equal holdup.
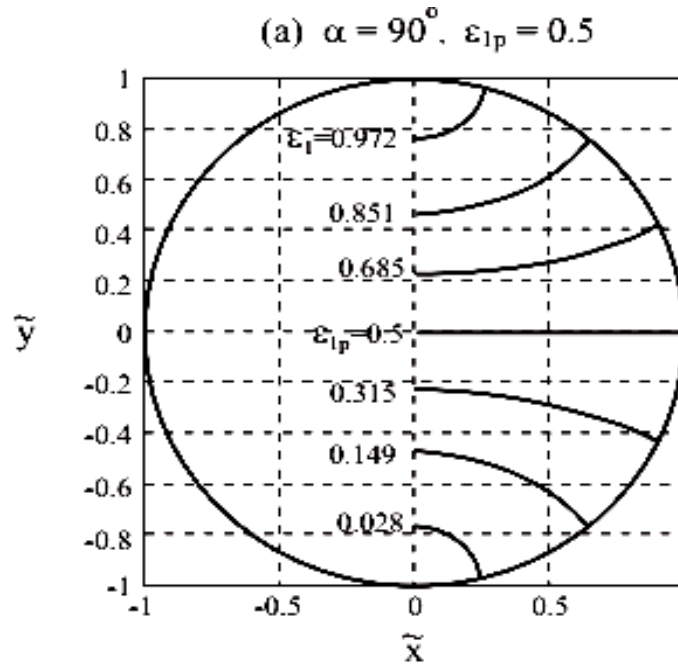
**Figure 2.18: Configuration of the interface for Bond number = 1 and contact angle = 90°
(Brauner, 1996)**

Gorelik and Brauner (1999) used similar procedure as Brauner (1996) in modeling the oil-

water interface shape and location but the difference lies in the method used in solving for the

interface shape. Gorelik and Brauner (1999) were able to obtain exact analytical solution for

the interface shape by solving the Young-Laplace equation with contact angle boundary

condition. The researchers concluded that the interface shape is a function of three parameters

namely the Bond number, water holdup and the contact angle (Zhang et al., 2019). For a given

Bond number and contact angle, the observation made for the change in the shape of the

interface as the holdup changes were similar to that of Brauner (1996). Also, for a constant

holdup and contact angle, given a small Bond number, the interface approaches a circular arc

while for a large Bond number, the interface is almost plane with a slight meniscus near the

pipe wall and finally in between these two extremes, the interface approximately becomes

elliptical. The researchers also observed that for a given Bond number and holdup, the interface

is approximately convex when the contact angle is high but at low contact angle, the interface

becomes concave.

Rodriguez and Baldani (2012) made an attempt to predict the pressure gradient and liquid holdup in a wavy-stratified oil-water flow across a 26.2 mm ID inclined pipe. The researchers modified the Two-Fluid model by incorporating a closure relation for the interfacial friction factor based on the new experimental data obtained on the wavy-stratified flow. In order to account for the shape of the interface, the researchers proposed an explicit equation based on the constant-curvature-arc model which is a function of the Bond number, contact angle and the liquid holdup. The radius of curvature for the curved interface was obtained by fitting a circular arc over the solution of Ng et al (2002) and the relation for the radius of curvature was given in equation (23).
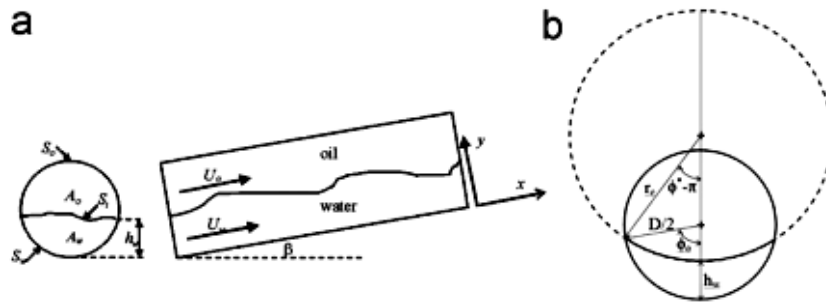
Figure 2.19: Schematic diagram of (a) Stratified oil-water wavy flow (b) Constant-curvature-arc model (Rodriguez and Baldani, 2012)

$$r_c = D\left[\psi_1(\theta) - \psi_2(\theta)e^{-E_o/\psi_3(\theta)}\right]e^{\psi_4(\theta)}\left\{g(h_w,\theta)\left[a(\theta) - \left(\frac{h_w}{D}\right)\right] + [1 - g(h_w,\theta)]\left[\left(\frac{h_w}{D}\right) - b(\theta)\right]\right\} \quad (2.30)$$

h_w, θ, D, E_o represents the water height (m), pipe inclination (radians), pipe internal diameter (m) and Bond number respectively.

The details of what each of the constants represented above can be found in Rodriguez and Baldani, (2012). On using the modified Two-Fluid model which accounts for the interface curvature and roughness to predict the liquid holdup and pressure gradient, there was an overall agreement when compared with other models and data from literature with an average deviation less than 15% for both the liquid holdup and the pressure drop.

Edomwonyi-Otu and Angeli (2015) attempted also to improve the prediction of the pressure drop and liquid holdup for curved and wavy interface in an oil-water flow across a 14 mm

horizontal acrylic pipe. The researchers used two conductance probes (parallel wire and ring probes) to determine the average oil-water interface height at the pipe centre and also at the pipe wall. Based on their experimental observations where the average oil-water interface heights at the pipe walls were always greater than the same measurement at the pipe centre, they concluded that the shape of the oil-water interface was concave for all the cases studied. An empirical correlation was developed that relates the average oil-water interface at the wall (h_w) and the average oil-water interface height at the middle (h_m) and it was obtained as:

$$h_m = \frac{1.065 h_w D}{0.014} - 0.0009 \tag{2.31}$$

The researchers equally determined the average wave amplitude using the time series data from the wire probe over the range of velocities studied and the value of the average wave amplitude was used as roughness in the interfacial friction factor correlation as proposed by Rodriguez and Baldani (2012).

$$f_i = f_k \left[1 + C_i \frac{\alpha}{D} \right] \tag{2.32}$$

Where f_k, α, D, C_i represents the wall friction factor of the faster phase, the average wave amplitude (m), internal pipe diameter (m) and a correction factor respectively.

On incorporating the effect of the interface curvature and roughness in the Two-Fluid model, the researchers observed that although the average pressure drop values does not seem to improve probably due to the very small wave amplitude observed, however the standard deviations reduced by almost 50% especially at low water velocities where the interface curvatures were much more pronounced.

Zhang et al., (2019) predicted the shape of the interface using the Young-Laplace equation and minimization of total energy model. The researchers used a 20 mm ID horizontal pipe where the oil-water interface shape was determined using a conductance parallel wire array probe (CPAP). Based on their experimental findings, the researchers observed that the prediction of the location and shape of the interface using the two models are very consistent, however, there

was a large deviation between the predicted interface shape from the models and the corresponding experimental values. Upon modifying the model by accounting for the dynamic contact angle, there was an agreement between the experimentally measured values and those predicted from the models.

2.9.2.1   Interfacial wave characteristics in stratified liquid-liquid flow system

The appearance of waves along the interface as a result of interfacial instability (Kelvin-Helmholtz instability) have been identified as the main factor that greatly impacts flow pattern transition from stratified to non-stratified flow, pressure drop estimation, liquid holdup distribution and heat transfer coefficients. In order to understand the behavior of these interfacial waves, several experimental campaigns have been undertaken to establish the relationship between the interfacial wave characteristics such as the wave amplitude, wavelength, frequency and wave speed and input flow parameters with the intent of developing empirical correlations between these parameters. Although earlier the attention of researchers working on interfacial waves in liquid-liquid system was primarily on core annular flow where it was demonstrated that the existence of interfacial waves is fundamental to the stability of the core annular flow pattern (Oliemans, 1986; Bannwart, 1998; and Rodriguez and Bannwart, 2006). However in this section emphasis will be on research efforts that focus on the stratified flow patterns including stratified wavy (SW) and stratified wavy with mixing at the interface (SW&MI).

Al-Wahaibi and Angeli (2011) were among the pioneers to conduct experimental studies of interfacial waves for the stratified flow pattern (SW) and at the onset of transition to dual continuous flow pattern (DC) across horizontal a 38 mm ID pipe. In order to study the interfacial wave characteristics at 2 m and 6 m from the inlet, the researchers used a parallel

wire conductivity probe to measure the instantaneous fluctuations of the interface and also images of the interfacial structures were taken using the fast speed camera. Based on the time series data obtained from the probe and images from the camera, the wave amplitude, wavelength and the wave speed were determined. On the basis of their experimental findings, the researchers noted that the wave amplitude increases as the superficial velocities of both phases increases and more importantly the interfacial waves need to reach a critical amplitude before drops are formed which signaled the point of transition from the stratified wavy (SW) to dual continuous flow (DC). The researchers equally observed that the wavelength of the interfacial wave is dependent on the relative velocity between the two fluids because the average wavelength decreases as the in situ relative velocity increases. The increase in the relative velocity between the phases have been identified by the researchers to cause an increase in interfacial shear stress which increases the instability and turbulence at the interface leading to a decrease in the wavelength and an increase in the wave amplitude. Although the researchers indicated that the wave speed was measured in their experiment, however no any information regarding the effect of the flow variables on the wave speed was found.

Castro et al., (2011) made an attempt to study the geometrical and kinematic properties of interfacial waves for a heavy oil-water flow across a 26 mm ID horizontal pipe. The authors captured the geometrical properties of the interfacial waves using the high speed camera and with the aid of a LabView-based software program, the wave amplitude and wavelength were determined while the wave celerity was obtained using the cross-correlation of two frames lagged in time. The interfacial waves observed were further classified based on the value of the normalized wavelength ($\frac{\lambda}{D}$ where λ is the wavelength (m) and D is the internal pipe diameter (m)) into short ($\frac{\lambda}{D} < 1$), intermediate ($1 < \frac{\lambda}{D} < 10$) and long ($\frac{\lambda}{D} > 10$) waves. Castro et al., (2011) only analyzed the intermediate waves because the short waves were considered to be ripples

while the long waves could not be entirely visualized in the film section. Based on their experimental observations, the authors were able to establish a relationship between the interfacial wave characteristics and some important hydrodynamic parameters such as the oil holdup and the relative velocity. Castro et al., (2011) observed that the normalized mean wavelength decreases with increasing oil holdup and relative velocity and similar trend was also observed for the normalized mean wave amplitude. Castro et al., (2011) were able to relate the observed trends with fundamental physics of interfacial instability where the relative velocity was suppose to have a destabilizing effect on the stratified flow based on Kelvin-Helmholtz instability criterion while the effect of the holdup was accounted for in the stabilizing effect of the gravitational force on the denser water phase. Also, on normalizing the wave celerity with the mixture velocity, the Castro et al., (2011) observed that the normalized wave celerity increases as both oil holdup and relative velocity increases.

In order to provide more insight into the properties of interfacial waves particularly for inclined pipes, Castro et al., (2012) conducted experimental campaigns to determine the geometrical and kinematic properties of interfacial waves in stratified oil-water flow across a 26 mm ID inclined pipe. The authors used 4 different pipe inclinations ($+10^o$, -10°, $+20^o$ and -20°) where the interfacial wave properties were captured using the high speed camera. A home-made LabView program was used to extract the properties of these interfacial waves from the flow images. Based on the experimental observations, the authors found that the wave properties are dependent on the relative velocity, holdup and pipe inclination and proposed a modified Froude number (Fr_M) to correlate their experimental data.

$$Fr_M = \frac{U_w - U_o}{\sqrt{g.cos\theta.\varepsilon_w.\frac{\pi.D}{4}}} \tag{2.33}$$

Where $U_w - U_o$ is the relative velocity (m/s), θ is the inclination angle (radians) ε_w is the water in-situ volumetric fraction, D is the internal diameter of the pipe (m) and g is the

acceleration due to gravity (m/s^2). Similar Castro (2011), the researchers categorized the interfacial waves observed based on the normalized wavelengths as short ($\frac{\lambda}{D}$ < 0.7), intermediate (0.7 < $\frac{\lambda}{D}$ < 2.15) and long ($\frac{\lambda}{D}$ >2.15) waves but only analyzed the intermediate waves. Upon plotting the wave aspect ratio which is the ratio between the average wavelength and amplitude ($\frac{\lambda_m}{\alpha_m}$) and the modified Froude number (Fr_M) for the different pipe inclinations, the researchers observed that the aspect ratio increases from downward to upward flow which implies that interfacial waves with longer wavelengths and shorter amplitudes are related to upward flow. The mean interfacial wave celerity normalized with the mixture velocity was found to increase as the modified Froude number increases.

Barral (2014) carried out experimental campaigns to study stratified wavy flow pattern for an oil-water flow across a 38 mm horizontal pipe using a specially designed fluid inlet device. The researcher used a high speed camera to capture the interfacial wave evolution at the fluid inlet device, but interestingly the interfacial wave did not propagate further down to the test section. In fact, the interfacial waves were only observed when the input ratio which is the ratio between the oil superficial velocity to water superficial velocity (r = $\frac{U_{so}}{U_{sw}}$) is less than unity or greater than unity but at values close to unity, interfacial waves were not observed at the fluid inlet device. The researcher explained that the dampening of the waves downstream was caused by the fluids adjusting their in-situ velocities to almost the same values, which implies the relative velocity will become almost zero downstream and thus removing the source of the instability. From the analysis of the experimental results, the researcher observed that the average wave amplitude decreases downstream the fluid inlet device while the average wavelength was found to increase along the fluid inlet device. Also, for all the flow conditions tested, the wave frequency was found to exist within the range of 11 – 20 Hz and the frequencies remained constant downstream the inlet section and as a result, the wave velocity increases.

The researcher equally noted that initially the wave velocities for all the tested flow conditions were found to be half the mixture velocity and is generally independent of the input ratio.

Castro and Rodriguez (2015) provided new experimental data on interfacial waves for stratified viscous oil-water flow across a 26 mm ID inclined pipe. The researchers used a high-speed camera to capture the evolution of the waves along the interface and applied several image analysis techniques using a Labview program to obtain the interfacial wave characteristics such as the wave amplitude, wavelength, wave shape and wave speed. One important improvement of this work compared to the previous efforts was that the researchers were able to correlate these interfacial wave properties with flow properties using dimensionless numbers such as Reynolds number, Froude number and Weber number which describes the physics of the system. Upon analyzing the experimental data and two other data from literature, the researchers obtained an empirical relationship between the wave aspect ratio and the Weber number (We). They observed that as the Weber number (We) increases as a result of increase in the relative velocity, the wave aspect ratio decreases asymptotically.

$$\frac{\lambda_m}{\alpha_m} = 84.4e^{-We/0.4} + 6.8 \tag{2.34}$$

Where λ_m, α_m, We represents the mean wavelength (m), mean amplitude (m) and the Weber number respectively.

Similarly, the researchers obtained two correlations for the normalized wave speed. They observed that as the modified Froude number increases, the normalized wave speed also increases asymptotically and they related the increase in the modified Froude number to a higher degree of instability. The same trend was also observed with the oil phase Reynolds number.

$$\frac{c}{(U_{sw} + U_{so})} = -2.6e^{-Fr/0.4} + 1.5 \tag{2.35}$$

$$\frac{c}{(U_{sw} + U_{so})} = -1.2 e^{Re_o/13.4} + 1.4 \tag{2.36}$$

where c, U_{sw}, U_{so}, Fr, Re_o represents the mean wave speed (m/s), water superficial velocity (m/s), oil superficial velocity (m/s), modified Froude number and oil phase Reynolds number respectively. Interestingly, the researchers were able to show with their experimental data the validity of the hypothesis that the lower and upper limit of the interfacial wave speed would be the phase's in-situ velocities which proves that waves are kinematic in nature (Wallis, 1969).

Premanadhan et al., (2019) carried out experimental investigations of interfacial waves in stratified oil-water flows across 40 mm ID, 54.8 mm ID and108.4 mm ID horizontal pipes. The researchers used high speed camera to capture the wave propagation along the interface and using the image processing suites in MATLAB, the interfacial wave properties (Wave amplitude and wavelength) were obtained. The researchers adopted similar technique of using modified Froude number to correlate the properties of the waves with flow parameters as Castro et al., (2012) and Castro and Rodriguez (2015) did but the difference between them is the inertia component of the Froude number. Premanadhan et al., (2019) used the in-situ mixture velocity while both Castro et al., (2012) and Castro and Rodriguez (2015) used the relative velocities to represent the inertia terms.

$$Fr_M = \frac{U_{iw} + U_{io}}{\sqrt{\frac{(\rho_w - \rho_o)}{\rho_w}.g.cos\theta.\frac{A_w}{S_w}}} \tag{2.37}$$

Where U_{iw}, U_{io}, ρ_w, ρ_o, A_w, S_w, g, θ represents the water in-situ velocity (m/s), oil in-situ velocity (m/s), water density (kg/m^3), oil density (kg/m^3), cross-sectional area occupied by the water phase (m^2), wetted perimeter of the water phase (m), acceleration due to gravity (m/s^2) and the inclination angle (in radians) respectively.

On the basis of their experimental findings on the 40 mm ID pipe, the researchers observed that the wave amplitude increased gradually as the modified Froude number increases and the

increase in amplitude attained a plateau at higher Froude number. On comparing their observation with experiments done on the 54.8 mm and 108.4 mm pipes, the researchers observed that the wave amplitudes measured across all the three pipes were found to increase with increasing Reynolds number of water until a plateau was reached close to 3 mm. On increasing the velocity of the phases beyond the 'plateau' point lead to droplets formation. The researchers identified the turbulence in the water phase as the main contributor to wave formation and growth in oil-water flows. Also, on correlating the wave aspect ratio($\frac{\lambda_m}{\alpha_m}$) with the modified Froude number, the researchers observed that the wave aspect ratio decreases with increase in modified Froude number and obtained the following correlation:

$$\frac{\lambda_m}{\alpha_m} = 40.46e^{(-1.125Fr_m)} + 8.86 \qquad (2.38)$$

2.10 Stability analysis of interfacial waves in oil-water stratified flow

The existence of waves along the interface in a two-phase gas-liquid or liquid-liquid system and its response to changes in the input flow parameters have been identified as the key element in the transition from stratified to non-stratified flow regimes (Trallero, 1995; Brauner and Moalem, (1992b), Al-Waibi, 2007). This transition is known to equally affect the pressure drop, liquid holdup distribution and heat/mass transfer coefficients. The stratified to non-stratified flow pattern transition have been widely studied in literature especially for gas-liquid flow (Taitel and Dukler, 1976; Barnea, 1990, Brauner and Maron, 1990, Guo et al., 2002, Salhi et al., 2010,) but only very few studies are available for the liquid-liquid flow (Brauner and Maron, 1992a,, Trallero, 1995; Al-Wahaibi and Angeli, 2007; Rodriguez and Bannwart, 2008; Al-Sarkhi et al., 2017). In the study of the transition from stratified to non-stratified flow, the one dimensional two-fluid model is usually used where the continuity and momentum equations are applied to each of the phases. In order to check the stability of the system, infinitesimal disturbances are introduce around the equilibrium position so that higher order

terms can be neglected and linearize the non-linear terms in the governing equations, hence this procedure is called linear stability analysis (Barnea and Taitel, 1989). The growth or decay in amplitude of this infinitesimal disturbance which are periodic will determine if the system is unstable or stable. Since in stratified flow, the two phases have different densities and are moving at different velocities, the classical Kelvin-Helmholtz (KH) instability analysis is used in determining the stability criterion. In developing the KH stability criteria, two methods of analysis are used of which one involves the use of shear stress terms in the two-fluid model and is called the viscous KH analysis (VKH) while the other method neglects the shear stress terms in the two-fluid model and is called the inviscid KH analysis (IKH).

Several researchers have made attempt in applying the KH stability analysis to develop models that can predict the flow pattern transition between the stratified and non-stratified flow. Taitel and Dukler (1976) applied the KH analysis to a gas-liquid horizontal channel flow where a finite wave exists on a flat liquid sheet. In order to simplify the analysis, the researchers neglected the surface effects and formulated the criterion for stable stratified flow as:

$$U_G - U_L \leq K_{TD}\sqrt{(\rho_L H_G + \rho_G H_L)\left[\frac{\rho_L - \rho_G}{\rho_L \rho_G} g cos(\theta) \frac{A}{dA_L/dh_L}\right]} \qquad (2.39)$$

Where U_G, U_L, ρ_L, ρ_G, H_L, H_G, A, A_L, h_L, θ are the gas velocity, liquid velocity, liquid density, gas density, liquid holdup, void fraction, cross-sectional area of the pipe, area of the pipe cross-section occupied by the liquid, the height of the liquid from the bottom of the pipe, and pipe inclination respectively. The term K_{TD} was added to account for the finite waves in the analysis and also according to Barnea (1990), the term equally accounts for the viscous effects especially at relatively low viscosities.

$$K_{TD} = (1 - \frac{h_L}{D}) \qquad (2.40)$$

where D is the pipe diameter.

Barnea (1990) attempted to study the effect of viscosity on the stability of stratified gas-liquid flow across different pipe inclinations to account for the viscous effect which was lacking in the criterion developed by Taitel and Dukler (1976). Based on the result of the stability analysis, the following stability criterion was given:

$$\left(\frac{e}{2b} - a\right)^2 + \frac{\rho_L \rho_G}{\rho^2 H_G H_L}(U_G - U_L)^2 - \frac{\rho_L - \rho_G}{\rho} g\cos(\theta)\frac{A}{dA_L/dh_L} < 0 \qquad (2.41)$$

The descriptions of all the variables are the same with the ones in equation (2.32) except for the following:

$\frac{e}{2b} = C_v$ is called the critical wave velocity at the inception of instability for viscous flow and is given as:

$$C_v = \frac{e}{2b} = \frac{\left(\frac{\partial \tau_i}{\partial H_L} - \frac{\partial \tau_{iL}}{\partial H_L}\right)_{U_{LS},U_{GS}}}{\left(\frac{\partial \tau_i}{\partial U_{GS}} - \frac{\partial \tau_{iL}}{\partial U_{GS}}\right)_{U_{LS},H_L} - \left(\frac{\partial \tau_i}{\partial U_{LS}} - \frac{\partial \tau_{iL}}{\partial U_{LS}}\right)_{U_{GS},H_L}} \qquad (2.42)$$

$\tau_i, \tau_{iL}, U_{GS}, U_{LS}$ represents the shear stress provided by the gas phase, interfacial shear stress needed for a steady state flow for any given U_G, U_L and R_L, gas superficial velocity and liquid superficial velocity respectively.

C_{iv} = a is called the critical wave velocity at the inception of instability for an inviscid flow where the shear stresses are neglected.

$$C_{iv} = a = \frac{\rho_L U_L H_G + \rho_G U_G H_L}{\rho_L H_G + \rho_G H_L} \qquad (2.43)$$

On putting the expression for C_{iv} and C_v into equation (34), the stability criterion now becomes:

$$(C_v - C_{iv})^2 + \frac{\rho_L \rho_G}{\rho^2 H_G H_L}(U_G - U_L)^2 - \frac{\rho_L - \rho_G}{\rho} g\cos(\theta)\frac{A}{dA_L/dh_L} < 0 \qquad (2.44)$$

While investigating the effect of viscosity on the stability of the stratified flow Barnea (1990) made an interesting observation where she said that the result of using equation (2.37) which is a VKH analysis compares well with the Taitel and Dukler (1976) model (equation 2.32) which is IKH analysis at low liquid viscosities. However, as the liquid viscosity increases, the Taitel and Dukler (1976) model under-predicts the experimental result which means that at higher liquid viscosity, using the Taitel and Dukler (1976) model will give incorrect prediction but for viscosities up to 100cP, the predictions are valid (Barnea 1990).

The stratified to non-stratified transition models proposed by Taitel and Dukler (1976), Barnea (1990) and other researchers predicts the transition of the stratified flow pattern to other bounding flow patterns to fall within the marginal stability boundary. But according to Brauner and Moalem (1990), such transition from stratified to non-stratified flow does not always occur along the marginal stability boundary but across a buffer zone which is defined when a combined condition for stability and reality of characteristics are considered. In an attempt to establish the entire stratified to non-stratified transitional boundaries, Brauner and Moalem (1990) formulated the governing equations using one-dimensional two-fluid model where continuity and momentum equations were written for each phase and linearized around the equilibrium positions. In order to obtain the condition for stability, the linearized governing equations are perturbed using the temporal stability formulation and the dispersion equation was obtained that relates the real wave number, k to the complex wave velocity, C

$$C = \frac{\omega}{k} \tag{2.45}$$

The solution of the dispersion equation in terms of the wave speed had both the real and imaginary components. On equating the imaginary part to zero, the so-called neutral stability conditions are obtained which gives a neutral stable wave number k_n and the corresponding wave speed C_{rn}. The Zero Neutral Stability line is obtained for all possible combinations of the

superficial velocities of the phases for which k_n approaches zero. This boundary line confines all possible smooth stratified flows. In order to test for reality of characteristic roots, the real part of the solution of the dispersion equation must be set to be greater than or equal to zero where the characteristic wave number k_{rc} is found. The Zero Real Characteristic (ZRC) boundary is obtained while searching for all the various combinations of superficial velocities of the phases which yield real characteristic roots for which $k_{rc} = 0$. Beyond the ZRC boundary, other flow regimes aside the stratified wavy exists. Therefore, the ZNS boundary delineates the transition from smooth stratified flow to stratified wavy flow while the ZRC boundary delineates the transition from stratified wavy to other flow patterns. The buffer zone is positioned in between the ZNS and ZRC boundaries and it includes the stratified flows with the existence of the interfacial waves. Suffice to say that the details of the rigorous mathematical formulations involve in developing these stability conditions can be found in Brauner and Moalem (1990).

Trallero (1995) carried out detailed modeling of the flow pattern transition between the stratified to non-stratified flow by employing similar procedure to what Barnea (1990) used. The classic Kelvin Helmholtz (K-H) analysis was applied to determine the stability of the interface which includes the viscous K-H (VKH) analysis that accounts for the shear stresses and the inviscid K-H (IKH) analysis which neglects the shear stresses. In a bid to improve the prediction of stratified/non-stratified transition, the researcher used a more rigorous two-fluid model which includes the interfacial tension between the phases and a closure relationship was developed for the interfacial stress that incorporates the sheltering effects which is a source of additional destabilizing force along the interface. The viscous stability criterion as formulated by the researcher can be obtained as:

$$(C_v - C_{iv})^2 + \frac{\rho_w \rho_o}{\rho^2 H_w H_o}(U_w - U_o)^2 - \frac{\rho_w - \rho_o}{\rho}\frac{g\cos(\theta)A}{S_i} - \frac{\sigma A}{\rho S_i}k^2 + \frac{\rho_{f(U_w - U_o)^2}C_s A}{\rho}\left(\frac{1}{A_w} - \frac{1}{A_o}\right) < 0$$

(2.46)

The whole of equation (2.39) represents the Viscous Kelvin-Helmholtz (VKH) analysis which can predict the stratified flow (ST) pattern whereas neglecting the first term (viscous term), the equation represents the Inviscid Kelvin-Helmholtz (IKH) analysis which can predict the stratified flow with mixing at the interface (ST&MI). The last two terms represents the interfacial tension term and sheltering effect term respectively. On comparing the stability criteria proposed by Brauner and Moalem (1992b,c), the researcher concluded that the ZNS/ZRC criteria are equivalent to the VKH/IKH criteria when the interfacial tension equals zero ($\sigma = 0$). The model proposed by Trallero (1995) performed remarkably well when compared with the experimental results, but on evaluating the model using some selected sets of published data (Russell et al., 1959;Guzhov et al., 1973; Oglesby 1979; Nadler and Mewes, 1995 and Cox, 1995), the performance of the model was also good though with some few points that were under-predicted.

Al-Wahaibi (2007) made an attempt to model the flow pattern transition from the stratified to non-stratified flow regime based on Kelvin-Helmholtz instability analysis. The researcher used the continuity equation and the balance of forces (which compete to deform or stabilize the interface) to develop the governing equations instead of the usual one dimensional two fluid model used by the previous researchers (Taitel and Dukler, 1976, Barnea, 1990, Brauner and Moalem, 1990,1992a,b and Trallero, 1995). In order for drops to form at the interface, the researcher stated that the wave amplitude must exceed a critical value and on that basis, model was eventually developed that could predict the critical wave amplitude for a given wavelength at which the waves in the stratified flow will become unstable.

$$\frac{1}{2}\rho_w \left[(U_w - C_v)^2 \; x \left(\left(\frac{A_w}{A_{w2}}\right)^2 - \left(\frac{A_w}{A_{w1}}\right)^2 \right) \right] +$$

$$\frac{1}{2}\rho_o \left[(U_o - C_v)^2 \; x \left(\left(\frac{A_o}{A_{o1}}\right)^2 - \left(\frac{A_o}{A_{o2}}\right)^2 \right) \right] - 2ga(\rho_w - \rho_o) - \frac{8\pi^2 a}{\lambda^2}\sigma \leq 0 \qquad (2.47)$$

Where ρ_w, ρ_o represents the water and oil density, A_{w1}, A_{o1} area occupied by the water and oil respectively at the crest side of the solitary wave, A_{w2}, A_{o2} area occupied by the water and oil respectively at the trough side of the solitary wave, C_v is the wave speed as defined by Wallis (1969), a is the wave amplitude, λ is the wavelength and σ is the interfacial tension. Please note that the details of the mathematical derivations of the stability criterion above can be found in Al-Wahaibi (2007).

For the different combinations of oil and water in situ velocities, different stability lines were drawn and a stable stratified flow is identified if the amplitude of all the waves fall below the stability line, whereas it is considered unstable if the amplitude of some waves fall above the stability line. On the assumption of a wave with a very long wavelength and very small amplitude, the equation (40) proposed by Al-Wahaibi (2007) gave similar predictions to the VKH analysis proposed by Trallero (1995). Also, using the experimental input parameters from Trallero (1995) to compare the predictions from the two models yielded similar results.

While developing the robust interfacial-tension-force model to be used in the stratified to non-stratified flow pattern transition, Rodriguez and Castro (2014) identified a new destabilizing term which is closely linked with the cross-sectional curvature of the interface. This destabilizing term was not included in the models developed by previous researchers (Taitel and Dukler, 1976, Barnea, 1990, Brauner and Moalem, 1990,1992a,b and Trallero, 1995) where they assumed a flat interface at the pipe cross-section. In modeling the pressure jump across the interface, Rodriguez and Castro (2014) used the two principal radii of curvature (the side view and the cross-sectional curvature radii) which can be seen below.

$$\frac{\partial(P_{io} - P_{iw})}{\partial x} = -\sigma \frac{\partial}{\partial x} \left\{ \frac{1}{h_w} \frac{\partial}{\partial h_w} \left[h_w \left(1 + \left\{ \frac{\partial h_w}{\partial x} \right\}^2 \right)^{-1/2} \right] \right\} \tag{2.48}$$

$$= -\sigma \frac{\partial}{\partial x} \left\{ \frac{\frac{\partial^2 h_w}{\partial x^2}}{\left[1 + \left(\frac{\partial h_w}{\partial x} \right)^2 \right]^{3/2}} - \frac{1}{h_w(x) \left[1 + \left(\frac{\partial h_w}{\partial x} \right)^2 \right]^{1/2}} \right\}$$

$$= -\sigma \frac{\partial}{\partial x} \left[\frac{1}{R_1(h_w)} - \frac{1}{R_2(h_w)} \right] \tag{2.49}$$

Where $R_1(h_w)$ and $R_2(h_w)$ represents the radius of curvature of the interface along the axial direction and the pipe cross-section respectively. The researcher asserts that the destabilizing action of the new interfacial tension term ($R_2(h_w)$) is strongly dependent on the cross-section curvature of the interface because the larger the cross-section curvature, the stronger its effect. This new interfacial tension term was included in the stability criterion proposed by the researcher and when tested against their experimental data, the prediction of the transition boundary between the stratified and non-stratified flow was good provided the stratified with mixing at the interface (ST&MI) flow pattern is included as part of the stratified flow. Similarly on testing the model using data from literature (Trallero, 1995; Alkaya, 2000; Brauner, 2001; Rodriguez and Oliemans, 2006; Mandhane, 2007), the prediction of the transition boundary was encouraging. The researcher also compared the performance of the newly proposed model with that of the IKH/VKH transition models proposed by Trallero (1995) and transition model of Brauner (2001) using the experimental data of Elseth (2001) and observed that at the region of low oil volume fraction, the new model and the IKH model had a better performance in predicting the stratified flow region of the flow map. However, at the region in the flow map where the superficial velocities are similar, the prediction of the new model and that of Brauner (2001) showed good result and are in close agreement with the experimental data of Elseth (2001).

2.11   Modeling pressure drop in liquid-liquid two-phase flow.

The pressure drop encountered in a liquid-liquid flow is strongly dependent on the flow regime. In order to develop a model that can be used to predict the pressure drop for a given input condition, the flow regime needs to known in the first place. For stratified flow patterns, the one-dimensional two-fluid model had been traditionally used to model the pressure drop since the flow are separately with a clearly defined interface while for the dispersed flow regimes, the homogeneous model is used.

2.11.1 The one-dimensional two fluid model.

The one-dimensional two-fluid model is used in the modeling of the pressure drop and determination of other hydrodynamic parameters such as the liquid holdup and in-situ velocities for a stratified flow where two different fluids flow together with a clearly defined interface between them. In applying the one-dimensional two-fluid model, separate continuity and momentum equations are written for each of the phase with some set of closure relations for the interfacial stress. Several researchers such as Taitel and Dukler, (1976), Brauner and Moalem, (1992b), Trallero (1995) and Al-Wahaibi et al., (2007) have applied the one-dimensional two-fluid model in the determination of pressure drop and other hydrodynamic parameters as mentioned above for the liquid-liquid system.

For a fully developed steady state flow and the fluids are assumed to be incompressible, isothermal and with a flat interface along the pipe cross-section, the integral form of the one-dimensional two-fluid model for the oil and water phase are given below:

$$-A_o \left(\frac{dp}{dz}\right)_o - \tau_o S_o \pm \tau_i S_i + \rho_o A_o \sin\alpha = 0 \qquad (2.50)$$

$$-A_w \left(\frac{dp}{dz}\right)_w - \tau_w S_w \pm \tau_i S_i + \rho_w A_w \sin\alpha = 0 \qquad (2.51)$$

The subscripts o and w denotes the oil and water phase while A_o, A_w, S_o, S_w, S_i, τ_o, τ_w, ρ_o, ρ_w, α denotes the cross-sectional area occupied by the oil phase, cross-sectional area occupied by the water phase, wetted perimeter for the oil phase, wetted perimeter for the water phase, length of the interface, shear stress of the oil phase, shear stress of the water phase, density of the oil phase, density of the water phase and pipe inclination respectively. Since the pipe geometry is of large diameter (127mm) pipe, the effect of surface tension on the curvature of the interface can be assumed to be negligible, therefore the interface can reasonably be assumed to be flat.

The oil, water and interfacial shear stresses (τ_o, τ_w, τ_i) can be expressed in terms of their corresponding friction factors (f_o, f_w, f_i) respectively.

$$\tau_o = f_o \frac{\rho_o U_o^2}{2} ; f_o = mRe_o^{-n} \tag{2.52}$$

Where Re is the Reynolds Number and can be represented as

$$Re_o = \frac{\rho_o U_o D_o}{\mu_o}$$

$$\tau_w = f_w \frac{\rho_w U_w^2}{2} ; f_w = mRe_w^{-n} \tag{2.53}$$

$$Re_w = \frac{\rho_w U_w D_w}{\mu_w}$$

$$\tau_i = f_i \frac{\rho_i (U_o - U_w)|U_o - U_w|}{2} ; f_i = mRe_i^{-n} = m\left(\left(\frac{S_i}{\pi}\right) \frac{U_i \rho_i}{\mu_i} \right)^{-n} \tag{2.54}$$

Where $U_i, \rho_i, \mu_i = \begin{cases} U_w, \rho_w, \mu_w, & if\ U_w > U_o \\ U_o, \rho_o, \mu_o, & if\ U_w < U_o \end{cases}$ \hfill (2.55)

The values of m and n are equal to 0.046 and 0.2 for turbulent flow and 16 and 1.0 for laminar flow respectively (Edomwonyi-Otu and Angeli, 2015).

In computing the Reynolds number for both the oil and water phase, hydraulic diameter is used which is dependent on in-situ velocity of the phases.

$$\text{For } U_w < U_o, D_o = \frac{4A_o}{(S_o + S_i)}, D_w = \frac{4A_w}{S_w} \tag{2.56}$$

For $U_w > U_o$, $D_w = \dfrac{4A_w}{(S_w + S_i)}$, $D_o = \dfrac{4A_o}{S_o}$ $\qquad\qquad$ (2.57)

For $U_w \approx U_o$, $D_o = \dfrac{4A_o}{S_o}$, $D_w = \dfrac{4A_w}{S_w}$ $\qquad\qquad$ (2.58)

On substituting equation (45) and (46) into equation (43) or (44) and on eliminating the $\tau_i S_i$ term, the expression for the pressure drop can be obtained as:

$$\left(\frac{dp}{dz}\right) = \frac{-\tau_w S_w - \tau_o S_o + \rho_o A_o \sin\alpha}{A} \qquad\qquad (2.59)$$

2.11.1.1 Geometric parameters used in the one-dimensional two-fluid model
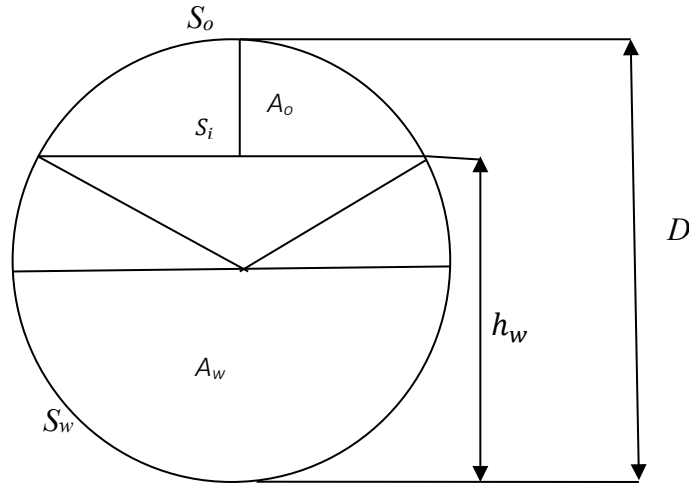
Figure 2.20: Schematic diagram of the pipe cross-section showing the flat interface and other geometrical parameters (Adapted from Al-Wahaibi et al (2011))

From figure 2.20 above, the relations for the geometric parameters characterizing the cross-section of a stratified flow with a flat interface can be given below without showing the details of the mathematical deductions.

Interfacial length (S_i) = $D * \left[1 - \left(2\frac{h_w}{D} - 1\right)^2\right]^{0.5}$

Wetted perimeter for the oil phase (S_o) = $D * Cos^{-1}\left(2\frac{h_w}{D} - 1\right)$ $\qquad$ (2.60a)

Wetted perimeter for the water phase (S_w) = $\pi D - S_o$

Cross-sectional area of the pipe (A) = $\dfrac{\pi D^2}{4}$

Cross-sectional area occupied by the oil phase (A_o) = $\dfrac{\pi}{4} * \left(So - Si * \left(2\frac{h_w}{D} - 1\right)\right)$

Cross-sectional area occupied by the water phase (A_w) = $A - A_o$

65

Oil holdup $(H_o) = \frac{A_o}{A}$

Water holdup $(H_w) = \frac{A_w}{A}$

(2.53b)

In-situ oil velocity $= \frac{U_{so}}{H_o}$

In-situ water velocity $= \frac{U_{sw}}{H_w}$

2.11.2 Homogeneous model

The homogeneous model is used for the prediction of pressure drop in dispersed flow regime where the dispersed and the continuous phases are assumed to be uniformly mixed. The model equally assumed that the two fluids flow together as a pseudofluid with a negligible slip velocity between the phases. The relation for the pressure drop using this model can be given as:

$$\frac{dP}{dx} = -\frac{1}{2}\frac{f_m \rho_m}{d} U_m^2 - \rho_m g \sin(\theta)$$

(2.54)

Where $\frac{dP}{dx}$, f_m, ρ_m, d, U_m, g, θ represents the pressure drop per unit length, friction factor for the mixture, mixture density, pipe diameter, mixture velocity, acceleration due to gravity and pipe inclination respectively.

$$\left.\begin{array}{l} U_m = U_w + U_o \\[6pt] \rho_m = \alpha_w \rho_w + \alpha_o \rho_o \end{array}\right\}$$

$$\alpha_w = \frac{U_{sw}}{U_m} \text{ (water holdup)}$$

(2.61)

$$\alpha_o = \frac{U_{so}}{U_m} \text{ (oil holdup)}$$

$$\alpha_w + \alpha_o = 1$$

For laminar flow, the friction factor can be obtained as:

$$f_m = \frac{16}{Re}$$

For Turbulent flow, the friction factor can be obtained as:

$$f_m = \frac{0.079}{Re^{0.25}}$$

$$Re = \frac{\rho_m u_m D}{\mu_m}$$

$$\mu_m = \mu_o \, (O.C) + \ \mu_w (W.C)$$

Where μ_m = Viscosity of the oil-water mixture

μ_o = Viscosity of oil

μ_w = Viscosity of water

O.C = Oil cut which corresponds to the inlet fraction of the oil phase

W.C = Water cut which corresponds to the inlet fraction of the water phase

2.12 Summary

This chapter gave a brief description of the different studies and applications of liquid-liquid flow system and also gave a historical perspective on the objective that undergirded such studies which was to enhance the transportation of heavy crude oil with minimal pressure drop requirement. Basic concepts that describe the physics of the flow for an oil-water mixture across a cylindrical pipe was also covered. A summarized description of all the flow patterns (as provided by Trallero, 1995) and flow pattern maps by different researchers across a horizontal and upwardly inclined pipes were also provided in this chapter. Different measuring techniques for the liquid holdup spanning across both the Intrusive and Non-intrusive methods were adequately discussed and a particular attention was paid on the Conductance method of measuring liquid holdup which was the method used in the current research (Flushed mounted ring conductance probe and Double Parallel Wire Probe). A detailed study on the interfacial characteristics in a gas-liquid flow system was carried out which served as a basis for

undertaking similar studies in the liquid-liquid flow systems because the basic principles are the same albeit the behaviour of the two systems are not the same due to differences in the physical properties of the phases. Studies on interfacial wave characteristics in a liquid-liquid flow system were carried out where relationships between the different wave characteristics, inlet flow conditions and also relevant dimensionless numbers were established. Consequently, the stability analysis of the interfacial waves in an oil-water two-phase flow system based on the Kelvin-Helmholtz stability criterion as given by different researchers was also carried out. Finally, a brief description of the different pressure drop models was also provided.

CHAPTER THREE
EXPERIMENTAL METHOD AND INSTRUMENT

3.0   INTRODUCTION

This chapter provides a detailed description of the liquid-liquid flow rig used in carrying out the experimental campaigns. It begins with the description and illustration of all the components contained in the experimental rig, followed by the description of the fluid properties, instrumentation and controls including their working principles, the experimental design, description of the data acquisition system and finally the description of the image analysis. Also included in this chapter are the detailed description of the procedure used in carryout each run of the experiment, the calibration methods for the Conductance Probes (CPs) and the Double Parallel Wire Probe (DPWP) and the detailed description of the method used in obtaining the interfacial wave amplitude, wavelength and wave speed from the flow images and videos.

3.1   DESCRIPTION OF THE LIQUID-LIQUID FLOW FACILITY

The liquid-liquid experimental rig used in this research is situated in the L3 main laboratory building of the Department of Chemical and Environmental Engineering, University of Nottingham and it was designed for the hydrodynamic study of the simultaneous flow of oil and water in both the horizontal and slightly inclined ($\pm 1^o, \pm 2^o, \pm 3^o, \pm 4^o, \pm 5^o$) directions. The major components that make up the rig are the test section, fluid inlet device, fluid storage tanks, pumps, instrumentations and control systems as shown in figure 3.1.

In carrying out the experiment, the flow of the silicone oil and water through the rig starts from the tank farm outside the laboratory building where the fluid storage tanks and the pumps are located. An E-line Dresser centrifugal pump with capacity of 120 m^3/h was used to pump the silicone oil from the silicone oil tanks while an Ingersoll-Dresser centrifugal pump with capacity of 36 m^3/h was used to pump water from the water storage tank. Both the silicone oil

and water flow pass through series of gate valves, by-pass valves and flow meters for flow

control and metering purposes before getting to the fluid inlet device where both fluids contact

each other.
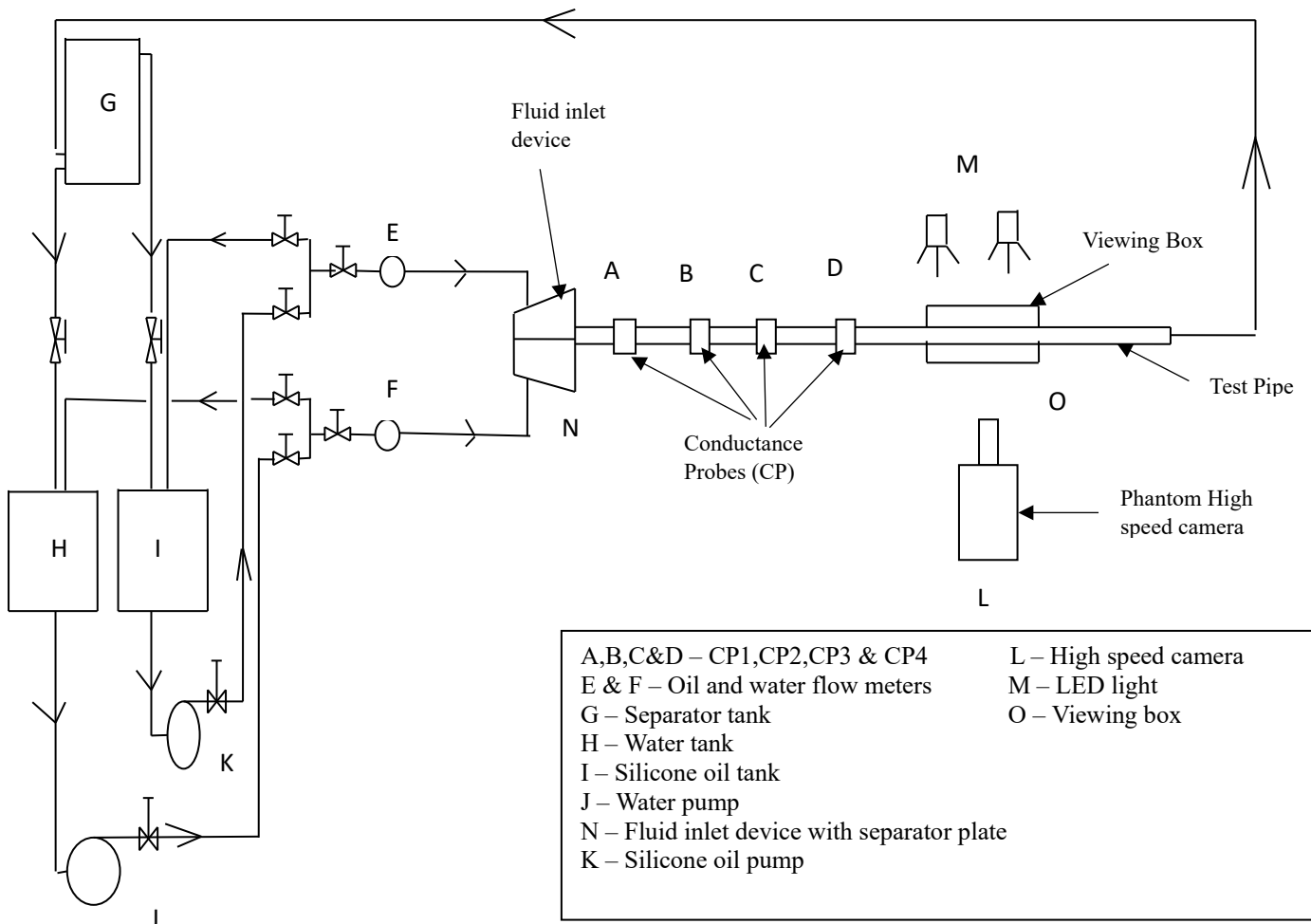
Figure 3.1: The schematic diagram of the liquid-liquid experimental rig showing the different components

From the fluid inlet device, the silicone oil and water mixture flow through the test section

where four (4) sets of conductance probes (CP) positioned at 9.6D (CP1), 19.2D (CP2), 28.8D

(CP3) and 56.6D (CP4) from the fluid inlet device (D is the internal diameter of the test pipe)

are used to measure the Oil Volume Fraction (OVF) and also the Double Parallel Wire Probe

(DPWP) used to measure the interfacial height. The viewing box filled with water was also

attached to the test section where the flow imaging was done using the high-speed camera. The importance of the viewing box filled with a refractive index matching fluid was to minimize image distortion due to the curvature of the pipe. The silicone oil/water mixture flow from the test section through a flexible hose and into the separator tank located in the tank farm where the silicone oil and water are separated. Silicone oil flows from the top of the separator tank into its storage tank while water flows by gravity to its storage tank.

The detail description of the various component in the liquid-liquid rig are given in the following sections.

3.1.1   THE TEST SECTION

The test section is a part of the liquid-liquid experimental rig where all the experimental data from the different probes and sensors are collected. It has an overall length of 7.7 m comprising of four (4) sections of transparent acrylic pipe, 0.127 m internal diameter (ID) and 1.3 m in length each and another section of transparent acrylic pipe with the same ID but 2.5 m in length.The pipe sections are connected through their flanges to the four (4) conductance probes (CPs) with a rubber gasket between each joint to prevent fluid leakage. The entire length of the test section including the measuring probes are mounted on a steel frame to provide support and also to permit the test section to be positioned at different inclinations $(\pm 1^o, \pm 2^o, \pm 3^o, \pm 4^o, \pm 5^o)$ with the help of the swivel joint at one end of the frame and a chain hoist at the other end. The transparent acrylic pipes allows the observation of the flow development through the pipes and equally permits the observation of the different flow patterns and their transition points. The viewing box measuring 60 cm x 30 cm x 30 cm made from an acrylic sheet and filled with water was also attached to the test section. Images of the flow were captured through the viewing box using the Phantom V.12 high speed camera for flow visualization, flow regime identification and interfacial wave analysis.
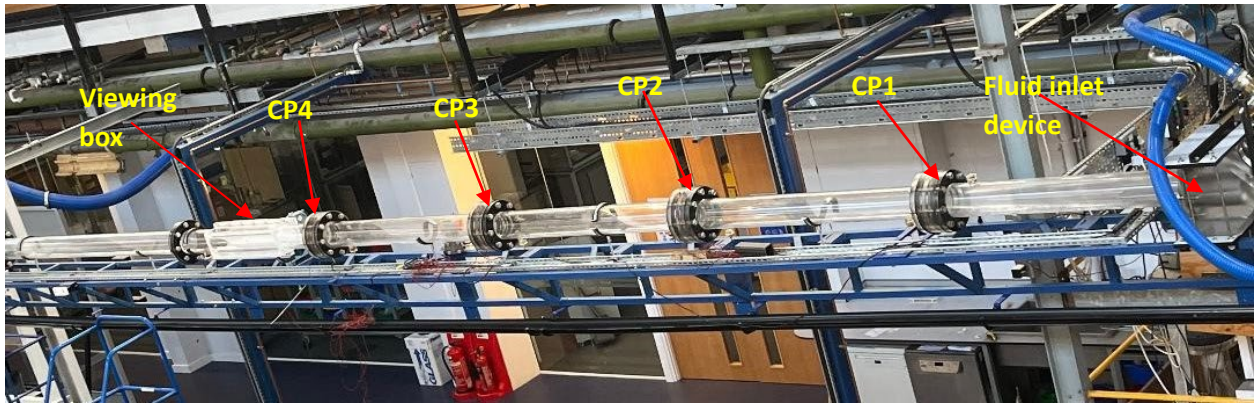
(a)

(b)

Figure 3.2: (a) Picture of the test section containing the conductance probes and the viewing box (b) Picture of the viewing box filled with water and a spirit level was used to check that the viewing box was placed horizontally.

3.1.2   FLUID INLET DEVICES

The oil and water pipes that convey the fluids from their respective storage tanks are connected using the flexible hoses to the fluid inlet device where both fluids contact each other and flow simultaneously into the test section. Two different types of fluid inlet devices were used in this research with different inlet flow configuration. One of the fluid inlet device was designed to minimize the mixing of the oil and water flow at the inlet so that flow stratification can be maintained as much as possible to allow the study of the interfacial waves. The fluid inlet

device was fabricated using clear acrylic block where the inlet holes of size 50.8 mm internal diameter (ID) for the oil (at the top) and water (at the bottom) were drilled in a slanted position at an angle of 90° between them and also an outlet hole of size 127 mm ID where the test section pipe is connected as seen in the Figure 3.3 below. A separator plate (0.45 m in length) was attached along the outlet of the fluid inlet device which also extends into the test section pipe to keep the flow separated and minimize droplets generation so that growth or decay of the interfacial waves can be reliably studied. The picture and engineering drawing of the fluid inlet device with the dimensions can be seen in Figures 3.3 and 3.4.
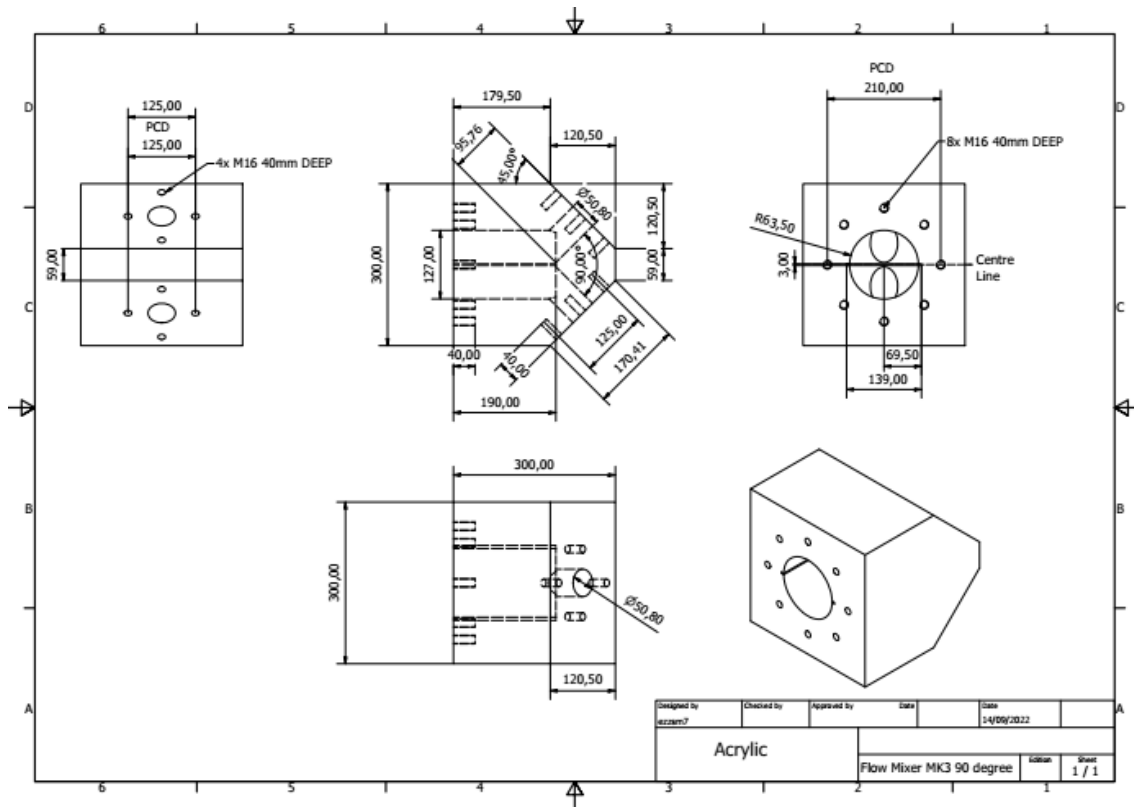
Figure 3.3: An engineering drawing of the fluid inlet device with relevant dimensions.
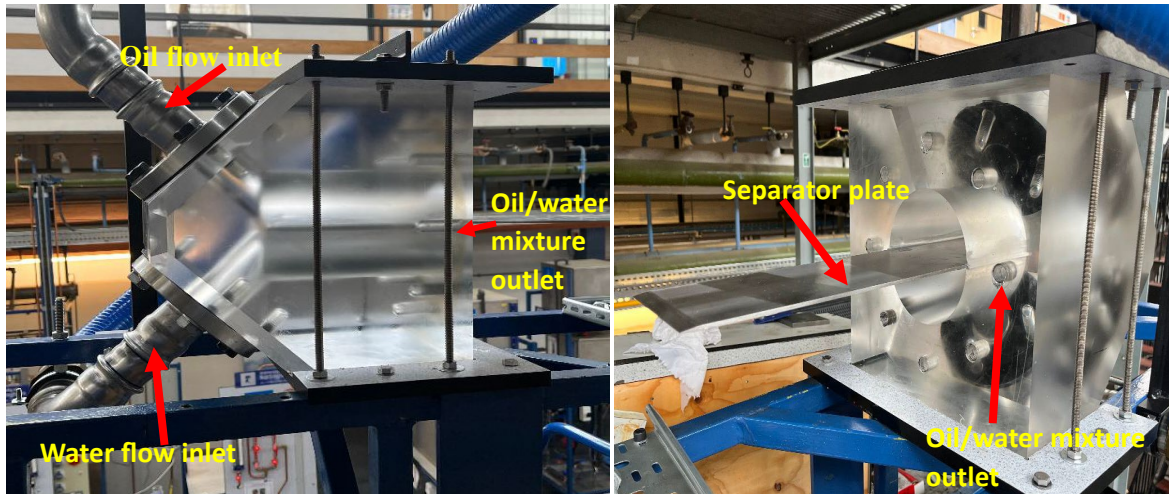
Figure 3.4a: Pictorial representation of the fluid inlet device and the separator plate

The second fluid inlet device used in the research is made from a perspex block where the silicone oil and water flow are connected to it in the horizontal plane and in the opposite direction. The size of the inlet holes are 50.8 mm ID while the size of the outlet hole from the is 76.2 mm ID. This fluid inlet device equally have a separator plate but the plate did not flush with the internal wall of the outlet hole, therefore the silicone oil and water flow experience some degree of mixing which generates some droplets that flows through the test section.
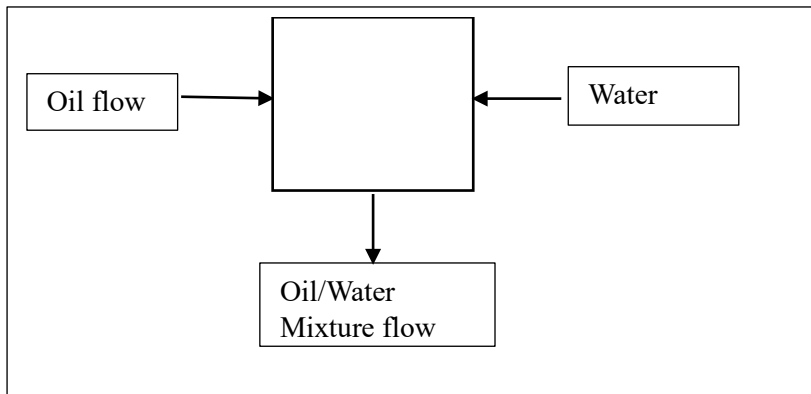
(a)
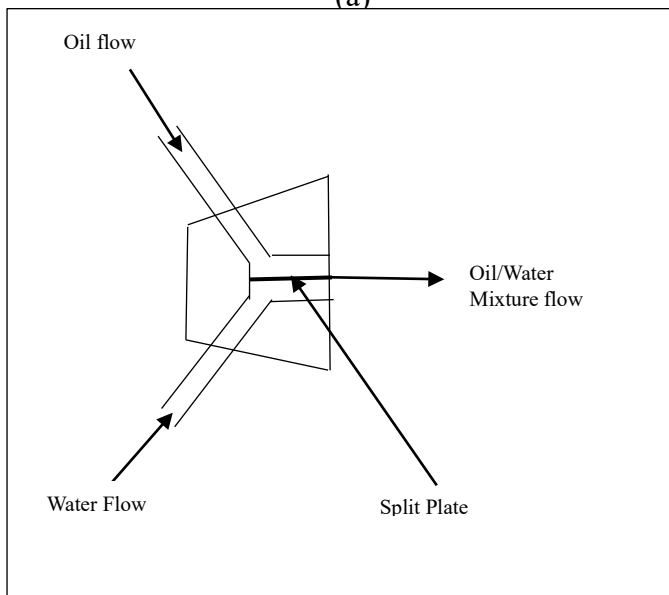
(b)
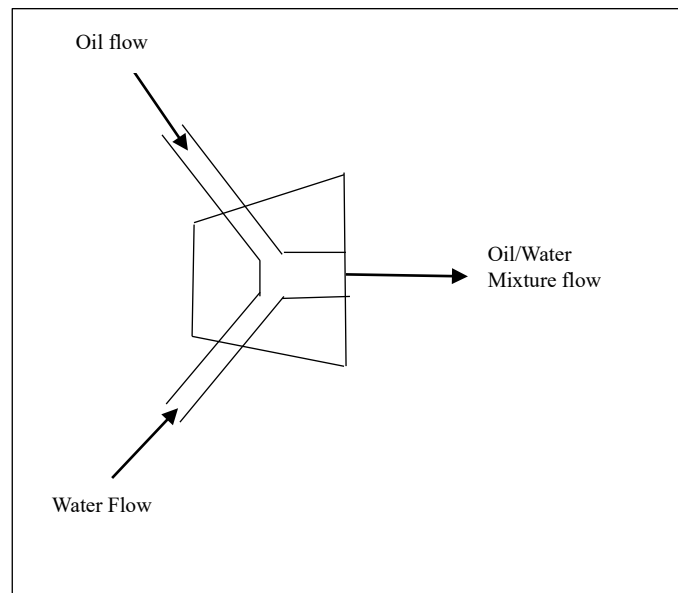
(c)

Figure 3.4b: Schematic diagrams of the fluid inlet devices (a) T- type fluid inlet device (b) Y-type fluid inlet device with split (separator) plate (c) Y- type fluid inlet device with a split (separator) plate

3.1.3 FLUID STORAGE TANKS

The liquid-liquid rig requires large volume of both the silicone oil and water to run effectively, therefore a tank farm was built outside the laboratory building where the storage tanks are kept. There are three (3) different types of the storage tanks; the separator tank, the oil tank and finally the water tank.

The separator tank is a vertical cylindrical vessel made from stainless steel where the oil and water mixture from the liquid-liquid rig are collected and separated. The diameter and height of the vessel are equal in size with the dimension of 2.438 m. To enhance the separation of the silicone oil and water, the separator tank has a 'knitmesh' coalescer cartridges containing very fine fibre glass wools that facilitate the coalescing of tiny oil droplets.The catridges has a dimension of ∅0.15 x 10 mm x 1 m long and manufactured by Knitmesh Ltd.

The silicone oil is stored in two equal size horizontal cylindrical vessels made from stainless steel while the water is stored in one horizontal cylindrical vessel with similar size with that of the silicone oil tank and the tanks have a dimension of ∅1.828 x 1.854 m . Both the silicone oil and water tanks are located within the tank farm outside the laboratory building. The separated silicone oil from the separator tank flows through a pipe connected at the top of the separator tank into the silicone oil tanks while the water at the bottom of the separator tank flow due to hydrostatic pressure into the water tank through a pipe connected at the bottom of the separator tank.

Figure 3.5: Fluid storage tanks showing the separator tank, oil tanks and the water tank

3.1.4   CONTROL SYSTEM

In order to safely operate the liquid-liquid rig, a control system is put in place which includes the pump switches and adjustable butterfly valves and they are all manually operated. Two sets of pump switches are used situated at the tank farm close to the pumps and also at the work space in the laboratory so that the pumps can quickly be switched off to prevent the pumps from running dry in the event the fluid level in the tanks becoming very low or in some cases to prevent the tanks from overflowing from the top. The adjustable butterfly valves are mounted at the inlet and outlets to the fluid storage tanks and also along the flowlines before the test section. The butterfly valve at the bottom of the separator tank plays a very important role because it can be manually manipulated to adjust the water level in the tank so that silicone oil can flow into the silicone oil tanks. Also, the adjustable butterfly valves located close to the flow meters can be used to adjust the flow rate of both the silicone oil and water to the desired value.

Figure 3.6: Components of the control system which includes the pump switches and the gate valves.

3.1.5 FLUID PROPERTIES

The fluids used in this research are silicone oil and tap water. Silicone oil was selected because of the need to study oil whose physical properties are comparable to the hydrocarbon commonly produced in the oil and gas fields. Also, silicone oil is non-toxic and its characteristic dielectric properties have been utilized to discriminate it from other fluids such as water or air using conductance or impedance probes. The table below gives a summary of the physical properties of the fluids used in this research.

Table 3.1: Physical properties of the fluids at 21°C

Fluid	Silicone Oil	Tap water
Density, ρ (kg/m³)	918	998
Viscosity, μ (kg/m.s or Pa.s)	0.0047	0.0010
Interfacial tension, σ (N/m)	0.0447	

The densities of both the silicone oil and water were obtained using the volumetric method (density bottle) while their viscosities were measured using the Ostwald viscometer type C.

3.2   EXPERIMENTAL TEST MATRIX

The methodology used in this experiment is to keep the mixture velocity (U_m) constant while varying the water cut (WC) for a given pipe inclination. In varying the WC, the water superficial velocity (U_{sw}) will also change but for constant U_m, the interfacial height will change alongside other hydrodynamic parameters such as the Oil Volume Fraction (OVF), water holdup, phase velocities and the flow regimes. The mixture velocities used are 0.08 m/s, 0.16 m/s, 0.24 m/s, 0.32 m/s and 0.4 m/s while the range of the water cut (WC) used are 10% - 70% with an interval of 10%. Only upward pipe inclinations were tested in this experiment i.e. $+1^o, +2^o, +3^o, +4^o, +5^o$. Attempts were made to test the flow both in the downward and horizontal positions but the fidelity of the measurement of the Oil Volume Fraction (OVF) cannot be guaranteed because the test pipe was not completely filled with the test fluids. The range of the U_m and WC selected were limited by the maximum flow rates obtained from both the water and silicone oil pumps. The summary of the experimental test matrix can be seen in Table 3.2.

3.3   INSTRUMENTATION

Various instruments were used to measure flow parameters such as flow rates, pressure drop, fluid temperature, interfacial height of the water and finally the Oil Volume Fraction (OVF). The descriptions of these instruments and their operating principles are given in the following sections.

3.3.1 Differential pressure transducer

A microprocessor-based smart pressure transducer manufactured by Kobold Instruments Inc, model PAD-DEE5S2NS00 was used in this research. It has a digital display that can show the differential pressure on the screen. The factory-set pressure range for calibration is 0 – 186.5 kPa which corresponds to the 4 mA and 20 mA current respectively. However, since the maximum differential pressure to be experienced in the system based on the prediction of the Two-fluid model is about 5 kPa, the differential pressure had to be re-range to give an Upper Range Value

Table 3.2: Experimental Test Matrix

U_m (m/s)	WC (%)	U_{sw} (m/s)	U_{so}(m/s)
0.08	10	0.008	0.072
	20	0.016	0.064
	30	0.024	0.056
	40	0.032	0.048
	50	0.04	0.04
	60	0.048	0.032
0.16	10	0.016	0.144
	20	0.032	0.128
	30	0.048	0.112
	40	0.064	0.096
	50	0.08	0.08
	60	0.096	0.064
	70	0.112	0.048
0.24	10	0.024	0.216
	20	0.048	0.192
	30	0.072	0.168
	40	0.096	0.144
	50	0.12	0.12
	60	0.144	0.096
	70	0.168	0.072
0.32	10	0.032	0.288
	20	0.064	0.256
	30	0.096	0.224
	40	0.128	0.192
	50	0.16	0.16
	60	0.192	0.128
	70	0.224	0.096
0.4	10	0.04	0.36
	20	0.08	0.32
	30	0.12	0.28
	40	0.16	0.24
	50	0.2	0.2
	60	0.24	0.16
	70	0.28	0.12

(URV) of 5 kPa which corresponds to the 20 mA so that the sensitivity of the differential pressure transducer can be improved. The accuracy of the transducer is $\pm 0.075\%$ of calibrated span. In order to connect the differential pressure transducer to NI 9203 module for data acquisition through the LabVIEW interface, a loop connection was made where the positive terminal of the transducer cable was connected to the positive terminal of the power source while the negative terminal of the transducer cable was connected to the desired channel in the NI 9203 module and finally the ground in the NI 9203 module was connected to the negative terminal of the power source.

The differential pressure transducer was calibrated using a column of water connected to the high pressure port. The pressure was calculated based on the height of the water column and the current corresponding to each height of water column was recorded. A plot of the pressure versus the current was made and a linear curve was obtained which gives the calibration equation as can be seen in figure 3.7.
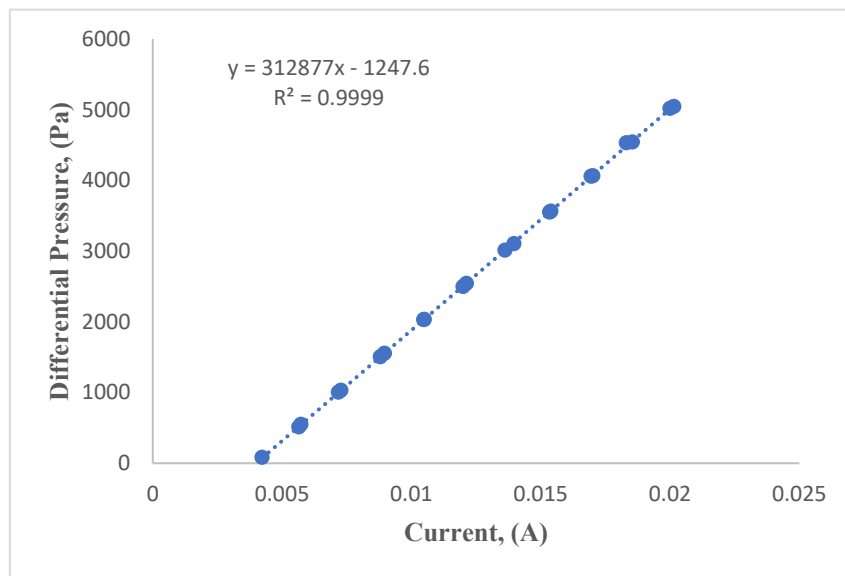
Figure 3.7: Calibration curve for the differential pressure transducer with accuracy of $\pm 0.075\%$ of calibrated span

Figure 3.8: The Smart PAD differential pressure transducer.

In Figure 3.7, it will be noted that a linear relationship between the differential pressure and the current output exist and the value of the current remains 4 mA at 0 Pa and 20 mA at 5045 Pa.

3.3.2 FLOWMETERS

Electromagnetic flowmeter was used to measure the flowrate of water at the inlet. The flowmeter was manufactured by Meatest with a model number M920 and accuracy of ±0.25% of reading value. It is an inductive type of flowmeter that was designed to measure and record both instantaneous and total flow of a conductive fluid flowing through its sensor based on the principle of Faraday's law of electromagnetic induction. The principle states that the magnitude of the voltage induced across the conductor when a conductive fluid passes through the magnetic field is directly proportional to the velocity of the conductor, length of the conductor and the strength of the magnetic field.

$$V = K \text{ (B.L.u)} \hspace{4cm} (3.1)$$

Where V = voltage (V)

B = Magnetic flux density (T)

L = Length = Diameter of the pipe (m)

u = Velocity (m/s)

The pictorial representation of the electromagnetic flowmeter can be seen in Figure 3.9.

Figure 3.9: Electromagnetic flowmeter for water flow rate measurement

The silicone oil flow rate was measured with a paddle wheel flowmeter, model TKM-50-RS-PVC and manufactured by Truflo. The flowmeter have an accuracy of ±1% of full scale (F.S) at 20°C. The maximum and minimum flow velocity across the flowmeter is 10 m/s and 0.3 m/s respectively with an operating pressure of 150 psi. This type of flowmeter uses the principle of mechanical displacement to measure the flow rate of silicone oil. It has several components which includes the paddle wheel with multiple blades, sensors, controllers, digital display and

pipe fittings. The flow of the silicone oil through the pipe causes the paddle wheel to rotate. The rotation of the paddle wheel is directly proportional to the velocity of the silicone oil and since the cross-sectional area of the pipe is constant, the flow rate of the silicone oil can be measured. The pictorial representation of the Paddle wheel flowmeter can be seen in Figure 3.10.

Figure 3.10: A Paddle wheel flowmeter for silicone oil flow rate measurement

3.3.3 MEASUREMENT OF OIL VOLUME FRACTION (OVF)

For a given set of flow condition where the mixture velocity (U_m) is kept constant while varying the Water-Cut (WC), the OVF is measured using the four (4) set of Conductance Probes (CP) positioned at 9.6D (CP1), 19.2D (CP2), 28.8D (CP3) and 56.6D (CP4) from the fluid inlet device once the flow is steady. A pictorial representation of the conductance probe showing the chromium plated brass conductors that facilitates the measurement of the electrical properties of the fluid mixture can be seen in Figure 3.11.The principle that governs the operation of the Conductance Probes was based on the differences in the electrical properties of the oil/water

mixture. Since water is a good conductor of electricity while silicone oil is resistive to the flow of electrical current, therefore a given oil/water mixture will present a unique resistance to the flow of electrical current which will be proportional to the composition of the mixture. In using this technique, a cross-sectional averaged OVF can be obtained given the relationship between the electrical impedance and the distribution of the phases as used by several researchers including Coney (1973), Andreussi et al., (1988),Tsochtzidis et al., (1992), and Fossa (1998).

3.3.3.1 ELECTRONIC CIRCUITRY FOR THE CONDUCTANCE PROBES

The fundamental design of the electronic circuits are based on that of (Fossa, 1998) which had three major segments including the Wheatstone bridge, operational amplifier and the full wave rectifier. The circuit diagram is given in Figure 3.12. From the circuit diagram, one may notice that the conductance probes are connected to the Wheatstone bridge which gives a precise measurement of the impedance associated with each combination of the oil/water mixture, while the operational amplifier helps to amplify weak electrical signal and finally the full wave rectifier helps in converting the alternating current (AC) into direct current (DC).
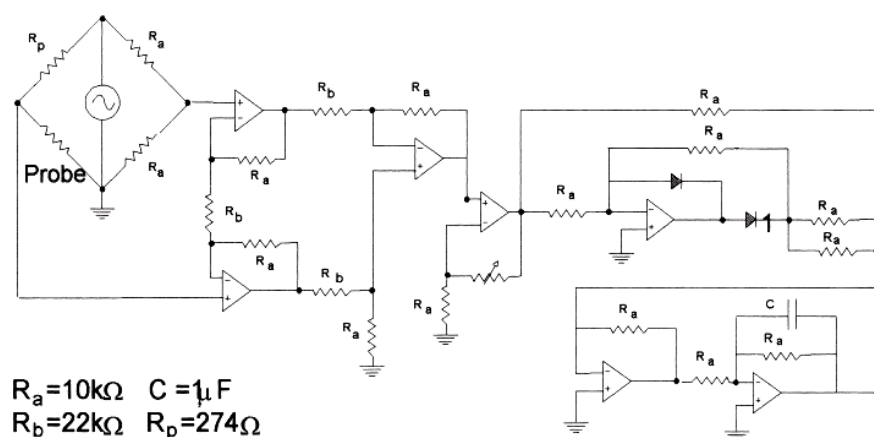
Figure 3.11: Original electronic circuit (Fossa,1998)

3.3.3.2 CALIBRATION OF THE CONDUCTANCE PROBES

The conductance probes were calibrated in order to establish a mathematical relationship between accurately known values of the Oil Volume Fraction (OVF) and the dimensionless conductance. On the basis of this mathematical relationship, a LabVIEW program was built which interfaces between the National Instrument (NI) modules and the conductance probes (CP) for data acquisition.

In determining the OVF, careful measurement of the water and silicone oil volumes were made using the 2000 ml measuring cylinder with an uncertainty of ±10 ml while the voltage measurements were made using the National Instrument Data Acquisition System (NI CDAQ-9178 series). The NI CDAQ-9178 series comprise of several modules one of which is the NI 9205 containing 32 channels capable of measuring voltage within the range of ±200 mV to ±10V. Meanwhile, there are factors that could affect the accuracy of the voltage measurement from the electronic box such as electromagnetic interference from the fluorescent lighting, uneven surface level where the test chamber was placed and the presence of air in the test chamber. In order to minimise the effect of these factors on the accuracy of the result and also to improve the fidelity of the measurement, several steps were taken such as placing the test chamber in a Faraday's cage while connecting it to a metal frame for the purpose of nullifying the effect of electromagnetic interferences (Hernandez-Perez, 2008), using a spirit level to ensure that the test chamber was placed horizontally on the test bench and by ensuring that the test chamber was completely filled with liquid using the tiny hole on one end of the chamber in order to expel the air within the chamber.

3.3.3.3 OFFLINE CONDUCTANCE PROBES CALIBRATION PROCEDURES

In calibrating the conductance probes, the first step is to do an offline calibration where the probes are calibrated using a test chamber and the Data Acquisition system (DAQ). The offline

calibration of the conductance probes was necessary to ensure that the voltage reading to be obtained while running the experiment is as close as possible to the true value. The test assembly comprises of the test chamber containing the fluid mixtures, the conductance probes, the end plates and the electronic circuit box. The calibration procedure was based on the work of Fossa (1998), who was one of the pioneers in using a conductance probe to measure hydrodynamic properties of a fluid.

The test chamber has a total volume of 4,945 litres where the different combinations of silicone oil and water are placed. The conductance probe was connected to one end of the test assembly and filled with 100% water, sealed with an end plate at both sides, then placed horizontally on a test bench and level confirmed using the spirit level. The terminal of the conductance probe was connected to the electronic circuit box (containing the Wheatstone bridge, operational amplifier, band filtering circuit and analogue-to-digital converter), and the corresponding voltage was read and recorded by the LabVIEW program on the computer through the National Instrument (NI) DAQ modules. The same procedure was repeated for 90% water and 10% silicone oil and the ratio continue to vary until it is 100% silicone oil in the test assembly.

One of the components of the electronic box (Wheatstone bridge box) is the Wheatstone bridge containing four (4) resistors i.e. one variable resistor R_x, one reference resistor R_{ref} and two other resistors of equal resistance, R_a. A sketch of the Wheatstone bridge showing all the four resistors and their corresponding voltages can be seen in Figure 3.13. The reference resistor R_{ref} was determined when the electronic box was built (R_{ref} = 50 Ω) and it helps in enhancing the precision of the liquid fraction measurement by expanding the range of the voltage output (Komonibo 2017).
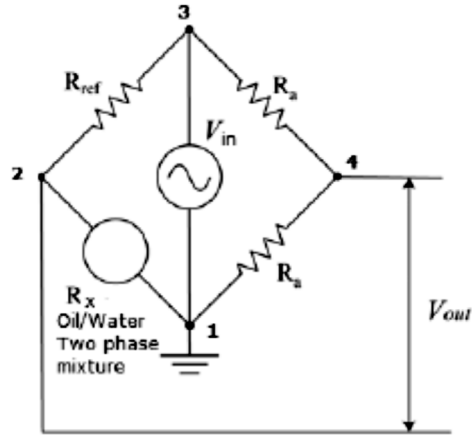
Figure 3.12: A diagram of the Wheatstone bridge showing the variable resistor that represents the oil-water mixture. (Source: Komonibo, 2017)

Considering the Wheatstone bridge in the diagram above and by applying Ohm's law:

$$V = I \: x \: R \tag{3.2}$$

Where V = Voltage (V)

I = Current (A)

R = Resistance (Ω)

From the Wheatstone bridge circuit,

$$V_{out} = V_{24} = V_{12} - V_{14} = \frac{V_{in}}{R_{ref} + R_X} R_x - \frac{V_{in}}{R_a + R_a} R_a \tag{3.3}$$

$$V_{out} = \frac{V_{in}}{2} \left[\frac{\left(\frac{R_x}{R_{ref}} - 1 \right)}{\left(\frac{R_x}{R_{ref}} + 1 \right)} \right] \tag{3.4}$$

$$E = \left[\frac{\left(\frac{R_x}{R_{ref}} - 1 \right)}{\left(\frac{R_x}{R_{ref}} + 1 \right)} \right] \tag{3.5}$$

88

In order to calibrate the conductance probes, the voltage output, V_{out} must be measured for each resistance selected on the variable resistor and then establish a linear relationship between the potential impedance, which is the term in the bracket in equation (3.12) and the voltage output, V_{out} The challenge is that due to the potential impedance in the electrical circuit, the actual voltage signal does not fit into equation (3.12), thus the need to calibrate the output voltage with known impedance. The linear relationship between the output voltage and the known impedance can be described with the equation below:

$$E = cV_{out} + k \tag{3.6}$$

Where E = Potential Impedance (Ω)

V_{out} = Output voltage (V)

c and k are constants.

The determination of the values of the constants c and k was made possible because a variable resistor was used in place of the two-phase oil-water fluid mixture in the Wheatstone bridge. The variable resistor was connected to the terminals of each of the conductance probes while the conductance probes were connected to the electronic box (precisely the Wheatstone bridge) and then to the NI DAQ module. As the resistance values, R_x in the variable resistor are varied, the corresponding voltage values too continue to change. The resistance was measured using the digital multimeter while the voltage values were read from the LabVIEW program. Since the resistance values from the variable resistor are known and also the reference resistance, R_{ref}, therefore, the potential impedance E, which is the term in bracket from equation (3.12) can be determined. In plotting the potential impedance, E and the voltage output, V_{out}, a linear graph is obtained with a slope and intercept equal to the values of the constants c and k for the

respective conductance probe. The calibration curves for the four conductance probes are shown in Figure 3.14.

The next step in the calibration procedure is to determine the voltage output for the known composition of the oil/water two-phase mixture. The variable resistor was replaced with different composition of silicone oil and water in the test assembly ranging from 0% silicone oil and 100% water to 100% silicone and 0% water in the mixture and the corresponding voltage, V_{out} reading was taken from the LabVIEW program. Since the potential impedance, E is the ratio of the resistance in the Wheatstone bridge as seen in equation (3.12) and the constants c and k are known from equation (3.14), then the resistance value for each of the oil/water mixtures can be determined using the equation (3.15) below:

$$E = \frac{\left[\left(\frac{R_x}{R_{ref}} - 1\right)\right]}{\left[\left(\frac{R_x}{R_{ref}} + 1\right)\right]}$$

$$E\left(\frac{R_x}{R_{ref}} + 1\right) = \left(\frac{R_x}{R_{ref}} - 1\right)$$

$$\frac{R_x}{R_{ref}}(E - 1) = -(1 + E)$$

$$\frac{R_x}{R_{ref}} = \frac{1+E}{1-E}$$

$$R_x = R_{ref}\left(\frac{1+E}{1-E}\right) \tag{3.7}$$
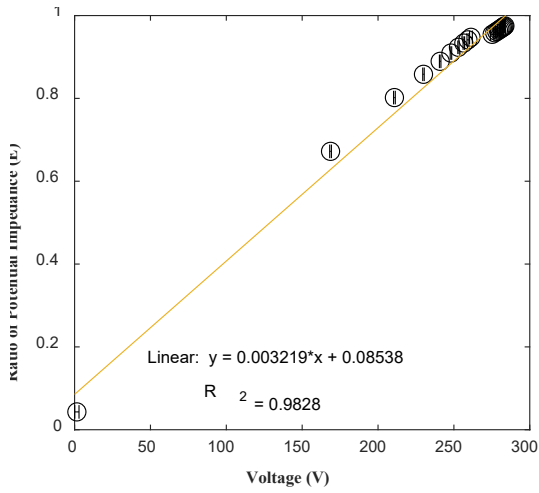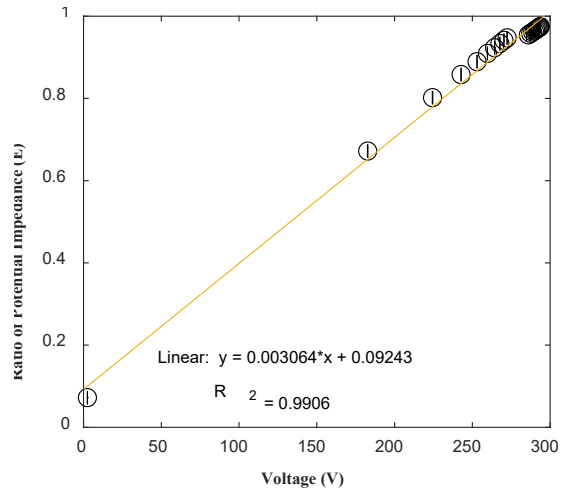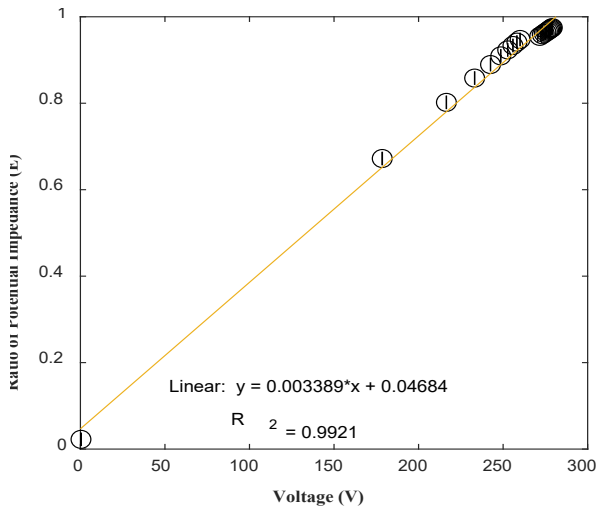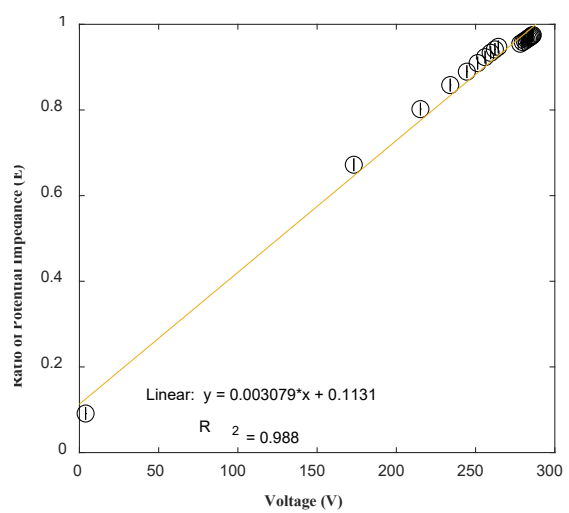
Figure 3.13 : A plot of the ratio of potential impedance and the voltage where the constants c and k are determined for each conductance probe

According to Fossa (1998), when conductance ring electrodes are used in determining the void fraction, a normalized conductance is used which is proportional to the apparent void fraction of the mixture. Therefore, the conductance value for each of the oil/water mixture is normalized using the conductance when the test assembly is full of water and the normalized conductance is called dimension

$$Ge^* = \frac{C_m}{C_w} \tag{3.8}$$

Where $Ge^* =$ Dimensionless conductance

$C_m =$ Conductance of the oil/water mixture (Ω^{-1})

$$= \frac{1}{R_x}$$

$C_w =$ Conductance when the test assembly is full of water (Ω^{-1})

$$= \frac{1}{R_w}$$

$$Ge^* = \frac{C_m}{C_w} = \frac{R_w}{R_x} \tag{3.9}$$

$$Ge^* = \frac{R_{ref}\left(\frac{1+E_w}{1-E_w}\right)}{R_{ref}\left(\frac{1+E_x}{1-E_x}\right)} \tag{3.10}$$

For each of the conductance probes, the dimensionless conductance values were obtained for the different Oil Volume Fraction (OVF) and a plot was made a using a 3rd degree polynomial function (Fossa, 1998) to fit the data and the values of the constants e, f, g and h were obtained.

$$\text{OVF} = e(Ge^*)^3 + f(Ge^*)^2 + g(Ge^*) + h \tag{3.11}$$

The calibration data for the four (4) conductance probes were plotted on a single graph and given in Figure 3.15 below.
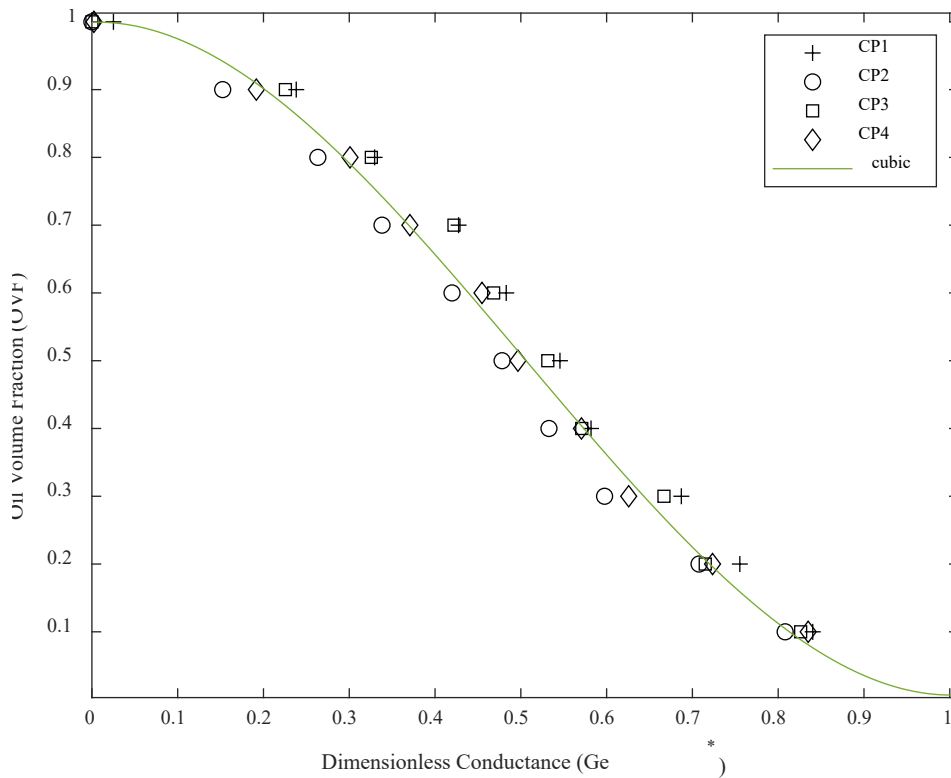
Figure 3.14: Calibration curve for the four (4) conductance probes CP1, CP2, CP3 and CP4 showing the relationship between the dimensionless conductance Ge* and the Oil Volume Fraction (OVF)

3.3.4 MEASUREMENT OF THE INTERFACIAL HEIGHT

The interfacial height was measured using the Double Parallel Wire Probe (DPWP) assembly which is an intrusive device that gives an indication of local fluctuations along the oil-water interface. The pictorial representation and the schematic diagram of DPWP can be seen in Figures 3.17 and 3.18 From the measurements of the instantaneous height of the oil/water interface, the wave amplitude can be determined which will reveal if the disturbance along the interface will grow or decay. The wave amplitudes were determined as the difference between local height of the wave crest and the average height of the oil/water interface for a given experimental condition.

The DPWP used in this research was designed and fabricated in the Department of Chemical and Environmental Engineering, University of Nottingham. The probe is made up of a pipe

section with flanges at both ends where two tiny holes are drilled through the centre of the pipe section and two (2) stainless steel parallel wires of 0.5 mm in thickness with a separating distance of 10 mm between them are connected using some bolts to provide support and for tensioning of the wires. The wires are placed perpendicular to the flow direction and tensioned using a specially designed bolt positioned at both ends so that the deformation experienced by the wires as a result of the flow will be minimized. The choice of the wire thickness and the separating distance was made to achieve high sensitivity between the electrodes so that accurate measurement of the voltages can be made.

Several researchers such as Huang et al., (2007), Lusheng et al., (2013), Zhai et al., (2014) and Zhou et al., (2020) have performed sensitivity analysis of the two electrodes in a DPWP using finite element methods and all agreed that the separating distance between the electrodes and the thickness of the electrodes directly affects the sensitivity of the probe. Based on the work of Lusheng et al., (2013), the maximum average sensitivity of the probe was attained when the thickness of the wire was 0.5 mm while at a separation distance of 10 mm, a very high average probe sensitivity was also attained, hence that informed the choice of the thickness and separating distance used in the current probe design.

A pair of wire is connected to the top of the two parallel electrodes and subsequently attached to an electronic box. In measuring the interfacial height, the mixture velocity (U_m) is kept constant while varying the Water-Cut (WC) for a given pipe inclination. The range of the mixture velocity used in this experiment is 0.08 m/s – 0.4 m/s with a step change of 0.08 m/s while the range of the WC used is 10% - 70% with a step change of 10%. Only upward inclination angle of $+1^o$, $+2^o$, $+3^o$, $+4^o$ and $+5^o$ were used in this research. For each set of flow condition, the flow is allowed to stabilize before measurements are made. The DPWP measures the conductance of the water layer to the flow of electricity in a separated flow and the thickness

of the water layer corresponding to a given oil/water combination will give a unique value of the conductance.

The probe was calibrated offline where the probe assembly was closed at both ends with blank flanges and the total volume of the probe assembly is 0.00374 m^3 (3.74 litres). Firstly, only water (100% water and 0% silicone oil) was introduced to fill the probe assembly completely and the corresponding voltage at a 1000 Hz sampling frequency was recorded through the LabView program. The program interfaces between the electronic box where the probe was connected and the National Instrument NI 9205 module. The recorded voltage for 100% water corresponds to the maximum interfacial height which equals the internal diameter of the pipe (0.127 m). The interfacial height was reduced by 10% to a value of 0.1143 m corresponding to 95% water and 5% silicone by volume and the voltage was read. The procedure was repeated until 100% silicone oil was used corresponding to zero interfacial height and the voltage was equally recorded. The uncertainty in the interfacial height measurement was calculated to be about 0.34%. A plot of the voltage and the interfacial height was made, and the equation of the curve obtained gives the calibration equation. The calibration equation was inputted into the LabView program for data acquisition.
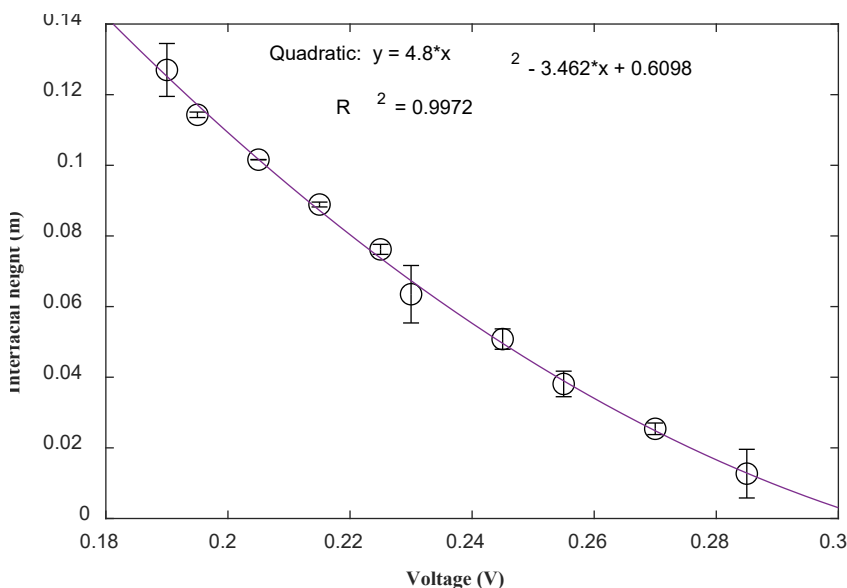
Figure 3.16: Calibration curve for the Double Parallel Wire Probe (DPWP)
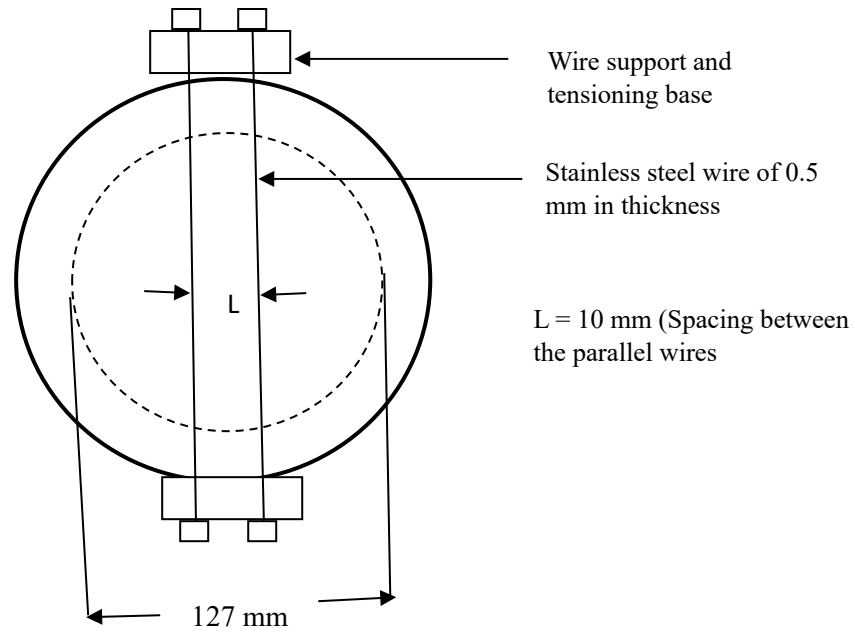
Figure 3.16: A schematic diagram of the Double Parallel Wire Probe (DPWP)
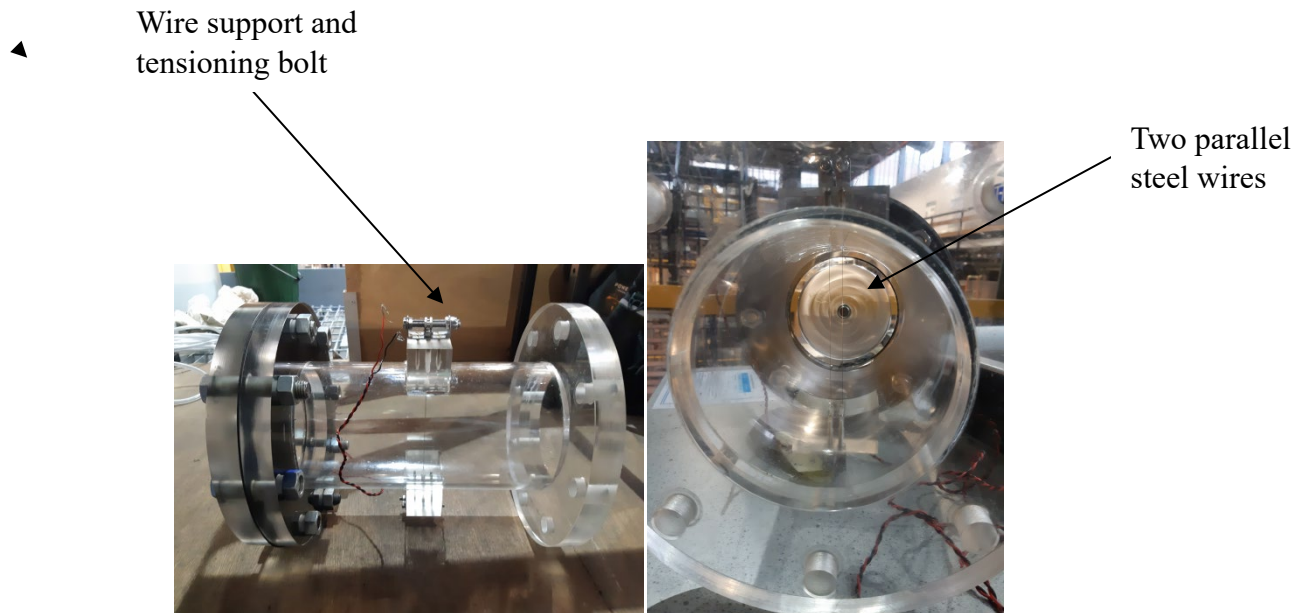
Figure 3.17: A picture of the Double parallel wire probe (DPWP) assembly showing the wire tensioning bolt and the two parallel wires.

3.4   DATA ACQUISITION SYSTEM

The Data Acquisition System (DAQ) used in this research is made up of the sensors, the
electronic box, the NI DAQ hardware (modules), the LabView software and the personal
computer as shown in the schematic diagram given in Figure 3.19.

Sensor block
representing all the
sensors used in
data acquisition

Electronic box
where the CP and
DPWP sensors are
connected

The NI Modules where
the analog –digital
signal conversion takes
place

Computer where the
LabView program was
installed and where the data
from the sensors are acquired
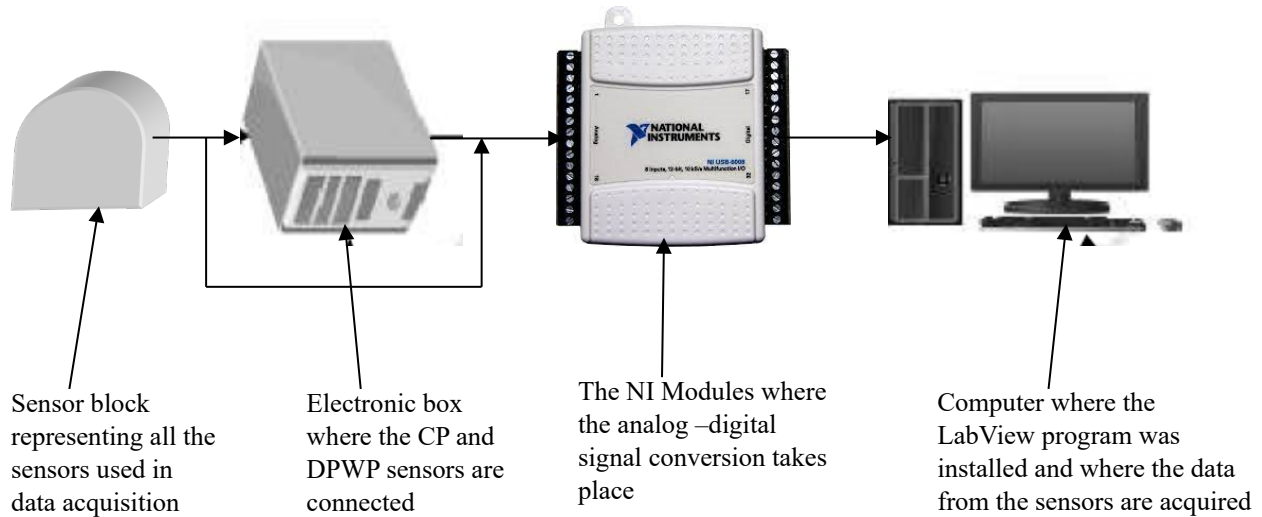
Figure 3.18: A block diagram of the Data Acquisition System (DAQ)

The sensors are the primary instrument that measures the experimental variables and provide
electrical signal in proportion to the quantity of the measured variable based on the calibration
equation. Some of the sensors such as the Conductance probes (CP) and the Double Parallel
Wire Probe (DPWP) are connected to the Wheatstone bridge box where specially designed
electronic circuits for the sensing of the variable resistance provided by the different oil/water
combinations are installed. Also, the signals from the sensors are filtered and amplified through
their various circuits in the Wheatstone bridge box. The Wheatstone bridge box was then
connected to the National Instrument NI 9205 modules. Other sensors such as the pressure
transducers and thermocouples are connected directly to the National Instruments NI 9203
modules. The NI modules converts the analog signals from the sensors into the digital signals
that can easily be read by the computer which provides the interface for the data to be acquired.
The NI 9205 module has a 16-bit Analog input with 32 signal channels and a voltage range of

+/-200mV to +/- 10V while the NI 9203 module is a 8-channel module with a 16-bit analog input signal resolution and has an input current of +/- 20mA. The sampling rate for the data acquisition is 1 kHz within the time frame of 12 minutes.

Figure 3.19: The data acquisition system comprising of the computer, NI modules and the electronic box.

3.5 HIGH SPEED IMAGING SYSTEM

The flow development and the interfacial wave behavior across the test section were observed using the high-speed camera. The setup of the imaging system includes the Phantom V12.1 high-speed camera, a Sigma 105 mm f/2.8 EX Macro lens, two (2) LED lights, tripod stand and the laptop computer where Phantom PCC 2.7 software was installed that provides the camera user interface. The imaging setups were placed in a scissor lift that helps in positioning the camera to the appropriate location on the rig. A pictorial representation of the camera setup can be seen in Figure 3.20.

Scissor lift frame

Viewing Section

LED lights

Phantom V-12 High speed camera

Laptop Computer
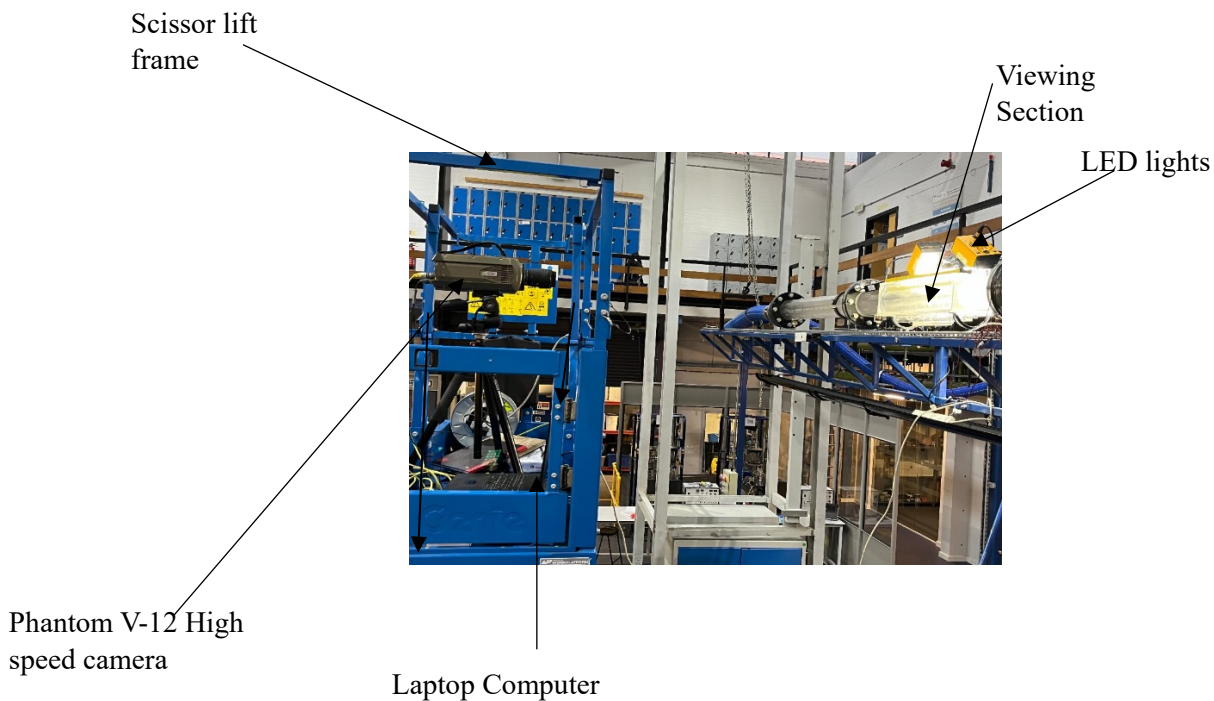
Figure 3.20: A picture showing the imaging setup comprising of the high speed camera mounted on a scissor lift, viewing section, LED lights and the computer for image acquisition. The maximum resolution (1280 pixels x 800 pixels) was used with a frame rate of 1000 fps for 6 seconds. A total of 6,000 frames were obtained for a given flow condition.

The wave speed can be roughly estimated using the Wallis (1969) kinematic wavy theory where it was stated that the wave speed should be in between the axial phase velocities of the water and oil phases, therefore an average of these phase velocities can be assumed to be the wave speed. The maximum oil and water phase velocities using the holdup values and the superficial velocities are 1.16 m/s and 3.39 m/s respectively, therefore the maximum wave speed will be in the order of 2.28 m/s. The length of the window on the viewing section captured by the high speed camera through which the wave travels is 0.36 m. The time it will take the fastest wave to travel through this window is 0.157 seconds. Since the frame rate is 1000 fps, then it will require about 157 frames to capture a single wave through the window in the viewing box, hence the frequency and the time allowed for each measuring point is sufficient to capture the waves and flow structures along the interface.

3.6.1 IMAGE ANALYSIS

The flow images obtained using the high-speed camera were analyzed using an image processing software called Image J. The parameters to be obtained using the image processing from Image J are the interfacial height and the wavelength while the wave speed will be obtained by analyzing the video of the flow using the Phantom PCC 3.8 software. The first step in using Image J is to upload the required image for processing unto the software and since all the images are inclined to a particular angle ($+1^o$,$+2^o$,$+3^o$,$+4^o$ and $+5^o$), the next step is to remove the inclination angle so that the image becomes horizontal. The subsequent step is to determine the resolution by relating the pixels of the image to the actual measurement using both the measuring tape attached to viewing section and also the diameter of the pipe as a reference. In using both methods, the length-to-pixel ratio obtained is the same (0.000276 metres per pixel) and the value is inputted into the Image J software. In determining the interfacial height, 30 images were selected and for each image, several measurements (at least 10) were made from the bottom of the pipe to the oil and water interface which was clearly defined on the image and the average of these measurements gives the average interfacial height. A sample image showing how the different measurements were taken on a given image can be seen in Figure 3.21. It is worth mentioning that attempt was made to ensure that the focus of the camera was on the centre plane of the viewing box so that the measurements of the interfacial height from the images can be compared with the one obtained using the DPWP where the measurement of the interfacial height was at the pipe centre. As a result of the large diameter of the pipe (127 mm), the interface curvature along the pipe cross-section was assumed to be planar due to the reduced effect of surface forces as noted from the corresponding low value of the $E\ddot{o}tv\ddot{o}s$ number ($Eo = 73.6$).

Figure 3.21: An image showing how the average interfacial height was determine by measuring at different locations from the bottom of the pipe to the oil-water interface.

Average interfacial height (h) $= \frac{1}{N} \sum_{i=1}^{N} \left(\frac{\sum_{i=1}^{n} H_i}{n} \right)$ (3.12)

Where n is the total number of measurements in a given image and N is the number of images used in the measurement of interfacial height (H_i).

The wavelength is determined as the horizontal distance between two consecutive wave crests or troughs. Similar method used for the average interfacial height was used in determining the wavelength. A number of images (at least 30) showing well-defined interfacial waves were used and for each image, horizontal distance between two consecutive troughs was measured and the average for all the images measured gives the average wavelength. A sample image showing the measurement of the wavelength can be seen in Figure 3.22.

Figure 3.22: A picture showing the measurement of wavelength.

The wave speed was determined using similar method by Al-Wahaibi et al., (2011) and Tripathy et al., (2017) where it is measured from the time taken for a wave crest or trough to travel between two fixed positions. The phantom PCC 3.8 software is used to display the flow video and attempt is made to locate the position of a relatively stable wave crest or trough by its frame number. The total number of frames involved for the identified wave crest or trough to move between two fixed locations of distance 0.01 m apart will be noted. This fixed distance was obtained using the ruler attached to the bottom of the viewing box and the distance is so small such that the shape of the wave does not significantly change as the interfacial wave traverses between the two fixed points. Since the frame rate used in acquiring the flow images was known at the beginning (1000 fps), then the time it takes the wave crest or trough to move between the two fixed locations of distance 0.01 m apart can be obtained by dividing the total number of frames involved in the movement of the wave crest

or trough between the two fixed locations (0.01 m apart) by the frame rate (1000 fps). The wave speed can be obtained once the time is calculated since the distance is fixed.

Frame 2339   Frame 2540   Frame 2720

Wave trough to
be tracked

Frame 2850   Frame 2940

Wave trough moving
through the fixed
positions after 381
frames

Final position
of the wave
trough
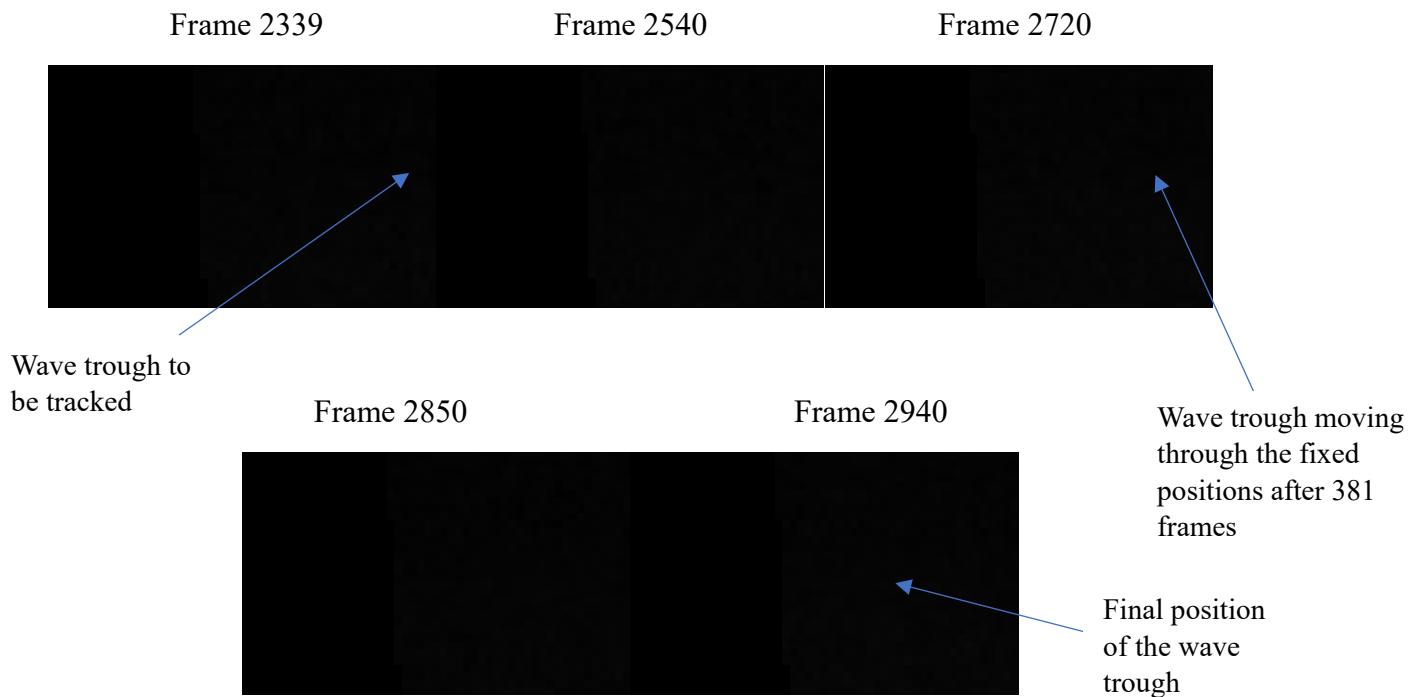
Figure 3.23: Pictures showing the movement of the wave trough across the fixed locations

3.6 EXPERIMENTAL UNCERTAINTIES

Measuring equipment suffer from a number of imperfections that limit our knowledge of the true value for any measurement which implies that there is always an uncertainty associated with any measured quantity. Uncertainty in measurement is unavoidable but the goal is to attempt to reduce it to the barest minimum if possible and the knowledge of the uncertainty is vital to correctly interpret the meaning of the measured value. The measuring instruments used in carryout the experimental campaigns have been provided with an estimate of the errors by the manufacturers and can be seen in the table below.

Table 3.3: Instrument Uncertainties

Instrument	Working range	Uncertainties
Truflo paddle wheel flow meter (Oil flow meter)	0 – 1200 litres/min	+/- 1%
Electromagnetic flow meter (water flow meter)	0 – 88.4 m^3/hr	+/- 0.25%
Differential pressure transducer	0 – 186.5kPa	+/-0.075%

The conductance probes (CP1, CP2,CP3 and CP4) and the double parallel wire probe (DPWP) were all properly calibrated in order to remove the systematic errors. The random errors in the measurement of the Oil Volume Fraction (OVF) and interfacial height were reduced by performing numerous measurements. The mean of the measurement is considered to be the best estimate while the standard deviation of the mean is taken as the uncertainty in the measurement which describes the reliability and repeatability of the measurement. The mean and standard deviation of the mean for the measurements are determined using statistical analysis.

$$\text{Mean} = \bar{x} = \frac{\Sigma_i^N x_i}{N} \tag{3.13}$$

$$\text{Standard deviation} = \sigma = \sqrt{\frac{\Sigma_i^N (x_i - \bar{x})^2}{N-1}} \tag{3.14}$$

$$\text{Standard deviation of the mean} = \sigma_{\bar{x}} = \frac{\sigma}{\sqrt{N}} \tag{3.15}$$

Since random measurements are described by the Gaussian distribution with a characteristic bell shape, the mean can be considered the best estimate of the measured variable while the standard deviation of the mean can also be considered as the measure of uncertainty for the given measured variable with 68% confidence.

3.7 SUMMARY

This chapter presents a comprehensive overview of the experimental rig used in the liquid-liquid experimental campaigns. It outlines the working principles and operational limits of selected components, including pumps, flow meters, conductance probes (CP), double parallel wire probes (DPWP), and pressure transducers. Additionally, it covers the design and configuration of the three different fluid inlet devices, which play a crucial role in how the inlet fluids contact and redistribute, leading to the formation of different flow patterns.

The chapter also includes a brief description of the physical properties of the fluids and the experimental matrix employed in the experiments. Special emphasis was also placed on the calibration methods and procedures for the instruments, particularly the CPs, DPWP, and pressure transducers. The underlying theory governing the performance of the CPs, along with the electronic circuitry responsible for transmitting signals, was thoroughly discussed.

Furthermore, a brief description of the Data Acquisition System (DAQ) was provided, which encompasses the electronic box that houses the circuitry powering the instruments, the National Instrument (NI) modules, and the computer system running LabView software for data acquisition. Lastly, the chapter presents an in-depth overview of the high-speed camera imaging system, detailing its setup, image capture process, image analysis, and the measurement of wave characteristics such as wavelength, wave speed, and wave amplitude.

CHAPTER 4

EXPERIMENTAL OBSERVATION OF THE FLOW CHARACTERISTICS IN OIL-WATER TWO PHASE FLOW ACROSS AN INCLINED PIPE

4.0   INTRODUCTION

This chapter presents the observations and results of the experimental work done using the T-type fluid inlet device where both the oil and water flow through a homogenizing mixer. The goal of the chapter is to study the various flow characteristics such as identifying the different flow patterns, developing the flow pattern maps and examining the distribution of the Oil Volume fraction (OVF) in the axial direction across all the conductance probes. The Conductance Probes (CP) are positioned 9.6D (CP1), 19.2D (CP2), 28.8D (CP3) and 56.6D (CP4) from the fluid inlet device. Also, attempt will be made to study the effect of other flow parameters on the hydrodynamic behaviour of the oil-water two phase flow such as the effect of pipe inclination and water-cut (WC) on the OVF and also the slippage characteristics between the phases will be presented.

4.1   FLOW PATTERN

In carrying out this research, four (4) distinct flow patterns were observed over the range of the investigated mixture velocities (U_m) and water-cut (WC) based on both visual observation and the images from the high-speed camera. The flow patterns include the stratified wavy with mixing at the interface (SW&MI), dispersed oil in water and water (Do/w&w), dispersed water in oil and oil (Dw/o&o) and finally dispersed oil in water (Do/w) as can be seen in Figure 4.0 below . It is interesting to note that a clearly separated flow with no droplets at the interface, such as the stratified flow (ST) and the stratified wavy (SW) flows were not observed in this research. The probable reason that such flow patterns were not observed could be attributed to the design of the fluid inlet device which favours the generation of droplets as a result of the

manner in which the two fluids contact. These droplets come in various sizes depending on the input flow conditions and they are carried downstream through the test section. The pictorial representation of the flow patterns and the flow pattern map are presented in Figures 4.0 and 4.1 respectively .

Stratified Wavy with Mixing at the Interface (SW&MI)

(b) Dispersed Oil in Water and Water (Do/w&w)

Dispersed oil droplets in water

(c) Dispersed Oil in Water (Do/w)
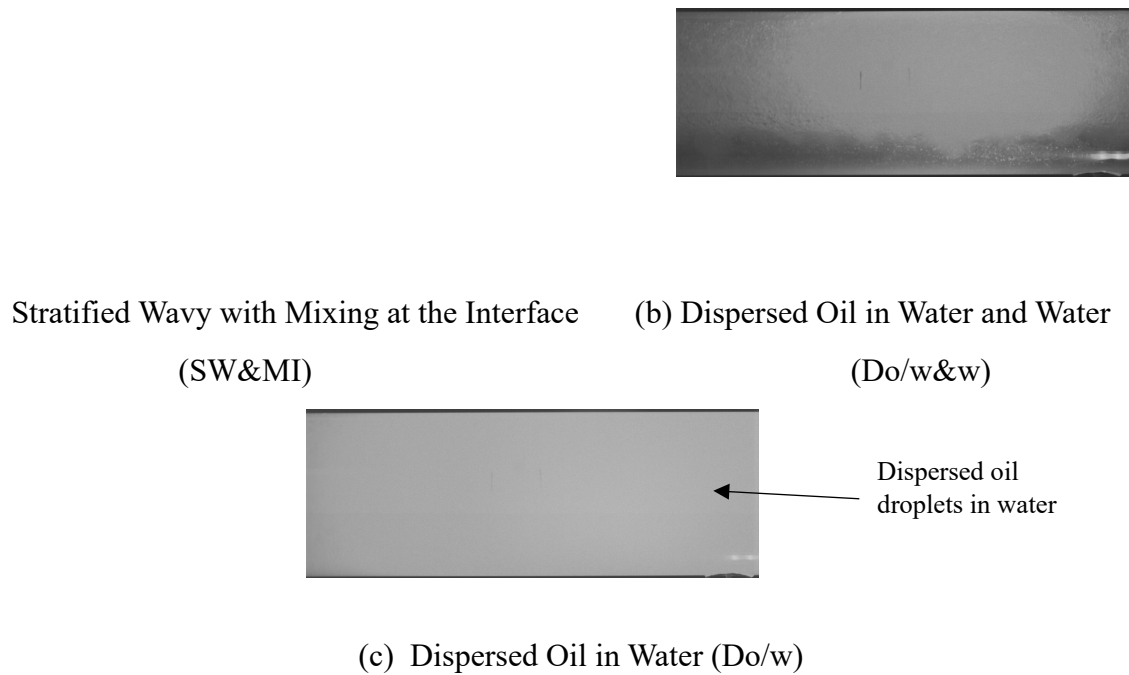
Figure 4.0: Pictorial representation of the flow patterns as captured using the high-speed phantom camera.
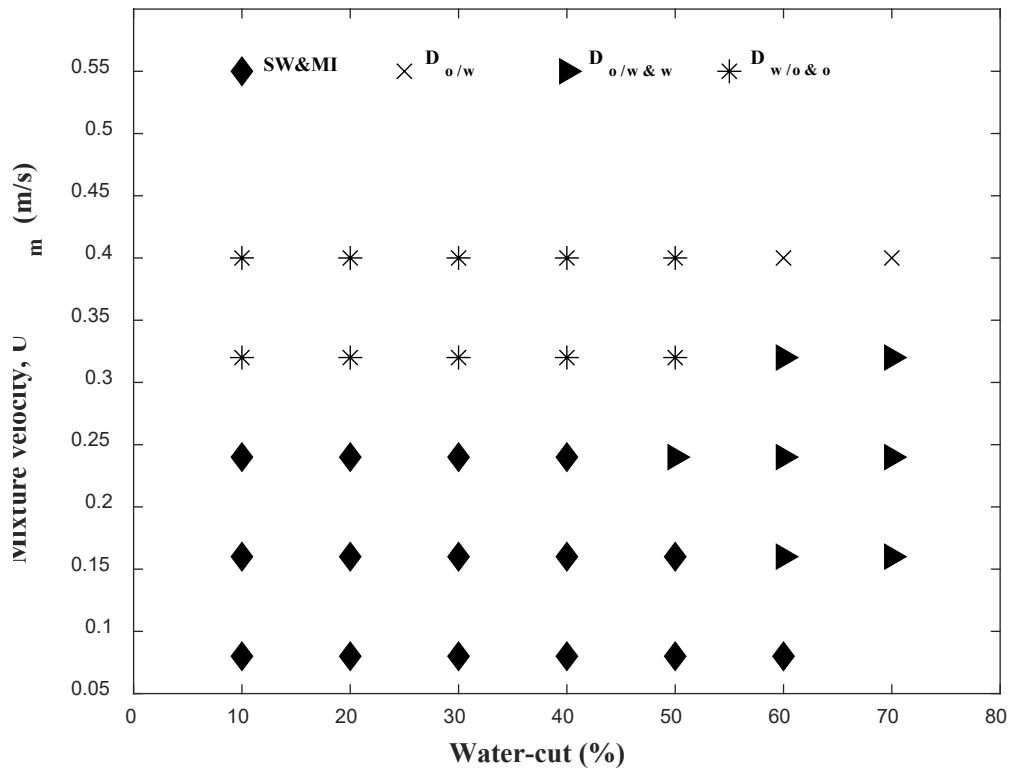
Figure 4.1: Flow pattern map for oil-water flow across a +1° inclined acrylic pipe

4.1.1 Stratified Wavy and Mixing at the Interface (SW&MI)

The SW&MI flow pattern is the first flow pattern observed even at lowest mixture velocity ($U_m = 0.08$ m/s) and for all water cuts (WC) as seen in Figure 4.1. In this type of flow pattern, both the oil and water phases maintain their continuity at the top and bottom of the pipe with a region around the interface where droplets are observed to agglomerate. According to Kumara et al., (2009), the existence of the droplets close to the interface could be due to the competition between the dynamic forces and the buoyant forces acting on the droplets. The buoyant force which enhances the settling of the droplets is stronger than the dynamic force which tends to spread the droplets across the pipe cross-section, hence the droplets remain close to the interface. From the flow pattern map (Figure 4.1), it was observed that increasing the mixture velocity (U_m) leads to a corresponding decrease in the size of the region occupied by the SW&MI flow pattern until there was a transition to another flow pattern. For instance, on

increasing the mixture velocity from 0.08 m/s to 0.24 m/s, the value of the WC needed to maintain the SW&MI flow pattern reduced from 60% to 40% and beyond this point, the SW&MI flow pattern transition to Dw/o&o.

4.1.2   Dispersed Oil in Water and Water (Do/w&w)

The Do/w&w flow pattern was observed within the window where the range of the WC is 50% $\leq WC \leq$70% and that of the U_m is 0.16 m/s $\leq U_m \leq$ 0.32 m/s which suggests that the water superficial velocity (U_{sw}) is relatively high. In this type of flow pattern, two separate layers are formed where the continuous water phase occupies the bottom layer while the dispersion of oil droplets in water occupied the top layer. This configuration was made possible because of the high superficial velocity of the water phase which produces high dispersive turbulent energy that enhances the dispersion of the oil droplets into the continuous water phase (Perera et al., 2018, Kumara et al., 2009). However, the buoyant forces acting on the droplets prevents the turbulent dispersive forces from distributing the droplets uniformly across the pipe section. Therefore, a dispersion of the oil droplets in the water phase are formed over a continuous water layer at the bottom of the pipe. This type of flow pattern can also be classified as a water dominant flow pattern. For the same the mixture velocity (U_m = 0.32 m/s) and at low WC, the oil becomes the dominant phase and therefore it maintain its continuity while the water phase becomes the dispersed phase.This type of flow pattern is termed Dw/o&o.

4.1.3   Dispersed Water in Oil and Oil (Dw/o&o)

The Dw/o&o flow pattern was observed within the region where the range of U_m is 0.32 m/s $\leq U_m \leq$ 0.4 m/s and that of WC is 10% $\leq WC \leq$50%. In this type of flow pattern, the oil phase remains the dominant (continuous) phase while the water phase is the dispersed phase. Since the mixture velocity (U_m) is quite high while the water-cut (WC) is relatively low, it implies that the superficial velocity for the oil phase will be relatively higher than that of the

water phase. Hence, the dispersive turbulent energy will be higher in the oil phase which is able to break the continuity of the thin water layer to form water droplets which are carried into the oil phase, while also maintaining a layer of the oil phase with no water dispersion in it. On further increase of the WC exceeding 50%, the water becomes the dominant phase and a flow pattern where the oil is fully dispersed and distributed in the continuous water phase is formed.

4.1.4 Dispersed Oil in Water (Do/w)

The Do/w flow pattern was observed at a very high mixture velocity ($U_m = 0.4$ m/s) and a very high water-cut (WC $\geq$ 60%). As a result of the high U_m and WC, the water superficial velocity becomes very high, hence, the dispersive turbulent energy of the water phase is sufficient to disperse and distribute the oil droplets homogeneously across the pipe section. Therefore, the water phase becomes the continuous phase while the oil phase becomes the fully dispersed phase. Also, in figure 4.0c, it can be observed that as a result of the finely dispersed oil droplets in the continuous water phase as a result of the high water superficial velocity and relatively low oil superficial velocity, the mixture was seen to be cloudy, forming an unstable emulsion which if left undisturbed will separate into water at the bottom and oil on top with a clear interface between them.
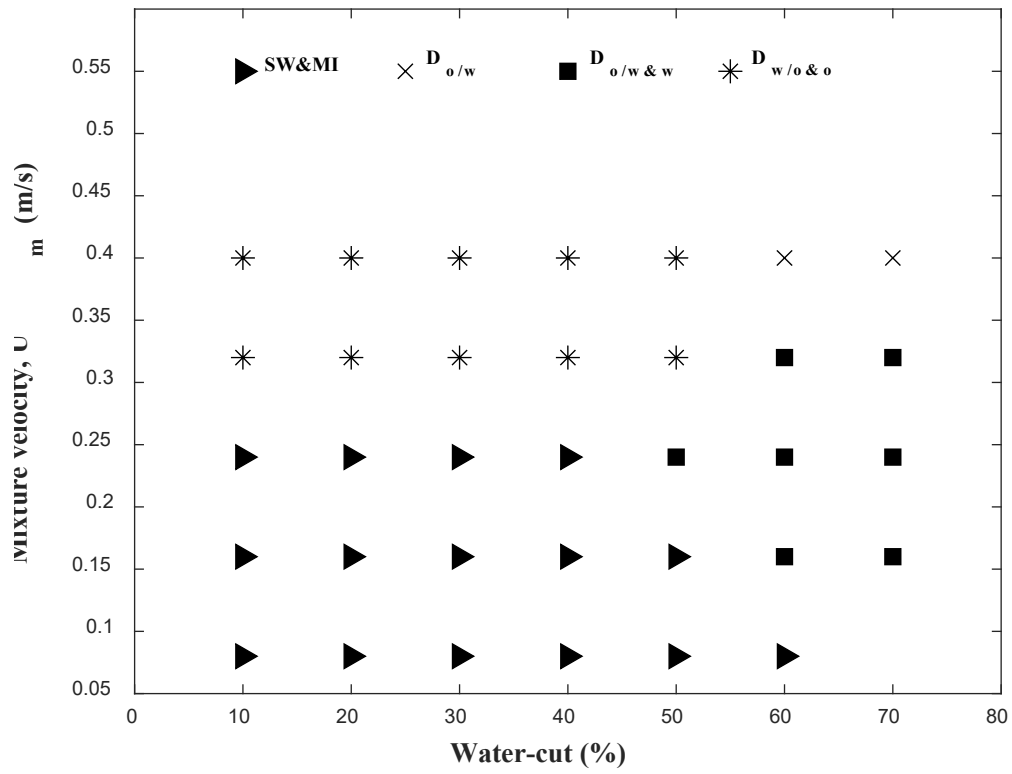
(b)
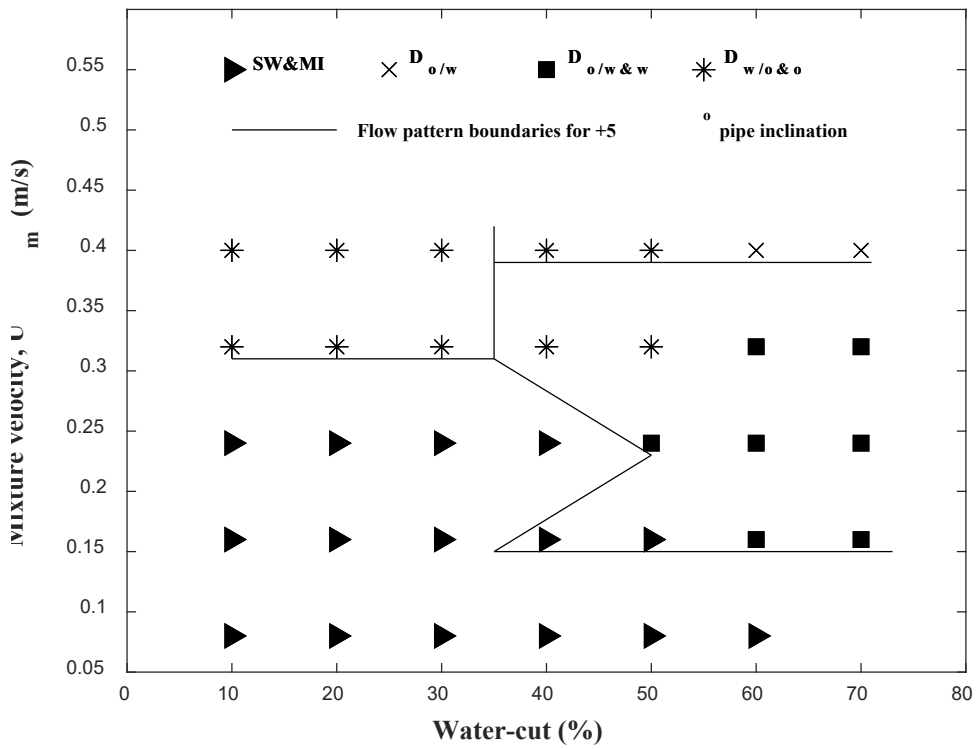
Figure 4.2: Flow pattern map for oil-water flow across pipe inclination (a) +1º (b) +1º with

+5º pipe inclination flow pattern boundary lines superimposed.

On comparing the flow pattern map for +1º pipe inclination and that of the +5º pipe inclination as depicted in Figure 4.2, it will be noticed that the pipe inclination affects the boundaries of the various flow pattern encountered for the same flow conditions. At low mixture velocity, U_m = 0.08 m/s, the flow pattern was not affected by the change in pipe inclination and it remained the same as SW&MI for all water cuts (WC). However, as the mixture velocity was increased to 0.16 m/s, the boundary between the SW&MI and Do/w&w shifted towards the left as the pipe inclination increases from +1º to +5º. Thus the Do/w&w flow pattern appeared earlier (at WC of 40%) for the +5º pipe inclination as against that of 1º which appeared at WC of 60%. Similar observation can also be made when the mixture velocity was further increased from 0.16 m/s to 0.4 m/s.

However, for the mixture velocity at 0.4 m/s, the boundary for the transition between Dw/o&o and Do/w was also shifted to the left as the pipe inclination increased to +5º which implies that the Do/w flow pattern appeared earlier at WC = 40% for the +5º pipe inclination compared to that of +1º pipe inclination which occur at WC = 60%. It is interesting to note that the change in the flow pattern transition boundary as a result of the increase in the pipe inclination serves to increase the size of the region where the water-dominant flow pattern such as Do/w&w and Do/w occupies. This is because the increase in the pipe inclination from +1º to +5º result in a corresponding action of the axial component of the gravitational force on the denser water phase which tends to retards its in-situ velocity, thereby leading to its accumulation in the pipe section, hence the presence of the continuous water layer as the pipe inclination increases.

In an attempt to compare the flow patterns observed in the current study with those obtained in the literature, the work of Kumara et al., (2009) and Perera et al., (2019) were selected because some of the operating conditions (i.e. mixture velocity and water-cut) used by these researchers are comparable to those used in the current work. However, there are fundamental differences such as the design of the fluid inlet devices, the size of the pipe geometry and the fluid

properties. Both Kumara et al., (2009) and Perera et al., (2019) used a separating plate (35 cm in length) to minimize the interfacial mixing close to the inlet whereas none was used in the current work.

Considering +1º pipe inclination, it will be noticed that for the range of the mixture velocity, 0.25 m/s ≤ U_m ≤ 0.5 m/s and for all water-cut (10% - 90%), Kumara et al., (2009) observed only one flow pattern which is ST&MI. However, for the current work where similar range of flow conditions were used, three (3) different flow patterns were identified which includes the Do/w&w, Dw/o&o and Do/w. The flow pattern identified by Kumara et al., (2009) can be classified as a separated flow pattern but for the current study, all the flow patterns identified for similar flow condition are classified as dispersed flow. The differences in the number and type of flow patterns between Kumara et al., (2009) and the current work can be attributed to the differences in size of pipe geometry used in both cases (56 mm ID) and also the presence of separator plate used by Kumara et al., (2009) which favours fluid segregation. However, in the current work, the pipe geometry is a large diameter pipe (127 mm ID) with no separator plate in the fluid inlet device, hence the manner in which the oil and water streams contact in the fluid inlet device enhances the generation of droplets and subsequent formation of the dispersed flow patterns.

Also, for the +5º pipe inclination, Kumara et al., (2009) observed two flow patterns namely ST&MI (for U_m = 0.25 m/s , WC ≤ 20%, and U_m = 0.5 m/s , WC ≤ 90%) and SW (for U_m = 0.25 m/s , 25% ≤ WC ≤ 92%. But for the current work, three different flow patterns as previously identified for the +1º namely Do/w&w, Dw/o&o and Do/w were observed within similar flow condition and the same explanation will suffice as given previously. Similarly when compared with the work of Perera (2018) for the +5º pipe inclination, it was noted that for U_m = 0.2 m/s, WC = 10% - 30%, the SW&MI flow pattern was obtained and interestingly, the same flow pattern was obtained in the current work despite that the pipe geometry and the

fluid properties in both cases are different. Similarly for the same mixture velocity ($U_m = 0.2$ m/s) and WC = 50% - 80%, the SW flow pattern was obtained by Perera (2018) whereas for the same flow condition, the Do/w&w flow pattern was obtained in the current work. This is because Perera (2018) used a split plate in the fluid inlet device which kept the oil and water phases separated and prevented mixing close to the inlet, hence the dispersed flow pattern was not observed by Perera (2018) unlike in the current work where the slip plate was not used and fluid mixing occur right at the inlet which favours the evolution of the dispersed flow pattern. Also, upon increasing the mixture velocity (U_m) from 0.2 m/s to 0.4 m/s, Perera (2018) observed SW&MI flow pattern for all water-cuts (10% - 80%) whereas for similar flow conditions, two (2) different forms of dispersed flow patterns were obtained in the current work and they include Dw/o&o flow pattern ($U_m = 0.4$ m/s, WC = 10% - 30%) and Do/w flow pattern ($U_m = 0.4$ m/s, WC = 40% - 70%) and this is attributed to the difference in the size of the pipe geometry and the design of the fluid inlet device in both cases as explained in the previous section.

Another point to note also is that since Kumara et al., (2009) and Perera (2018) used the same pipe geometry (56 mm ID) which is about half the size of the pipe used in the current work (127 mm ID), the $E\ddot{o}tv\ddot{o}s$ number (E_o) which measures the interaction between the buoyant forces (inertial forces) and surface forces (interfacial tension) is low in the former ($E_o = 149.5$) whereas the value is about twice in the latter ($E_o = 283.2$). The implication of this is that the buoyant forces (inertial forces) are lesser in the case of Kumara et al., (2009) and Perera (2018) compared to the current work since the interfacial tension and fluid properties in both cases are similar, hence the appearance of separated flow patterns in Kumara et al., (2009) and Perera (2018) and dispersed flow patterns in the current work for similar flow conditions.

4.2   COMPARISON BETWEEN THE IN-SITU WATER HOLDUP AND THE INLET WATER-CUT(WC)

The in-situ water holdup was not measured directly in this work but was indirectly obtained from the measurement of the Oil Volume Fraction (OVF) using the conductance probes. Since the OVF gives an average measurement of the cross-sectional area occupied by the oil phase and for a two-phase system, the sum of the OVF and the in-situ water holdup must be equal to one, therefore the in-situ water holdup can easily be determined once the OVF measurements are obtained. In Figure 4.5 a-c, the comparison between the in-situ water holdup and that of the inlet water-cut (WC) for mixture velocities of 0.16 m/s, 0.24 m/s, 0.32 m/s and 0.4 m/s at $+1^\circ$, $+3^\circ$ and $+5^\circ$ pipe inclinations respectively are presented. Also included in the plot is the diagonal line that represents the no-slip condition (homogeneous flow model) where it is assumed that the in-situ velocity of both the oil and water phases are the same, therefore the values of the in-situ water holdup and the inlet water-cut is the same for each flow condition along the diagonal line.

From the plots, it will be observed that at low pipe inclination $(+1^\circ)$, the in-situ water holdup was lower than the water-cut (WC) for all the mixture velocities (U_m) and water-cuts (WC) except at low mixture velocity $(U_m = 0.16$ m/s) and low water-cut $(WC = 10\% - 20\%)$. However, upon increasing the pipe inclination from $+1^\circ$ to $+3^\circ$, an increase in the number of data points above the no-slip condition line were observed particularly at low mixture velocities $(U_m = 0.16$ m/s and $U_m = 0.24$ m/s) and low water-cuts $(WC = 10\% - 40\%)$, which suggest that the in-situ water holdup was greater than the WC for these flow conditions while for high mixture velocities $(U_m = 0.32$ m/s and $U_m = 0.4$ m/s) and for all WCs, the in-situ water holdup was lower than the inlet WC, hence all the points fell below the no-slip condition line. These observations suggest that the response of the in-situ water holdup to changes in pipe inclination is more significant at low mixture velocities $(U_m = 0.16$ m/s and $U_m = 0.24$ m/s) and low water-cuts $(WC = 10\% - 40\%)$. However, for higher mixture velocities $(U_m = 0.32$ m/s and $U_m = 0.4$ m/s) and for all water-cuts, no significant change in in-situ water holdup was observed. Similar

observation can also be made for the +5° pipe inclination. Apparently, the observations made above indicates clearly the presence of slip between the oil and water phases which suggests that they are flowing at different in-situ velocities, hence the homogeneous flow model cannot adequately describe the flow hydrodynamics observed in this study.
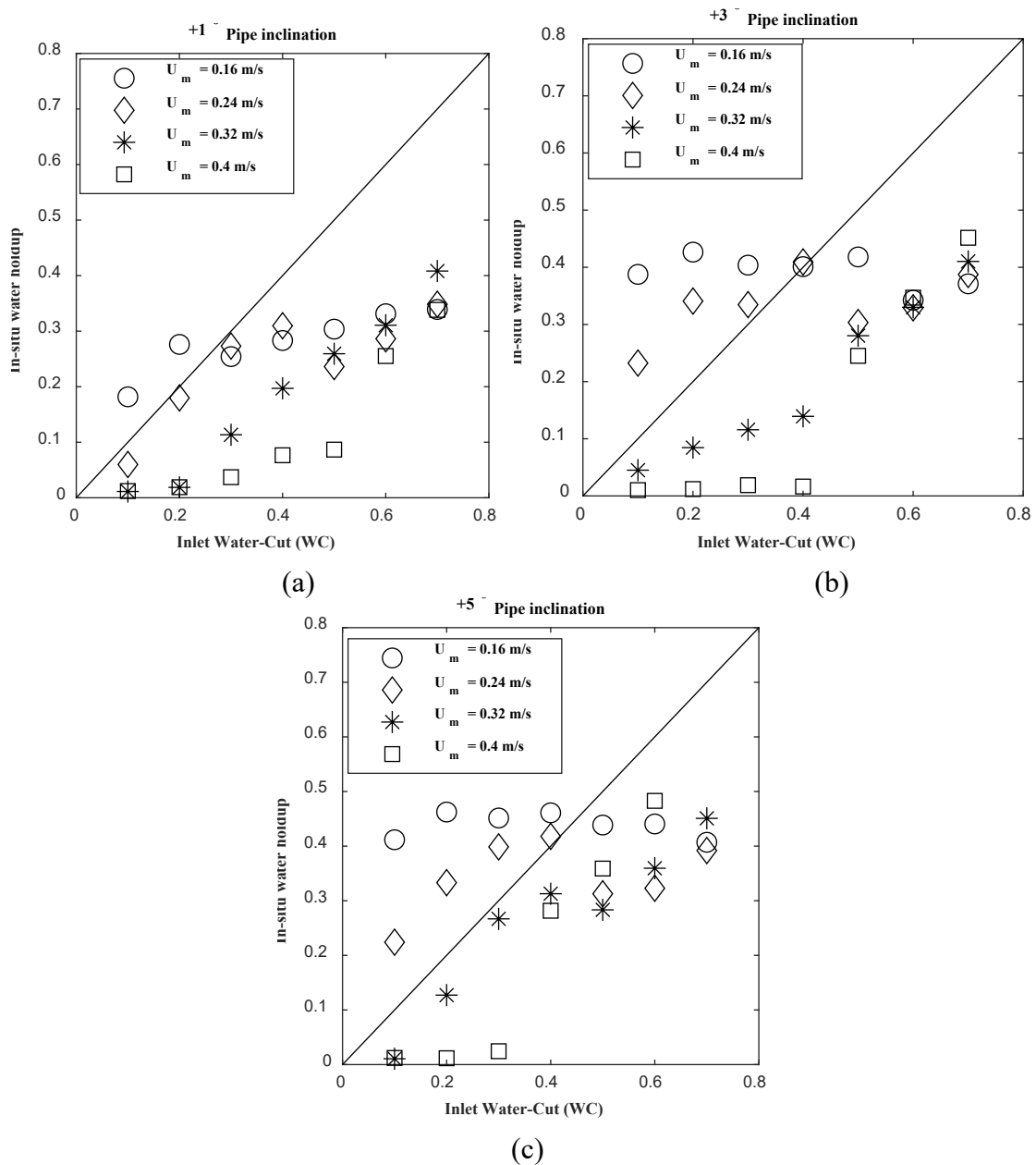
Figure 4.3: A plot showing the comparison between the in-situ water holdup for different mixture velocities and the homogeneous flow model at (a) +1° pipe inclination (b) +3° pipe inclination (c) +5° pipe inclination

4.3 EFFECT OF INLET WATER-CUT ON THE DISTRIBUTION OF OIL VOLUME FRACTION (OVF)

The Oil Volume Fraction (OVF) in the context of this research is referred to the time-averaged in-situ oil fraction which is the fraction of the pipe section occupied by the oil phase. It is a very important hydrodynamic parameter which is quite critical in the design and optimization of two-phase liquid-liquid system and three-phase gas-liquid-liquid systems because it determines the flow regime, pressure drop, heat and mass transfer coefficients and also the determination of the mixture properties of the fluid such as the mixture density and viscosity. The distribution of OVF in a given geometry is dependent on the water-cut among several other variables such as the fluid properties, pipe inclination and design of fluid inlet device and the nature of such dependency can be seen in the Figures 4.6.

Figures 4.6a-c showed the variation of the OVF with the WC for the $+1^{\circ}$, $+3^{\circ}$ and $+5^{\circ}$ pipe inclinations considered in this research work. For all pipe inclinations, it can be observed that the OVF decreases in response to increase in the WC. However, one may notice that the change in OVF as a function of the pipe inclination is dependent on the mixture velocity (U_m). For instance, at low mixture velocity ($U_m = 0.16$ m/s), the OVF decreases as the pipe inclination increases due to slip between the oil and water phases and this will be discuss in great detail in subsequent sections. However, for high mixture velocity ($U_m = 0.4$ m/s), there was no significant change change in OVF as pipe inclination increases particularly at low WC (10% - 30%) where there was dispersion of water droplets in the continous oil phase as a result of the high inertial force in the oil phase.

Another interesting point to note is that the length of the error bars which gives an indication of the variation of the OVF for a given flow condition appears to be a function of the mixture velocity (U_m), water-cut (WC) and ultimately the flow pattern. For instance, for all the pipe

inclinations, it appears that for low mixture velocity (U_m = 0.16 m/s), the error bars are longer which suggest higher fluctuations in OVF which could be due to the appearance of interfacial waves or evolution of oil droplets along the interface. Interestingly, the flow patterns observed for this flow condition (U_m = 0.16 m/s) across all the pipe inclinations are predominantly SW&MI and Do/w&w where there was both the interfacial waves and oil droplets appearing at the interface.

<table>
<tr><td>(a)</td><td>(b)</td></tr>
</table>
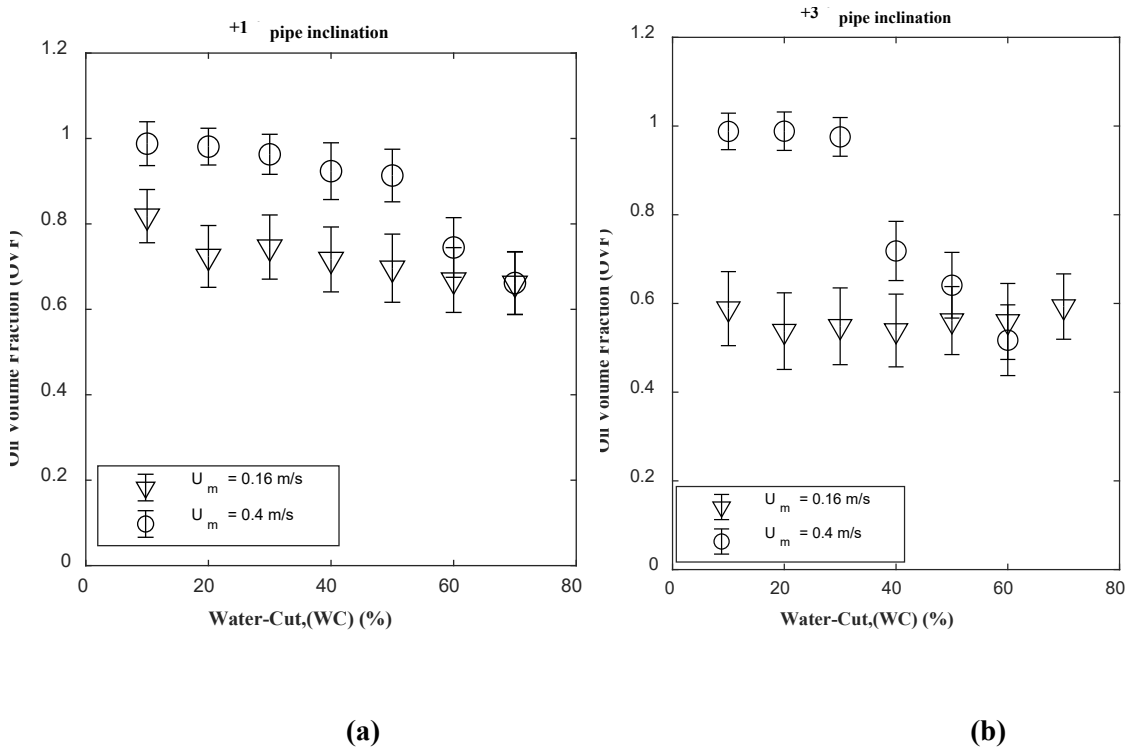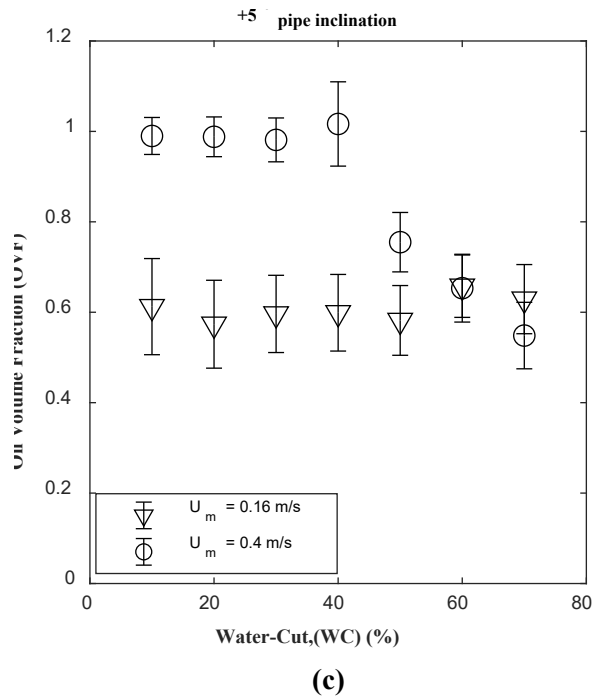
Figure 4.4: Effect of the water-cut (WC) on the oil volume fraction (OVF) across (a)+1° pipe inclination (b)+3° pipe inclination and (c)+5° pipe inclination

However, for higher mixture velocity (U_m = 0.4 m/s), the length of the error bar is dependent on the WC. For instance, the length of the error bars are shorter for all the pipe inclinations particularly at WC = 10% - 40% which suggest a low fluctuation in OVF and beyond WC = 10% - 40% region, there was an abrupt drop in the value of OVF in addition to the longer error bars observed suggesting higher fluctuations in OVF. Upon comparing this findings with the experimental observation, it was noted that at the same flow condition, the Dw/o&o flow pattern was observed which corresponds to the section on the plots with shorter error bars. The presence of the water droplets did not lead to higher fluctuations in OVF probably due to its small size as a result of the high inertial force in the oil phase which was able to disperse the water phase into small droplets. Also, for the same mixture velocity (U_m = 0.4 m/s), and at higher WC (40% - 70%), the error bars were longer suggesting higher fluctuations of the OVF and for all the pipe inclinations, the flow pattern observed was Do/w which is a water-dominated flow pattern with the oil phase dispersed in the continuous water phase. The

presence of the oil droplets of different sizes could possibly explain the wider fluctuations in OVF at these flow conditions.

4.4 AXIAL DISTRIBUTION OF OIL VOLUME FRACTION (OVF)

From the experiment, it was observed that as a result of the upward pipe inclination, the oil-water interfacial height vary all through the test section. The oil/water interface has a gradient where the portion occupied by the oil phase was seen to increase from the inlet and towards the end of the test section. In other words, there is an axial variation of the OVF along the test section and this observation is consistent with that made by Lakis and Nguyen (2016) though they worked on a turbulent gas-liquid flow system. Similarly, Zhou et al (2020) stated that in an oil-water two-phase flow across an inclined pipe, the thickness of the water layer changes along the axial direction and as a result, the water holdup also changes axially. The objective of this section is basically to seek to understand how the OVF changes in the axial direction taking into cognizance the changes in pipe inclination, WC and mixture velocity (U_m).

(a)   (b)
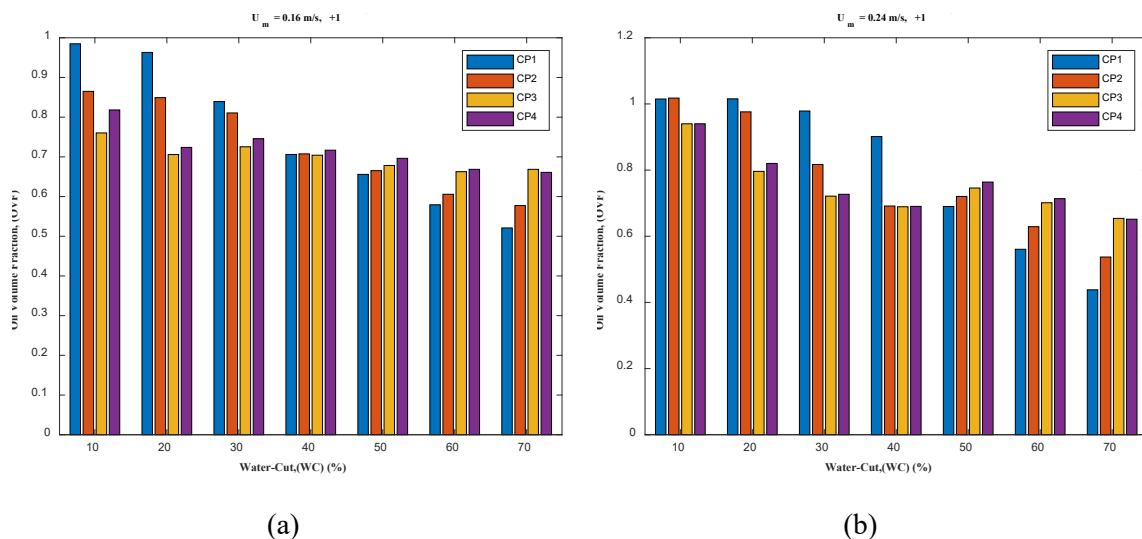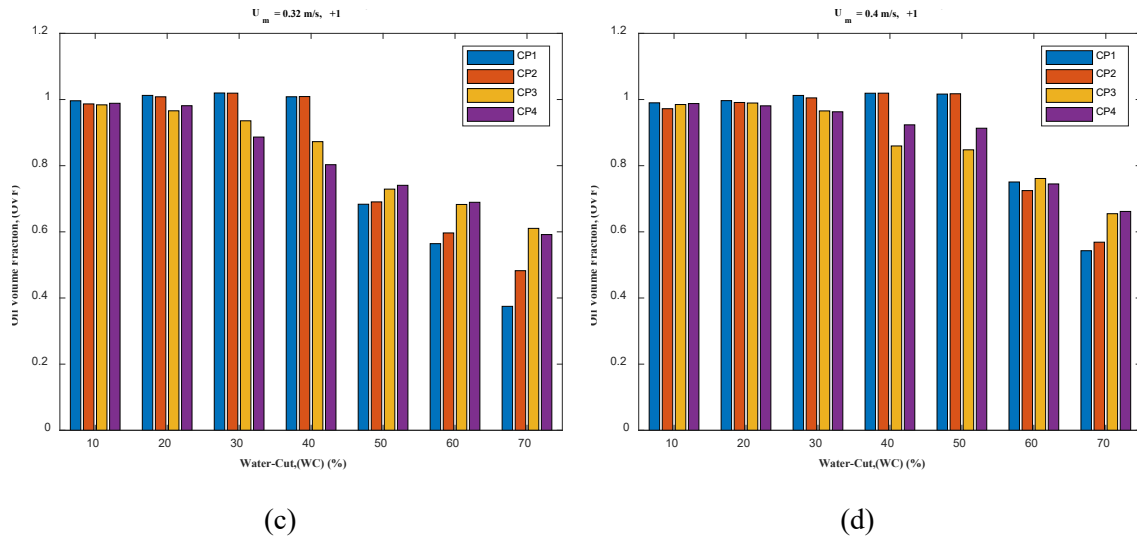
Figure 4.5: Axial distribution of OVF across the test section at +1° pipe inclination and for the mixture velocity, U_m (a) 0.16 m/s (b) 0.24 m/s (c) 0.32 m/s (d) 0.4 m/s.

From Figure 4.7 above, it can be observed that the Oil Volume Fraction (OVF) vary in the axial direction as WC increases and for all U_m. In other words, the fraction of the cross-sectional area occupied by the oil phase increases in the axial direction which clearly demonstrate that there is a greater degree of separation between the oil and water phase along the axial direction particularly for the separated flow regimes. From the experiment, it was physically observed that the height of the oil-water interface decreases axially and this is because of the effect of buoyant forces which tend to push the oil phase to occupy upper region of the test section due to its lower density as against the denser water phase which tends to occupy the lower regions of the test section. However, from the measurements of OVF by the conductance probes, it was noticed that the axial distribution of the OVF at low WC (10% - 40%) and high WC (50% - 70%) are different for all mixture velocities (U_m). It appears that at low WC, the value of the OVF measured by CP1 and CP2 which were placed 9.6D and 19.2D from the fluid inlet device were higher than that of CP3 and CP4 which were placed 28.8D and 56.6D from the same fluid inlet device probably due to the high inertial force in the oil phase as a result of the high superficial velocity. However, at high WC (50% - 70%) and for all U_m, it appears also that the

effect of the slippage between the oil and water phase becomes very pronounced, hence the increase in the OVF in the axial direction as measured by the four conductance probes. Upon considering the axial distribution of the OVF for $U_m = 0.16$ m/s and $U_m = 0.24$ m/s, it will be observed that across all the four (4) conductance probes, there was a gradual decrease in OVF as the WC increases which was quite expected since the flow patterns observed for these flow conditions are the SW&MI and Do/w&w where there is dispersion of oil droplets and a continuous water layer in both cases. However, for $U_m = 0.32$ m/s and $U_m = 0.4$ m/s, the OVF measured by the four (4) conductance probes were almost the same up until WC = 40% and WC = 50% respectively and thereafter an abrupt decrease in OVF across all the four (4) conductance probes was observed and it is suggested that this abrupt decrease in OVF could indicate the phase inversion point. This is because on the flow pattern map, for ($U_m = 0.32$ m/s, WC = 40 %) and ($U_m = 0.4$ m/s, WC = 50%), the Dw/o&o flow pattern was observed while for the same U_m and higher WC, the Do/w&w and Do/w flow patterns were observed in the two cases respectively. Though, the Dw/o&o and Do/w&w flow patterns are not a fully dispersed flow patterns like the Do/w and Dw/o, yet one phase can be observed to be the continuous phase (oil phase) and the other phase will be the dispersed phase (water phase) and therefore the transition from the oil dominant flow pattern (Dw/o&o) where oil is the continuous phase and water is the dispersed phase to the water dominant flow patterns (Do/w&w and Do/w) where water is the continuous phase and oil is the dispersed phase can be suggested to be called the phase inversion point. It is very important to know the phase inversion point most especially for flow of oil and water mixture across pipelines or other process equipment because it will determine the phase in contact with the pipe wall which will affect its extent of corrosion and the pressure drop to be encountered in the system (Arirachakarn et al., 1989). In comparing the findings above regarding the phase inversion point with the values in literature, Mukherjee et al. (1981) observed the phase Inversion Point (PIP)

in their work at water cut (WC) between 40% -50% for all pipe inclinations except -30º, whereas Angeli and Hewitt (1998) observed the PIP at a WC between 37% - 41%. Though the values of the PIP obtained by these researchers are different from the one obtained in this current study, the difference could be attributed to the type of fluids used by the researchers with different physical properties, the size and type of pipe geometry and finally the pipe inclination.

4.5 EFFECT OF PIPE INCLINATION ON THE AXIAL DISTRIBUTION OF OIL VOLUME FRACTION (OVF)

In conducting this research, the angle of inclination was varied between +1º to +5º and and the objective was to study how the OVF responds to changes in pipe inclination.

(a)   **(b)**
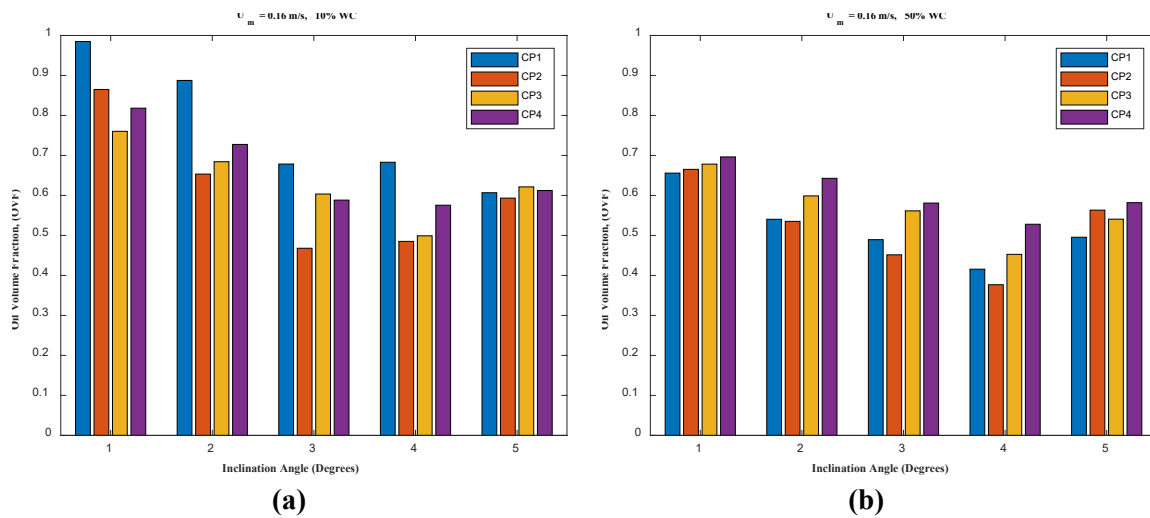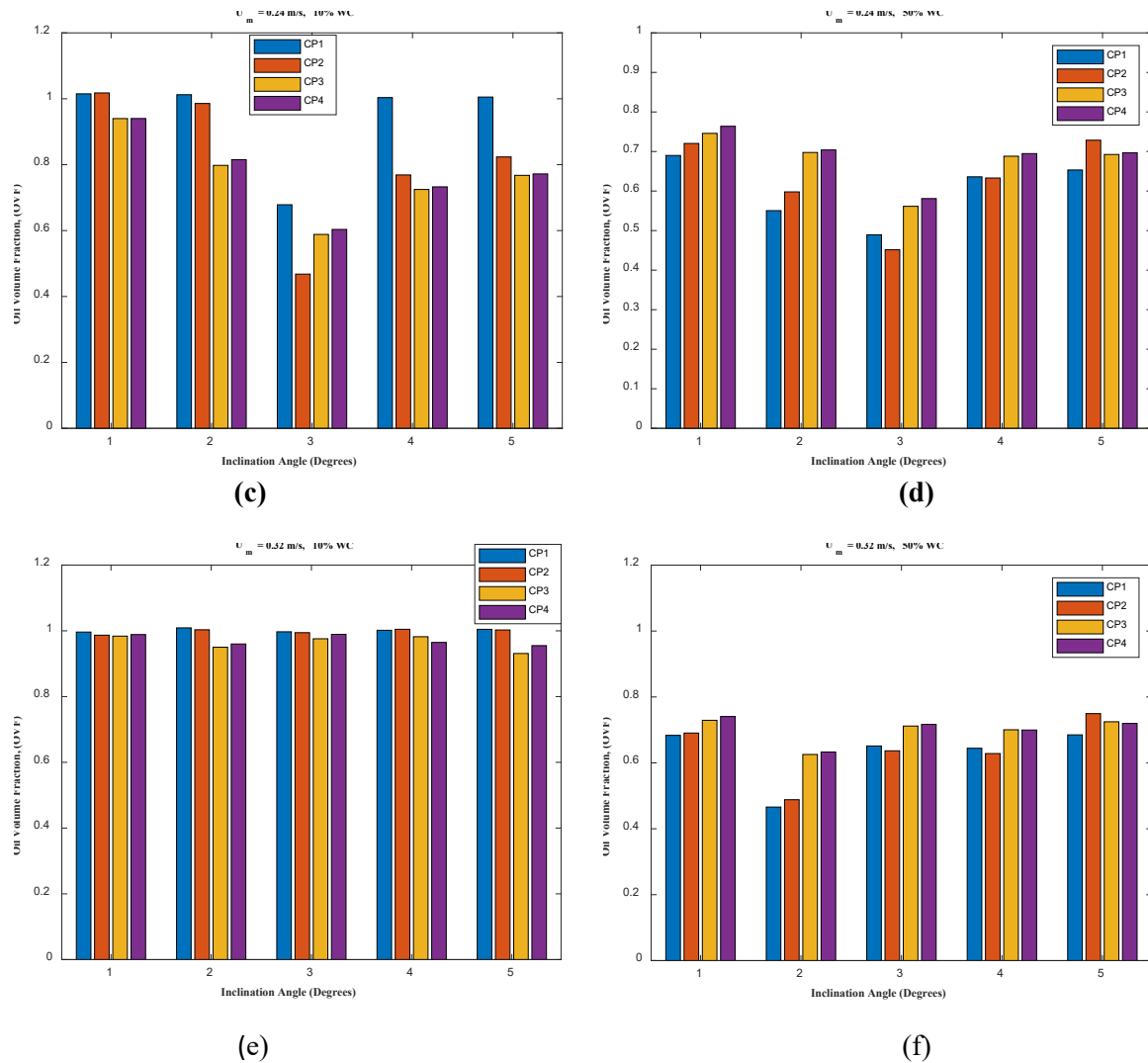
Figure 4.6: Effect of pipe inclination on oil volume fraction (OVF) (a) U_m = 0.16 m/s, WC = 10%; (b) U_m = 0.16 m/s, WC = 50%; (c) U_m = 0.24 m/s, WC = 10%; (d) U_m = 0.24 m/s, WC = 50%; (e) U_m = 0.32 m/s, WC = 10%; (f) U_m = 0.32 m/s, WC= 50%.

The Figure 4.8 above showed the effect of pipe inclination on the Oil Volume Fraction (OVF).

A little background to explain the forces at play in determining the flow across an inclined pipe

will help in understanding the phenomenon being revealed by the graphs. The predominant

forces that determines the flow of fluid through the inclined pipe includes:

- The Inertia force

- Force due to gravity

- Interfacial tension

- Shear stress (due to viscosity of the fluids)

124

For a slightly inclined pipe and for a given fluid combination (oil and water) subjected to the same flow conditions, the shear stress and the interfacial tension are assumed to be constant. Therefore, the two competing forces that govern the flow in an inclined pipe are the inertia and gravitational forces. The force due to gravity has two components i.e. the component normal to the flow direction which aids in the fluid stratification just as in a flow across horizontal pipe, while the component acting along the axis of the pipe opposes the flow for an upward inclined pipe and enhances the flow for a downward inclined pipe. The component of the fluid mixture that will experience the greater retarding force will be the denser fluid. As a consequence of the flow retardation experienced by the denser fluid, it will tend to occupy the greater portion of the cross sectional area at a particular point and therefore the greater volume fraction as compared to the less dense fluid (Lum et al., 2006, Xu et al., 2016).

From Figures 4.8 (a-f), it can be observed that the response of OVF to change in pipe inclination is a function of the mixture velocity (U_m). For instance at low mixture velocity,(U_m = 0.16 m/s) and for a given water-cut (WC = 10% and WC = 50%), the OVF decreases across all the measurements from the four (4) conductance probes (CPs) as the pipe inclination increases up to a minimum at +4º and thereafter the OVF increases for +5º pipe inclination. Similar observation was made upon increasing the mixture velocity (U_m) to 0.24 m/s but in this instance, the OVF attained a minimum at +3º. It appears that the competition for dominance between the inertial force and gravitational force seems to be the phenomenon governing the response of the OVF to changes in pipe inclination. For instance, the response of the OVF up to the minimum point (+3º and +4º) for both U_m = 0.16 m/s and U_m = 0.24 m/s respectively represents the region where the gravitational force overcomes the inertial force and therefore the action of the axial component of the acceleration due to gravity on the denser water phase becomes very significant, leading to increase in the water holdup and the corresponding decrease in the OVF. However, beyond the minimum points attained by the OVF on increasing

the pipe inclination represents the region where the inertial force overcomes the gravitational force and the effect of the axial component of the acceleration due to gravity on the denser water phase becomes less significant, leading to a decrease in the water holdup and subsequent increase in OVF.

Further, upon increasing the mixture velocity (Um) to 0.32 m/s, two interesting observations were made. First, it appears that at low water-cut (WC = 10%) and relatively high mixture velocity (U_m = 0.32 m/s),the change in pipe inclination does not seem to have a significant effect on the OVF. One possible reason for this observation is that at this flow condition and for all the pipe inclinations, the water phase appear as tiny droplets in the continuous oil phase (Dw/o&o flow pattern across all pipe inclinations) and the presence of these droplets did not seem to significantly affect the OVF measurements by the CPs. As such the OVF measured appears to be that of a continuous oil phase, hence the OVF was between 0.98 to 1.0 across all the pipe inclinations. However, on increasing the WC to 50% and for the same U_m = 0.32 m/s, the water phase becomes the continuous phase while the oil phase is the dispersed phase (Do/w&w flow pattern), hence a significant drop in the OVF as a result of the continuous water layer across all the pipe inclinations. Although, there was a small dip in the OVF at +2º OVF, but overall it appears that the OVF did not significantly change with the change in pipe inclination for the given flow condition.

4.6   VELOCITY RATIO (SLIP RATIO) BETWEEN THE WATER AND OIL PHASES

In the simultaneous flow of two or more phases, the input volume fraction and the in-situ volume fractions are not always the same and as a result, the in-situ velocities of the phases are different. Although for a very dispersed flow where the continuous phase is moving at the same velocity with the dispersed phase and based on the homogeneous theory, the input volume

fraction can be assumed to be the same as the in-situ volume fraction. However, for other flow patterns, the difference in the in-situ velocities of the phases is as a result of a phenomenon known as slip. According to Lovick(2004), the difference in the in-situ velocity between the oil and water phase could be as a result of changes in certain flow parameters such as the variations in the velocity profiles within the oil and water phases. These variations could be due to differences in the physical properties of the phases (i.e. viscosity), and the preferential wetting of the pipe wall by the phases which inevitably determines the wall contact area occupied by the phases and the eventual frictional drag experienced by the phase. Besides, the slip is also dependent on several other variables such as physical properties of the phases, pipe geometry, flow patterns and the pipe inclination (Xu et al., 2008, Hapanowicz, 2008)

The slip velocity can be determined as the difference between the in-situ velocities of the less dense phase and that of the denser phase. Alternatively, the slip ratio can be quantitatively determined as the ratio of the in-situ velocity of the less dense phase to the in-situ velocity of the denser phase. For a specific case of oil/water two-phase flow, the slip ratio can be expressed as the ratio of the in-situ oil velocity (U_o) to in-situ water velocity (U_w) since the density of the oil phase is less than that of the water phase.

$$S = \frac{\beta_o/H_o}{\beta_w/H_w} = \frac{\beta_o/\beta_w}{H_o/H_w} \tag{1}$$

The value of the slip ratio S can give an indication on which of the phases is moving faster than the other. If $S > 1$, it means that $U_o > U_w$ and the oil phase is moving faster than the water phase whereas if $S < 1$, it means that $U_w > U_o$ and the water phase is moving faster than the oil phase. However, if $S = 1$, it means that $U_o = U_w$ and both phases are moving at the same velocity and this usually occur in a fully dispersed flow where the dispersed droplets are moving at the mean velocity of the continuous phase. The slip ratio for the oil and water flow in this experimental campaign can be seen in Figure 4.9.

From figure 4.9 (a), it can be observed that the slip ratio is directly affected by the mixture velocity (U_m), water-cut (WC) and pipe inclination. Upon increasing the inclination angle from $+1^o$ to $+5^o$, the slip ratio values progressively becomes greater than one (S > 1) particularly for mixture velocities (U_m = 0.16 m/s – 0.32 m/s) and water-cuts (10% - 40%). This implies that the in-situ velocity of the oil phase becomes greater than that of the water phase as pipe inclination increases for these flow conditions, hence the oil phase travels faster than the water phase which is consistent with the findings of Scott (1985), Alkaya (2000) and Lum et al., (2004).

However, for the high mixture velocity (U_m = 0.4 m/s), the change in pipe inclination did not significantly affect the slip ratio and it was noted that for all pipe inclinations and WC, the slip ratio was below one (S < 1), suggesting that the water phase was travelling faster than the oil phase for the given flow conditions. Interestingly, the flow patterns encountered within the range of the given flow conditions are predominantly Dw/o&o flow pattern and since water is the dispersed phase, it therefore implies that the in-situ velocity of the water droplets will be greater than that of the continuous oil phase which invariably will experience the greatest drag as a result of the large contact area between the internal pipe wall and the oil phase.
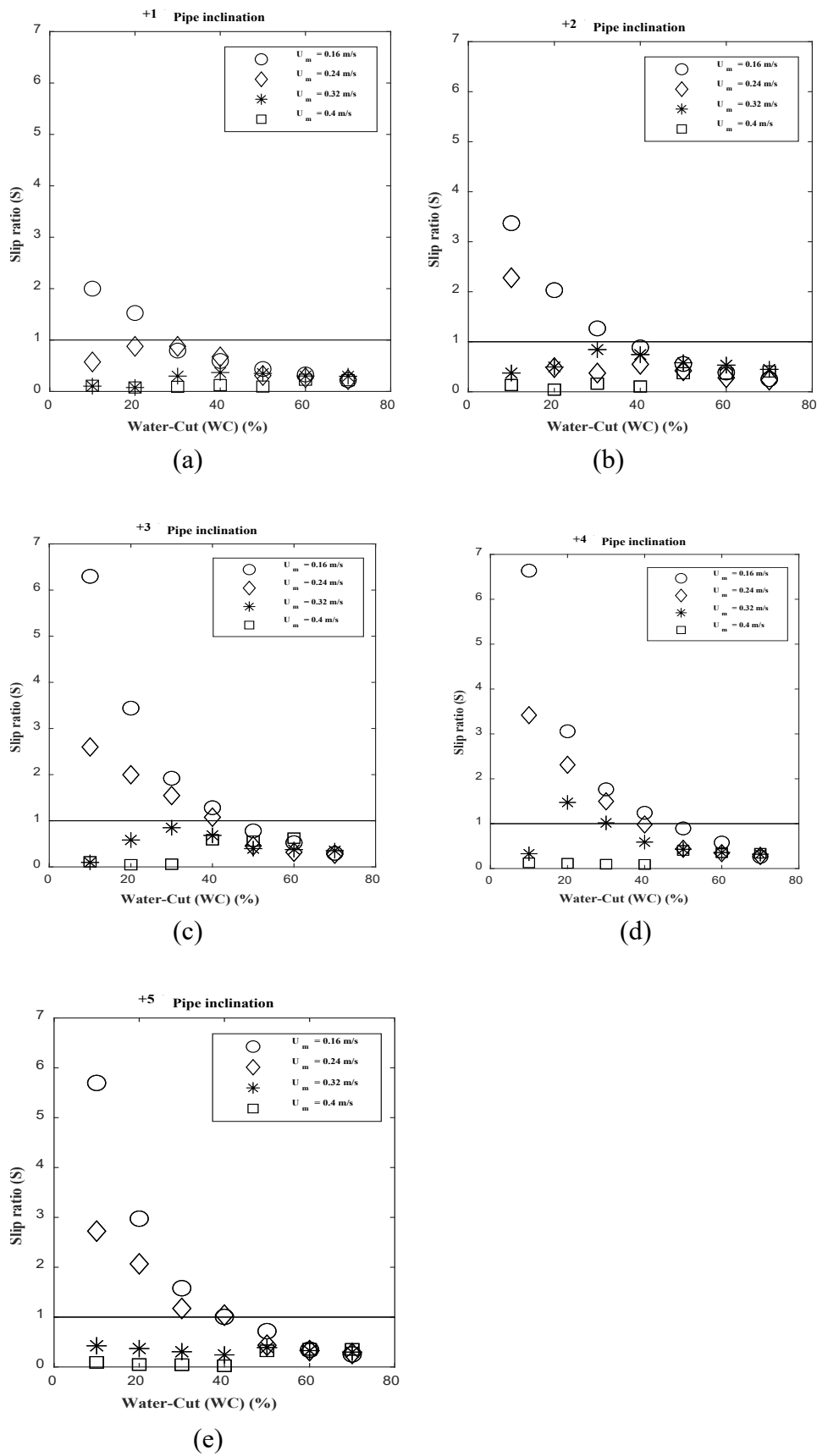
Figure 4.7: A figure showing the effect of water-cut, pipe inclination and mixture velocity on the slip ratio at 56.6D from the inlet (CP4)

129
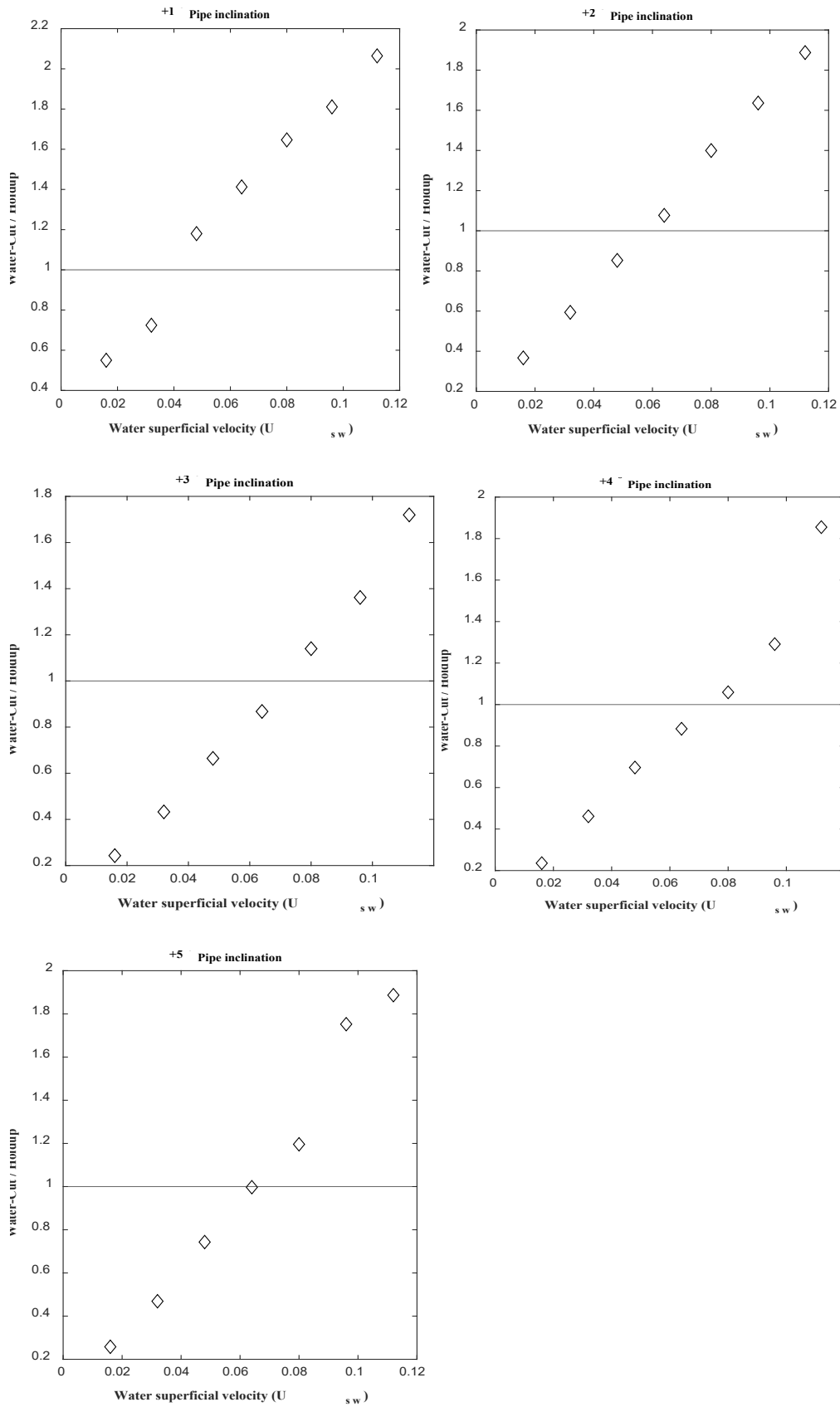
Figure 4.8: A figure showing the effect of the water superficial velocity on the oil-water slippage across the +1º , +2º, +3º, +4º and +5º pipe inclination .

In order to further understand the slippage between the oil and water phase, the concept of in-situ phase accumulation (holdup ratio) will be explored which give a relative representation of the slip between the phases and it can be represented by the ratio of the water cut and the in-situ holdup $\left(\frac{WC}{H_w}\right)$ (Trallero, 1995, Rodriguez and Oliemans, 2006; Atmaca et al; 2008).

Figure 4.10 above shows an alternative representation of the slippage between the oil and water phase. The ratio between the water-cut and the in-situ holdup can give an indication of the in-situ phase accumulation most especially for flow across an inclined pipe. By phase accumulation, reference is made to the phase that accumulates within the pipe as a result of the effect of the axial component of the gravitational force which retards its motion and therefore reduces its in-situ velocity. When $\frac{WC}{H_w} < 1$, it means that there is more phase accumulation as a result of an increase in the liquid holdup and by implication, the in-situ velocity of the more dense phase (i.e. water) had reduced and therefore the less dense phase (i.e. oil) will slip passed the water phase. However, for $\frac{WC}{H_w} > 1$, it means that there is less phase accumulation which implies that the holdup had reduced and which could probably mean that the in-situ velocity of the more dense phase (i.e. water) is higher than that of the less dense phase (i.e. oil) and finally for $\frac{WC}{H_w} = 1$, it means that the in-situ holdup is equal to the inlet holdup (water-cut) and therefore the in-situ velocity of both phases are the same and this can happen in a fully dispersed flow where the homogeneous theory can be applied. In Figure 4.10a it can be observed that at low U_{sw} (0.016 – 0.032 m/s), the $\frac{WC}{H_w} < 1$, which implies that the in-situ velocity of water phase, U_w is less than the in-situ velocity of the oil phase, U_o. However, as the U_{sw} increases beyond 0.032 m/s, the $\frac{WC}{H_w} > 1$, meaning that the $U_w > U_o$ and all of these findings are consistent with the previous findings in Figure 4.9a. Moreso, as the pipe inclination increases from +1° to +5°, it can be observed that more of the points fell below the unity line (i.e. $\frac{WC}{H_w} < 1$) which imply that

there is a phase accumulation of the water phase which causes the holdup to increase with pipe inclination. The increase of the holdup could be as a result of the action of the axial component of the gravitational force on the water phase because of its higher density and thereby retarding its in-situ velocity which inevitably leads to its accumulation.

4.7 SUMMARY

In this chapter, a T-type fluid inlet device was employed, leading to the identification of four distinct flow patterns: stratified wavy with mixing at the interface (SW&MI), dispersed oil in water and water (Do/w&w), dispersed water in oil and oil (Dw/o&o), and dispersed oil in water (Do/w). Flow pattern maps were developed for different pipe inclinations (+1° and +5°), showing that an increase in inclination from +1° to +5° shifted the flow pattern transition line leftward, expanding the regions dominated by water-dominant flow patterns (Do/w and Do/w&w).

The flow pattern maps generated in this study were compared with those from Kumara et al. (2009) and Pereira et al. (2019), and key differences were observed. These discrepancies were attributed to variations in fluid properties, pipe geometry, and the use of an inlet plate by Kumara et al. and Pereira et al., which promoted fluid stratification.

A comparison between in-situ water holdup and inlet water cut (WC) was also performed. It was found that at low WC (10%–40%) and mixture velocities (Um = 0.16 m/s and Um = 0.24 m/s), in-situ water holdup were greater than the WC as pipe inclination increased from +1° to +3°. However, at higher mixture velocities (Um = 0.32 m/s and Um = 0.4 m/s), and across all WCs, in-situ water holdup was lower than the inlet WC.

A detailed analysis of the effect of inlet WC and pipe inclination on the axial distribution of oil volume fraction (OVF) was conducted. It was observed that OVF decreases as both WC and pipe inclination increase. Additionally, a comprehensive discussion on the slippage

characteristics of oil/water two-phase flow highlighted the significant influence of mixture velocity and pipe inclination on the slip ratio between the oil and water phases. For instance, with an increase in inclination angle from +1° to +5°, the slip ratio progressively exceeded one (S > 1), particularly at mixture velocities of 0.16 m/s to 0.32 m/s and water cuts of 10% to 40%.

CHAPTER 5

EFFECT OF FLUID INLET DEVICE ON OIL-WATER TWO PHASE FLOW CHARACTERISTICS.

5.1   INTRODUCTION

The hydrodynamic characteristics (flow patterns, void fraction and pressure drop) of oil-water two-phase flow is dependent on several factors one of which is the design of the fluid inlet device. In order to form the two-phase oil-water flow mixture, single phase oil and water flow separately and then combine at the fluid inlet device. The manner in which the two streams combine in the fluid inlet device will determine whether the initial flow pattern formed will be dispersed or separated flow and according to Mandal et al., (2007) the initial configuration of the two-phases once formed does not change far downstream as a result of the inertia of motion of the fluids. Also, according to Mandal et al., (2007), Kawaji et al., (2009) and Ibarra et al., (2015), the fluid entrance design exerts great influence in the geometrical distribution of the fluids (flow patterns) and its corresponding transition boundaries. As a result, this chapter seeks to present the experimental findings that examines the dependence of the hydrodynamic characteristics such as the flow pattern, flow pattern transition boundaries, liquid holdup and the slip velocity on three (3) configurations of the fluid inlet device. The T-type inlet mixer design which could also be referred to as the first fluid inlet device which allows the oil and water to contact and mix from the opposite direction in the horizontal plane. The Y-type inlet mixer design without a split plate also referred to as the second fluid inlet device was designed such that the oil flowed from the top while the water flowed from the bottom and the two inlet holes form an external angle of 90° with the centre line. Finally, the Y-type inlet mixer design with a split plate also referred to as the third fluid inlet device (third mixer) is similar to the second mixer except that a split plate was added to keep the oil and water flow separated until they get to the test pipe where mixing occur.

5.2   EFFECT OF THE FLUID INLET DEVICE ON THE FLOW PATTERNS

The three (3) different fluid inlet devices were used to introduce the oil and water flow into the test section and for similar operating conditions, the flow patterns were identified using both visual observation and the images from the high speed camera. The flow pattern observations and the flow images were taken through the viewing box filled with water and located at position 4.5 m (35.4D) from the fluid inlet device (where the flow is assumed to be fully developed). For a given pipe inclination (i.e. $+1^{\circ}$), four (4) flow patterns which includes stratified wavy with mixing at the interface (SW&MI), dispersed oil in water and water (Do/w&w), dispersed water in oil and oil (Dw/o&o) and dispersed water in oil (Dw/o) were observed when the first fluid inlet device was used. While for the same flow condition and pipe inclination, five (5) flow patterns were identified which includes stratified smooth (ST), stratified smooth with mixing at the interface (ST&MI), dispersed oil in water and water (Do/w&w), dispersed water in oil and oil (Dw/o&o) and dispersed water in oil (Dw/o) when the second fluid inlet device was used and finally for the third fluid inlet which is similar to the second fluid inlet device but with a split plate, only three (3) flow patterns were identified and they include stratified smooth (ST), stratified wavy (SW) and stratified wavy with mixing at the interface (SW&MI). The summary of all the flow patterns observed for $+1^{\circ}$ pipe inclination can seen in Table 5.1 and Figure 5.1 respectively.

Table 5.1 Flow patterns observed for each of the fluid inlet device used at $+1^{\circ}$ pipe inclination

First fluid inlet device	Second fluid inlet device	Third fluid inlet device (with split plate)
SW&MI	ST	ST
$D_{o/w\&w}$	ST&MI	SW
$D_{w/o\&o}$	$D_{o/w\&w}$	SW&MI
$D_{w/o}$	$D_{w/o\&o}$	
	$D_{w/o}$	

135
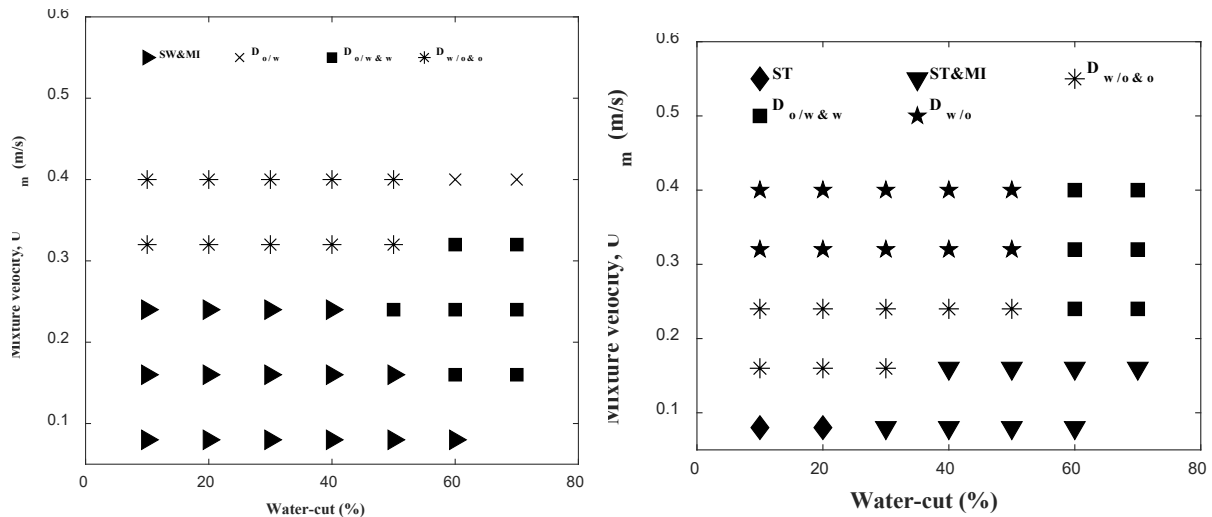
(a)

(b)
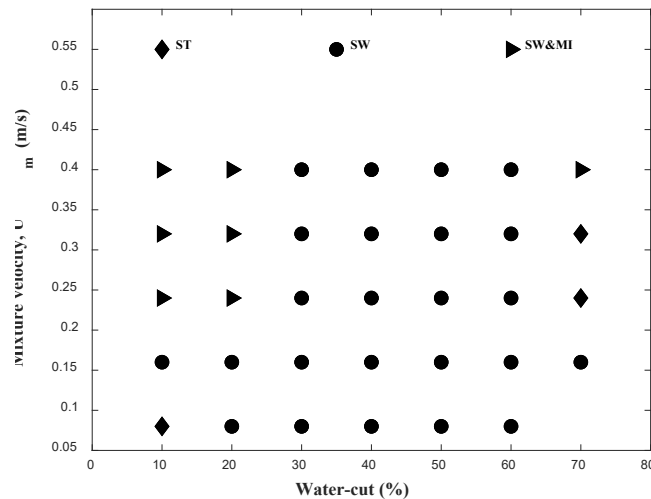
(c)

Figure 5.1: Flow patterns observed at +1° pipe inclination for (a) T-type fluid inlet device (First mixer) (b) Y-type fluid inlet device with no split plate (Second mixer) and (c) Y-type fluid inlet device with split plate (Third mixer).

In figure 5.1a-c, the influence of the fluid inlet device on the distribution of oil and water phases can be clearly seen. For instance, in figures 5.1a and 5.1b, the fluid inlet device used permits the oil and water phases to contact and mix before flowing into the test pipe, hence both the separated flow patterns (ST, ST&MI and SW&MI) and the dispersed flow patterns ($D_{o/w\&w}$, $D_{w/o\&o}$ and $D_{w/o}$) are formed depending on the input flow rates of the oil and water phases.

Although, both the separated and dispersed flow patterns were observed in the first and second fluid inlet device (fluid inlet devices), one may note that in figure 5.1a, stratified smooth (ST) flow pattern was never observed. For all the observed flow patterns (SW&MI, $D_{o/w\&w}$, $D_{w/o\&o}$ and $D_{w/o}$), there appears to be an agglomeration of droplets along the interface or the dispersion of droplets of one phase into another. This implies that the design of the first fluid inlet device (first fluid inlet device) favours the generation of droplets due to the high impact force created when the oil and water streams flowing from the opposite direction in the horizontal plane contact each other. Thus, the initial flow patterns formed will be dependent on the distribution of these droplets in the continuous phase which is also a function of the inlet velocity of the phases.

Further, on replacing the first fluid inlet device (first fluid inlet device) with the second fluid inlet device (second fluid inlet device) while keeping all other flow conditions and pipe inclination constant, one may observe remarkable change in the number and type of flow patterns encountered. For instance, stratified smooth (ST) flow pattern was observed which indicates that at low water cut (10% - 20%) and low mixture velocity (0.08 m/s), the interface was smooth with no droplets, suggesting the presence of small disturbance along the interface. The design of the second fluid inlet device (second fluid inlet device) which allows the oil stream to flow from the top at an angle to the bottom water stream ensures a smooth contact between both streams and at low water cut (10% - 20%) and low mixture velocity (0.08 m/s), separated flow is maintained with no evolution of droplets, but at higher mixture velocities, fluid dispersion occurs where the droplets of one fluid appear in the continuous layer of the other fluid and flow patterns such as ST&MI, $D_{o/w\&w}$, $D_{w/o\&o}$ and $D_{w/o}$ are formed.

However, the flow pattern map shown in figure 5.1c which was obtained using the third fluid inlet device (third fluid inlet device) showed only three (3) flow patterns which are all separated flow patterns (ST, SW and SW&MI) and no any form of dispersed flow patterns were observed.

This observation clearly showed that the presence of the split plate at the fluid inlet device serves to keep the oil and water flow separated and minimizes the mixing of the two streams even for higher mixture velocities and water-cut, thus the flow patterns formed all have continuous oil and water layer at the top and bottom with a smooth (ST) or wavy (SW) interface containing some droplets in some cases (SW&MI). This observation is consistent with the work of Kumara et al., (2009) who used a split plate in the fluid inlet device and observed separated flow regime (ST&MI) for similar experimental condition with the current work, but for higher mixture velocities and water-cut beyond the range of the current work, the researchers observed dispersed flow patterns. However, in contrast to Barral (2014) where he observed that the split plate had a detrimental effect to fluid stratification by reducing the region in the map where stratified flow exist and also by suppressing the evolution of 2D waves at the junction, experimental observations from this work showed clearly that the presence of the split plate enhanced fluid stratification and greatly reduce dispersion of one fluid into the other and also interfacial waves evolve on increasing the water-cut and mixture velocity, thus SW flow pattern was observed in the current work. The reason for the differences between the current work and that of Barral (2014) could probably be due to the large diameter pipe and low fluid flow rates used in the current.

The observations made thus far in this current work is in agreement with the observations made by Kawaji et al., (2009) and Ibarra et al., (2015) where the fluid inlet device was said to determine the flow patterns for a co-current two-phase. For instance, for the first fluid inlet device (first fluid inlet device)at both low and high mixture velocities and water-cut, fluid stratification was not favoured, rather droplets were formed which favours the formation of the dispersed flow patterns as a result of the manner in which the fluids contact within the fluid inlet device. Again, for the second fluid inlet device (second fluid inlet device), the design favours fluid stratification at low mixture velocity and water-cut, thus separated flow patterns

are formed while at high mixture velocities and water-cut, droplets are formed and this favours the formation of the dispersed flow patterns. However for the third fluid inlet device (third fluid inlet device) containing the split plate, the design favours the formation of separated flow patterns where continuous fluid layers appear at the top and bottom of the pipe with a smooth or wavy interface and occasionally containing some droplets at the interface.

5.3   EFFECT OF PIPE INCLINATION ON THE FLOW PATTERN BOUNDARIES FOR THE THREE FLUID INLET DEVICES.

In this section, attempt will be made to understand how the change in pipe inclination will affect the flow pattern transition boundaries for each of the three fluid inlet devices. The flow pattern maps at $+1^\circ$ and $+5^\circ$ pipe inclinations for each of the three fluid inlet devices can be seen in figures 5.2, 5.3 and 5.4 respectively.
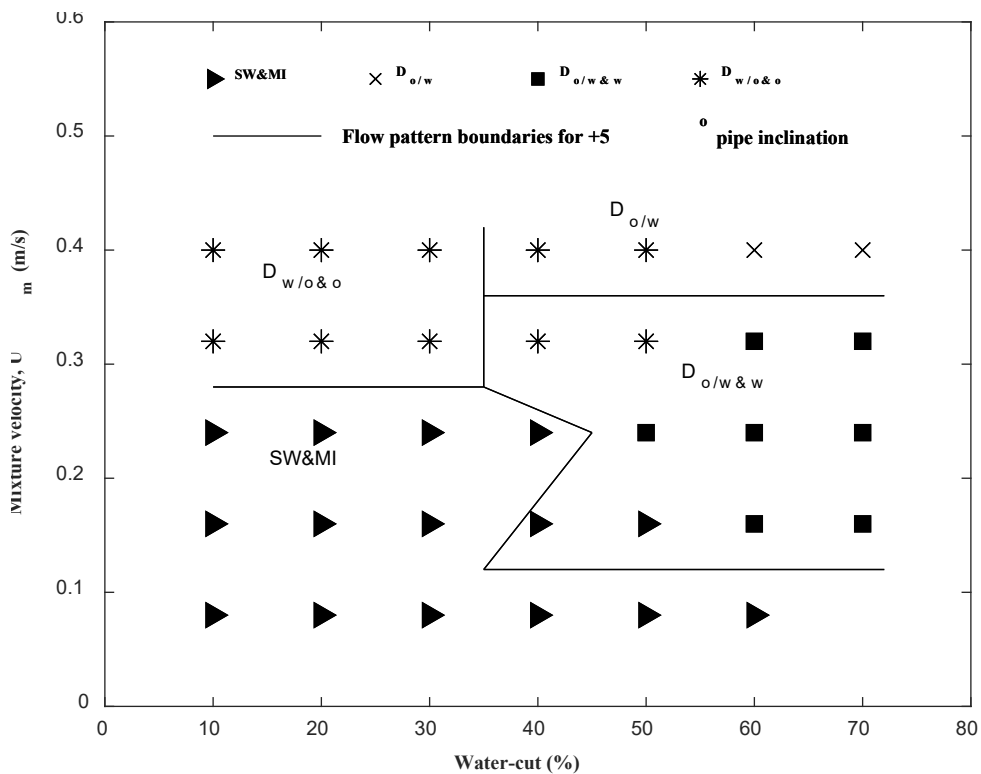
Figure 5.2: Flow pattern map for the T-type fluid inlet device (first fluid inlet device) at $+1^\circ$ pipe inclination with the flow pattern boundaries at $+5^\circ$ pipe inclination superimposed.

In figure 5.2, one may notice that on increasing the pipe inclination from +1º to +5º, the flow pattern transition boundary between the SW&MI and Do/w&w flow patterns shifted towards the left at higher pipe inclination (+5º) where the region occupied by the Do/w&w flow pattern increased at +5º compare to that of +1º. Similarly, the transition boundary between the Dw/o&o and Do/w flow patterns shifted towards the left and the region occupied by the Do/w flow patterns enlarges at +5º when compared to +1º pipe inclination. These observations suggest that increasing the pipe inclination enhances the disturbance at the oil and water interface and it had been agreed by several researchers (Oddie et al., 2003; Lum et al., 2004; Kumara et al., 2009 and Perera et al., 2019) that as a consequence of increased disturbance, fluid dispersion appear at lower velocities in inclined flows than in horizontal flows, thus the dispersed flow patterns (Do/w&w, Dw/o&o and Do/w) appeared at lower water-cut at +5º pipe inclination than +1º pipe inclination. Also, on increasing the pipe inclination from +1º to +5º, the parallel component of the gravitation force retards the flow of the water phase which is denser leading to the accumulation of water (higher water holdup), hence the water-dominant flow patterns (Do/w&w and Do/w) observed occupied larger areas at higher inclination angles (+5º) compared to similar observation at +1º pipe inclination.
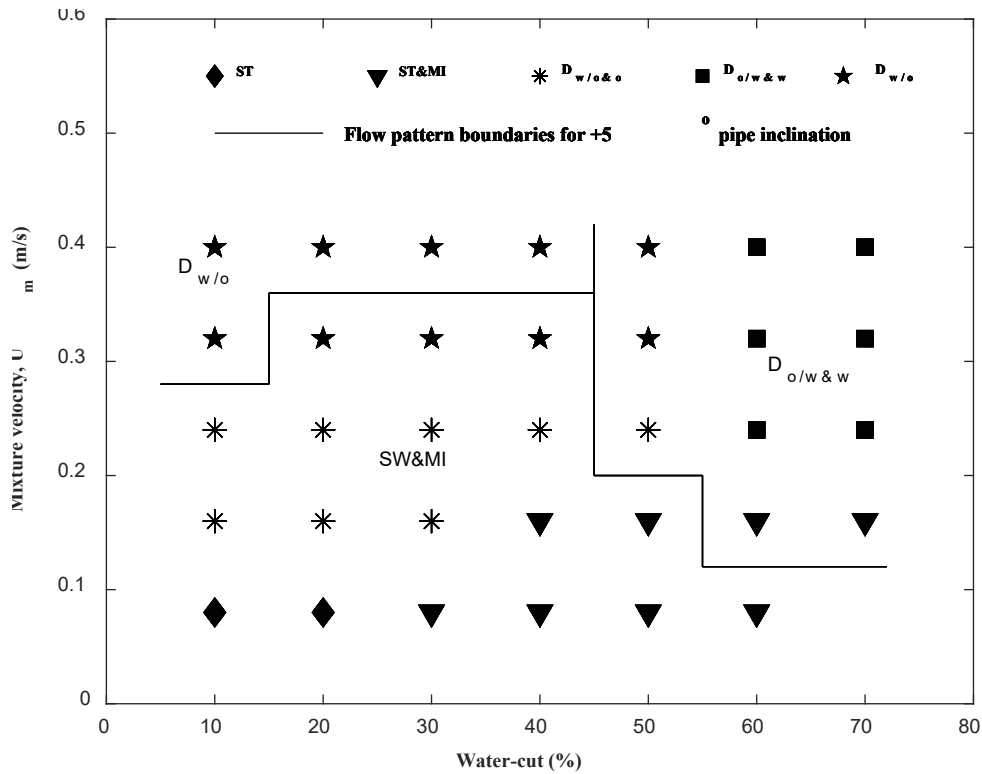
Figure 5.3: Flow pattern map for the Y-type fluid inlet device with no split plate (second fluid inlet device) at +1º pipe inclination with the flow pattern boundaries at +5º pipe inclination superimposed.

In figure 5.3, the flow pattern maps obtained using the second fluid inlet devices (second fluid inlet device) at +1º and +5º pipe inclinations are presented. On increasing the pipe inclination from +1º to +5º, remarkable changes in the number and types of flow patterns including their transition boundaries can be observed. For instance, at +1º pipe inclination, five (5) flow patterns namely stratified smooth (ST), stratified smooth with mixing at the interface (ST&MI), Dispersed oil in water and water (Do/w&w), dispersed water in oil and oil (Dw/o&o), and finally dispersed water in oil (Dw/o) were observed. While at +5º pipe inclination, only three (3) flow patterns namely stratified wavy with mixing at the interface (SW&MI), dispersed oil in water and water (Do/w&w) and dispersed water in oil (Dw/o) were observed. Besides the differences in the number of flow patterns observed between the +1º and +5º pipe inclinations, one may notice also that at +1º pipe inclination, less interfacial disturbances are encountered at low mixture velocity ($U_m = 0.08$ m/s) and the flows are gravity-dominated, therefore ST flow

pattern was observed at 10-20% water-cut. However, on increasing the water-cut, interfacial disturbances increases which results in droplets formation and the droplets were seen to agglomerate around the smooth interface, thus ST&MI flow patterns were observed between 30%-60% water-cut. Further, on increasing the mixture velocity to 0.16 m/s and above, dispersed flow patterns were observed where there is a dispersion of one fluid into the other.

On increasing the pipe inclination from +1º to +5º while maintaining similar flow conditions, ST or SW flow patterns were not observed, rather SW&MI flow pattern was identified even at the lowest mixture velocity (0.08 m/s) and lowest water-cut which suggest an increase in flow disturbance as a result of increase in pipe inclination. Also, on the +5º flow pattern map, one may notice an increase in the region occupied by the water-dominant flow pattern (Do/w&w) and a decrease in the region occupied by the oil-dominant flow pattern (Dw/o) in comparison with that of the +1º flow pattern map and it is as a result of the effect of the axial component of the acceleration due to gravity acting on the denser water phase which reduces its velocity leading to the accumulation of the denser water phase (Increased holdup).
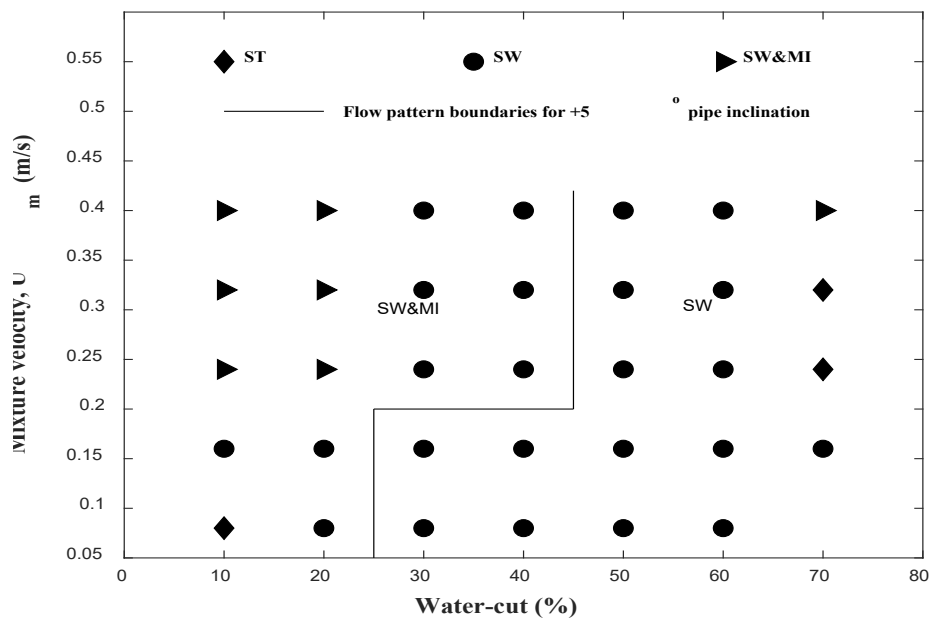
Figure 5.4: Flow pattern map for the Y-type fluid inlet device with split plate (second fluid inlet device) at +1º pipe inclination with the flow pattern boundaries at +5º pipe inclination superimposed.

In figure 5.4, the flow pattern maps for the third fluid inlet devices (third fluid inlet device) are presented for the +1° and +5° pipe inclinations respectively. Interestingly, separated flow patterns (ST, SW and SW&MI) were observed at both +1° and +5° pipe inclinations which is quite expected owing to the effect of the split plate which tends to keep the flow separated at the inlet. However, there are important points to note for the +1° pipe inclination which includes the observation of the ST flow pattern, large region of the map occupied by SW flow pattern and finally a small region of the map occupied by the SW&MI flow pattern. These observations suggest that high interfacial disturbances were only encountered within a limited region (U$_m$ $\geq 0.24\ m/s\ and\ 10\% - 20\%\ WC$) where droplets were formed around the interface (SW&MI), but for the remaining portion of the map, the interfacial disturbances were small and flows were completely separated with either a smooth or wavy interface (ST or SW). But for the +5° pipe inclination, the flow disturbance was enhanced as a result of the increase in pipe inclination and as such no ST flow pattern was observed and there was considerable increase in the region of the map occupied by the SW&MI flow pattern (10% - 20% WC for U$_m$ $\leq$ 0.16 m/s and 10% - 40% WC for U$_m$ $\geq 0.24\ m/s$) and a corresponding reduction in the region of the map occupied by the SW flow pattern.

5.4 RELATIONSHIP BETWEEN THE OIL VOLUME FRACTION (OVF) AND FLOW PATTERN TRANSITION FOR THE DIFFERENT DESIGNS OF THE FLUID INLET DEVICES

The change in the distribution of the oil phase within a given pipe cross-section as measured by the conductance probe (CP) have been observed to relate directly with the region where transition from one flow pattern to the other occur.
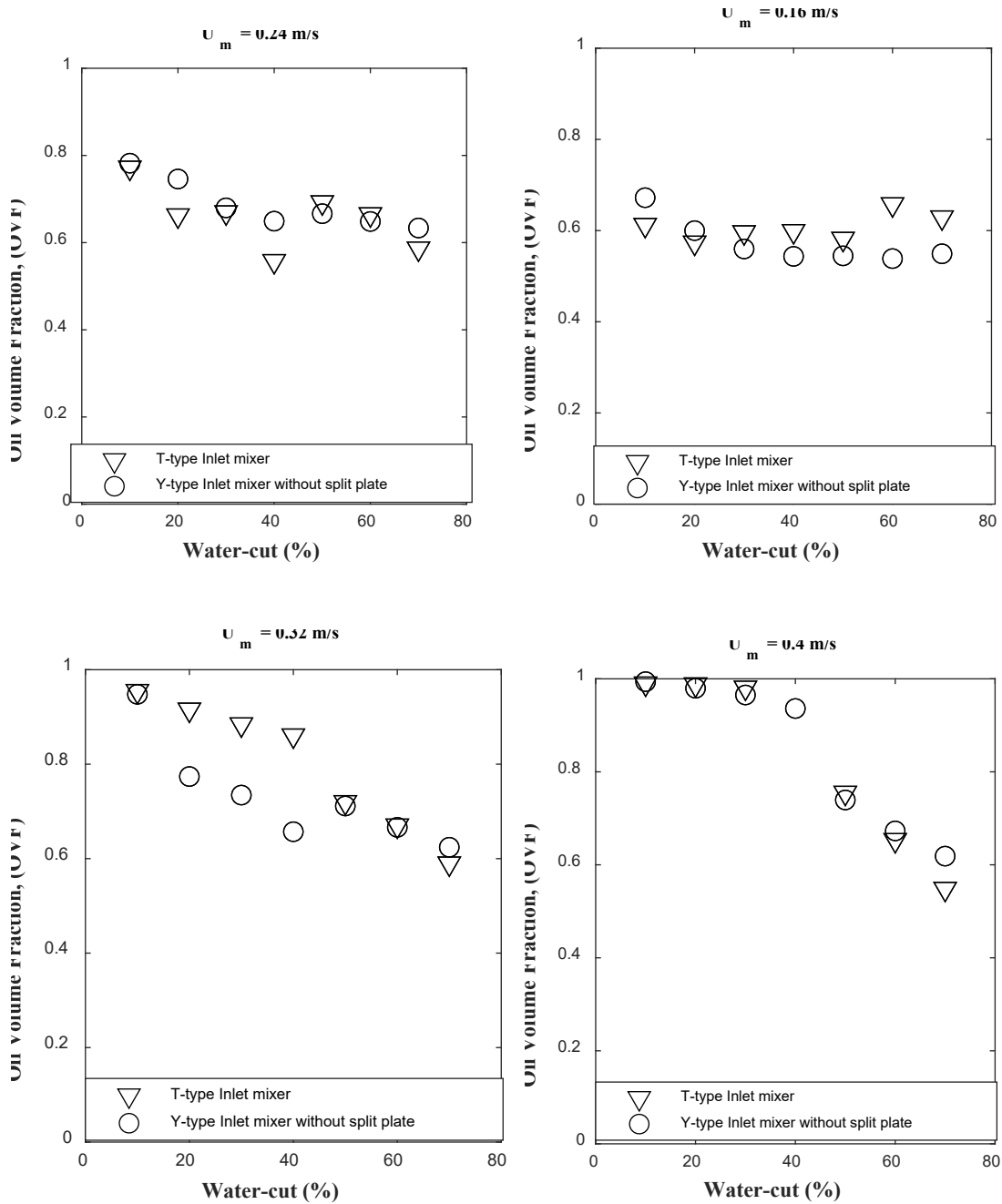
Figure 5.5: The distribution of Oil Volume Fraction (OVF) on using the first and second fluid inlet devices at +5° pipe inclination.

Figure 5.5 depicts the distribution of the OVF as the water-cut (WC) and mixture velocity (U_m) changes while using the first and second fluid inlet devices for the +5° pipe inclination. The distribution of OVF across these two fluid inlet devices are compared because both mixers do not have a split plate and the oil and water flow streams contact right within the fluid inlet device. The only difference is that the first fluid inlet device is a form of a T-junction while the

second fluid inlet device is a form of a Y-junction. In figure 5.5, it will be observed that for Um = 0.16 m/s, the OVF reduces though marginally on increasing the WC for the first fluid inlet devices (first fluid inlet device) which was quite expected up till WC = 50% and then there was a sudden increase in OVF from WC = 60% which indicates a change in the distribution of OVF and might possibly suggest flow pattern transition. Interestingly, on the flow pattern map, a flow pattern transition was seen to have occurred earlier at WC = 40% between SW&MI and Do/w&w. The discrepancy between the transition point on the flow pattern map and the OVF distribution plot is that on the basis of physical observation, the Do/w&w first appeared at WC = 40%, a further increase in the WC did not appreciable led to an increase in the oil dispersion and the OVF remained almost constant until the WC was increased to 60% where there was a sudden increase in the oil dispersion as a result of increased turbulence in the water phase, thus an increase in the OVF. However, for the second fluid inlet device, a sudden increase in OVF at WC = 60% coincided with the point on the flow pattern map where a transition from SW&MI and Do/w&w occurred.

Further, on increasing the mixture velocity from U_m = 0.16 m/s to U_m = 0.24, the OVF distribution using the two fluid inlet devices are very similar. In fact, a decrease in OVF as WC increases was observed up till WC = 40% which correspond to the region where the SW&MI flow pattern appeared on the flow pattern maps using both the first and second fluid inlet devices. A sudden increase in OVF from WC =50% was observed for the first and second fluid inlet devices which corresponds to the point where the flow pattern transition from the SW&WI to Do/w&w occurred. Similar observation can also be made on increasing the mixture velocity to U_m = 0.32 m/s and U_m= 0.4 m/s. However, for U_m = 0.4 m/s, the OVF remained constant on increasing WC up till WC = 30% and thereafter it dropped abruptly from WC > 50%. The abrupt decrease in the OVF correspond to the Dw/o&o flow pattern transition to Dw/o flow pattern.
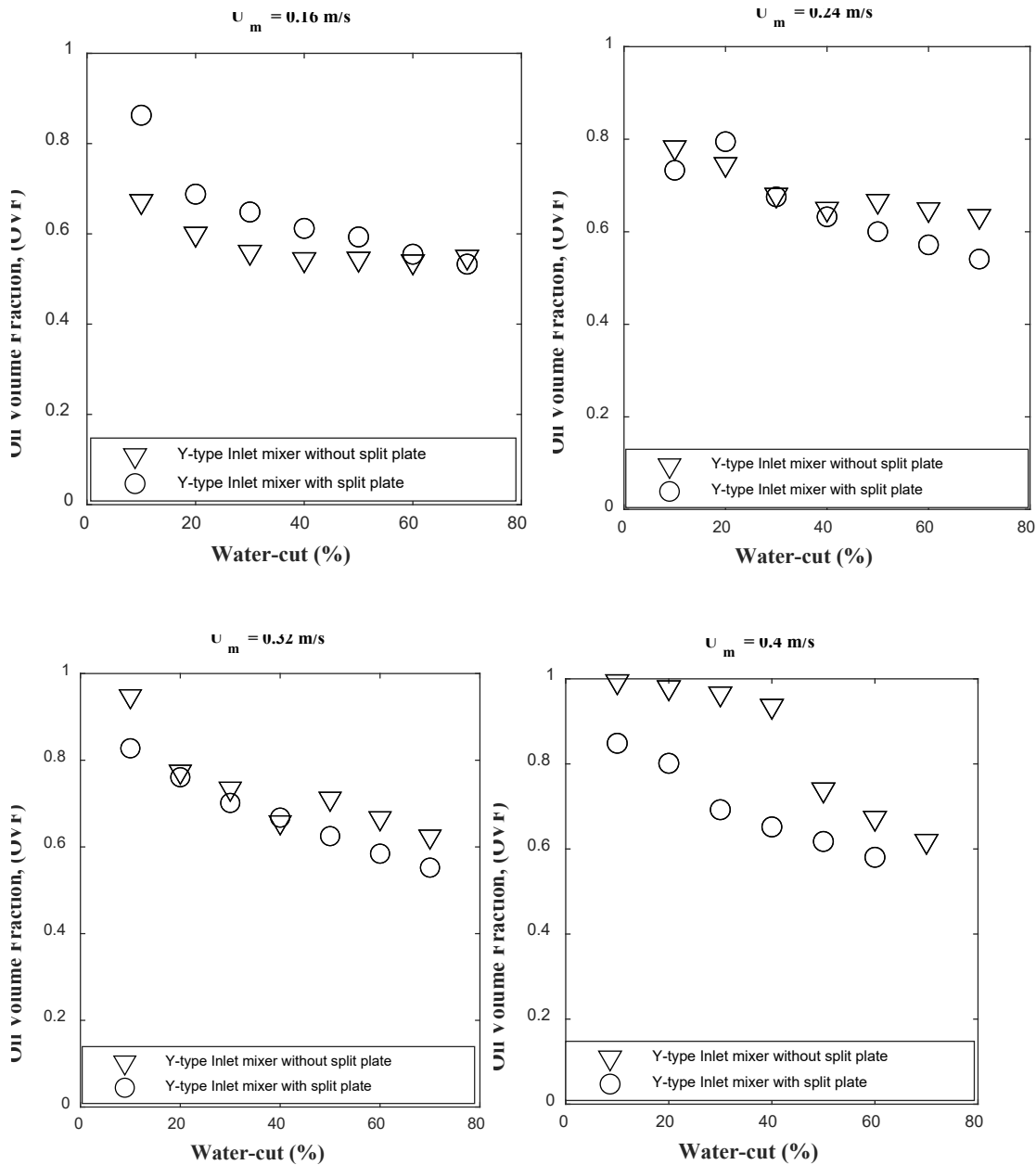
Figure 5.6: The distribution of OVF on using Y-type fluid inlet devices with and without the split plate at +5° pipe inclination.

Figure 5.6 presents the OVF distribution and how it is been affected by changes in water-cut (WC) and mixture velocity (U_m). Similar observations made in figure 5.5 which involve the use of the first and second fluid inlet devices can equally be extended to figure 5.6 which equally involves the use of the second and third fluid inlet devices. It will be observed that for low mixture velocity, $U_m = 0.16$ m/s, the OVF decreased progressively on increasing the water-

cut and the trend did not give any indication of a flow pattern transition when using the third fluid inlet devices (third fluid inlet device). However, on the flow pattern map, SW&MI flow pattern transitioned to SW flow pattern at WC = 30% which indicates that the change in the distribution of OVF cannot be used to accurately predict the flow pattern transition between SW&MI and SW flow patterns for the third fluid inlet devices (third fluid inlet device). However, for the second fluid inlet devices (second fluid inlet device), similar decrease in OVF was observed on increasing the WC, but there was a marginal increase in OVF at WC > 50% which suggest a change in the phase distribution indicating the possibility of a flow pattern transition. On comparing with the flow pattern map, it was observed that a flow pattern transition between SW&MI and Do/w&w flow patterns occurred at WC > 50%.

Further, on increasing the mixture velocity (U_m) to 0.24 m/s, 0.32 m/s and 0.4 m/s, similar observations were made of a sudden increase in OVF at WC > 40% for Um = 0.24 m/s and Um = 0.32 m/s which corresponds to a flow pattern transition between SW&MI and Do/w&w flow patterns in both cases using the second fluid inlet devices (second fluid inlet device). Meanwhile, for the third fluid inlet devices (third fluid inlet device), it was observed that there was a continuous decrease in OVF as the WC increases for all the mixture velocities (Um = 0.24 m/s, 0.32 m/s and 0.4 m/s) and there was no any indication of an abrupt change in OVF with respect to the WC which could probably indicate a flow pattern transition. However, on the flow pattern map, a flow pattern transition between the SW&MI and SW for all the mixture velocities occur at WC = 30%. Therefore, it can be said that the flow pattern transition between SW&MI and SW cannot be adequately predicted using the change in the distribution of OVF as the WC changes.

5.5 TIME SERIES OF THE OIL VOLUME FRACTION (OVF) AND THE PROBABILITY DENSITY FUNCTION (PDF) FOR THE DIFFERENT FLUID INLET DEVICES.

In order to gain further insight in the distribution of the oil and water phases within the pipe section when using the different designs of fluid inlet devices, the statistical analysis of the OVF- time series data will be carried out. The Probability Density Function (PDF) will be used as the main statistical tool to analyse the OVF-time series data which will produce a histogram whose shape and size will give an indication of the distribution of OVF and a characteristic signature of the flow pattern encountered.

5.5.1 Time Series Plots of OVF On Using The T-type Fluid Inlet Device (First Fluid inlet device)

The plots of the time series of the OVF for the first fluid inlet devices can be seen in Figure 5.7.
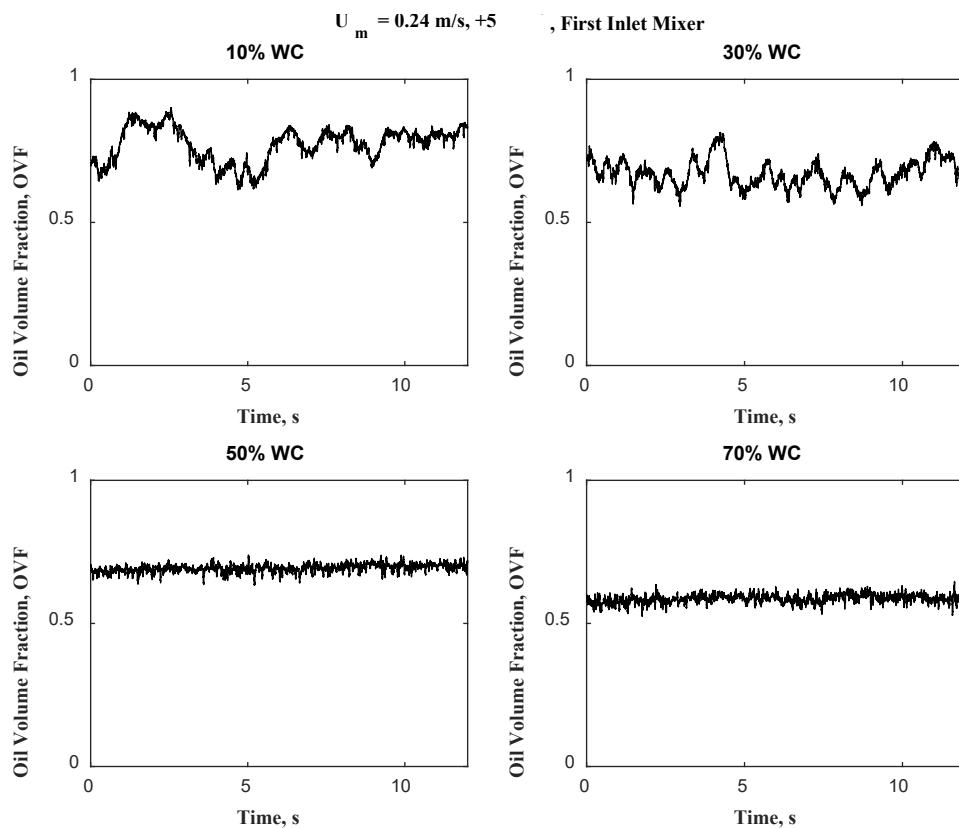
Figure 5.7: Time series of the oil volume fraction (OVF) for the T-type fluid inlet device at +5° pipe inclination using the mixture velocity, U_m = 0.24 m/s.

Figure 5.7 depicts the evolution of the OVF with time for a given mixture velocity (U_m = 0.24 m/s) and four (4) different values of water-cut (WC) ranging from low WC (10% - 30%), medium WC (50%) and high WC (70%) for a +5° pipe inclination. It will be noticed that the signature of the time series at 10% WC and 30% WC are similar where there is a wide fluctuation of the OVF as a result of the waves present along the interface as shown on the chart. Similar observation can also be made for the time series data at 50% WC and 70% WC which are quite similar and the OVF fluctuated within a smaller range such that the interface seems to be devoid of any well-defined wavy structure. However, from experimental observation, it was noticed that at U_m = 0.24 m/s and 10% WC, interfacial waves of large amplitude were present along the interface bounded by a continuous layer of oil and water at the top and bottom respectively. Also, along the wavy interface, oil droplets of different sizes were seen floating and moving with the interface. On increasing the WC to 30%, the thickness of the continuous water layer increases while the interfacial waves were still present but with reduced amplitudes. Also as a result of the increased turbulence within the water layer, more oil droplets appear along the interface. The presence of interfacial waves and droplets of different sizes along the oil-water interface for WC 10% and 30% accounts for the wide fluctuations observed on the OVF-time series charts.

Further, on increasing the WC from 30% to 50%, it was observed that as a result of the increased turbulence in the water phase, the continuity of the oil phase was broken and the oil droplets were seen dispersed in the continuous water layer with yet another continuous water layer where no oil droplets were observed. Similar observation was also made on increasing the WC to 70%. The presence of the oil droplets of different sizes flowing in the continuous water phase accounts for the small fluctuations in the OVF-time series chart shown in figure 5.7.

Figure 5.8: The Probability Density Function (PDF) of the OVF showing its distribution and characteristic signature at $U_m = 0.24$ m/s and +5° pipe inclination using the T-ype fluid inlet devices (first fluid inlet device).

Figure 5.8 showed the PDF as a function of the Oil Volume Fraction (OVF) which gives an indication of how the OVF is distributed within the given pipe section for a particular time interval. It will be noticed that the characteristic signature of the histograms at 10% WC and 30% WC are similar because in both cases, the histogram forms a dome asymmetrical shape where several prominent peaks can be noticed within the OVF range (0.65 – 0.9) and (0.6 – 0.8) for 10% WC and 30% WC respectively and these occur as a result of the interfacial waves and the presence of oil droplets of different sizes along the interface which creates the variability in the measurement of OVF. On critically examining the shape of the time series charts and their corresponding PDFs as a function of the OVF for the 10% WC and 30% WC, one may infer that the flow pattern identified will likely be the SW&MI and this is consistent with flow pattern map at these conditions. The shape of the PDF curve produced by the group

of histograms in the present study which characteristically identify the SW&MI flow pattern is similar to that of Jana et al., (2007) who identified the Mixed (Three layer) flow pattern. The description of the Mixed (Three layer) flow pattern by Jana et al., (2007) is similar to the SW&MI flow pattern observed in the current study, hence the similarity in the shape of the corresponding PDF curves.

However, on increasing the WC from 30% to 50% and subsequently to 70%, a significant change in the shape of the PDF curves were observed. For instance, the number of the prominent peaks had reduced significantly, the width of the curves had equally reduced and the curves appear to be symmetrical about specific OVF values of 0.7 and 0.6 (points where the highest peaks were observed) corresponding to 50% WC and 70% WC respectively. The shape of the time series curves and that of the PDFs as a function of the OVF at 50% WC and 70% WC are consistent and they correspond to the Do/w/w flow pattern on the map at these flow conditions. The highest peaks in both cases corresponds to the measurement of OVF of the finely dispersed oil droplets in the continuous water layer with another water layer underneath where no oil droplets were observed.

On increasing the mixture velocity (U_m) to 0.4 m/s while maintaining the same water-cut (WC) and pipe inclination, remarkable changes in the time series and the shape of the PDF curves as a function of the OVF were observed. For instance at 10% WC and 30% WC, small fluctuations on the time series curves in figure 5.9 were observed and these curves were almost close to the OVF value of one (1) suggesting that the pipe section is almost filled with the oil phase with tiny droplets of water dispersed across it. However, on increasing the WC to 50% and 70% respectively, the size and number of water droplets increased and these water droplets are dispersed in the continuous oil phase. Meanwhile, just like in the previous cases of low WC, the time series charts showed small fluctuations which is as a result of the effect of the water droplets of different sizes on the measurement of OVF.
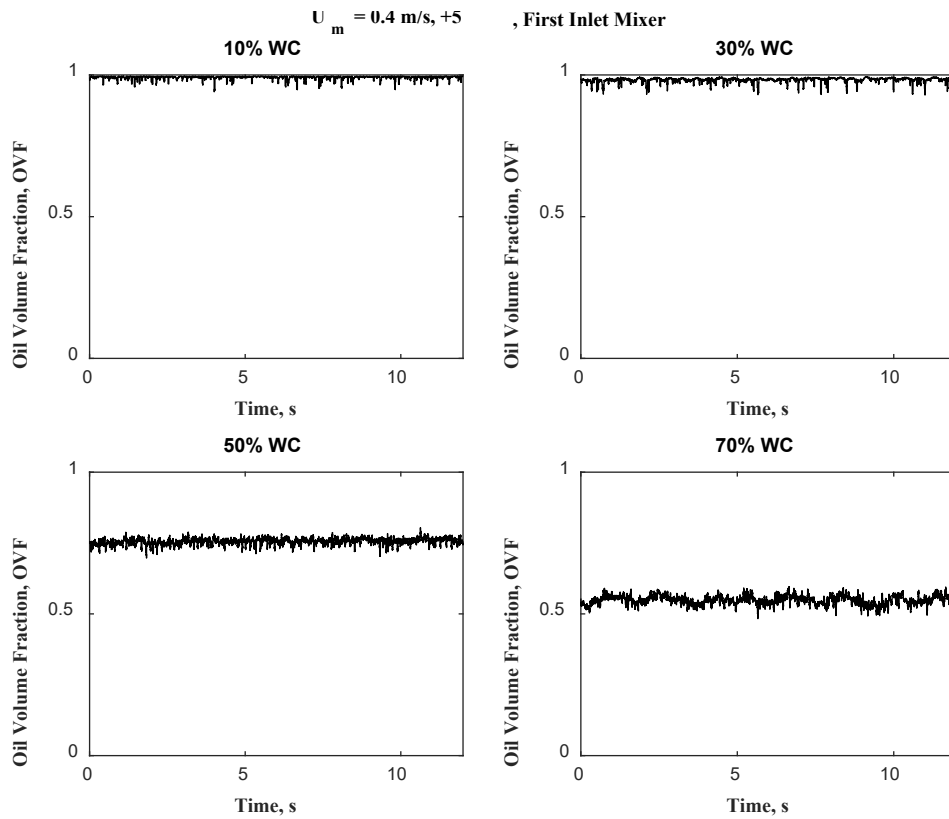
Figure 5.9: Time series of the oil volume fraction (OVF) for the T-ype fluid inlet devices (first fluid inlet device) at +5° pipe inclination using the mixture velocity, U_m = 0.4 m/s.

Considering the PDF curves as a function of OVF in figure 5.10, one may notice that at 10% and 30% WC, the shape of the PDFs are asymmetrical and skewed towards the right with a single prominent peak corresponding to the OVF measurement of the continuous oil layer with small water droplets dispersed in it. Although the shape of the time series curve and the PDFs at 10% WC and 30% WC are slightly different yet the specific characteristics of the flow patterns identified are the same. For instance, at 10% WC and 30% WC, Dw/o&o flow pattern was identified where there is a continuous oil layer with a region at the bottom of the pipe where the water droplets are dispersed. However, on increasing the WC to 50% and subsequently to 70%, the shape of the PDF curve changed considerable where the curves seemed to be symmetrical with more prominent peaks compared to the previous cases of low WC (10% and 30%). The peaks corresponds to the measurement of the OVF for the continuous

oil phase and the variability in the OVF were as a result of the presence of water droplets of

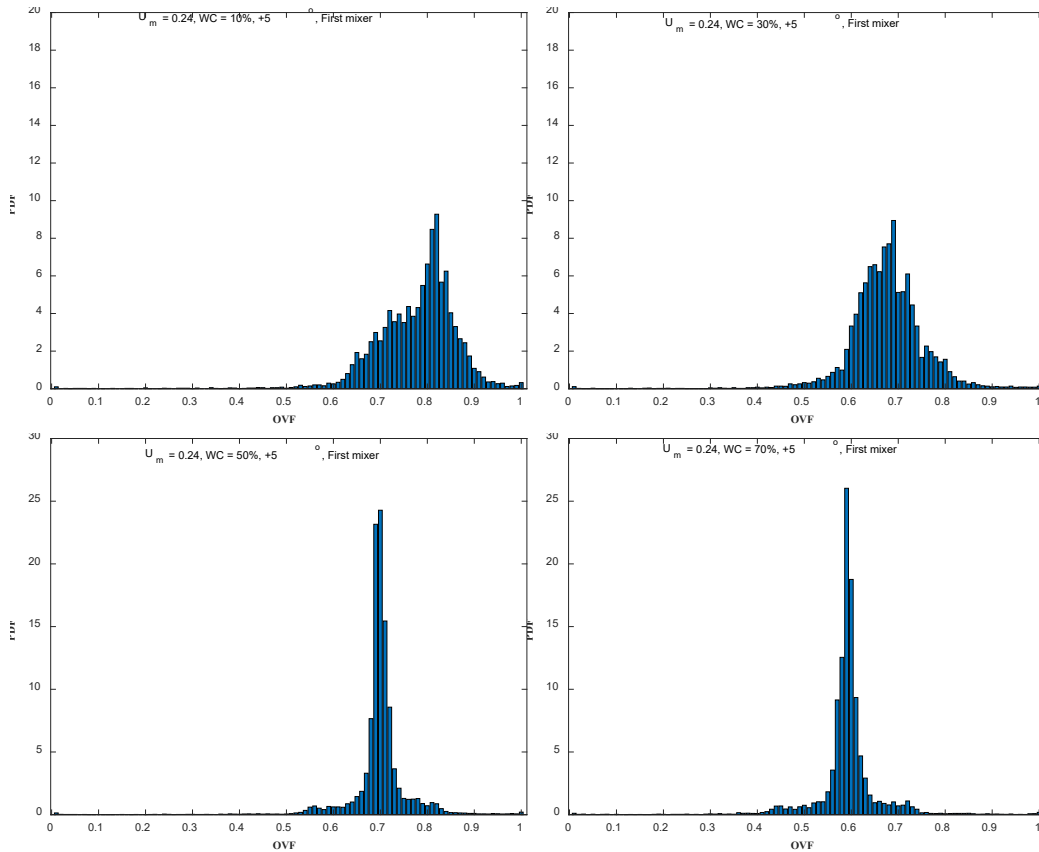different sizes, therefore at 50% WC and 70% WC, Dw/o flow pattern was observed.
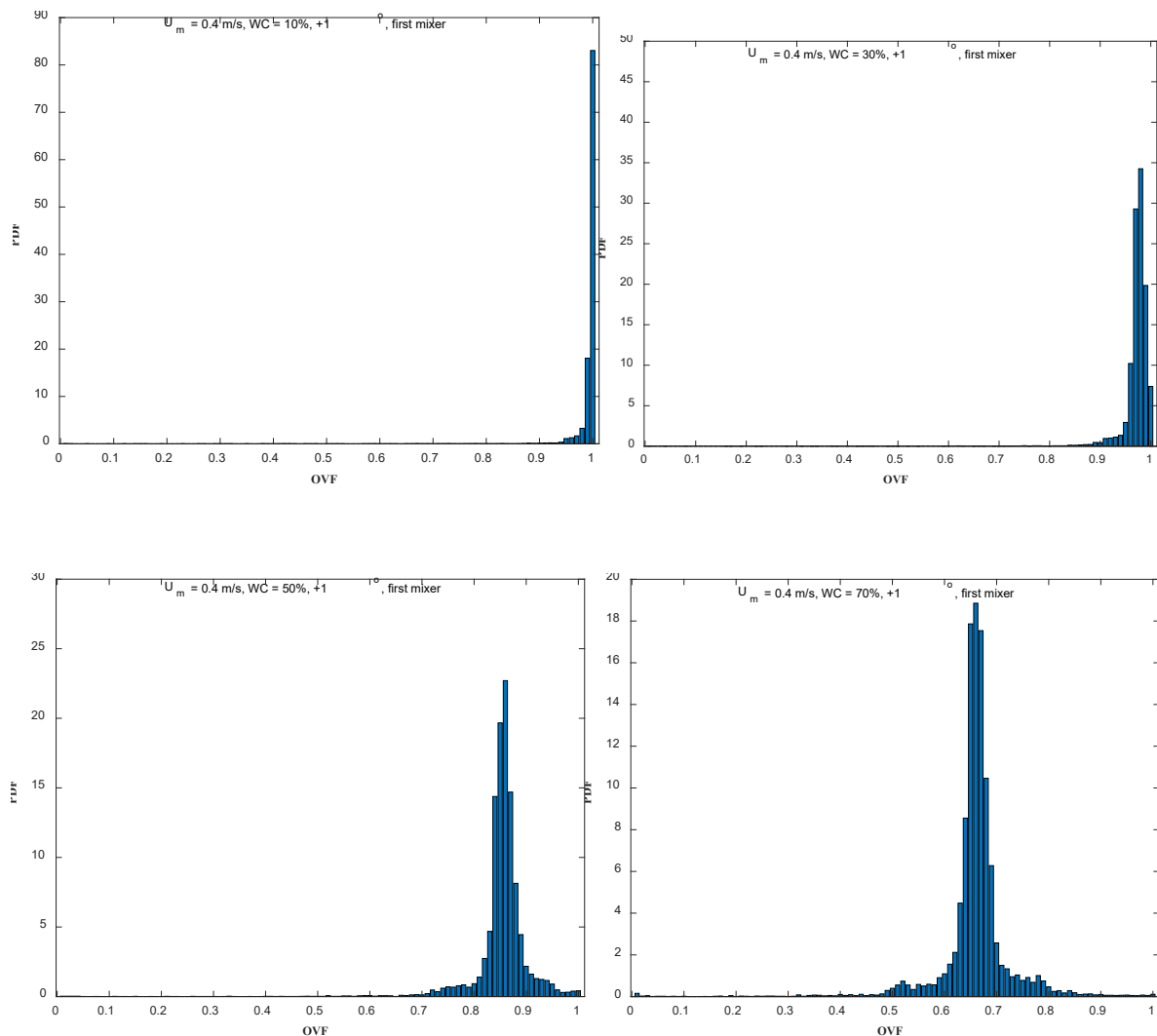
Figure 5.10: The Probability Density Function (PDF) of the OVF showing its distribution and characteristic signature at $U_m = 0.4$ m/s and $+5°$ pipe inclination using the T-ype fluid inlet devices (first fluid inlet device).

5.5.2 Time Series Plots of OVF On Using The Y-type Fluid Inlet Device with no split plate (Second Fluid inlet device)

The time series data and the PDFs as a function of the OVF when the second fluid inlet device (second fluid inlet device) was used can be seen in figures 5.11 and 5.12 for the mixture velocity, $U_m = 0.24$ m/s and in figures 5.13 and 5.14 for the mixture velocity, $U_m = 0.4$ m/s. In figure 5.11, it will be observed

that the signature of the time series across all the water cuts (10%, 30%, 50% and 70%) for Um = 0.24 m/s are similar to the ones observed in figure 5.7 when the first fluid inlet device was used. In both cases, the fluctuating nature of the time series curve suggests the presence of interfacial waves at 10% WC and 30% WC and on the flow pattern map, the SW&MI flow patterns were observed at these flow conditions. Also, for the high WC (50% and 70%), the nature of the time series curves suggest that there is a rapid change in OVF within small time interval and the interface appears slightly wavy though the wave structure are not well defined compared to when the WC was 10% and 30%, therefore it can be suggested that the disturbances on the interface were as a result of the ripples moving across the interface with a possible dispersion of oil in the continuous water phase. From the flow pattern map, the flow pattern corresponding to these time series curves is the Do/w&w which was the same flow pattern identified using the first fluid inlet device at the same flow condition.

Figure 5.11: Time series of the oil volume fraction (OVF) for the Y-type fluid inlet device without split plate (second fluid inlet device) at +5° pipe inclination using the mixture velocity, $U_m = 0.24$ m/s.

On carefully examining figure 5.12, one may notice that the plot of the PDF as a function of the OVF formed a group of histograms whose shapes are asymmetrical and dome-like with an appearance of several peaks for the 10% and 30% WC. This observation is also similar to the previous one made for the first fluid inlet device, therefore the same explanation is applicable, thus the signature of the PDF corresponds to the SW&MI flow pattern on the flow pattern map for the same flow condition.

Similarly, for 50% WC and 70% WC, the shape of the PDF curve appears to be symmetrical with smaller number of peaks which is about the same behaviour observed for the first fluid inlet device, therefore similar explanation is applicable, thus the signature of the PDF curve suggest the existence of Do/w&w flow pattern which is consistent with the observation from the flow pattern map at the same flow condition.

Figure 5.12: The Probability Density Function (PDF) of the OVF showing its distribution and characteristic signature at $U_m = 0.24$ m/s and $+5°$ pipe inclination Y-type fluid inlet device without split plate (second fluid inlet device).
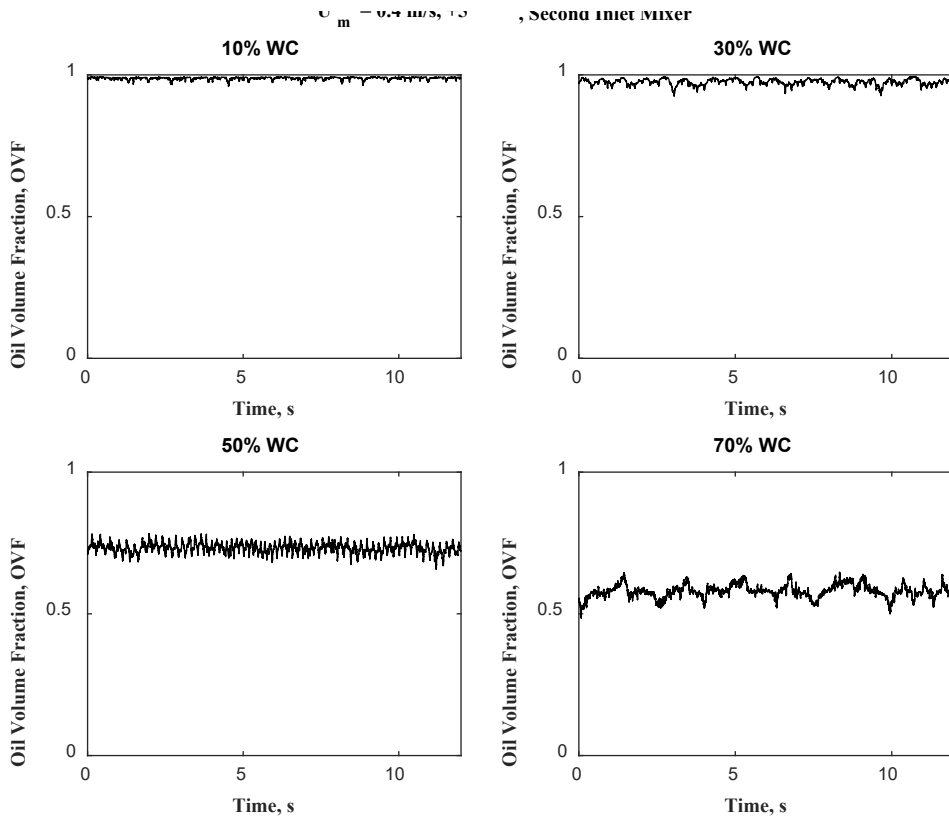
Figure 5.13: Time series of the oil volume fraction (OVF) for the Y-type fluid inlet device without split plate (second fluid inlet device) at $+5°$ pipe inclination using the mixture velocity, $U_m = 0.4$ m/s.

In figures 5.13 and 5.14, the plot of the time series and the PDFs as a function of OVF are presented and it will be noticed that at 10% WC, it appears that the pipe is almost filled with

the oil phase and the time series almost coincide with OVF = 1 with some tiny fluctuations suggesting the presence of small water droplets. This observation is consistent with the PDF plot where the prominent peak was found to coincide with OVF = 1. This signature of the PDF and the time series curves correspond to the Dw/o flow pattern on the flow pattern map.

On increasing the WC to 30%, the flow is still oil-dominant with a high OVF which can be seen on both the time series and PDF plots in figures 5.13 and 5.14 respectively. However, it appears that a small continuous layer of water-phase was seen flowing at the bottom, while a thick continuous layer of the oil phase flows at the top and a wavy interface with some droplets separating the two continuous layers and at this flow condition, the flow pattern corresponds to the SW&MI on the flow pattern map. Although, the shape of the PDF curve for this flow condition (30% WC) is different from the dome-shaped curves with multiple peaks observed in figures 5.8 and 5.12, it should be noted that the design of the fluid inlet device may have probably affected the distribution of the phases since other factors such as the flow conditions and the pipe inclination are the same, thus, the flow patterns may appear the same based on visual observations, but the distribution of the OVF may be different.

Further increasing the WC to 50% and 70%, the time series showed small fluctuations in the OVF which suggest the presence of small amplitude interfacial waves and oil droplets and on comparing with the symmetrical-shaped, narrow peak curve of the PDF which is similar to the curves in figures 5.8, 5.10 and 5.12 at the same condition, it can be said that the unique shape of the time series and the PDF correspond to the Do/w&w flow pattern on the flow pattern map.

5.5.3 Time Series Plots of OVF On Using The Y-type Fluid Inlet Device with split plate (Third Fluid inlet device)

The time series and the PDF curves on using the third fluid inlet device (third fluid inlet device) can be seen in figures 5.15 and 5.16 respectively for $U_m = 0.24$ m/s and in figures 5.17 and 5.18 for $U_m = 0.4$ m/s respectively. For the flow conditions considered, one may notice that the time series curves in figures 5.15 and 5.17 are similar for all water cuts (10%, 30%, 50% and 70%) and in all cases, the OVF fluctuates in a wave-like form which suggest the probable appearance of interfacial waves. However, on considering the shape of the PDF curves in figures 5.16 and 5.18, one may notice that at 10% WC for $U_m = 0.24$ m/s (10% WC and 30% WC for $U_m = 0.4$ m/s) the group of histogram form a dome-shaped curve with multiple peaks which is a characteristic signature of the SW&MI flow pattern which is consistent with the observation on the flow pattern map.
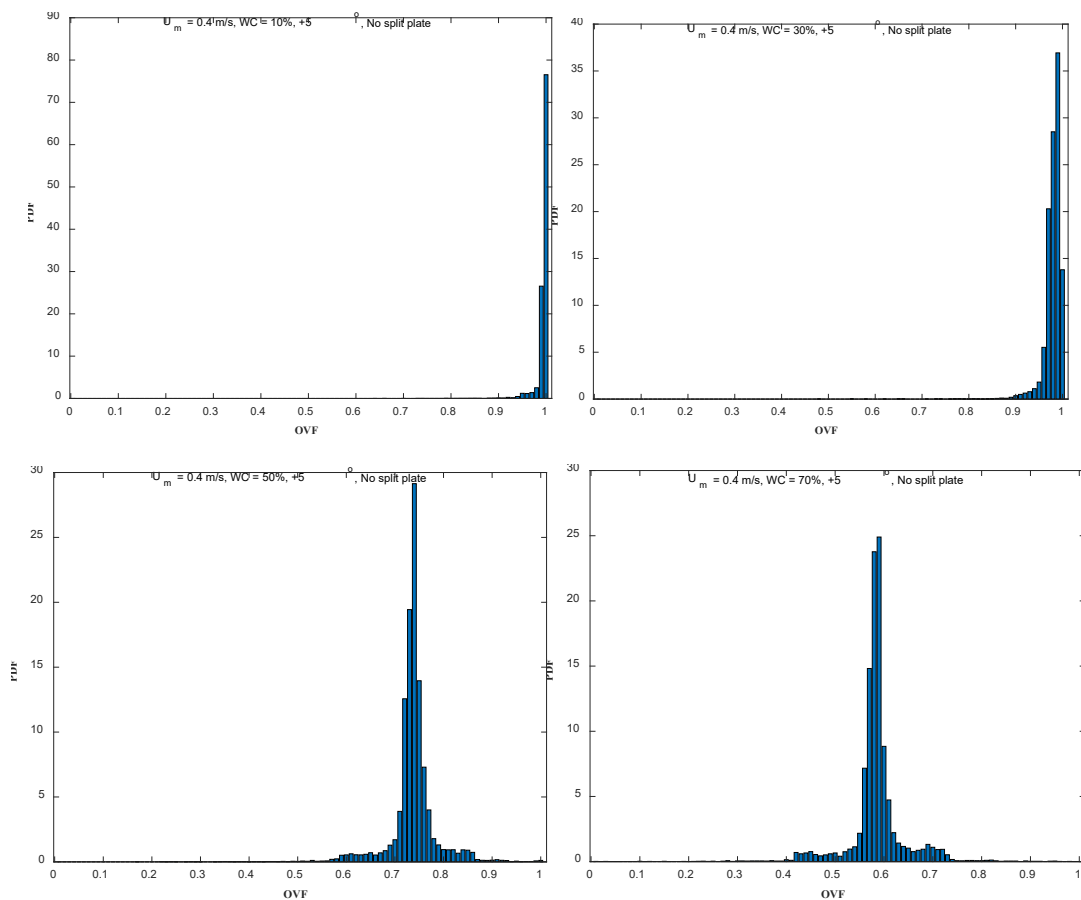
However, for 30% WC, 50% WC and 70% WC with the same mixture velocity (Um = 0.24 m/s), the shape of the PDF curves appear to be symmetrical, though with multiple peaks and these corresponds to the SW flow pattern on the flow pattern map.
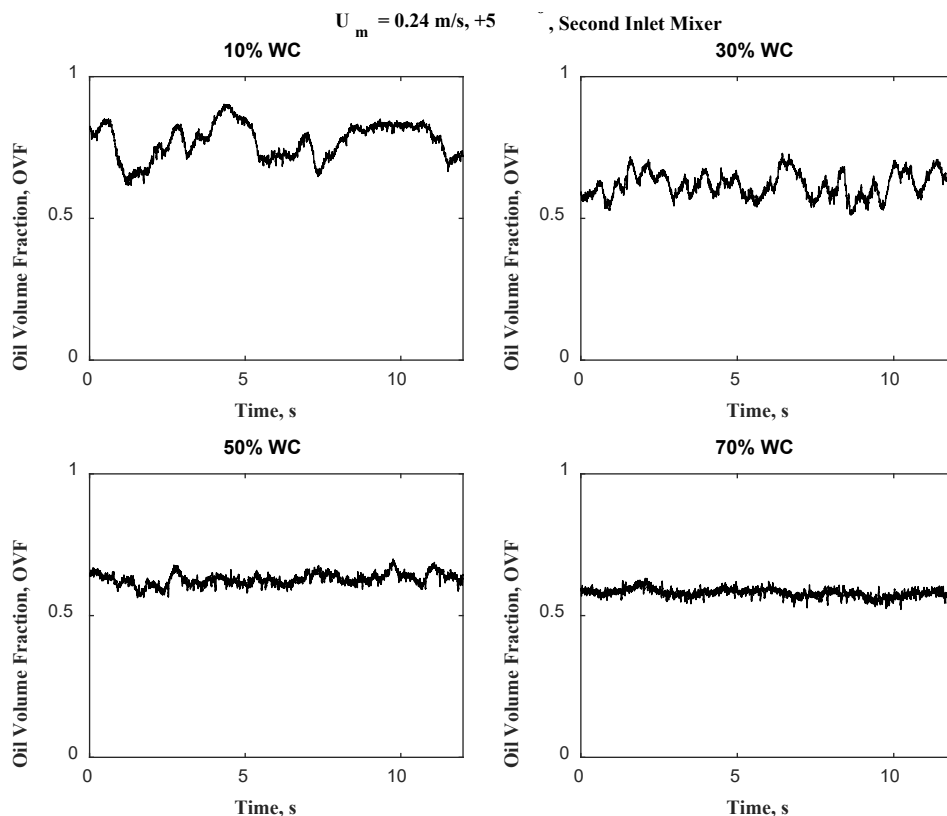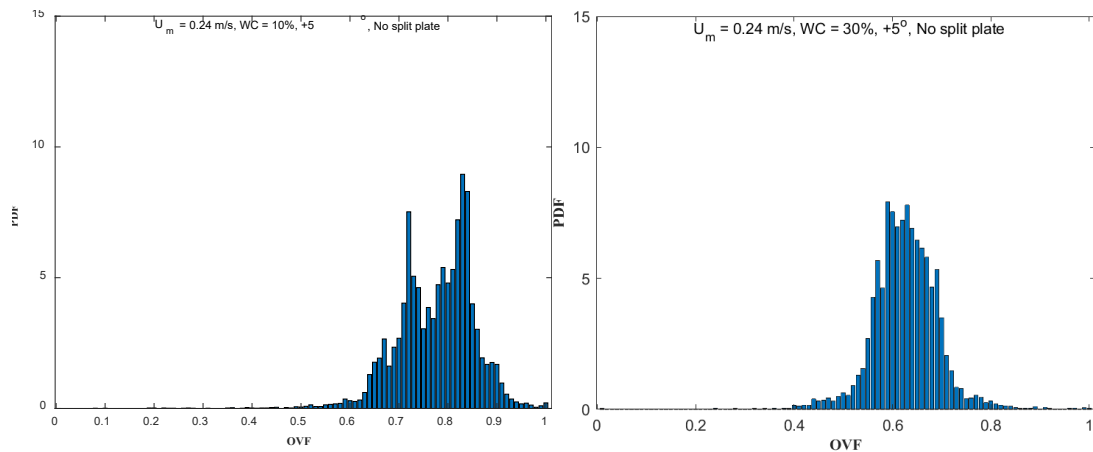
U_m = 0.24 m/s, +5 , Third Inlet Mixer
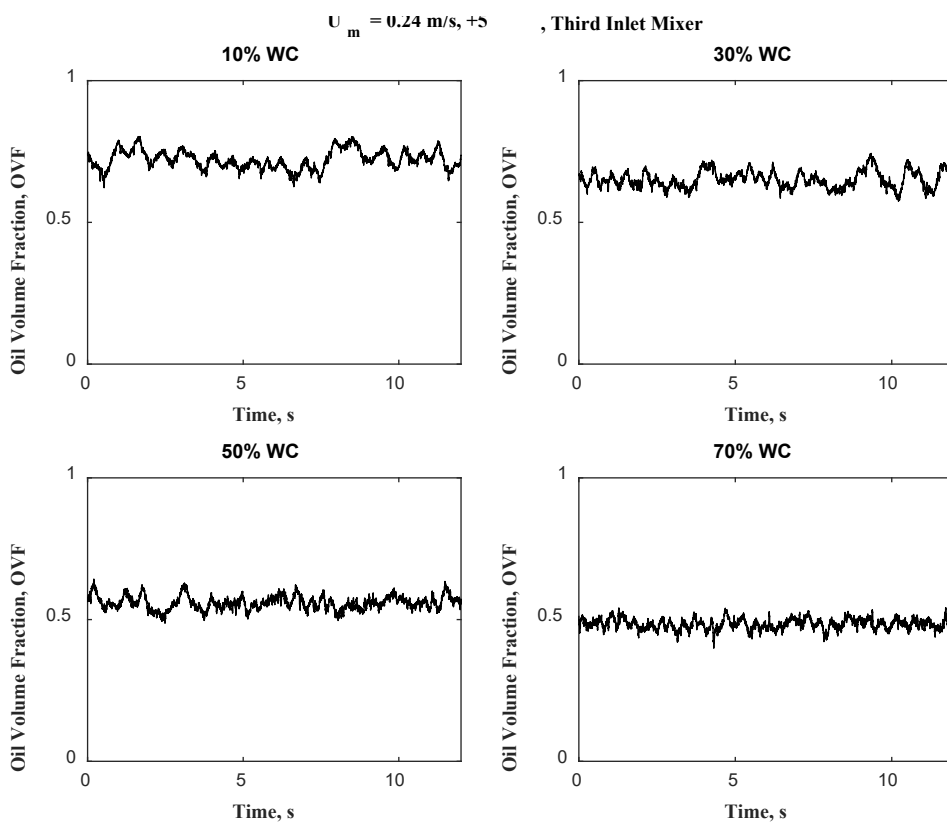
Figure 5.15: Time series of the oil volume fraction (OVF) for Y-type fluid inlet device with split plate (third fluid inlet device) at +5° pipe inclination using the mixture velocity, U_m = 0.24 m/s.
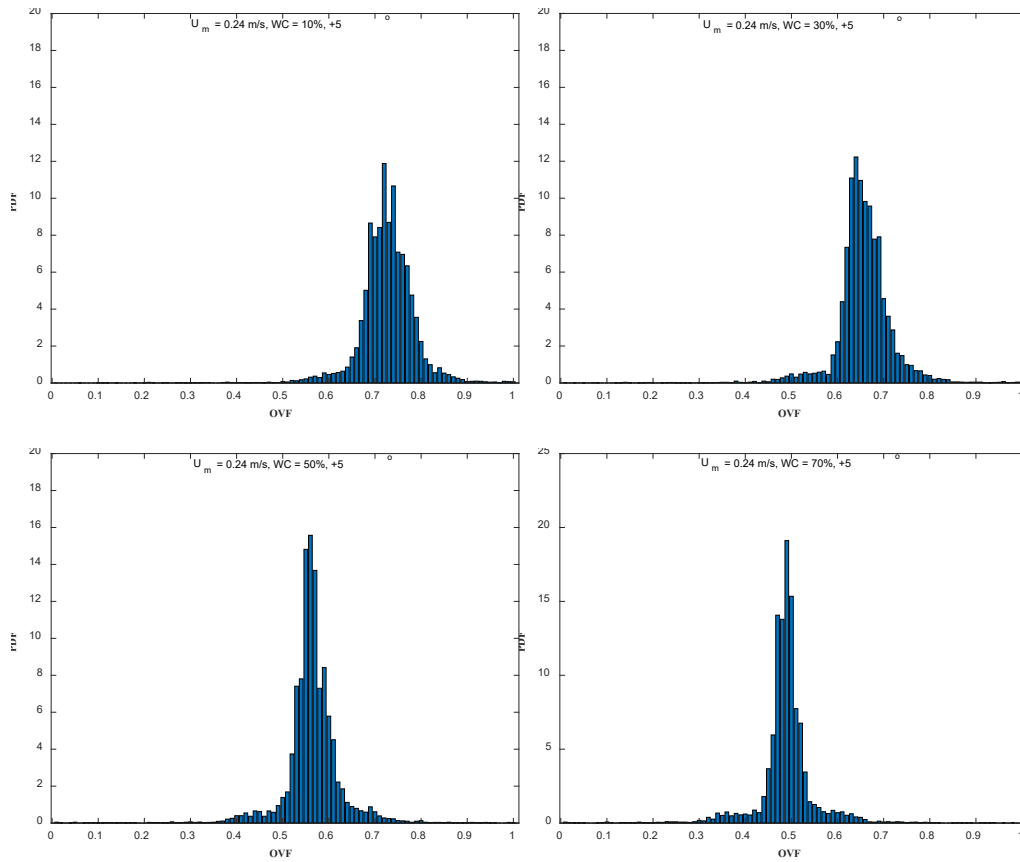
Figure 5.16: The Probability Density Function (PDF) of the OVF showing its distribution and characteristic signature at U_m = 0.4 m/s and +5° pipe inclination using Y-type fluid inlet device with split plate
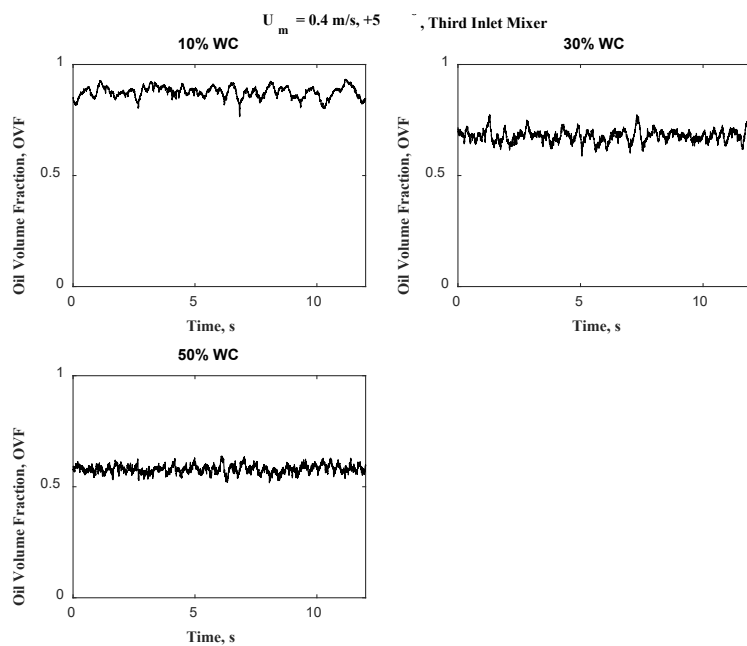
Figure 5.17: Time series of the oil volume fraction (OVF) for Y-type fluid inlet device with split plate (third fluid inlet device) at +5º pipe inclination using the mixture velocity, $U_m = 0.4$ m/s.
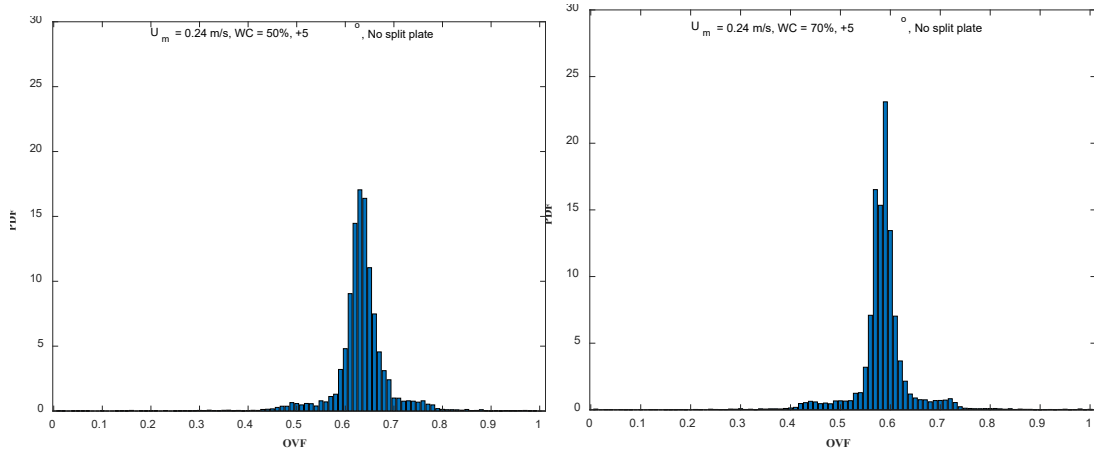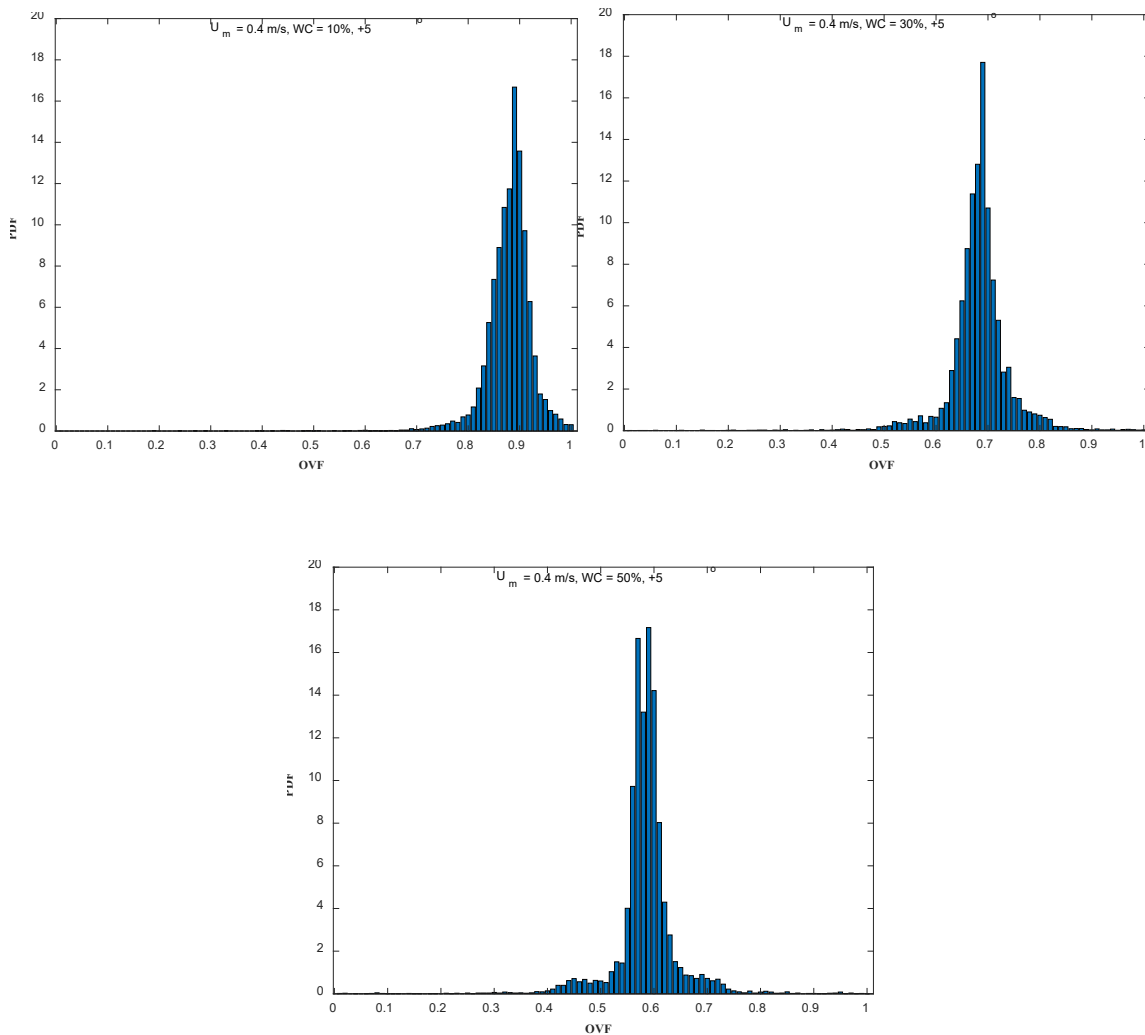

Figure 5.18: The Probability Density Function (PDF) of the OVF showing its distribution and characteristic signature at $U_m = 0.4$ m/s and +5º pipe inclination using Y-type fluid inlet device with split plate (third fluid inlet device).

5.5 RELATIONSHIP BETWEEN THE DESIGN OF THE FLUID INLET DEVICE AND THE SLIPPAGE CHARACTERISTICS OF THE DIFFERENT FLOW PATTERNS.

In section 5.1, it was clearly stated that the design of the fluid inlet device will determine the contacting method between the oil and water phase which will eventually dictate the geometrical configuration of the interface otherwise called the flow patterns. Moreso, for the different flow patterns, the slippage characteristics which measures the degree to which one

phase travels faster than the other are different. The slippage characteristic is often determined as a ratio between the in-situ or phase velocity of the oil phase and that of the water phase, hence it is termed the slip ratio (S). By convention, when S < 1, it means that the in-situ velocity of the oil phase is less than that of the water phase which means that the water phase travels faster than the oil phase. Also, for S > 1, it means that the in-situ velocity of the oil phase is greater than that of the water-phase, hence the oil phase is travelling faster than the water phase. However, for S = 1, it implies that the in-situ velocities of the oil and water phases are the same, hence both phases travel at the same uniform velocity. In this section, attempt will be made to study the effect (if any) of the design of the fluid inlet device on the slippage between the oil and water phases. The plot of the slippage as a function of the WC can be seen in Figure 5.19 at +1° and +5° pipe inclinations for different values of the mixture velocities (U_m).

In figure 5.19, the relationship between the slip ratio and the water-cut for each of the three fluid inlet device was presented for +1° and +5° pipe inclination. It will be observed that for most of the data, the slip ratio decreases as the water-cut and mixture velocity increases which implies that the in-situ velocity of the oil phase decreases while that of the water phase increases as the water-cut or mixture velocity increases which agrees with the findings of Lum et al., (2004), Morgan et al., (2013) and Xu et al., (2016) among others.

(e) +1º   (f) +5º
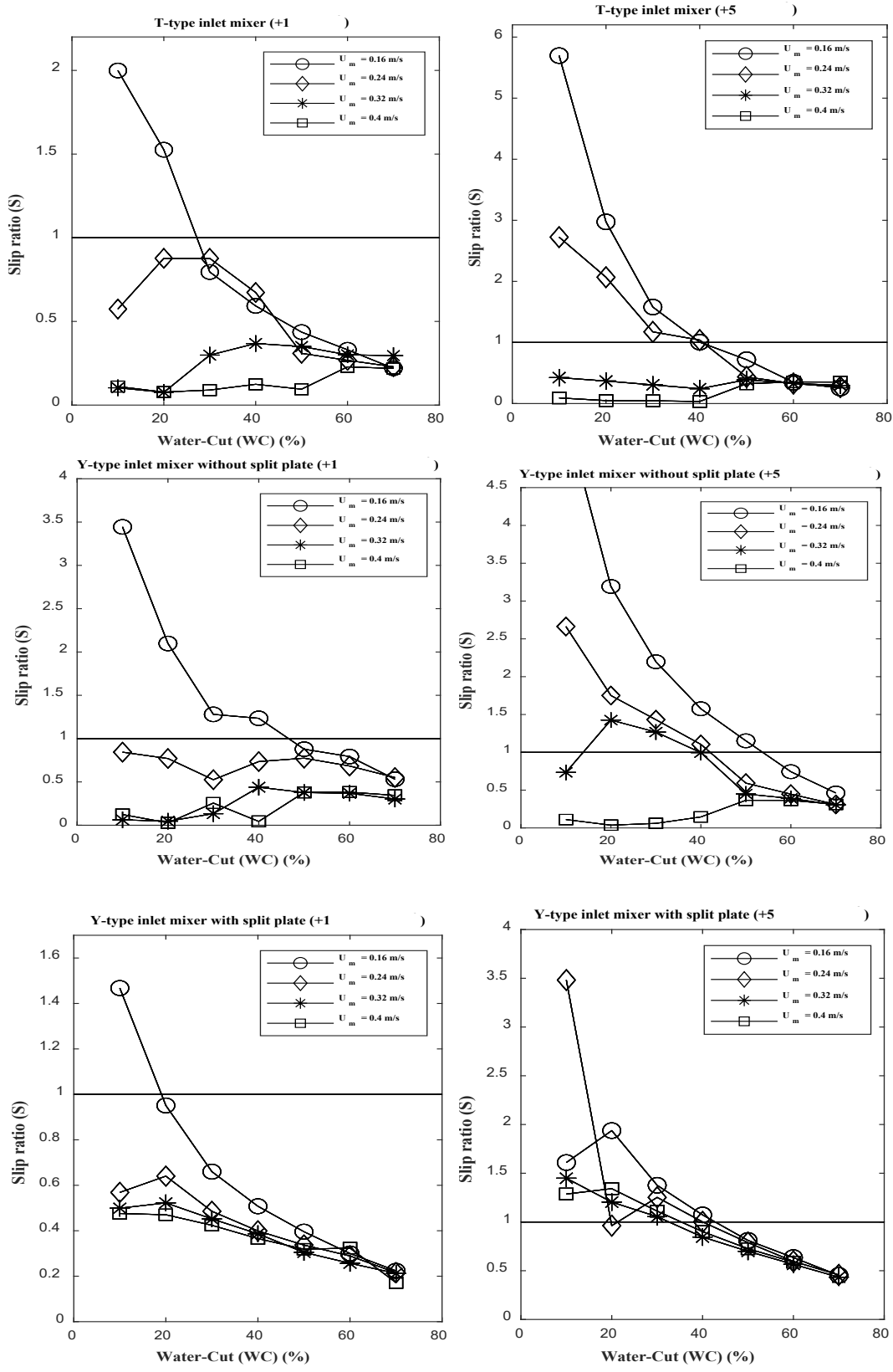
Figure 5.19: Effect of the fluid inlet device design on the slip ratio across +1º and +5º pipe inclinations for the T-type inlet mixer, Y-type inlet mixer without split plat and Y-type inlet mixer with split plate.

On examining figure 5.19, one may notice some fundamental differences in the slippage characteristics for each of the fluid inlet device for both pipe inclinations. For instance, at +1°

pipe inclination, the slippage characteristics when the first and third fluid inlet device (Figure 5.19a and 5.19e) are used are similar. The similarity stems from the fact that most of the slip ratios for the tested flow conditions are less than one which means that the in-situ velocities of the water phase are greater than that of the oil phase except at the point where the mixture velocity (U_m) is 0.16 m/s and 10% water-cut (WC). At this flow condition (U_m =0.16 m/s and WC = 10%), the observed flow patterns are the SW&MI and SW and the slip velocity is greater than one for the first and third fluid inlet devices respectively which implies that the in-situ velocity of the oil phase is greater than that of the water phase.

This is because at this flow condition, the water phase had the lowest input flow rate and as a result of the considerable inertial force produced by the high input flow rate of the oil phase and in addition to the action of the gravitational force due to the pipe inclination on the denser water phase, the in-situ velocity of the oil phase was found to be greater than that of the water phase, hence the increase in the slip ratio value above the S = 1 line.

However, for the second fluid inlet device and at +1° pipe inclination (Figure 5.19c), while most of the slip ratio data points fell below the S = 1 line, yet for a number of the flow conditions (U_m = 0.16 m/s, WC = 10% - 40%) which were significantly higher than those observed in the first and third fluid inlet devices, the slip ratios were observed to be above the S = 1 line and at these conditions, the observed flow patterns are Dw/o&o and ST&MI. For these flow conditions, water droplets of different sizes are produced and they are distributed at the bottom and also close to the interface for the Dw/o&o and ST&MI flow patterns respectively. The interaction between these water droplets and also between the droplets and

the pipe wall coupled with the action of the gravitational force on the denser water phase results in the in-situ velocity of the water phase to be retarded while enhancing that of the oil phase, hence the increase in the slip ratio.

Interestingly, on increasing the pipe inclination from +1° to +5°, a considerable number of the data points across all the three fluid inlet devices were found to be above the S = 1 line. This suggest that as a consequence of increasing pipe inclination, the in-situ velocity of the oil phase is greater than that of the water phase due to the action of the parallel component of the gravitational force on the denser water phase which retards its in-situ velocity. For instance, on considering the first fluid inlet device(first fluid inlet device) in figure 5.19b, and within the range of 0.16 m/s – 0.24 m/s for the mixture velocity and 10% - 40% for water-cut, the slip ratio for these data points were above the S = 1 line and they correspond to the SW&MI and Do/w&w flow patterns where the continuous oil phase and the dispersed oil droplets slip past the continuous water layer due to the action of the gravitational force retarding the flow of the water layer. Similarly, for the second and third fluid inlet devices in figures 5.19d and 5.19f, there is a progressive increase in the number of the data points above the S = 1 line particularly for the third fluid inlet device where the slip ratio values are greater than one for all the mixture velocities (U_m = 0.16 m/s – 0.4 m/s) and 10% - 40% water-cut and the flow pattern observed at these points are predominantly SW&MI with a few SW occurring at U_m = 0.16 m/s. Generally, it can be said that at low pipe inclination (+1°), the slippage characteristics where the water phase slipped past the oil phase such that the slip ratio is less than one (S < 1) is more predominant when the first and third fluid inlet device were used compared to the second fluid inlet device. However, on increasing the inclination angle to +5°, there seem to be a considerable change in the slippage characteristics for all the three fluid inlet devices where the oil phase slipped past the water and as a result, S > 1 and this is found to be more

predominant in the third fluid inlet device where it occurred for all mixture velocities (Um = 0.16 m/s – 0.24 m/s and 10% - 40% WC).

5.7   SUMMARY

The chapter attempted to study the effect of the design of fluid inlet device on the oil-water two phase flow characteristics with a particular focus on its effect on flow pattern and flow pattern transition, OVF distribution and slippage characteristics. The design of the fluid inlet device was found to determine the number and type of flow patterns observed. The first fluid inlet device favours the formation of droplets, hence most of the flow patterns are formed as a result of the dispersion of one phase into the other. Whereas for the third fluid inlet device, it favours the formation of separated flow due to the presence of the split plate, hence the flow patterns are predominantly separated flow patterns. However, the second fluid inlet device seems to have a combined characteristics of both the first and third fluid inlet devices where both separated and dispersed flow patterns are obtained depending on the flow condition.

Relationship between the OVF and the flow pattern transition was also explored for the three fluid inlet devices and in most of the cases, a sudden change in the distribution of the OVF as a function of WC corresponds to a region on the flow pattern map where there is a corresponding transition from one flow pattern to another. In addition, the nature of the OVF-time series chart and the shape of the PDF curves clearly identified and categorize the different flow patterns. Finally, the slippage characteristics as a consequence of using each of the three fluid inlet devices was also explored. Thus, at low pipe inclination (+1°), the first and third fluid inlet devices favours the water phase to travel faster than the oil phase, hence the slip ratio, S < 1 in most cases. However, for higher pipe inclination (+5°), the in-situ velocity of the oil phase was found to be greater than that of the water phase in most cases, hence S > 1 for all

the three fluid inlet devices, but the observation was more predominant in the third fluid inlet device.

CHAPTER 6

EXPERIMENTAL OBSERVATION OF FLOW DEVELOPMENT AND INTERFACIAL BEHAVIOUR IN OIL-WATER FLOW ACROSS THE LARGE DIAMETER INCLINED PIPE.

6.1 INTRODUCTION

This chapter reports all the results obtained from the experimental investigations of the flow development including the identification of the different flow patterns and their transition using both physical observations and the images from the high-speed camera. The characterization of the interfacial waves which occur along the oil-water interface will also be reported in this chapter using the interfacial height measurements from the double parallel wire probe (DPWP) and the analysis of the images from the high-speed camera and thereafter a discussion on stability of the interfacial waves will be made.

6.2 FLOW PATTERN IDENTIFICATION

In conducting the experiments, the flow patterns were identified both physically and with the use of the Phantom V.12 high-speed camera. The flow imaging was done through the viewing box positioned 4.5 m from the fluid inlet device and all the observations were made using the Y-type fluid inlet device with a separator (split) plate that minimizes fluid mixing at the inlet. The design of the fluid inlet device ensured that within the limit of the experimental flow conditions, no any form of fluid dispersion were observed, therefore the dispersed flow patterns were absent across all the pipe inclinations. The flow patterns observed are the stratified smooth (ST), stratified wavy (SW) and stratified wavy with mixing at the interface (SW&MI).

| (a) | (b) | (c) |
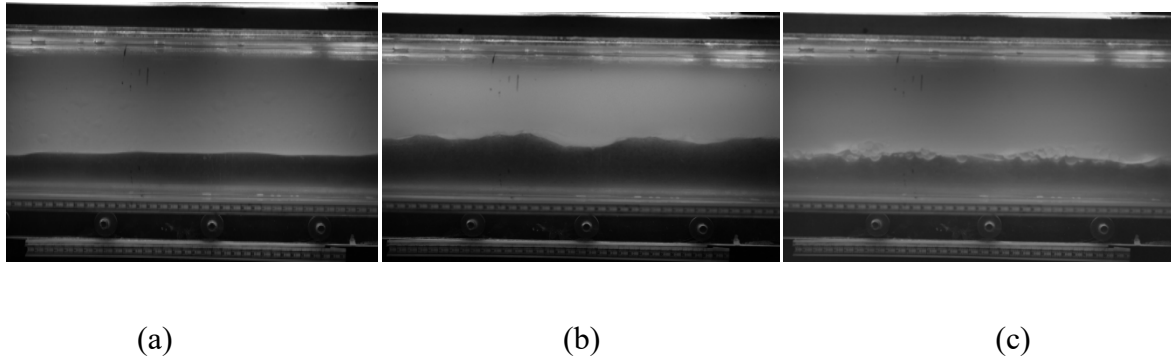
Figure 6.1: Representative samples of the flow patterns observed in the experiment (a) Stratified Smooth (ST) (b) Stratified wavy (SW) and (c) Stratified wavy with mixing at the interface (SW&MI).

The stratified smooth (ST) flow pattern is characterized by a clearly defined smooth interface with no waves or drops and a continuous layer of oil at the top and water at the bottom. The observation of stratified smooth flow pattern for a +1° pipe inclination is very interesting because such flow pattern normally occur in horizontal pipes which are gravity-dominated but rarely observed in flows across inclined pipes.

The stratified smooth (ST) flow pattern was observed only at the lowest pipe inclination (+1°) where the effect of flow disturbance due to higher inclination angle is low. From the experimental observation, the ST flow pattern occurred at three separate points and they include - the lowest mixture velocity and water cut (U_m = 0.08 m/s, WC = 10%), the intermediate mixture velocity and highest water cut (U_m 0.24 m/s and WC = 70%) and finally at high mixture velocity and the highest water cut (U_m 0.32 m/s and WC = 70%).

| (a) | (b) | (c) |
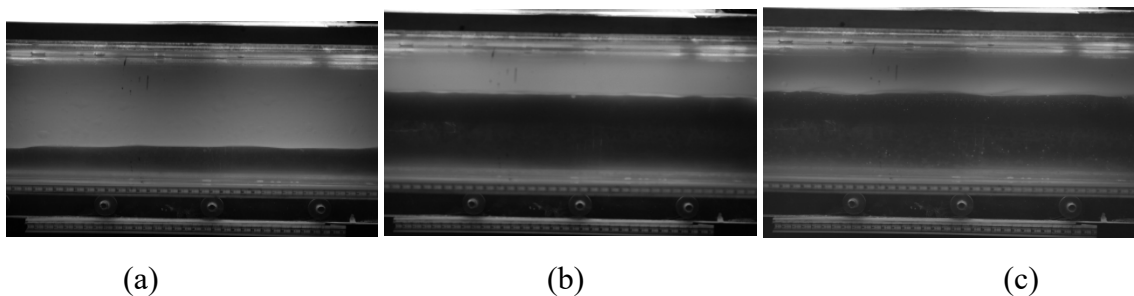
Figure 6.2: Images of the stratified smooth flow pattern at different flow conditions (a) U_m = 0.08 m/s, WC = 10%   (b) U_m = 0.24 m/s, WC = 70%   (c) U_m = 0.32 m/s, WC = 70%

At the first point where the stratified flow (ST) pattern occurred, both the mixture velocity (U_m = 0.08 m/s) and the water-cut (WC = 10%) were at their lowest values which implies that the oil and water superficial velocities (U_{so} and U_{sw}) are equally low (although the U_{so} is greater than U_{sw}) and therefore the flow becomes gravity-dominated leading to the segregation of the phases with a smooth interface between them. In addition, for low mixture velocity (U_m = 0.08 m/s) and water-cut (WC = 10), both the flow of the oil and water phases are laminar (Re_w = 486 and Re_o = 2148) therefore there are no turbulent dispersive forces in both phases that could promote the appearance of droplets or waves along the interface, hence the interface at this flow condition appeared to be smooth and stable.

On comparing this observation with those made by other researchers, it will be noted that the stratified smooth flow pattern was predominantly observed for flows across the horizontal pipe (Scott, 1985; Abduvayt et al.,2004; Lum et al., 2006; and Kumara et al., 2009) but for oil-water flows across an upwardly inclined pipe, stratified smooth flow pattern was rarely observed for all pipe inclinations studied as a result of the flow disturbance induced by the effect of the pipe inclination.

However, Kurban (1997), Alkaya (2000) and Rodriguez and Oliemans (2006) all identified stratified smooth (ST) flow pattern for oil-water flows across a +1° inclined pipe which is in agreement with the findings of this research effort. Also for the other two points where the stratified smooth flow pattern was observed, the mixture velocities (U_m =0.24 m/s and 0.32 m/s) were relatively high while the water-cut were at the highest level (WC = 70%). From experimental observations, it was noted that interfacial waves with droplets along the interface were formed as the mixture velocity increases. However, at a given mixture velocity (U_m =0.24 m/s or 0.32 m/s), it was equally observed that on increasing the water-cut, the amplitude of the interfacial waves began to decrease which makes the interface to get smoother as a result of

the reduction in fluctuations along the interface. The reduction in the interfacial wave amplitude could be as a result of the decrease in the Reynolds number of the oil phase from a highly turbulent condition at low water-cut (WC = 10%) and gradually approaching the laminar condition as the water-cut increases which is consistent with observations made by Al-Wahaibi and Angeli (2011) and Perera et al., (2019). The flow images in figure 3.3 showed the progressive change in flow pattern from stratified flow with mixing at the interface (SW&MI) which occurred at low water-cut (WC) to a stratified smooth (ST) which occurred at high water-cut (WC).
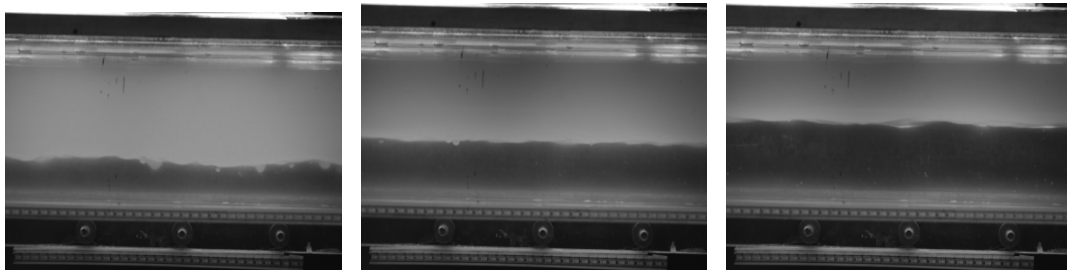
U_m = 0.24 m/s, WC = 10%   (b) U_m = 0.24 m/s, WC = 20%   (c) Um 0.24 m/s, WC = 40%
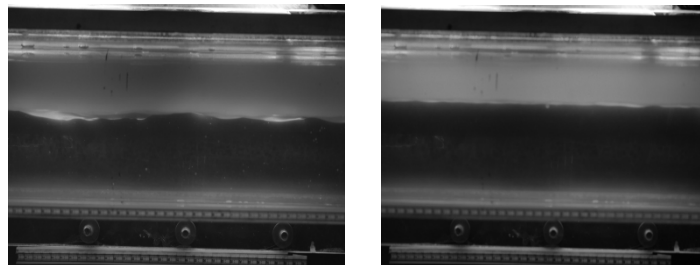
(d) Um 0.24 m/s, WC = 50%   (e) Um 0.24 m/s, WC = 70%

Figure 6.3: A figure showing the effect of increasing water-cut on the evolution of flow pattern at a given mixture velocity

6.3   FLOW PATTERN MAPS

The different flow patterns observed in this experimental work can be presented in a 2D plot called the flow pattern map with the axes of the plot corresponding to the input parameters (mixture velocity, U_m and water-cut,WC) while the different points on the map represents the various flow patterns observed.

Figure 6.4 shows the different flow patterns observed for the $+1^\circ$ pipe inclination. Three different flow patterns are represented in the flow pattern map which includes the stratified smooth (ST), stratified wavy (SW) and stratified wavy with mixing at the interface (SW&MI). The stratified smooth (ST) flow pattern was observed at very low mixture velocity and water-cut (Um = 0.08 m/s) and WC = 10%) and also at high water-cut (WC =70%) for intermediate to high mixture velocities (Um = 0.24 m/s and 0.32 m/s). Detail discussion on this observation was done in the previous section. Stratified wavy (SW) flow pattern was observed for all the mixture velocities and predominantly within 30% - 60% water-cut. The presence of stable interfacial waves with no droplets along the interface typically characterizes the stratified wavy flow (SW) pattern and these waves appear due to interfacial shearing as a result of increase in the relative velocity between the oil and water phases.
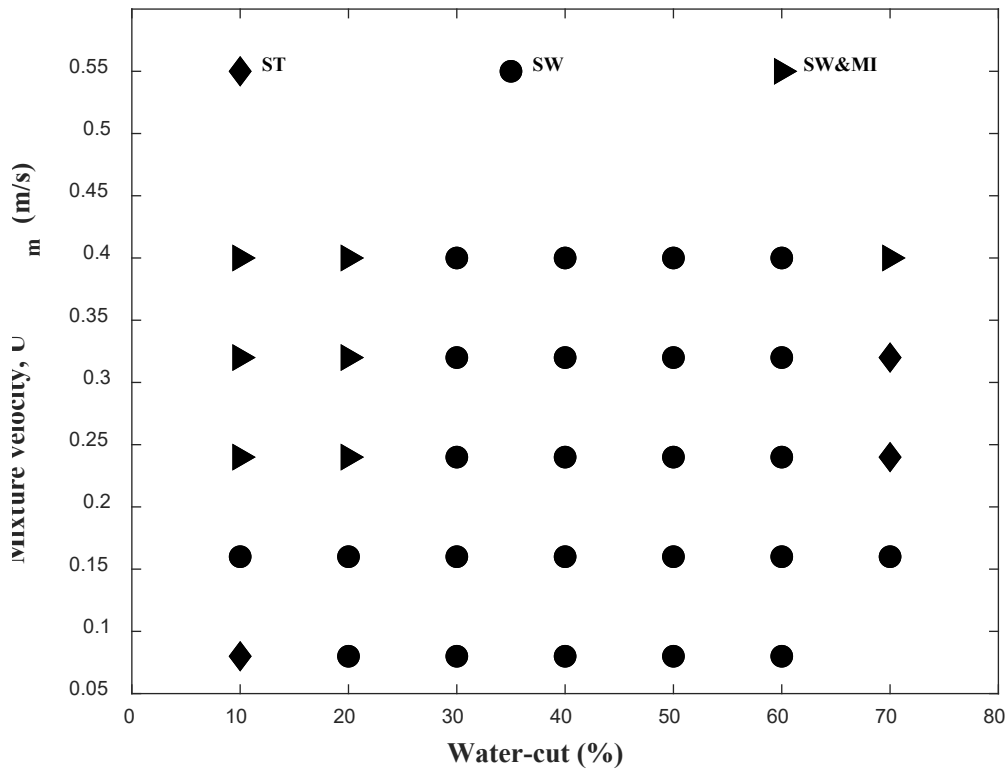
Figure 6.4: Flow pattern map for +1° pipe inclination showing the different flow regimes and their corresponding transition boundaries.

. The stratified wavy with mixing at the interface (SW&MI) flow pattern appeared at low water-cut (WC = 10% and 20%) and at medium to high mixture velocity (U_m = 0.24 m/s, 0.32 m/s and 0.4 m/s). The evolution of droplets along the interface can be explained by considering the turbulent dispersive force that exist in the phases as a result of high Reynolds number and also the interfacial shearing effects that occur due the changes in the relative velocity between the phases. For instance, at 10% WC, the flow condition in the oil phase is turbulent with single phase Reynolds number **of 6416.4, 8530.9 and 10670.1 corresponding to the mixture velocities of 0.24 m/s, 0.32 m/s and 0.40** m/s respectively while the flow condition in the water phase is laminar with the Reynolds number less than 2,300 for all the three mixture velocities. Similarly, for each of the mixture velocity, the relative velocity between the oil and water phase is lowest at 10% WC and increases progressively as the WC increases. Therefore, the appearance of droplets along the wavy interface to form the stratified wavy with mixing at the interface (SW&MI) flow pattern could be as a result of the high Reynolds number of the oil

173

phase which suggests the existence of high turbulent dispersive forces that can potentially promote the formation of droplets along the interface since the effect of the shearing force as a result of the relative velocity is low. This is in agreement with Al-Wahaibi and Angeli (2011) and Perera et al., (2019) who both asserts that the turbulent oil phase greatly impacts droplet formation compared to the shearing effects for a given mixture velocity and pipe inclination. Although, the turbulent oil phase is thought to be responsible for the appearance of droplets, yet the action of the buoyant forces on the droplets as a result of the density difference between the oil and water phase serves to prevent the drops from spreading across the pipe, instead they are localized around the interface.

On increasing the inclination angle to $+3^{\circ}$ and $+5^{\circ}$, a number of changes in the flow structures including the region of flow pattern transition and the characteristics of the interfacial waves were observed. Essentially, for these two inclination angles, stratified smooth (ST) flow pattern was not observed probably due to increased flow disturbance introduced as a result of the increase in pipe inclination, hence only stratified wavy (SW) and stratified wavy with mixing at the interface (SW&MI) flow patterns were identified as presented in the following flow pattern maps shown in figures 6.5 and 6.6.

Figure 6.5 presents the flow pattern map for the $+3^{\circ}$ pipe inclination and it will be observed that at low mixture velocity (Um =0.08 m/s and 0.16 m/s) and for all water-cut, the stratified wavy (SW) flow pattern was identified. On increasing the mixture velocity to 0.24 m/s and for 10% WC, drops began to appear along the interface as a result of the turbulent oil phase layer which indicates the transition to another flow pattern called stratified wavy with mixing at the interface (SW&MI). The SW&MI flow pattern exist only within a small window when $U_m \geq$ 0.24 m/s and WC $\leq$ 30%. Similarly in figure 6.6, the flow pattern map for the $+5^{\circ}$ pipe inclination was shown in which for all mixture velocity, SW&MI flow pattern was observed for
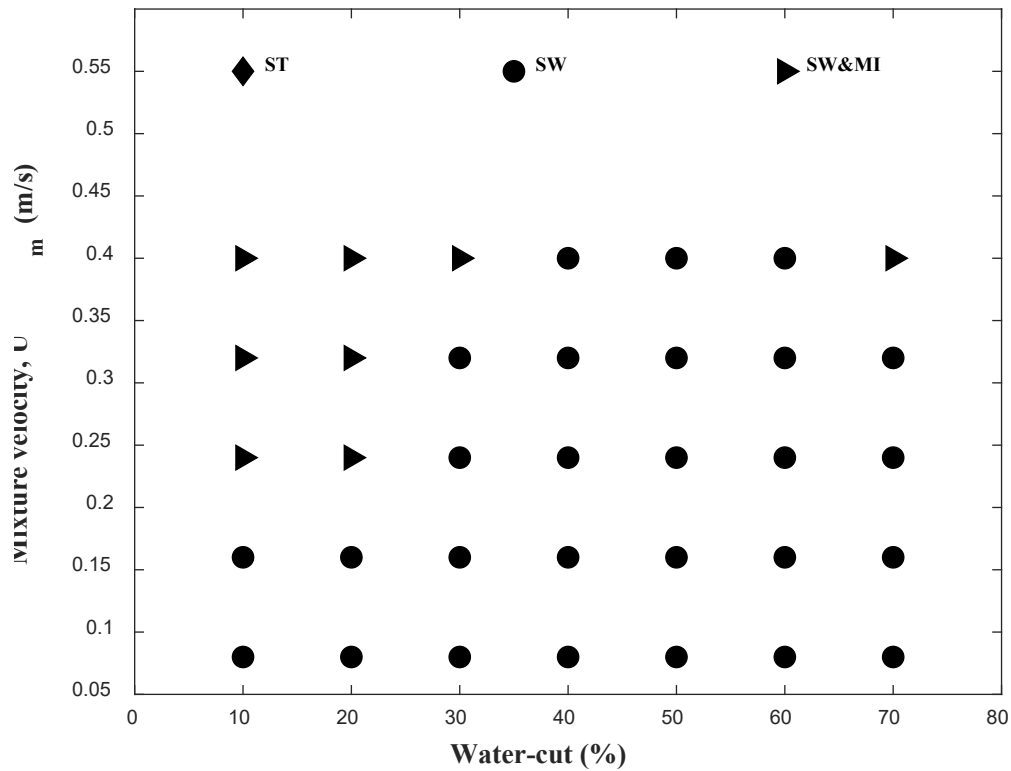
Figure 6.5: Flow pattern maps showing the SW and SW&MI flow patterns for a +3º pipe inclination

WC ≤ 40%. The SW flow pattern occurs only at high WC (WC ≥ 40%) and across all mixture velocities.

On comparing the flow pattern maps for +1º, +3º and +5º pipe inclinations, a number of observations can be made which are brought about by changes in the pipe inclination. The first thing to note is the increase in the region on the flow pattern map occupied by SW&MI flow pattern as the pipe inclination increases which suggests that for the same flow condition, the increase in pipe inclination enhances the evolution of droplets due to the increase in flow
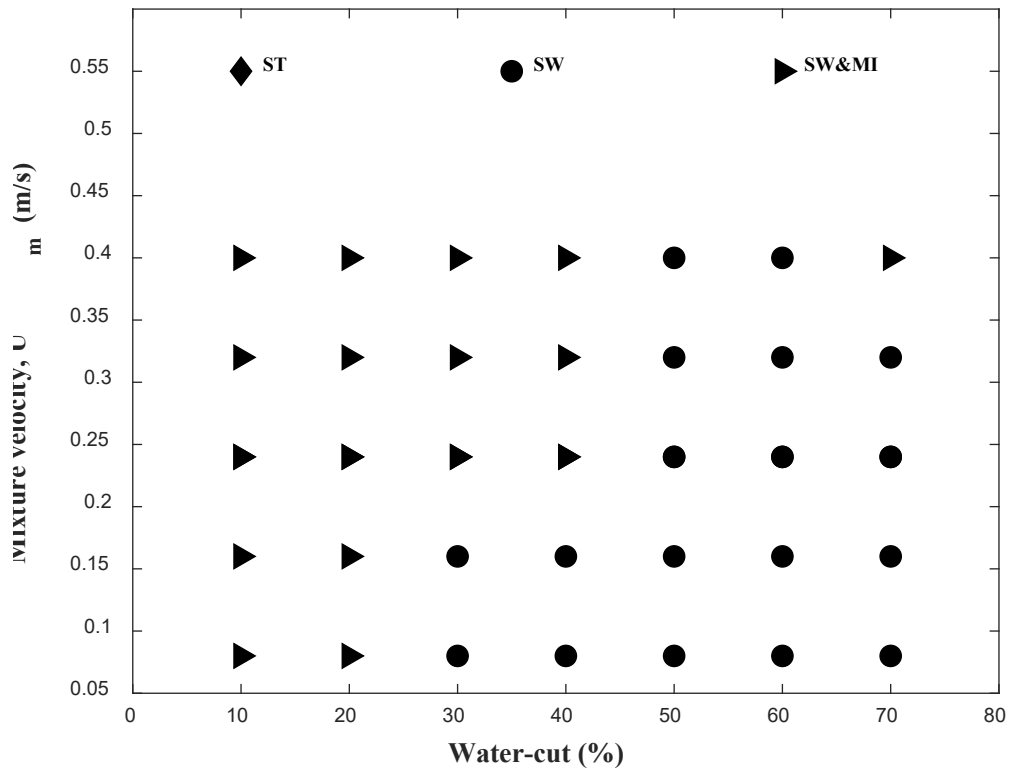
Figure 6.6: Flow pattern maps showing the SW and SW&MI flow patterns for +5º pipe inclination
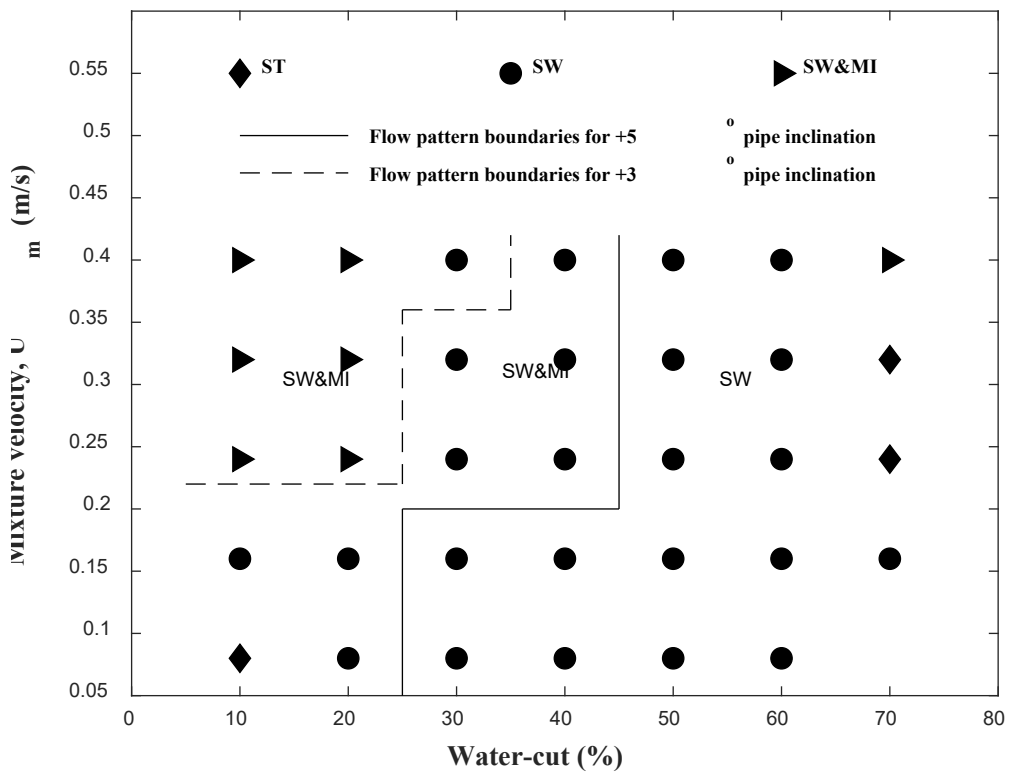
Figure 6.6a: Flow pattern map for the Y-type fluid inlet device with split plate (second fluid inlet device) at +1º pipe inclination with the flow pattern boundaries at +3º and +5º pipe inclinations superimposed.

disturbance introduce as a result of the higher inclination angle. Another interesting observation is that for all the pipe inclinations considered, there was a transition from SW to SW&MI flow pattern at the highest mixture velocity (U_m = 0.4 m/s) and highest water-cut (WC = 70%). It will be noted that at this point (U_m = 0.4 m/s and WC = 70%) the Reynolds number for the water phase are 31,280, 37,045 and 34,655 for +1º, +3º and +5º pipe inclination respectively which are far greater than the corresponding Reynolds number for the oil phase, hence the turbulent dispersive forces in the water phases could be the possible cause of droplets formation along the interface. Therefore, it appears that the turbulent dispersive forces in the oil phase contributes to the droplet generation at lower water cut whereas at higher water-cut, the generations of droplets along the interface are determined by the turbulent dispersive forces in the water phase.

(a) +1º   (b) +3º
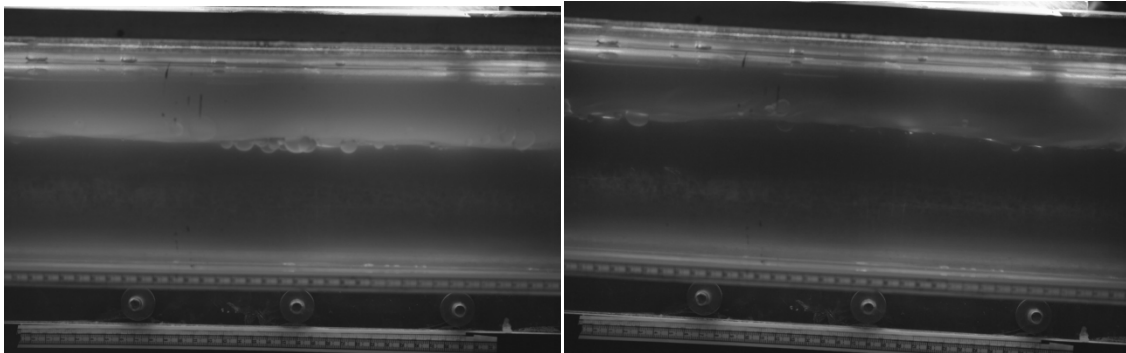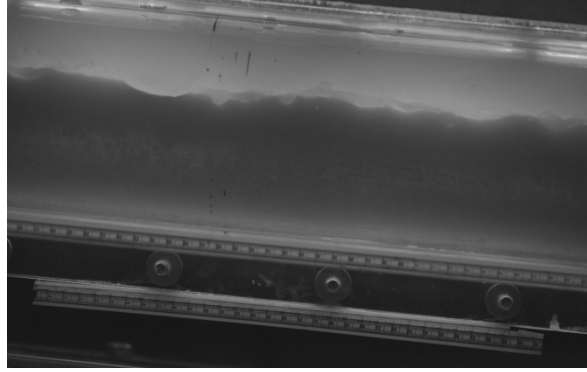
(c) +5°

Figure 6.7: Images showing the droplets along the interface for the different pipe inclination at WC = 70% and U_m = 0.4 m/s.

The flow patterns observed in this experimental work can be compared with those of Kumara et al., (2009) and Perera et al., (2018). At low mixture velocity (Um = 0.08 m/s) and for water-cut (WC < 90%), Kumara et al., (2009) observed stratified smooth with mixing at the interface (ST&MI) flow pattern and stratified smooth (ST) flow pattern was not identified for the +1° pipe inclination. On comparing with the current work, it will be observed that though the experimental flow conditions are similar, yet there are fundamental differences in the type and number of flow patterns observed. For instance, in the current work, stratified smooth with mixing at the interface (ST&MI) flow pattern was not observed, however stratified smooth (ST), stratified wavy (SW) and stratified wavy with mixing at the interface (SW&MI) were all observed within similar region in the flow pattern map of Kumara et al., (2009) where only ST&MI was observed. These differences could be attributed probably to the differences in size of the pipe geometry and the fluid properties used.

Similarly, for the +5° pipe inclination, Kumara et al., (2009) observed the SW flow pattern within the range of $25\% \leq WC \leq 90\%$ and for Um = 0.24 m/s while the SW&MI flow pattern was observed within the range of $5\% \leq WC \leq 10\%$ and for Um = 0.24 m/s. On comparing the region on the flow pattern map for the +5° pipe inclination where the SW and SW&MI flow patterns are located in the current work and that of Kumara et al., (2009), it will be observed

that they are quite similar although the inlet flow conditions (water-cut and mi xture velocity) for Kumara et al., (2009) are larger, therefore the boundaries for these flow pattern extends beyond that of the current work.

Perera et al., (2019) did not plot a detail flow pattern map for all the flow patterns identified, rather they provided a table that highlighted all the flow conditions where the various flow patterns were observed. For the +3º pipe inclination and for mixture velocity, U_m = 0.24 m/s, the researchers observed a stratified wavy (SW) flow pattern across all the water-cut which is consistent with the observations made in the current study. On increasing the mixture velocity to 0.32 m/s, the researchers observed SW&MI flow pattern at 10% WC, SW at 50% WC and SW&MI at 80% WC which is a similar observation made in the current study except that SW flow pattern was observed at 70% WC. Further increasing the mixture velocity to 0.4 m/s results in the appearance of the SW&MI flow patterns for all water-cut except at 90% where the researchers observed a different flow pattern called distinct oil droplet clusters in water (D-OC/W). In contrast with the current study, it appears that the region where SW&MI flow pattern appeared seemed to be smaller and falls within the range of WC ≤ 30% and also at the point where WC = 70%. In between these points, the SW flow pattern was observed. Similar observations were made for the +5º pipe inclination. The range of the water-cut and mixture velocities where the SW and SW&MI flow patterns were identified in the current work are in agreement with that of Perera et al., (2019) except that at Um = 0.4 m/s and WC = 50%, SW flow pattern was observed in the current work while Perera et al., (2019) observed SW&MI flow pattern and also the plug flow pattern at WC = 90% which was outside the experimental range of the current work.

6.4 Time-averaged interfacial height and Oil Volume Fraction (OVF)

The interfacial height normalized with the diameter of the pipe cross-section (D) and Oil Volume Fraction (OVF) are two important variables measured in this experimental work. The

former gives an indication of the thickness of water layer in a given pipe cross-section but more importantly the wave characteristics can equally be obtained using this measurement which will be discussed in later sections while the latter gives an indication of the area of the pipe cross-section occupied by the oil phase. The double parallel wire probe (DPWP) which consist of two sets of stainless steel wires stretched perpendicularly to the direction of flow was used to measure the interfacial height while the conductance probe (CP) was used to measure the OVF. Additionally, the OVF was also calculated from the measurement of the interfacial height by the DPWP in conjunction with the geometrical properties from the one dimensional two fluid model. The interfacial height and OVF were observed to be dependent on the flow conditions and the section following will attempt to examine and discuss the nature of such dependence.

6.4.1 Effect of the water-cut (WC) and mixture velocity on the normalized averaged interfacial height and OVF

The water-cut (WC) is an input variable which gives an indication of the fraction of the water phase in the inlet oil/water combined stream. The change in the water-cut (WC) directly affects in-situ water height (interfacial height) which in turn determines the area of the pipe cross-section occupied by the oil phase (OVF).

Figure 6.8 (a) showed that for a given mixture velocity, the normalized average interfacial height increases as the water-cut (WC) increases. Since the flow regimes observed (ST, SW and SW&MI) can all be classified as separated flow where there is continuous oil and water phases at the top and bottom of the pipe separated by an interface, then an increase in the water-cut (WC) for a given mixture velocity (U_m) essentially increases the thickness of the water layer, thus an increase in the normalized averaged interfacial height. The increase in the thickness of the water layer will lead to a corresponding decrease in the thickness of the oil layer which invariable will cause a decrease in the OVF as water-cut (WC) increases as seen in figures 6.9 (b) and (d) for +1° and +5° pipe inclinations respectively.

Also, for a given WC, it was observed that the normalized average interfacial height

decreases as the mixture velocity increases which can clearly be seen in figures 6.9 (a) and

(b)
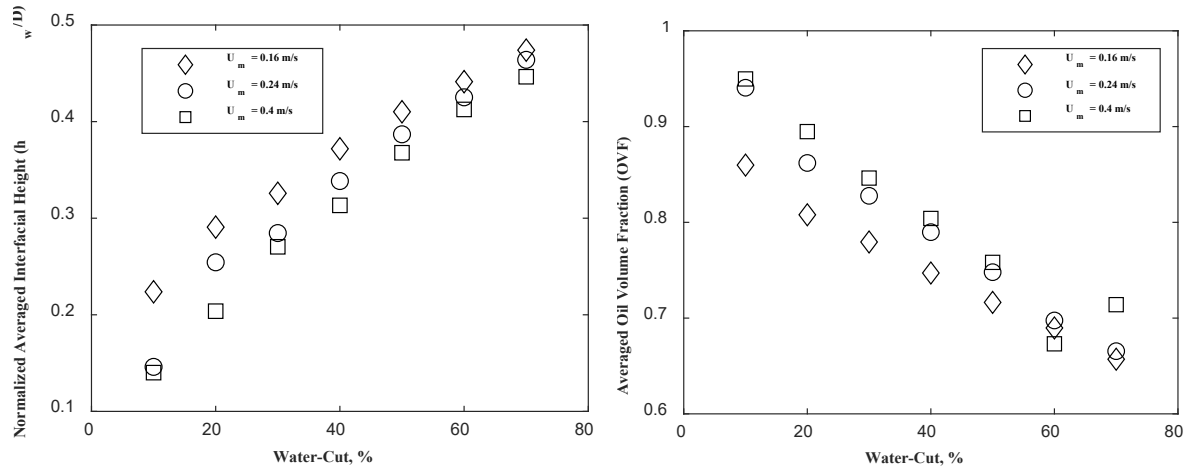
(a)
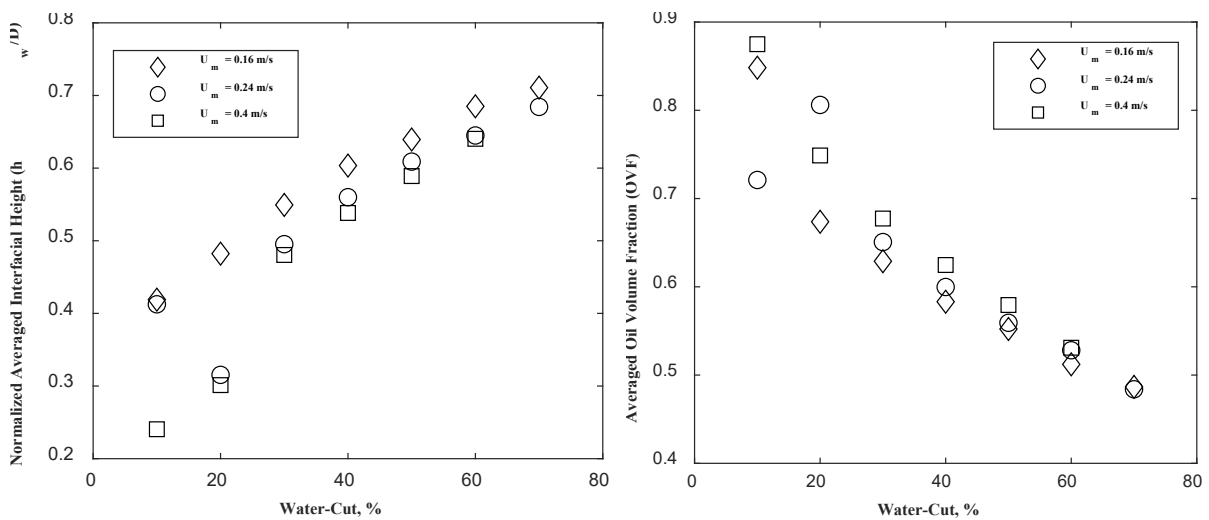
(b)

Figure 6.8: Effect of water-cut (WC) on (a) Normalized averaged interfacial height for +1° pipe inclination (b) Averaged Oil Volume Fraction (OVF) for +1° pipe inclination, (c) Normalized averaged interfacial height for +5° pipe inclination (b) Averaged Oil Volume Fraction (OVF) for +5° pipe inclination.
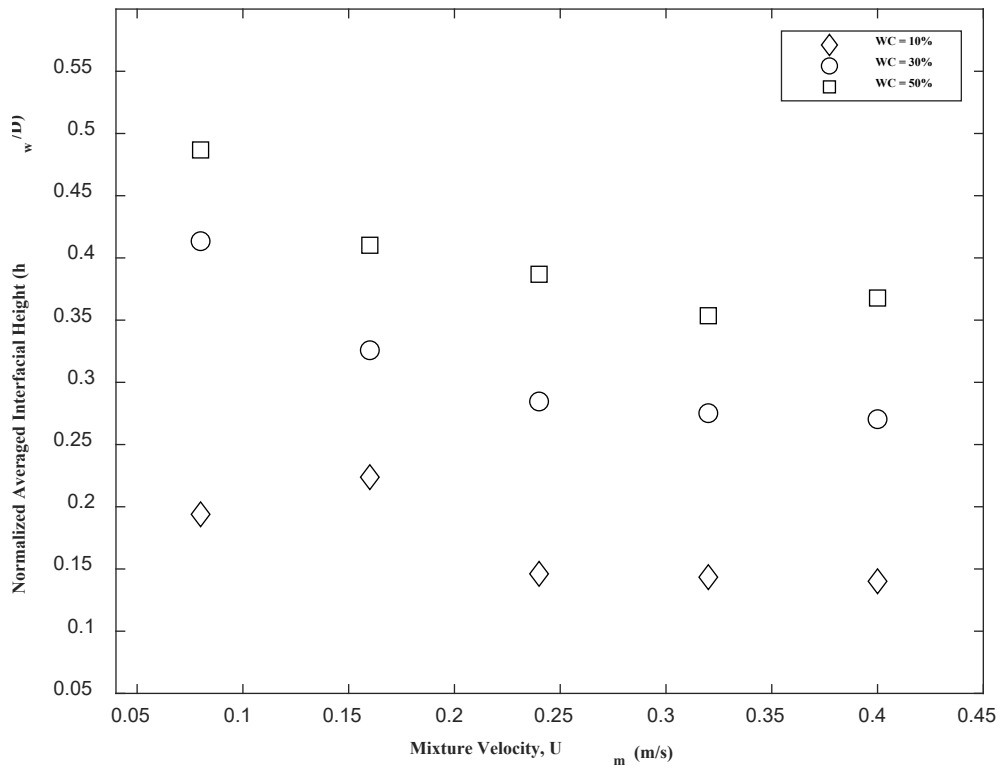
(a)
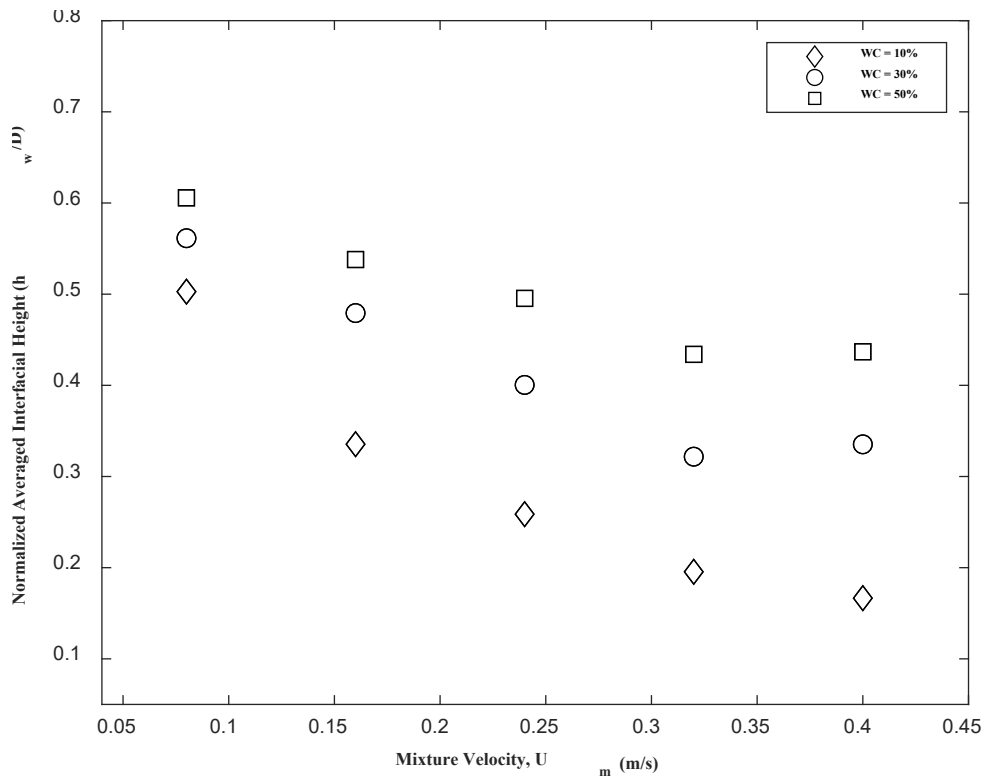
(b)

Figure 6.9: The effect of mixture velocity on the normalized averaged interfacial height for (a) +1º pipe inclination (b) +3º pipe inclination

The decrease in the normalized averaged interfacial height on increasing the mixture velocity for a given water-cut (WC) and pipe inclination could be associated with the increase in the cross-sectional area of the pipe occupied by the oil phase with corresponding decrease in the cross-sectional area occupied by the water phase, hence the decrease in the normalized averaged interfacial height.

6.4.2 Effect of pipe inclination on the normalized averaged interfacial height and OVF

The change in pipe inclination angle have been identified as one of the parameter that affects the distribution of the phases within a given pipe cross-section due to the action of gravitational force. The gravitational force acting on the fluid particle for flows across an inclined pipe can be resolved along two directions i.e. the axial direction which acts parallel to the direction of flow and also in the perpendicular direction which leads to flow segregation as a result of density difference.
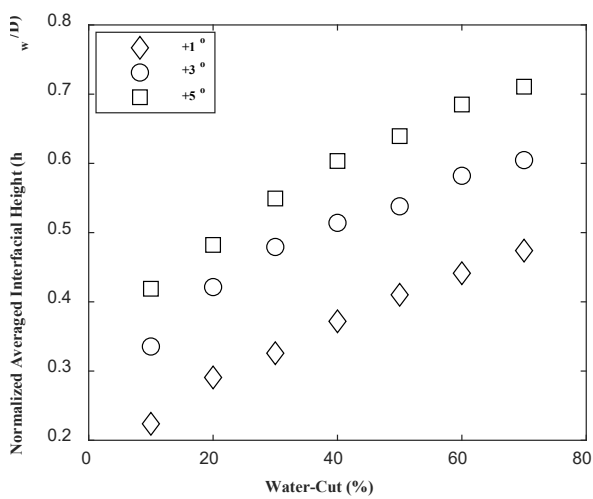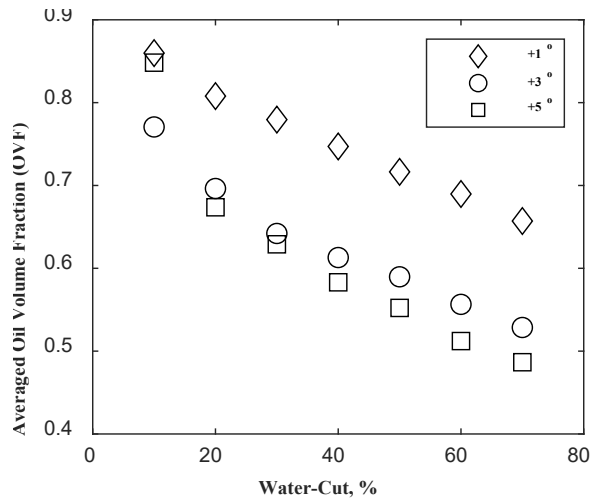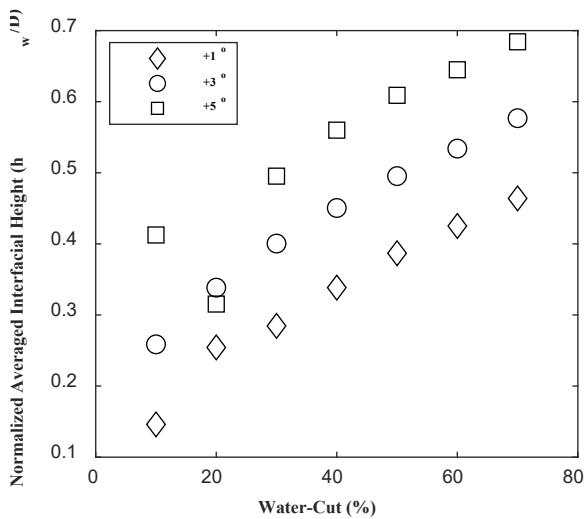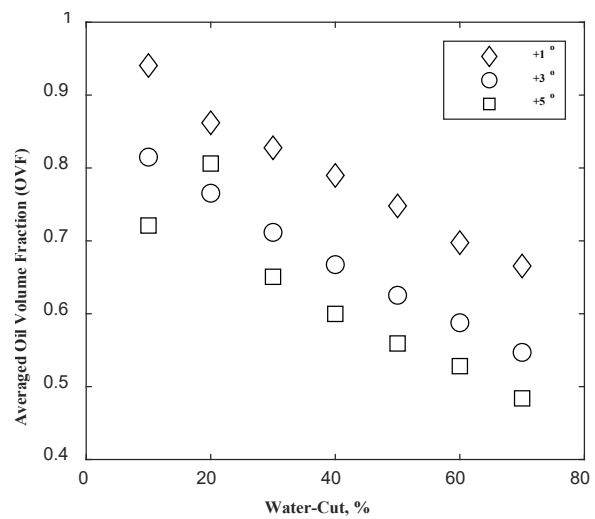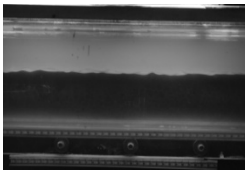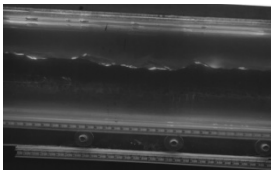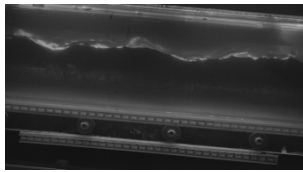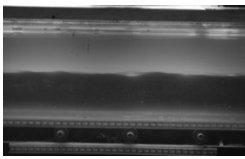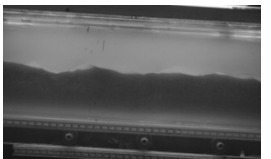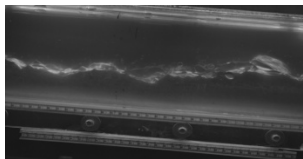
Figure 6.10: Figures showing the effect of pipe inclination on (a) normalized averaged interfacial height at mixture velocity, $U_m = 0.16$ m/s (b) OVF at mixture velocity, $U_m = 0.16$ m/s (c) normalized averaged interfacial height at mixture velocity, $U_m = 0.24$ m/s (d) OVF at mixture velocity, $U_m = 0.24$ m/s

Figures 6.10 (a) - (d) showed the effect of the pipe inclination angle in the upward direction on the normalized averaged interfacial height and the Oil Volume Fraction (OVF). It will be observed that for a given mixture velocity, $U_m = 0.16$ m/s, the normalized averaged interfacial height increases with increase in pipe inclination angle in the upward direction. As stated earlier, the parallel component of the gravitational force acts in the opposite direction to the

flow and therefore retards the flow of the denser water phase leading to its accumulation in the pipe. The effect of the parallel component of the gravitational force increases as the pipe inclination angle increases from $+1^\circ$ to $+5^\circ$, hence the thickness of the water layer also increases which invariably leads to increase in the normalized averaged interfacial height. Also, it can be observed that in both figures 6.10 (a) and (b), the averaged Oil Volume Fraction (OVF) decreases as the pipe inclination angle increases. It should be pointed out that the normalized averaged interfacial height and Oil Volume Fraction (OVF) behave in an opposite manner in response to the change in pipe inclination. For instance, as stated earlier, the normalized averaged interfacial height increases as the pipe inclination angle increases as a result of the action of the axial component of the gravitational force on the water phase. The increase in the thickness of the water layer in a given pipe cross-section increases the water holdup and since the water holdup and the OVF sums up to unity, it therefore means that the OVF will decrease as the pipe inclination angle increases. In other words, the thickness of the oil layer will decrease as the pipe inclination angle increases and this is consistent with the images of the flow taken at those conditions as shown in table 6.1.

Table 6.1: Images showing the effect of pipe inclination on thickness of water layer and OVF

U_m (m/s) / WC (%)	$+1^\circ$	$+3^\circ$	$+5^\circ$
0.16 / 40			
0.24 / 40			

		186	

6.4.3 Comparison between the interfacial height from the parallel wire probe and image analysis.

The interfacial heigh which gives an indication of the thickness of the water layer was measured using the double parallel wire probe (DPWP) which essentially consist of two steel wires positioned at the central plane of the pipe. Also, the flow images obtained from the high-speed camera were analyzed using image-J image analysis software and the interfacial heights were measured from selected images.

Figure 6.11: Representative of the interfacial height measurement from image analysis
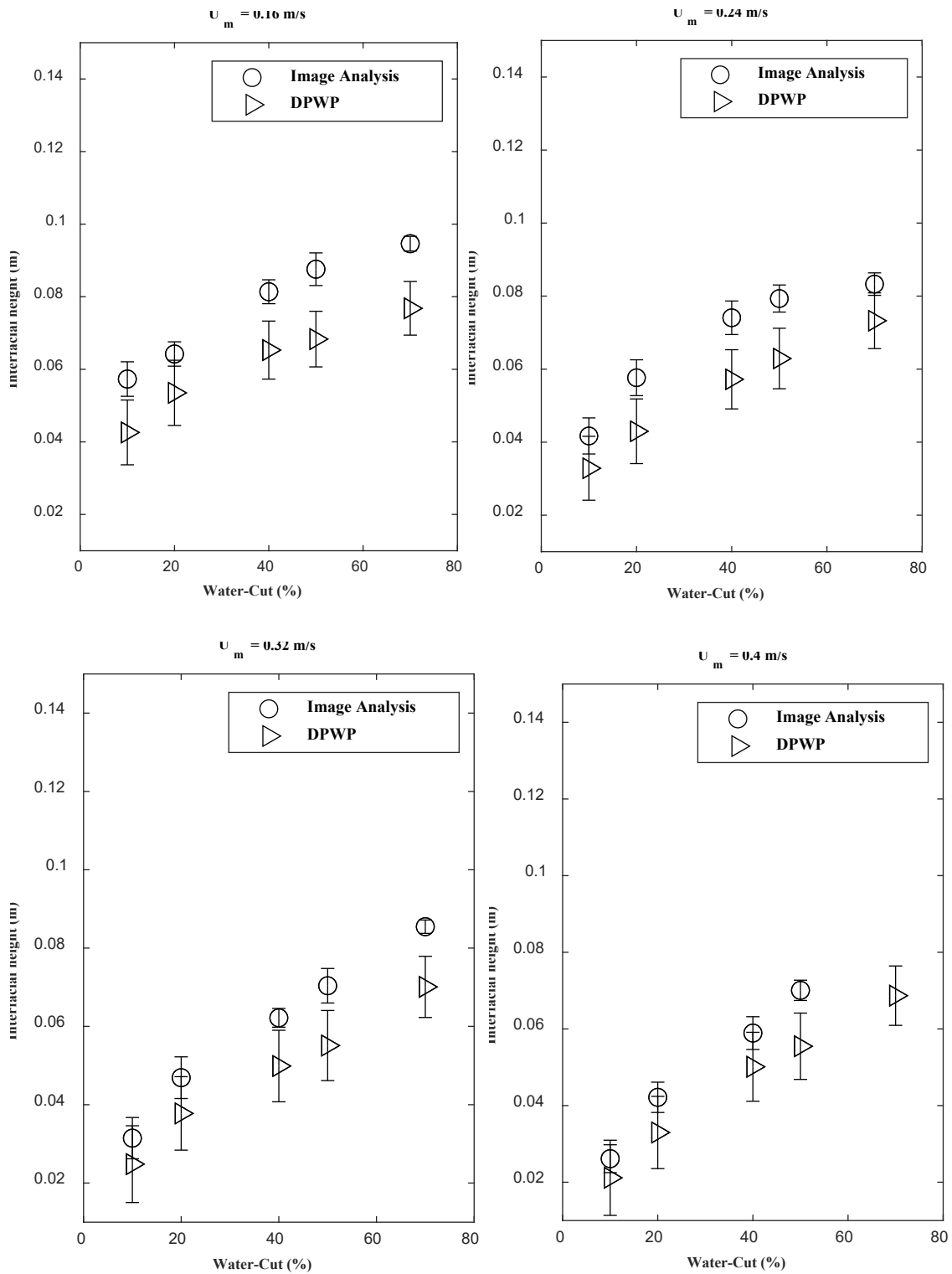
Figure 6.12: A plot of the mean interfacial height measured from the double parallel wire probe (DPWP) and the image data for mixture velocities Um = 0.16 m/s, 0.24 m/s, 0.32 m/s and 0.4 m/s at +3° pipe inclination

Figure 6.12 showed the comparison between the interfacial height obtained from DPWP and those from the image analysis. The assumption of a flat interface along the pipe cross section was made in this study as a result of a large pipe diameter (0.127 m) which increases significantly the Bond number. The increase in the Bond number is as a result of the reduction in the surface forces which essentially reduces the interface curvature, hence the assumption of the flat interface is valid. It will be observed that the interfacial height from both measurements are in good agreement and the mean absolute percent errors (MAPE) are 26.1%, 26.1%, 25.0% and 23.8% for the mixture velocities (U_m) 0.16 m/s, 0.24 m/s, 0.32 m/s and 0.4 m/s respectively. It is also worth noting that the interfacial height increases linearly with the Water Cut (WC), however, the rate of increase of the interfacial height decreases as the interfacial height approaches towards the pipe centre where the largest pipe curvature is obtained. Also, one may notice that the interfacial height measurement using the DPWP are higher than those obtained from the image analysis across all the mixture velocities probably due to the fact that in using the DPWP, 12,000 data points which covers a wider range of interface fluctuations were used in calculating the mean interfacial height. But in using the image analysis, 20 images were selected and for each image, at least 10 different locations were used in measuring the interfacial height and the average for each image was obtained. Also, the difference in the two measurements could be as a result of droplets of different sizes appearing at the interface that could interfere with the accurate measurement of the interfacial height from the DPWP.

6.5 WAVE EVOLUTION ALONG THE OIL-WATER INTERFACE

The evolution of waves along the oil-water interface have been identified as one phenomenon that influences pressure drop, holdup distribution and the transition from stratified to non-stratified flow. In this experimental work, the evolution of interfacial waves are captured using the high speed camera positioned 450 cm from the fluid inlet device and also with the use of double parallel wire probe (DPWP) that captures the in-situ fluctuations of the interfacial height

as a result of the movement of the waves. In order to study the growth or decay of the wave amplitude along the axial direction, the DPWP was placed in two locations i.e. 140 cm and 450 cm from the fluid inlet device and the detail discussion of this will be done in the subsequent section on stability analysis.

In a bid to understand the growth or decay of the waves along the interface, several studies were conducted to monitor the response of the interfacial height to various sets of input conditions (water-cut (WC) and mixture velocity (U_m)). From the experimental findings, it was observed that for all the pipe inclinations and for a given mixture velocity, the largest interfacial wave amplitude appeared at the lowest water-cut and the wave amplitude was found to progressively decay as the water-cut increases

Figure 6.13 (a) – (c) showed the behavior of the interface with time in response to the wave motion. It will be observed that for all the pipe inclinations ($+1^o$, $+3^o$ and $+5^o$), the interfacial waves with the largest amplitudes were obtained at the lowest water-cut (WC = 10%) while at the highest water-cut (WC = 70%), the interfacial waves have the lowest amplitude. Although, this observation was not so obvious at $+1^o$ pipe inclination, however as the inclination angle increases ($+3^o$ and $+5^o$), the trend appears to be more noticeable. At 10% WC and for U_m = 0.24 m/s, the average interfacial wave amplitude are 5.08 mm, 6.41 mm and 8.15 mm for $+1^o$, $+3^o$ and $+5^o$ pipe inclination respectively whereas for the same mixture velocity and pipe inclination with WC = 70%, the average interfacial wave amplitude are 4.84 mm, 6.52 mm and 4.52 mm respectively. This result equally shows that the interfacial wave amplitude increases with increase in pipe inclination angle. Interestingly, the appearance of droplets were first observed when WC = 10% which corresponds to the point with the largest interfacial wave amplitude and the swarm of these droplets were localized along the interface, thus the stratified wavy with mixing at the interface (SW&MI) flow pattern was found to exist at this point.

The origin of the droplets can be attributed to the shearing of the high amplitude interfacial waves as a result of the high relative velocity between the oil and water phases. Droplet generation due to turbulent mixing of the oil and water phases at the inlet have been minimized through the design of the fluid inlet device that keeps the fluids separated with the aid of a separator plate. Since droplets were not observed when $U_m < 0.24$ m/s and for all water-cuts particularly

(a)   (b)

(c)
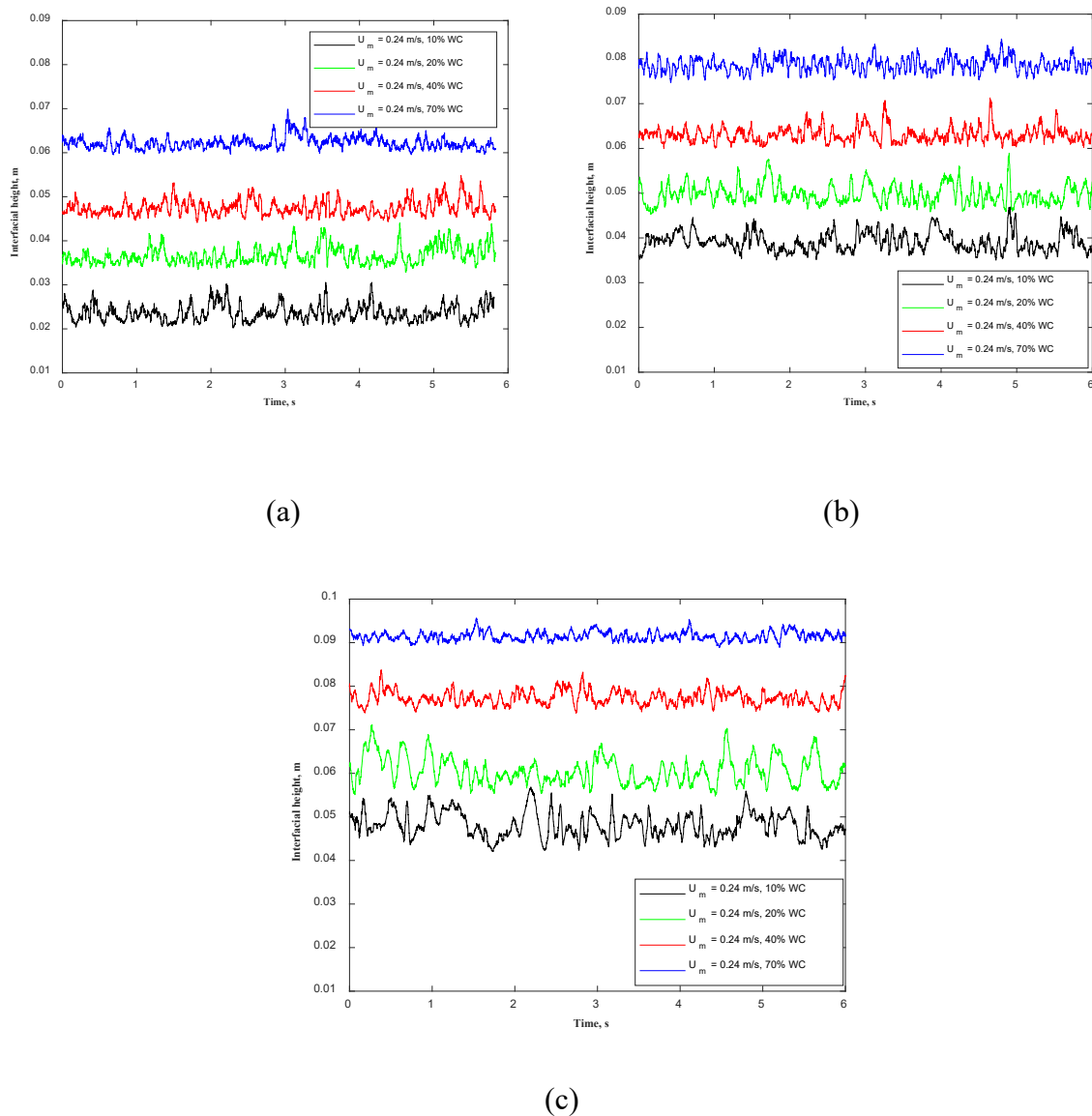
Figure 6.13: Time trace of the interfacial height which shows the fluctuating nature of the interface for $U_m = 0.16$ m/s at (a) +1° pipe inclination (b) +3° pipe inclination and (c) +5° pipe inclination

for +1º and +3º pipe inclinations, then it can be said that the onset of liquid entrainment which marks the point where the first droplets were observed for these experimental conditions occurs when U_m = 0.24 m/s and WC = 10%. However, for the +5º pipe inclination, the first droplets were observed when U_m = 0.08 m/s and WC = 10% which implies that the droplets appeared earlier compared to the +1º and +3º pipe inclinations probably as a result of increased disturbance introduced as a result of increased pipe inclination angle. Beyond the point where the droplets were first observed (onset of entrainment), the interfacial wave amplitude were observed to decrease progressively for all the pipe inclination angles.

6.6 INTERFACIAL WAVE CHARACTERISTICS

The presence of waves along the oil-water interface have been known to play a very significant role in flow pattern transition from stratified to non-stratified flows and to equally have an impact on the pressure drop and holdup distribution. In order to characterize these interfacial waves, certain attributes such as the wave amplitude, wavelength and wave speed needs to be identified and also their responses to changes in the experimental input conditions needs to be understood. The following section will attempt to describe these interfacial waves in terms of the attributes mentioned above and their corresponding responses to different input conditions.

6.6.1 Distribution of interfacial wave amplitude

Based on experimental observations, it was noted that for a given mixture velocity and water-cut, interfacial waves of different sizes exist and the wave amplitude ranges from 0.5 mm to 16 mm, thus one of the ways to describe the variation of these amplitudes with input condition is to consider its distribution using the Probability Density Function (PDF). The wave amplitude is considered to be the vertical distance normal to the interface and measured between the wave crest or trough and the mean height of the interface.

In the literature, there was no any general criteria for wave categorization in terms of wave amplitude for a liquid-liquid flow system, however some researchers made effort to categorize the waves based on their wavelength (de Castro et al., 2011, 2012). But, in this research work and in order to systematically analyze the waves, attempt was made to categorize the waves based on the size of their amplitudes into small amplitude waves ($\alpha \leq 2$ mm), intermediate amplitude waves ($2mm \leq \alpha \leq 10$ mm) and large amplitude waves ($\alpha \geq 10$ mm). Within this categorization, the two extremes are the small amplitude waves (ripples) which are short waves that may eventually decay as they travel along the length of the test pipe and the large amplitude waves which appear less frequently and have the lowest number density (pdf). Therefore, majority of the waves that propagates along the interface can be classed as intermediate waves.

6.6.1.1 Effect of water-cut (WC) on the distribution of interfacial wave amplitude

The water-cut (WC) is the quantity that gives an indication of the fraction of water in the inlet stream and in combination with the mixture velocity; it can determine the superficial velocities of both the water and oil phase. Since the water-cut (WC) have an effect on both the superficial and in-situ velocity of the phases, therefore the relative velocity (the difference between the water and oil in-situ velocity) which determines the growth of the interfacial wave amplitude will equally be affected by the water-cut (WC), hence the extent to which the water-cut (WC) will affect the interfacial wave amplitude distribution will be examined in this section while the effect of relative velocity on the mean interfacial wave amplitude will be dealt with in subsequent section.
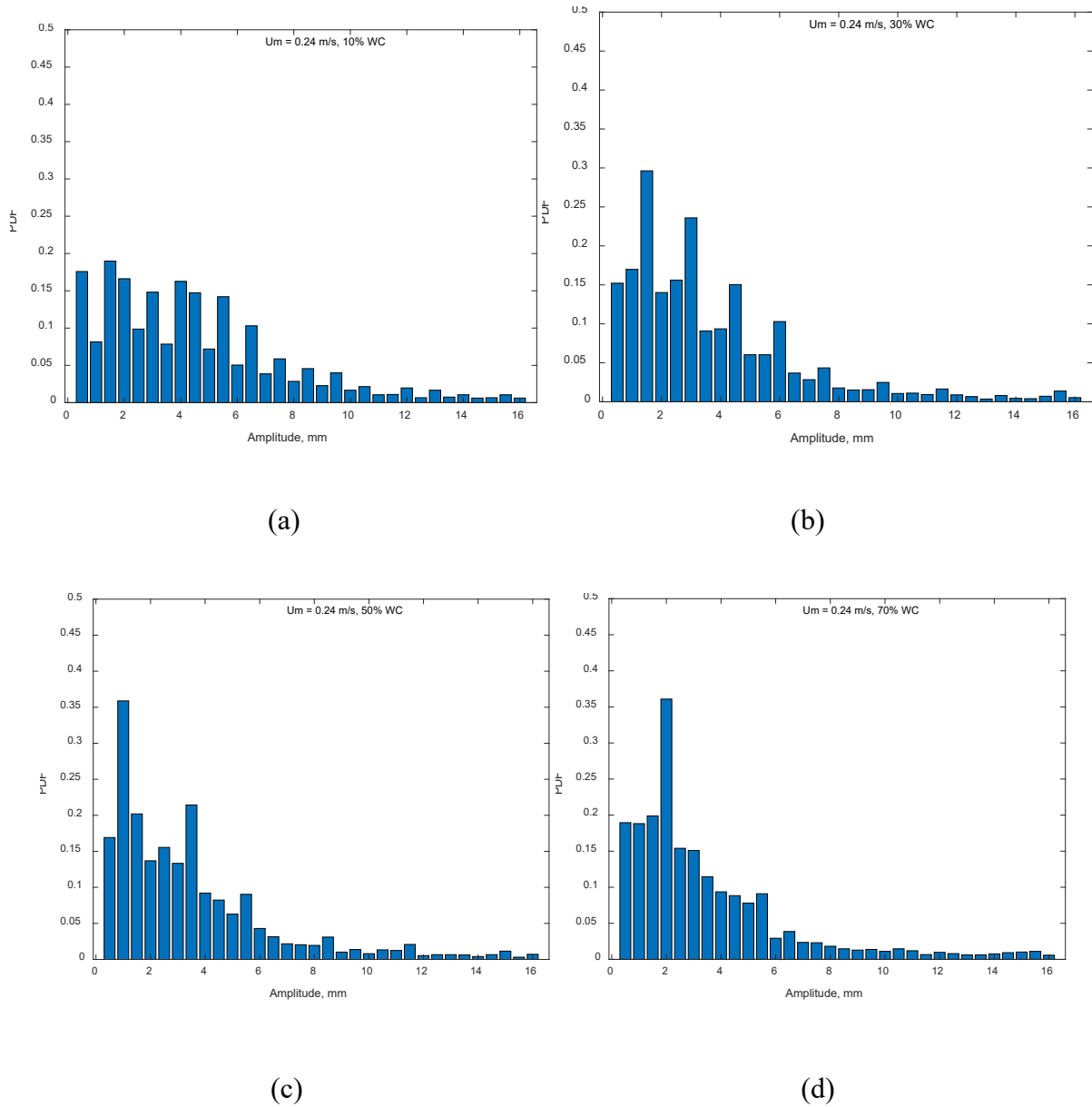
Figure 6.14: Distribution (PDF) of interfacial wave amplitude for the mixture velocity (U_m = 0.24 m/s) at (a) 10% WC (b) 30% WC (c) 50% WC and (d) 70% WC.

Figure 6.14 (a) – (d) shows the effect of water-cut on the interfacial wave amplitude distribution for mixture velocity (U_m = 0.24 m/s) and +3° pipe inclination.

In order to understand how the wave amplitude are distributed in response to change in the water-cut (WC), the number densities of each of the wave categories will be used. Considering the small amplitude waves ($\alpha \leq 2$ mm), for change in WC from 10% to 70%, the number

density (which is the sum of the pdf of wave amplitude within each category) changes from 0.61 to 0.94 which implies that at 10% WC, there are less small amplitude waves compared to when the WC = 70%. Again, for the intermediate amplitude waves ($2mm \leq \alpha \leq 10$ mm), the number density changes from 1.25 to 0.96 on changing the WC from 10% to 70%. This means that intermediate amplitude waves were seen to appear more at WC = 10% compared to that of 70% WC. Finally, for the large amplitude wave ($\alpha \geq 10$ mm), the number density changed from 0.13 to 0.10 on increasing the WC from 10% to 70% which means that more of large amplitude waves appear at WC=10% compared to that of WC = 70%. Overall, it can be seen that at 10% WC, there appears to be more of the intermediate amplitude and large amplitude waves with less of the small amplitude waves compared to that of 70% WC. This implies that the interface is more disturbed at WC =10% with more appearance of waves of larger amplitude as against when WC =70% where more of the small amplitude waves exist and the interface is relatively stable. This observation is consistent with the experimental images taken at those experimental conditions as seen in figure 6.13.
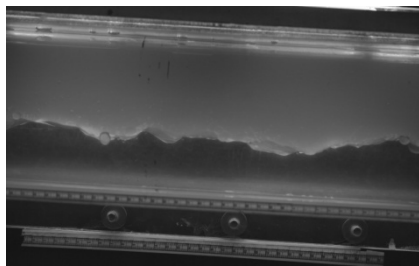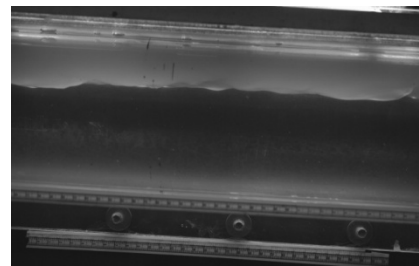
(a) U_m = 0.24 m/s, 10% WC   (b) U_m = 0.24 m/s, 70% WC

Figure 6.15: Images showing the decrease in interfacial wave amplitude for +3° pipe inclination.

6.6.1.2 Effect of pipe inclination angle on the distribution of interfacial wave amplitude.

The change in pipe inclination angle in the upward direction have been known to affect the growth of the waves propagating across the interface as a result of the increased action of the axial component of acceleration due to gravity (which affects the slip velocity), hence its effect on the wave amplitude distribution. In figure 6.16 (a) – (d), the distribution of the wave amplitude across +3º and +5º pipe inclination angles are presented. For mixture velocity, U_m = 0.24 m/s and water-cut (WC = 10% and 70%), it will be observed that distribution of the histograms are similar for both the +3º and +5º pipe inclinations. However, on critically examining the distribution of the different categories of waves as described in the previous section, it will be observed that for the small amplitude waves ($\alpha \leq 2$ mm), the number density decreased from 0.61 to 0.57 for +3º and +5º pipe inclination respectively. The decrease in the number density implies that increasing the pipe inclination angle from +3º to +5º will result in fewer small amplitude waves present in the flow at +5º inclination compared to +3º pipe inclination. Considering also the intermediate amplitude waves ($2mm \leq \alpha \leq 10$ mm), it was observed that the number density for +3º pipe inclination was 1.25 and decreased to 1.13 on increasing the pipe inclination to +5º. This means that fewer intermediate amplitude waves are present at +5º pipe inclination compared to the +3º pipe inclination. However, for the large amplitude waves ($\alpha \geq 10$ mm), the number density increased from 0.13 to 0.30 on increasing the pipe inclination from +3º to +5º implying that more waves of larger amplitude are present on increasing the pipe inclination from +3º to +5º for the same flow condition.
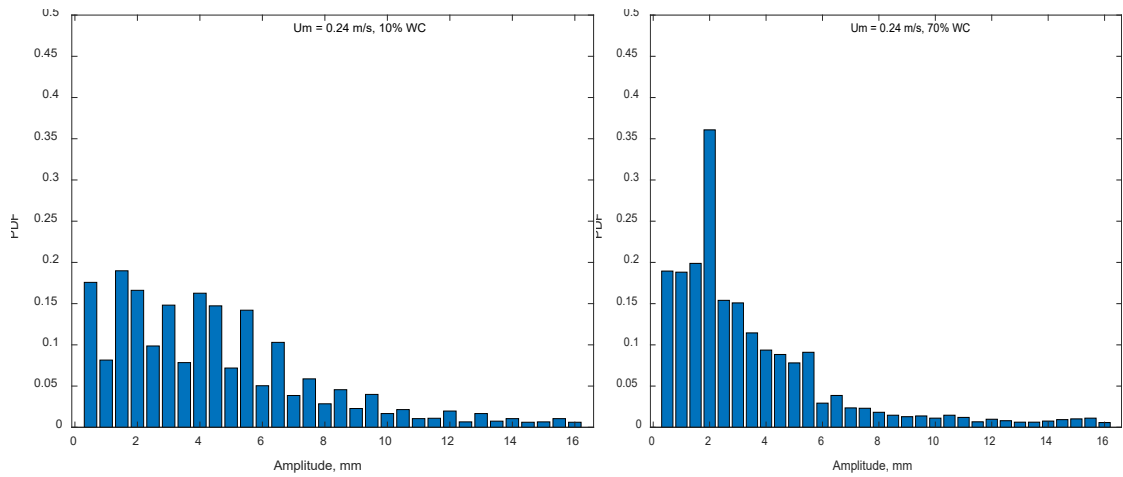
(a) $U_m = 0.24$ m/s, 10% WC, +3º (b) $U_m = 0.24$ m/s, 70% WC, +3º
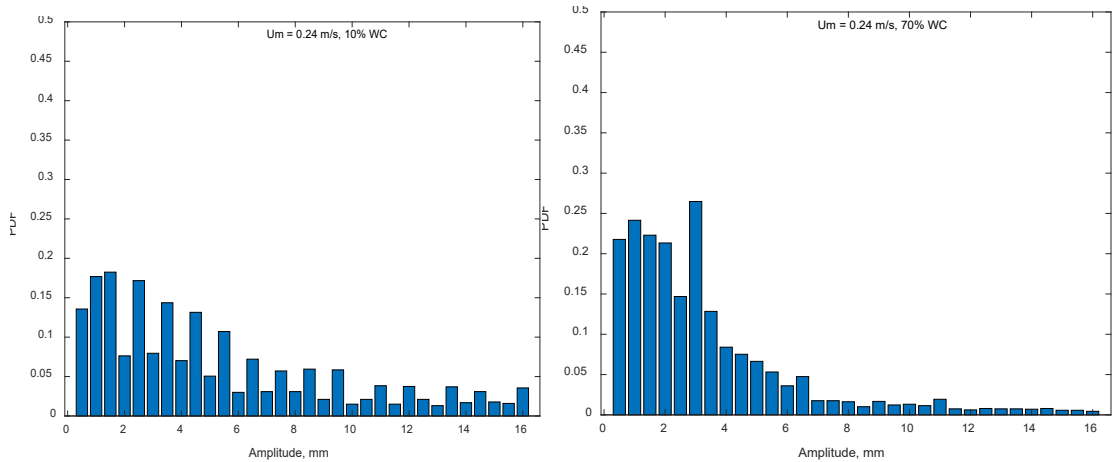
(c) $U_m = 0.24$ m/s, 10% WC, +5º (d) $U_m = 0.24$ m/s, 70% WC, +5º

Figure 6 .16: A figure showing the effect of pipe inclination angle on the wave amplitude distribution for mixture velocity, Um = 0.24 m/s, water-cut (WC = 10% and 70%) and inclination angle (+3º and +5º)

Similarly, on increasing the mixture velocity to 0.4 m/s, it appears also that the distribution of the wave amplitude shifted to the right which means that larger amplitude waves are formed when the pipe inclination angle increased from +3º to +5º as seen in figure 6.17 (a) – (d).
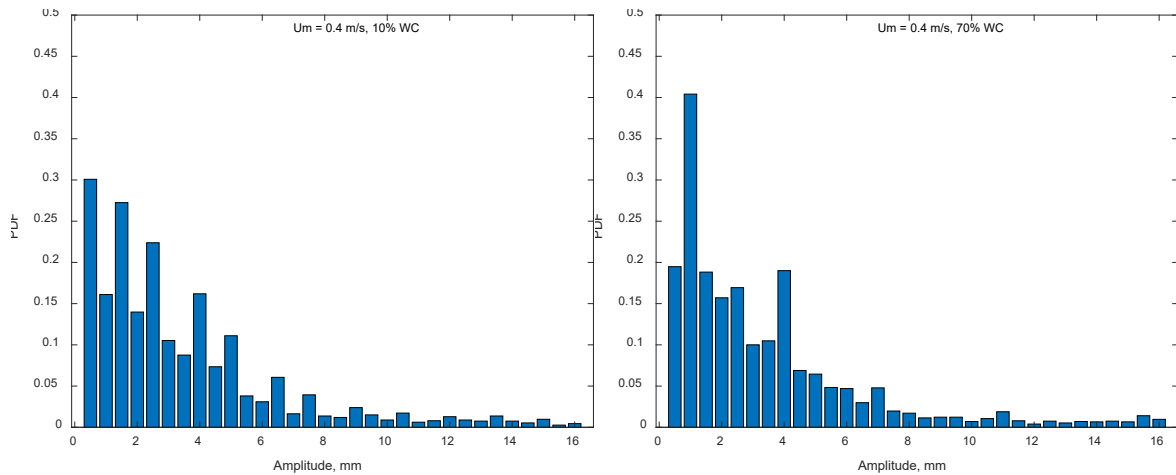
(a) $U_m = 0.4$ m/s, 10% WC, +3°　　　　　　(b) $U_m = 0.4$ m/s, 70% WC, +3°
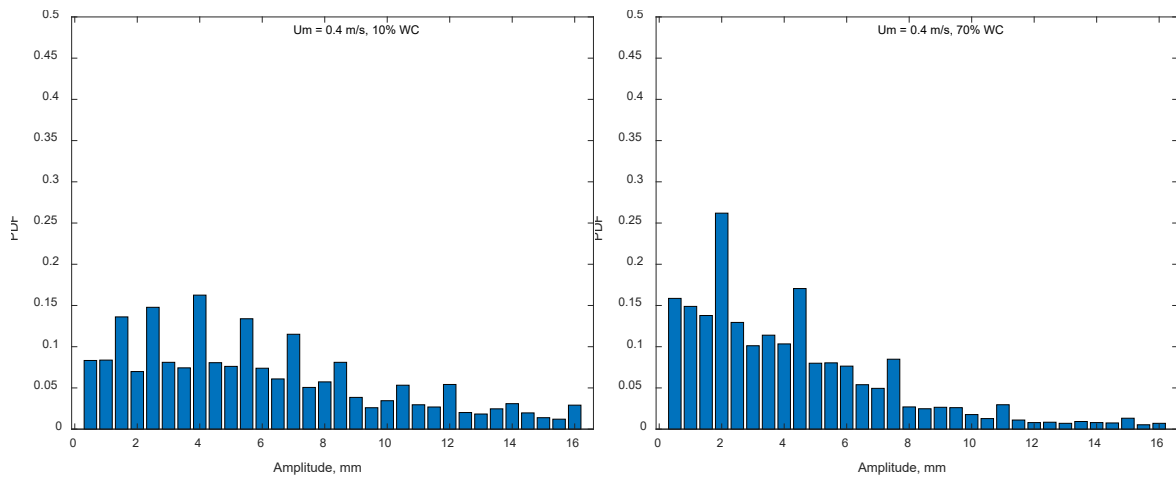
(c) $U_m = 0.4$ m/s, 10% WC, +5°　　　　　　(d) $U_m = 0.4$ m/s, 70% WC, +5°

Figure 6.17: A figure showing the effect of pipe inclination angle on the wave amplitude distribution for mixture velocity, Um = 0.4 m/s, water-cut (WC = 10% and 70%) and inclination angle (+3° and +5°)

Considering also the distribution of the different categories of waves and their corresponding number densities, it will be obseved that in figure 6.17 (a) and (c), the number density for the small amplitude waves ($\alpha \leq 2$ mm) decreased from 0.87 to 0.37 on increasing the pipe inclination from +3° to +5° which connotes a decrease in appearance of short amplitude waves at the +5° inclination angle compare to the +3° angle. Also, for the intermediate amplitude waves, the number density increased from 1.02 to 1.29 as the inclination angle was increased

from +3° to +5° which clearly shows that there is an increase in the appearance of intermediate amplitude waves at the higher inclination angle. However, for the large amplitude waves, it was noticed that the number density increased from 0.10 to 0.33 which shows that there is a considerable increase in the appearance of large amplitude waves as the inclination angle was increased from +3° to +5°. Similar argument can also be made when the water-cut (WC) was increased to 70% where it was observed that there was a decrease in the appearance of small amplitude waves and increase in the appearance of both intermediate and large amplitude waves based on the changes in their corresponding number densities on increasing the pipe inclination from +3° to +5° as shown in figure 6.17 (b) and (b). Generally, from all the observation made from both figures 6.16 (a) – (d) and 6.17 (a) – (d), it can be said that on increasing the inclination from +3° to +5° for both low and high water-cuts (10% and 70%), there were less appearances of short amplitude waves ($\alpha \leq 2$ mm) while the intermediate amplitude waves ($2mm \leq \alpha \leq 10$ mm) and large amplitude waves ($\alpha \geq 10$ mm) were found to increase in appearance for both mixture velocities ($U_m = 0.24$ m/s and $U_m = 0.4$ m/s) as can be seen in figure 6.18 (a) – (d).

(a)   (b)

<p style="text-align:center;">(c)   (d)</p>
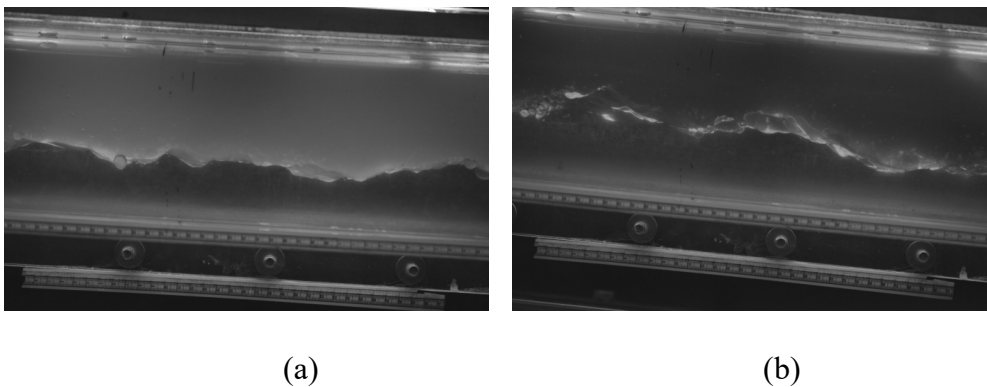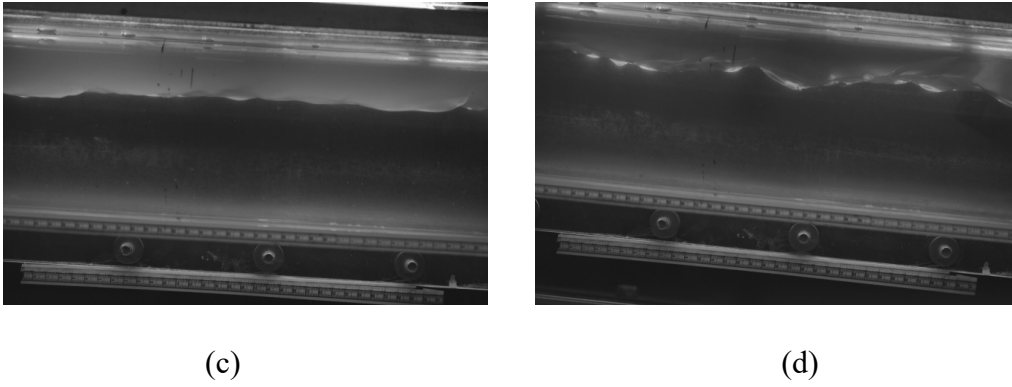
Figure 6 18: Images of the interfacial waves showing the increase in the wave amplitude as the pipe inclination angle was increased from +3º to + 5º for (a) U_m = 0.24 m/s, WC = 10%, +3º (b) U_m = 0.24 m/s, WC = 10%, +5º (c) U_m = 0.24 m/s, WC = 70%, +3º and (d) U_m = 0.24 m/s, WC = 70%, +5º

6.6.2 Effect of water-cut (WC) on mean interfacial wave amplitude.

In the previous section and on the basis of the distribution of the interfacial wave amplitude, it was stated that the intermediate amplitude waves ($2mm \leq \alpha \leq 10$ mm) and the large amplitude waves ($\alpha \geq 10$ mm) were seen to appear more at the lowest water-cut (WC = 10%) when compared to similar appearances for the highest water-cut (WC = 70%). In order to clearly understand the trend of how the interfacial wave amplitude vary with the water-cut, the mean of the interfacial wave amplitude for each experimental conditions were determined and plotted against the water-cut (WC) as seen in the figures 6.19a and 6.19b.

According to figure 6.19a, there is a clear indication that the interfacial wave amplitude decreases linearly with increase in water-cut across all the mixture velocities. This shows that the interface experiences larger disturbances at low water-cut where larger amplitude waves seem to appear more frequently whereas at high water-cut, the interface appears to be relatively stable
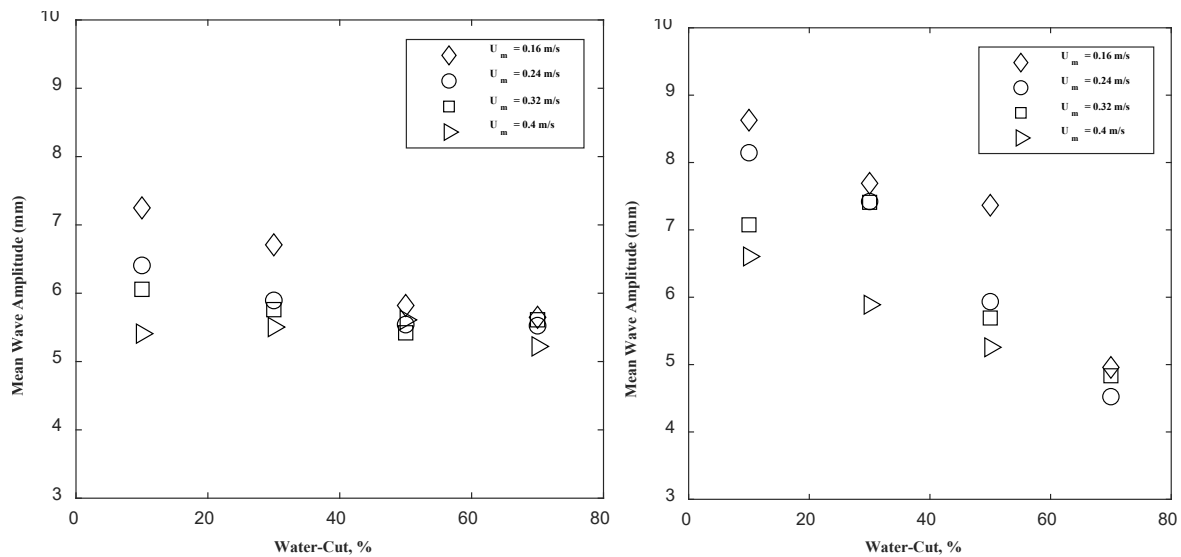
Figure 6.19: A figure showing the effect of water-cut on the mean interfacial wave amplitude for different mixture velocities at (a) +3° pipe inclination and (b) +5° pipe inclination.

with small amplitude waves appearing more frequently. Also, for all water-cuts, the mean interfacial wave amplitude appears to decrease on increasing the mixture velocity (U_m). Considering the mixture velocity, U_m = 0.16 m/s, large amplitude interfacial waves appeared at low water-cut (WC = 10% and 20%) and there was no appearance of any droplets along the interface, hence the flow pattern observed was the stratified wavy (SW) for all the water-cuts. However, on increasing the mixture velocity, Um = 0.24 m/s, large amplitude waves appeared at 10% - 20% WC with droplets equally observed which implies that the stratified wavy with mixing at the interface (SW&MI) flow patterns prevails at these conditions. The appearance of droplets at these conditions could be as a result of increase in the shear forces along the interface due to increased turbulence in both the water and oil phase as the mixture velocity increases. The oil and water phase Renolds numbers (Re_o and Re_w) increased from 5819.3 to 8067.6 and from 5234.8 to 9022.1 respectively as the mixture velocity (U_m) increased from 0.16 m/s to 0.24 m/s at 10% WC. The increased turbulence which results in the shearing of the interface leading to the formation of more droplets along the interface could somewhat explain the decrease of the mean interfacial wave amplitude from 7.25 mm to 6.41 mm on increasing

the mixture velocity from $U_m = 0.16$ m/s to $U_m = 0.24$ m/s for 10% WC. Further increase in the mixture velocity from $U_m = 0.24$ up to $U_m = 0.4$ m/s results in an increase in the number of droplets appearing at the interface, hence the resultant decrease in the mean interfacial wave amplitude.

(a) Um = 0.16 m/s, WC = 10%

(b) Um = 0.24 m/s, WC = 10%

(c) Um = 0.32 m/s, WC = 10%

(d) Um = 0.4 m/s, WC = 10%
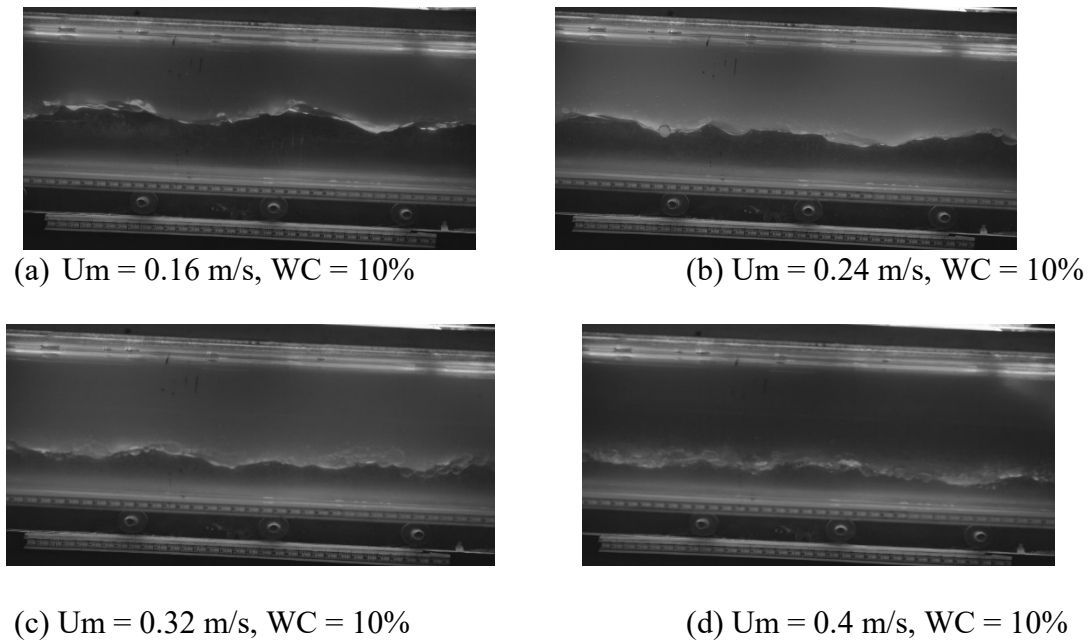
Figure 6.20: Images showing the decrease in interfacial wave amplitude on increasing the mixture velocity (U_m from 0.16 m/s to 0.4 m/s) at 10% WC and +3° pipe inclination.

6.6.3 Effect of relative velocity on the mean interfacial wave amplitude.

The relative velocity which is the difference in the in-situ velocities of both the water and oil phases have been identified by several researchers such as Al-Wahaibi and Angeli (2011), Barral (2014), Castro et al.,(2012) and Perera et al., (2019) as one of the primary variable that determines the size of the interfacial wave amplitude. This section attempts to examine the nature of the dependence of the mean interfacial wave amplitude on the relative velocity.
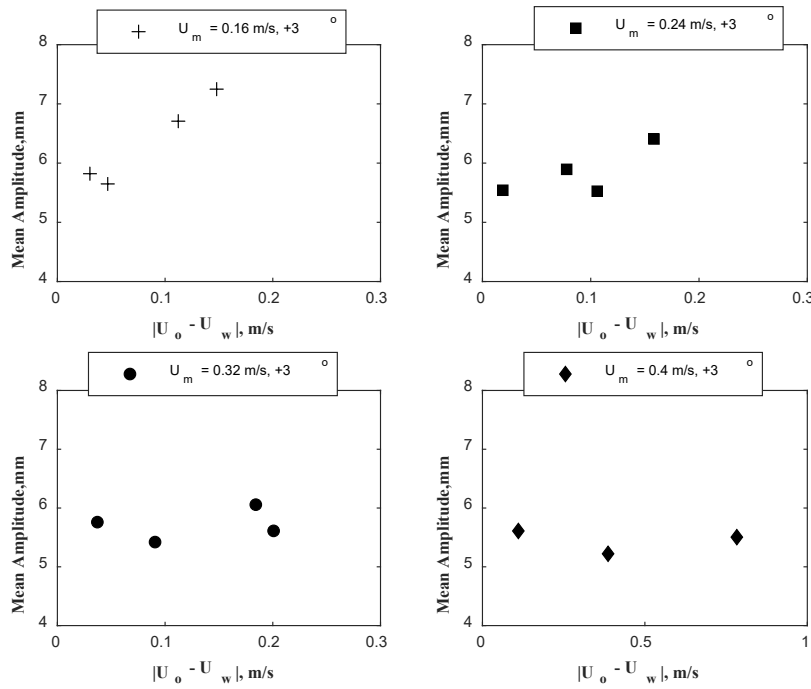
Figure 6.21: A figure showing the effect of the relative velocity on mean amplitude for mixture velocities Um = 0.16 m/s, 0.24 m/s, 0.32 m/s and 0.4 m/s across a +3° pipe inclination

In Figure 6.21, one may notice that at low mixture velocity (Um = 0.16 m/s and 0.24 m/s), there is an upward trend when the mean amplitude was plotted against the relative velocity between the oil and water phases. This suggest that there is a direct relationship between the mean amplitude and the relative velocity. For the mixture velocities, Um = 0.16 m/s and 0.24 m/s, it should be noted that the highest values of both the relative velocity and the mean amplitude were obtained at the lowest water-cut (WC = 10%) while the lowest values of both the relative velocity and the mean amplitude were obtained at the highest water-cut (WC = 70%). This implies that an increase in relative velocity increases the relative movement between the oil and water phases which results in increased interfacial disturbance and shear along the interface. The increase in the interfacial disturbance potentially leads to increase in the wave amplitude and the formation of droplets once the critical wave amplitude is exceeded (Al-Wahaibi et al., 2011). In this case, for mixture velocity, Um = 0.16 m/s and at 10% WC, the interfacial waves with the largest amplitude were obtained but no droplets at the interface were

observed (SW flow pattern) and as expected, it coincided directly with the point where the relative velocity is the highest. On the other hand, the interfacial waves with the lowest amplitudes were obtained at 70% WC and coincided with the point where the relative velocity was the lowest and apparently no droplets were also formed (SW flow pattern). However, on increasing the mixture velocity to 0.24 m/s and at 10% WC, the largest mean amplitude was obtained with some droplets formed along the interface (SW&MI flow pattern) and at this point, the largest relative velocity was also obtained. Similarly, the lowest mean amplitude was obtained when the relative velocity is also the lowest (70% WC).

On increasing the pipe inclination angle to $+5^{\circ}$, similar observations were also made as can be seen in figure 6.22. However, it should be noted that at Um = 0.16 m/s and 10% WC, the largest mean amplitude was observed with some droplets at the interface (SW&MI) and also at this point, the relative velocity was the largest. Interestingly, there was a reduction in the size of the mean amplitude after the droplet formation. For instance, between 20% WC and 30% WC, the mean amplitude reduced from 9.1 mm to 7.7 mm which corresponded to the point of transition between SW&MI and SW flow patterns. Similar observations are obtained when the mixture velocities were further increased to 0.24 m/s and higher and these observations are consistent with that of Al-Wahaibi and Angeli (2011) and Perera et al., (2019)
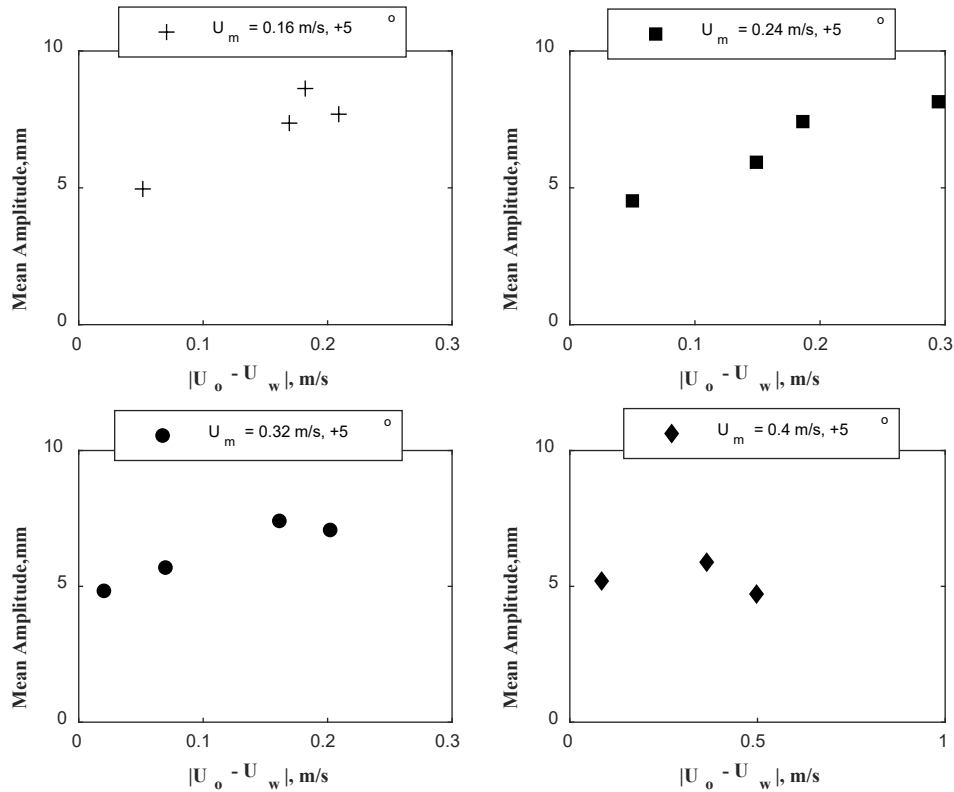
Figure 6.22: A figure showing the effect of the relative velocity on mean amplitude for mixture velocities Um = 0.16 m/s, 0.24 m/s, 0.32 m/s and 0.4 m/s across a +5º pipe inclination

6.6.4 Effect of Water-cut on mean wavelength

The wavelength was measurement as the horizontal distance between two consecutive wave crest from the flow images obtained using the high speed camera. In order to understand the effect of flow properties on the wavelength, the mean of the wavelengths was obtained and a plot of the water-cut which is one of the important input variable was made against the mean wavelength as presented in figure 6.23.
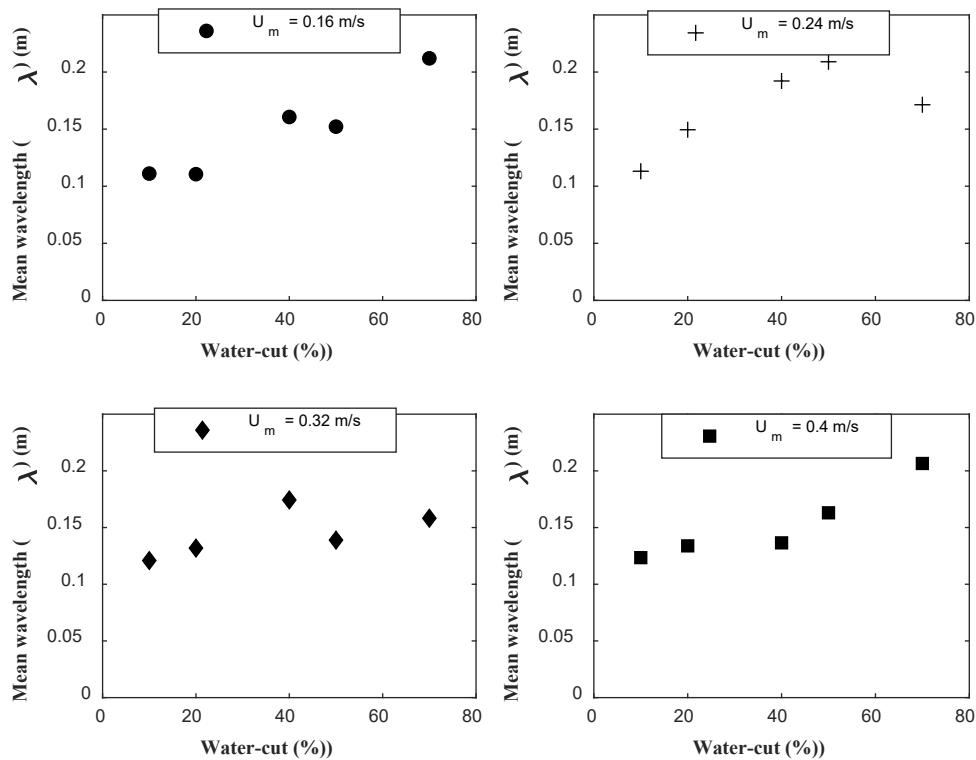
Figure 6.23: A plot of water-cut and mean wavelength for different mixture velocities at +3°
pipe inclination.

In Figure 6.23, one may notice that within the range of the mixture velocity used in this research

work (Um = 0.16 m/s – 0.4 m/s), there is an upward trend of mean wavelength as the water-

cut increases.   At low water-cut (10%), the interfacial waves experiences the greatest

disturbance due to the high relative velocity between the oil and water phases and as a result,

the interfacial shear increases which further leads to an increase in the wave amplitude and a

decrease in the wavelength. On increasing the water-cut, it was observed that the relative

velocity which is responsible for the growth of interfacial wave amplitude (Al-Wahaibi and

Angeli, 2011) decreases, consequently the wave amplitude decreases and the wavelength

increases. On considering the mixture velocities 0.24 m/s, one may notice that for water-cut

10% and 20%, droplets were formed along the interface as a result of the shearing of the waves

with large amplitude and short wavelength (SW&MI) and beyond that (WC 40%, 50% and

70%), there was a flow pattern transition to SW where the wave amplitude reduces and the wavelength increases. Similar observations were also made on increasing the mixture velocity to 0.32 m/s and 0.4 m/s and these findings are consistent with experimental observations and the images taken from the high speed camera. On close examining the wave spectrum, one may notice that the range of wavelength for the interfacial waves fall within 0.46D to 1.53D where D is the internal pipe diameter of the test pipe .

6.6.5 Wave aspect ratio

The wave aspect ratio also known as the wave steepness is a very important attribute that characterizes the geometrical structure of the wavy oil/water interface. It can be described as the ratio between the mean wavelength and the mean wave amplitude (λ_m/α_m). Since the wave aspect ratio is a non-dimensional parameter which characterizes the growth or decay of interfacial structures, it is therefore said to be a function of the modified Froude number (Fr_m).

$$Fr_M = \frac{U_w - U_o}{\sqrt{g.cos\theta.\varepsilon_w.\frac{A_w}{S_w}}}$$

The modified Froude number was chosen because for flows across an inclined pipe, it gives the relationship between the inertia force due to the relative velocity between the phases and the gravitational force as a result of the pipe inclination angle. The plot of the wave aspect ratio and the modified Froude number can be seen in figure 6.24.

In figure 6.24, it can be observed that the wave aspect ratio decreases asymptotically with the modified Froude number. The inertia force component of the modified Froude number is provided by the relative velocity between the water and oil phase and it also governs the growth of the interfacial wave amplitude. On increasing the modified Froude number, the relative
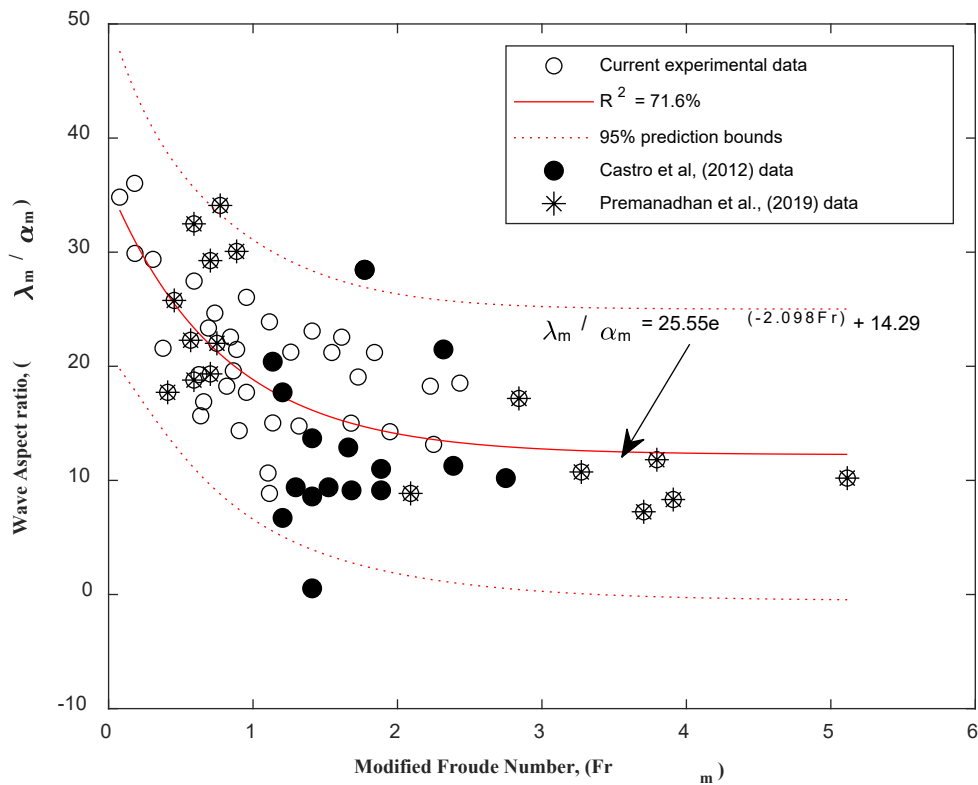
Figure 6.24: Plot of the wave aspect ratio and the modified Froude number using current experimental data and also data from Castro et al., (2012) and Premanadhan et al., (2019).

velocity increases and therefore the wave amplitude also increases. Since an increase in the wave amplitude implies a decrease in the wavelength, then the wave aspect ratio will eventually decrease on increasing the Froude number. Interfacial waves with low aspect ratio suggests that the wave amplitude is large while the wavelength is small and in such a situation, the possibility of shear force breaking the tip of the wave to form droplets is high (unstable waves), thus the stratified wavy with mixing at the interface flow pattern (SW&MI) is obtained. Therefore, it can be said that the probability of SW&MI flow pattern to occur is high when the wave aspect ratio is low and modified Froude number is high while SW flow pattern will likely occur at high wave aspect ratio and small modified Froude number. In order to test the validity of the relationship between the wave aspect ratio and the modified Froude number, data from Castro et al., (2012) and Premanadhan et al., (2019) were plotted along with the current

experimental data and all the data follow similar trend and fell within 95% prediction bounds in spite of the differences in the pipe diameter and physical properties of the fluids. Based on the fitted curve of the experimental data, the relationship between the aspect ratio and the modified Froude number can be proposed as:

$$\frac{\lambda_m}{\alpha_m} = 26.55e^{(-2.098Fr_m)} + 14.29 \qquad (6.1)$$

6.6.6 Relationship between normalized wave speed and the Reynolds number of the phases.

The interfacial wave speed was determined from the analysis of the flow images obtained from the high speed camera. Two positions were selected along the test pipe section within the viewing box of distance 0.01 m apart and the movement of a stable wave crest was monitored. The time it takes for a given wave crest to travel across the fixed position was noted and thereafter the wave speed can be obtained. The time was determined from the frame rate used in the experiment. Since 1000fps was used, then it means that successive images were taken at 0.001 seconds. Once the total number of frames it will take the given wave crest to cross the fixed position have been identified, then using the frame rate, the total time can be determined.

The wave speed obtained was normalized using the mixture velocity for the purpose of comparison.Wang et al., (2020) who worked in an air-water wavy stratified flow posited that a relationship exist between the wave speed and the Reynolds number of the liquid phase. However, for the case of an oil-water two-phase, both phases are liquid therefore it will be proposed that the wave speed will be affected by the Reynolds number of both the water and oil phases.
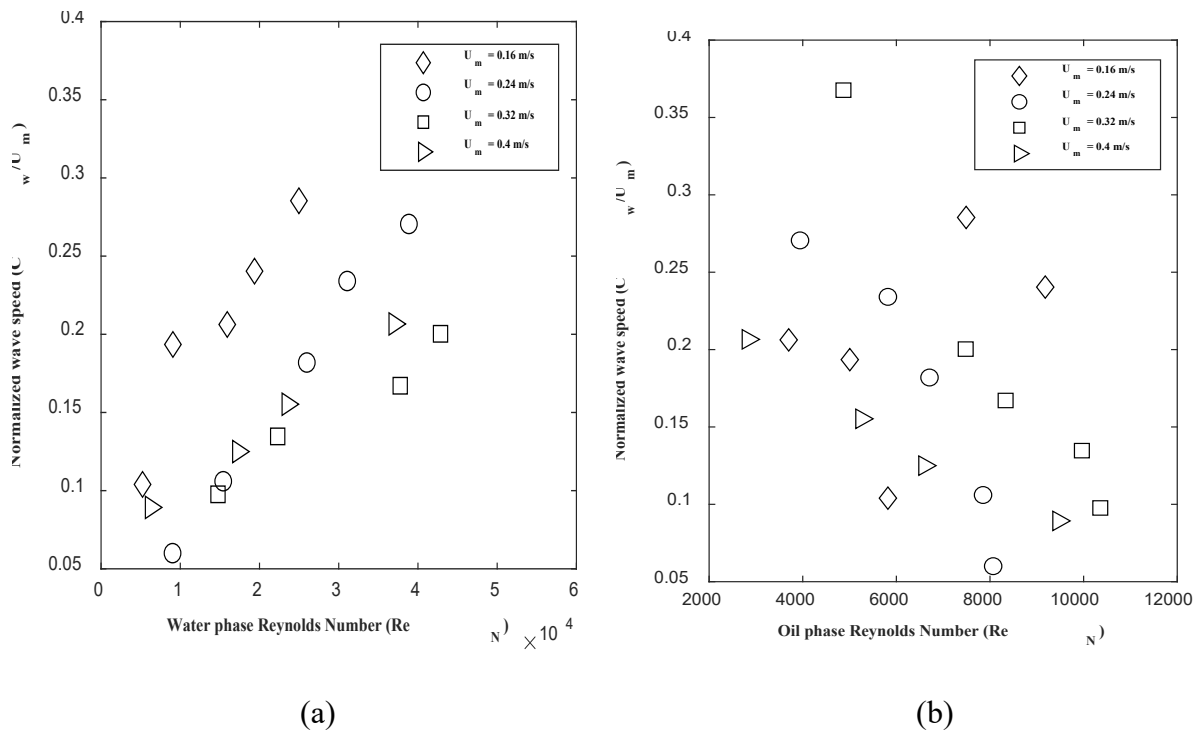
Figure 6.25: Effect of Reynolds number on the normalized wave speed. (a) Water phase Renolds number versus the normalized wave speed (b) Oil phase Reynolds number and the normalized wave speed.

In figure 6.25(a), it will be observed that the normalized wave speed generally increases with increasing water phase Reynolds number (Re_w) which is consistent with the observation made by Wang et al (2020) while the reverse trend was observed in figure 6.25(b) where the normalized wave speed generally decreased with increase in the oil phase Reynolds number (Re_o). It should be noted also that the both the Re_w and Re_o were calculated using the in-situ velocity of the water and oil phases respectively. Since the Reynolds number measures the interaction between the inertia forces and the viscous forces and for a given fluid combination where the viscosity of the phases are assumed to remain constant, then the Reynolds number will be a function of the inertia force which directly relates to the velocity of the phases. The increase in the water phase Reynolds number from 5234.7 to 24,973 as observed in figure 6.25(a) is closely associated with an increase in the water phase in-situ velocity from 0.38 m/s to 0.52 m/s which increases the inertia forces while a decrease in the oil phase Reynolds number

from 10,703 to 2830.2 as noted in figure 6.25(b) is also closely linked with a decrease in the oil-phase in-situ velocity from 0.4 m/s to 0.26 m/s which leads to a decrease in the inertia forces.

6.7   Interfacial Stability Analysis

Interfacial waves were observed for almost all the flow conditions used in carryout the experimental campaigns. Waves of finite amplitude and wavelength were seen propagating in the axial direction and the concept of stability analysis is used to know whether the sinusoidal disturbance which manifest on the interface as sine waves grows or decays with time. If the disturbance grows with time, it means the interfacial wave is unstable and there is a likelihood of a transition to another flow pattern. However, if the disturbance decays with time, it means the interfacial wave is stable.

 In the literature, several authors such as Barnea (1990), Trallero (1995), Al-Wahaibi and Angeli (2011), Rodriguez and Castro (2014) and Zhai et al., (2024) have made propositions on the stability criteria that governs transition from a stratified to non-stratified flow based on the principle of Kelvin-Helmholtz (K-H) stability analysis. The stability criteria proposed by Trallero (1995) will be used in this work since the criteria successfully capture the interplay of the important forces that tend to stablize or destabilize the interface and is given as:

$$(C_v - C_{iv})^2 + \frac{\rho_w \rho_o}{\rho^2 H_w H_o}(U_w - U_o)^2 - \frac{\rho_w - \rho_o}{\rho}\frac{g\cos(\theta)A}{S_i} - \frac{\sigma A}{\rho S_i}k^2 + \frac{\rho_{f(U_w - U_o)^2}C_s A}{\rho}\left(\frac{1}{A_w} - \frac{1}{A_o}\right) < 0$$

(6.2)

The first, second and fifth terms accounts for the viscous force, inertia force and the force due to the sheltering effect which are all destabilizing forces and tend to amplify the presence of any interfacial disturbance while the third and fourth terms accounts for the gravitational and

surface tension forces which are stabilizing. Since in this research work, the viscosity of the silicone oil used is low (4.7 cP), the inviscid Kelvin-Helmholtz stability criteria will be used where the first term of equation 6.2 will be dropped. Also since the sheltering effect term does not affect the speed of the interfacial wave (Trallero 1995) and also according to Rodriguez and Castro (2011), the term was artificially included in the stability criteria equation, though it has a physical basis, therefore in the context of this analysis, the sheltering effect term will also be dropped. Hence, the IKH stability criteria used will be:

$$\frac{\rho_w \rho_o}{\rho^2 H_w H_o}(U_w - U_o)^2 - \frac{\rho_w - \rho_o}{\rho}\frac{g\cos(\theta)A}{S_i} - \frac{\sigma A}{\rho S_i}k^2 < 0 \tag{6.3}$$

Equation (6.3) can equally be written in the form:

$$(U_w - U_o)^2 < \left[\frac{\rho_w - \rho_o}{\rho}\frac{g\cos(\theta)A}{S_i} + \frac{\sigma A}{\rho S_i}k^2\right]\frac{\rho^2 H_w H_o}{\rho_w \rho_o}$$

$$U_w - U_o < \left\{\left[\frac{\rho_w - \rho_o}{\rho}\frac{g\cos(\theta)A}{S_i} + \frac{\sigma A}{\rho S_i}k^2\right]\frac{\rho^2 H_w H_o}{\rho_w \rho_o}\right\}^{\frac{1}{2}} \tag{6.4}$$

In equation 6.4, the only destabilizing term is the $(U_w - U_o)$ which is the relative velocity between the water and oil phase, while the other two terms are stabilizing i.e. the gravitational force and force due to surface tension. For a damped system where any disturbance introduced vanishes with time (stable system), the inertia force due to the effect of the relative velocity must be less than the sum of the gravitational force and the force due to surface tension. But for an unstable system, the reverse will be the case. The limit of stability as given in equation (6.4) will be tested using the experimental data from this research work to determine if the system is stable or not.

The variables U_w and U_o are the in-situ velocity of water and oil phases, ρ_w and ρ_o are the water and oil density, S_i is the interfacial length, σ is the interfacial tension, k is the wave

number which is a function of the wavelength, A is the cross-sectional area of the pipe, H_w and H_o are the liquid holdup for water and oil phases, θ is the pipe inclination angle and ρ is the weighted mixture density which can be given as:

$$\rho = \frac{\rho_w}{H_w} + \frac{\rho_o}{H_o} \qquad (6.5)$$

On substituting the values of the physical properties of silicone oil and water including the cross-sectional area of the pipe geometry, the IKH stability criteria (equation 6.4) for a $+3^o$ pipe inclination becomes

$$U_w - U_o < \left[\left(\frac{99.32 + 0.00567k^2}{\rho S_i}\right)\left(\frac{\rho^2 H_w H_o}{916164}\right)\right]^{0.5} \qquad (6.6)$$

The parameters in equation (6.6) which includes the interfacial length (S_i), water and oil holdups (H_w, H_o), weighted mixture density (ρ) and the wave number (k) are all dependent on the input flow conditions. Therefore, the criterion for stability as stated in equation (6.6) will be tested for all the inlet flow conditions for both the $+3^o$ and $+5^o$ pipe inclinations. The plot for some of the flow conditions can be seen in Figure (6.26) and Figure (6.27).

The stability criterion revealed that the system will be stable and all disturbances will be damped on the condition that the relative velocity between the phases will be less than the stability limit. In both Figures (6.26) and (6.27), it can be seen that the relative velocities for all the tested flow conditions fell below the stability limit which suggests that the system is stable and by implication, it means any disturbance introduced at the inlet will decay with time as the flow traverses in the axial direction.
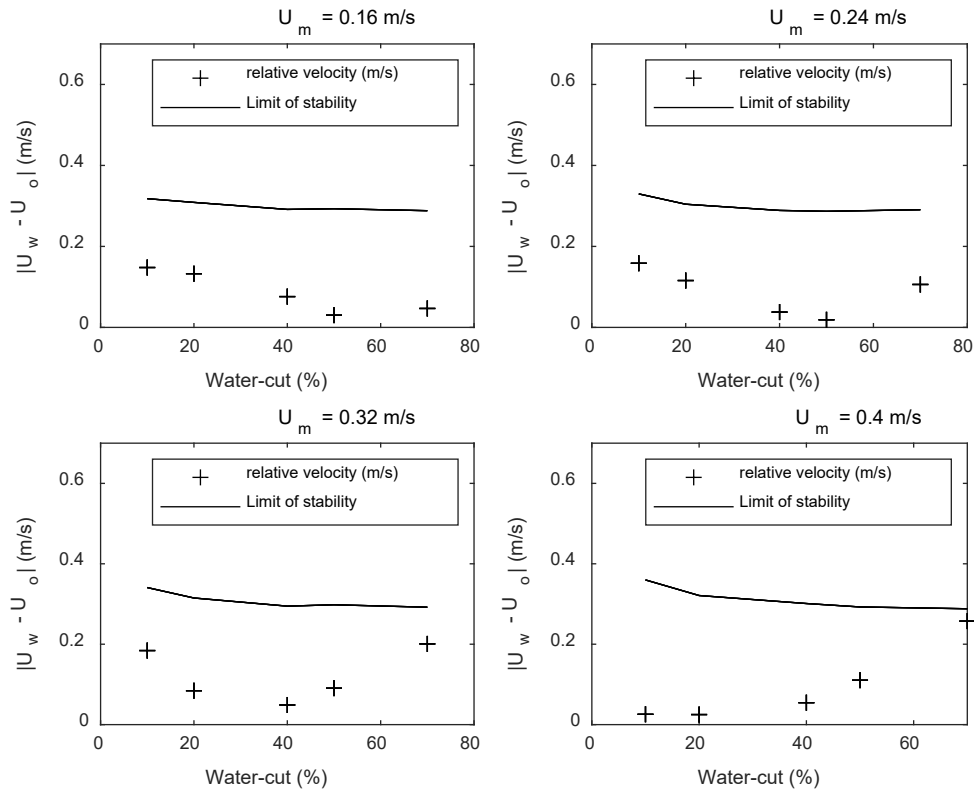
Figure 6.26: A plot showing the limit of stability and the relative velocity as a function of water-cut for mixture velocities (U_m = 0.16 m/s, 0.24 m/s, 0.32 m/s and 0.4 m/s) at +3° pipe inclination.

On relating this result with experimental observation, it was noticed that interfacial waves propagate from the inlet of the test pipe up till the exit for all the tested flow conditions. In order to further check the stability of the system, the interfacial wave amplitude was measured along two points i.e. 140 cm and 450 cm from the fluid inlet device using the double parallel wire probe (DPWP).
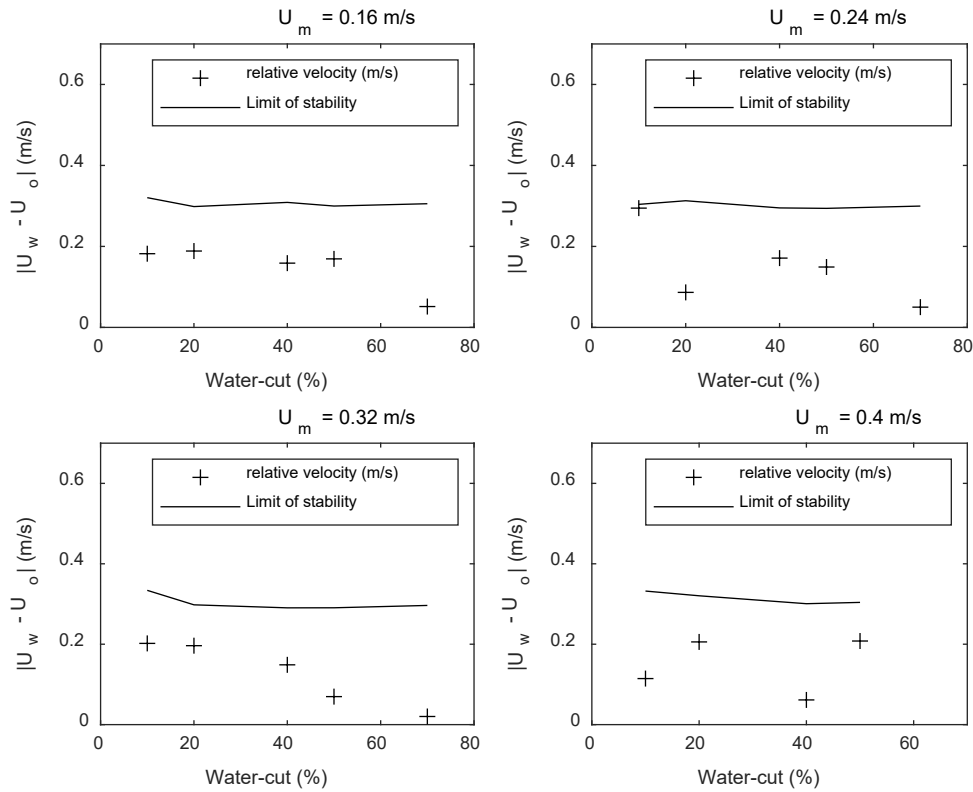
Figure 6.27: A plot showing the limit of stability and the relative velocity as a function of water-cut for mixture velocities (U_m = 0.16 m/s, 0.24 m/s, 0.32 m/s and 0.4 m/s) at +5° pipe inclination.

The wave amplitude was selected to track the growth or decay of the interfacial wave because of the very important relationship that exist between the wave amplitude and wave energy where high energy waves have high amplitude and vice versa (Perera et al., (2019). The proposition adopted here is that if there is a decrease in the mean wave amplitude along the two locations in the flow direction, then it implies that there is a probability that the disturbance will be damped and decay in the flow direction which could probably suggest that the system is stable. However, an increase in the mean amplitude along the two locations in the flow direction will suggest an amplification of disturbance which will result to an unstable system. Plots of the mean wave amplitude along the two locations can be seen in the figure 6.28.
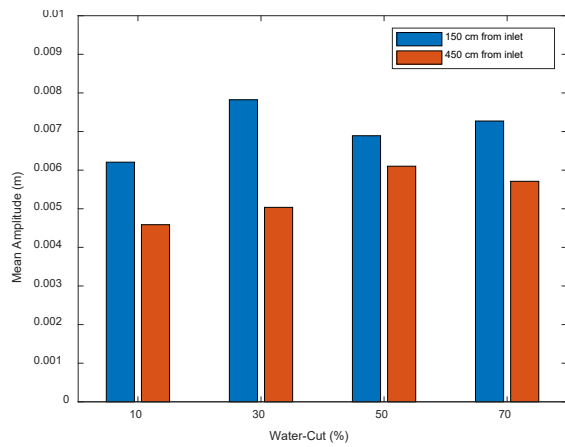
(a)
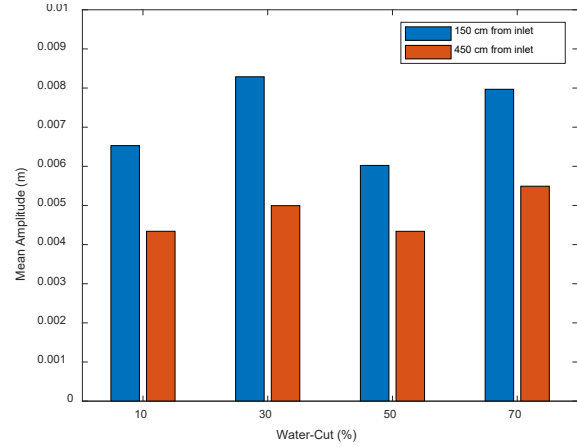
(b)
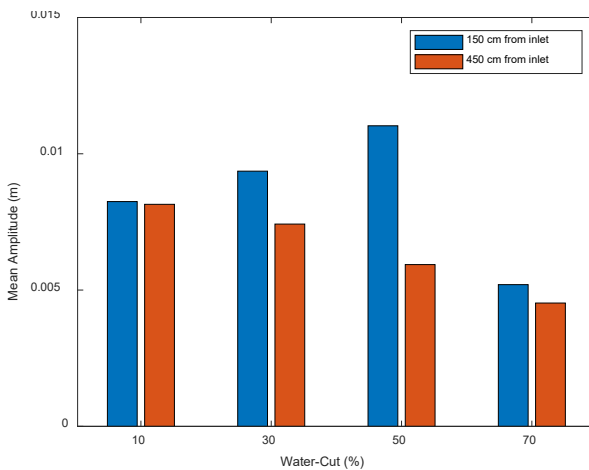
(c)
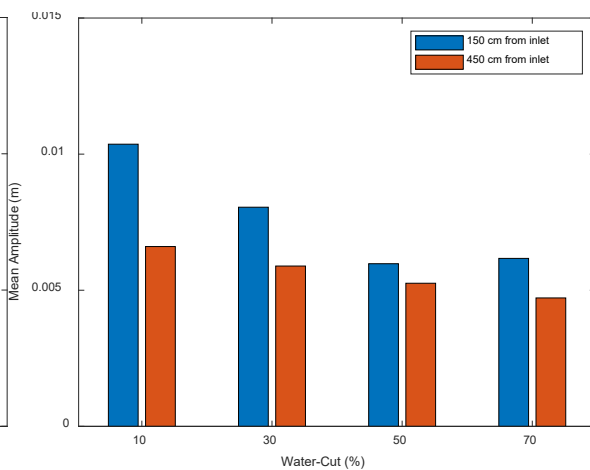
(d)

Figure 6.28: Comparison plot of mean amplitude versus water-cut at 150 cm and 450 cm from the fluid inlet device for (a) U_m = 0.24 m/s, +3° pipe inclination (b) U_m = 0.4 m/s, +3° pipe inclination (c) U_m = 0.24 m/s, +5° pipe inclination and (d) U_m = 0.4 m/s, +5° pipe inclination

Table 6.2: A table showing the Reynolds number of the phases at both 140 cm and 4540 cm from the fluid inlet device for mixture velocity (U_m) = 0.4 m/s and +3° pipe inclination.

Water_Cut (%)	Reynolds Number of the phases (Re)			
	140 cm from inlet (Re_w)	450 cm from inlet (Re_w)	140 cm from inlet (Reo)	450 cm from inlet (Reo)
10	25378	2103	11134	10703
30	42598	11482	10778	8013
50	62569	23548	8322	5256

215

70	80556	37046	5309	2830

In Figure 6.28, one may notice that for the stated flow conditions, the mean amplitudes for the interfacial waves at 140 cm from the fluid inlet device appears to be higher than the mean amplitude downstream at 450 cm from the fluid inlet device. This decrease in the mean amplitude along the flow direction which is independent of the changes in inclination angle or mixture velocities suggest a dampening of the interfacial waves which potentially could make the system stable. Also, the Reynolds number (Re) which measures the interplay of inertia force over the viscous force was determined at these two locations and the values for the mixture velocity $U_m = 0.4$ m/s at $+3^\circ$ pipe inclination was shown in table 6.2. It was observed that for all the pipe inclinations and mixture velocities investigated, there is a decrease in the Reynolds number of both the water and oil phase (Re_w and Re_o) along the flow direction which implies that at 140 cm from fluid inlet device, the high turbulence within the phases will enhance the shearing effects which inevitably leads to higher disturbance at the interface resulting to the growth of wave amplitude.

However, at 450 cm from the fluid inlet device, the Reynolds number for both the water and oil phase was found to considerably decrease and this suggest a reduction in turbulence which enhances the shearing effects at this location and by implication, the disturbance along the interface will also reduce leading to a decrease in the wave amplitude. These results in combination with experimental observation suggests that the interfacial waves generated as the oil and water flow simultaneously across the test pipe is stable and the evolution of any inlet disturbance was seen to decay along the flow direction. Barral (2014) made similar observation where high amplitude 2D interfacial waves were observed in the fluid inlet device but these 2D waves were not seen downstream of the fluid inlet device, rather a 3D fluctuation of the interface.

6.8   SUMMARY

In this chapter, a Y-type fluid inlet device with a split plate was used, resulting in the identification of three distinct flow patterns due to flow segregation: stratified smooth (ST), stratified wavy (SW), and stratified wavy with mixing at the interface (SW&MI). These flow patterns were presented on a flow pattern map for pipe inclinations of +1°, +3°, and +5°. A comparison of these flow pattern maps with those of Kumara et al. (2009) and Perera et al. (2018) revealed significant differences in both the types and number of flow patterns. For instance, in the current study, the stratified smooth with mixing at the interface (ST&MI) pattern was not observed. However, stratified smooth (ST), stratified wavy (SW), and stratified wavy with mixing at the interface (SW&MI) were present in similar regions of Kumara et al.'s (2009) flow pattern map, where only ST&MI was observed in the current study.

The effects of water cut (WC) and mixture velocity (Um) on the normalized average interfacial height and Oil Volume Fraction (OVF) were also examined. It was noted that for a given mixture velocity, the normalized average interfacial height increased with increase in WC, while OVF decreased. Additionally, effect of changes in pipe inclination were studied, showing that for a given mixture velocity, increasing the pipe inclination led to an increase in the normalized average interfacial height. This increase in interfacial height corresponded to a decrease in OVF, and this is driven by the influence of the parallel gravitational force component on the denser water phase.

A comparison between interfacial heights obtained from the Double Parallel Wire Probe (DPWP) and image analysis showed strong agreement, with mean absolute percent errors (MAPE) of 26.1%, 26.1%, 25.0%, and 23.8% for mixture velocities of 0.16 m/s, 0.24 m/s, 0.32 m/s, and 0.4 m/s, respectively. The evolution of waves along the oil-water interface was studied using the DPWP to measure interfacial fluctuations. It was observed that, in most flow

conditions, the largest amplitude interfacial waves occurred at the lowest WC (10%), while small-amplitude waves were seen at the highest WC (70%). For example, at 10% WC and Um = 0.24 m/s, the average interfacial wave amplitudes were 5.08 mm, 6.41 mm, and 8.15 mm for pipe inclinations of +1°, +3°, and +5°, respectively. At 70% WC and the same conditions, the amplitudes were 4.84 mm, 6.52 mm, and 4.52 mm.

Interfacial waves were categorized based on the size of interfacial wave amplitude (α) into small ($\alpha \leq 2$ mm), intermediate (2 mm $\leq \alpha \leq 10$ mm), and large amplitude waves ($\alpha \geq 10$ mm). The effects of WC and pipe inclination on wave distribution were studied using number density, which represents the sum of the probability density for each wave category. For a given pipe inclination (+3°), it appears that a significant number of the intermediate amplitude and large amplitude waves were observed along the interface at 10% WC and $U_m = 0.24$ m/s based on the analysis of their corresponding number densities compared to similar observations at 70% WC where the appearance of the small amplitude waves was very significant. This implies that for a given pipe inclination and mixture velocity, the interfacial disturbance at 10% WC is more significant with the appearance of large amplitude waves as against similar observation at WC = 70% where there is considerable reduction in interfacial disturbance with the appearance of small amplitude waves. The observation is consistent with the flow images taken at those conditions.

Upon increasing the pipe inclination from +3° to +5° (for both $U_m = 0.24$ m/s, $U_m = 0.4$ m/s and WC = 10%, WC = 70%) there were less appearances of short amplitude waves while there was a significant appearance of both the intermediate amplitude and large amplitude waves which implies that increasing pipe inclination enhances the interfacial disturbances.

A direct correlation was found between relative velocity and mean wave amplitude. Additionally, the impact of WC on mean wavelength was examined, showing that for a given mixture velocity, the mean wavelength increased with WC.

The wave aspect ratio which characterizes the growth or decay of interfacial structures was found to decrease asymptotically with the modified Froude number. Experimental data from Castro et al., (2012) and Premanadhan et al., (2019) were plotted along with the current experimental data and all the data follow similar trend and fell within 95% prediction bounds. Furthermore, the relationship between normalized wave speed and Reynolds number was investigated, showing a direct relationship with the water phase and an inverse relationship with the oil phase. Finally, a stability analysis of interfacial waves was conducted using a simplified Inviscid Kelvin-Helmholtz (IKH) stability criterion and for all flow conditions studied in this current work, the interface remained inherently stable due to the fact the difference between the in-situ velocity of the phases was lower than the IKH stability criterion for all the flow conditions.

CHAPTER 7
CONCLUSIONS AND RECOMMENDATIONS

The challenge of producing and transporting crude oil mixed with large quantity of water economically and safely across long stretches of undulating pipelines is one of the primary concerns of the petroleum industry. The knowledge of the operational limits that permits the existence of the different flow regimes will be particularly helpful in the design of the pipelines since knowing the phase that will be in contact with the pipe wall will determine the pressure drop and pumping requirement and also corrosion management protocol.

In order to address this problem, this study was undertaken with the sole aim of investigating the flow development and interfacial behaviour of oil-water two-phase flow across a large diameter inclined pipe. The primary objective of the study was to understand how the hydrodynamic behaviour of the oil-water mixture such as the Oil Volume Fraction (OVF), water holdup, spatial distribution of the phases (flow patterns) and slippage responds to changes in input flow conditions and pipe orientations.

In conducting the experiments, significant amount of data were collected, analysed and the results were presented in the preceeding chapters of the thesis. The main conclusions arising from the study are presented below followed by the recommendations for future work.

7.1   Flow patterns

- The flow patterns identified in this study were found to depend on the inlet water-cut (WC), mixture velocity (U_m), pipe inclination and the design of the fluid inlet device.

- Three types of fluid inlet devices were used and they include the T-type, Y-type and the Y-type with a separator plate fluid inlet devices.

- For the T-type fluid inlet device, four (4) different flow patterns were identified including SW&MI, Do/w&w, Dw/o&o, Do/w. Stratified flow with smooth or wavy

interface (ST and SW) were never identified even at the lowest flow condition (U_m = 0.08 m/s and WC = 10%).

- Based on the design of the T-type fluid inlet device, intense mixing was observed at the inlet which generates droplets that are carried downstream, hence all the flow patterns observed have one form of droplet dispersion or the other.

- For +1° pipe inclination, and within the operating range where $U_m \leq$ 0.24 m/s and WC $\leq$ 60%, the flow was segregated with droplets at the interface (SW&MI). However, at high water cut (WC$\geq$ 60%) and $U_m \geq$ 0.16 m/s), water-dominant flow patterns were observed (Do/w&w and Do/w) while at high mixture velocity (0.32 m/s $\leq U_m \leq$ 0.4 m/s) and WC $\leq$ 50%, oil-dominant flow pattern was observed (Dw/o&o).

- Upon increasing the pipe inclination from +1° to +5°, no significant change was observed in the flow pattern even at the lowest mixture velocity (U_m = 0.08 m/s). However, for higher mixture velocities ($U_m \geq$ 0.08 m/s), significant increase in the region on the flow pattern map occupied by the water-dominant flow patterns was observed due to the action of the axial component of the gravitational force on the denser water phase.

- Similarly, for the Y-type fluid inlet device, five (5) different flow patterns were identified for +1° pipe inclination including ST, ST&MI, Do/w&w, Dw/o&o and Dw/o. Stratified smooth (ST) flow pattern was observed only at the lowest mixture velocity (U_m = 0.08 m/s) and low water cut (WC = 10% - 20%) due to the design of the fluid inlet device that minimizes fluid mixing at the inlet. The water-dominant flow patterns (Do/w&w) are formed within the flow region ($U_m \geq$ 0.24 m/s) and (WC$\geq$ 60%) while the oil-dominant flow patterns are formed within the flow region $U_m \leq$ 0.16 m/s and WC $\leq$ 50%.

- On increasing the pipe inclination from +1º to +5º, the number of flow patterns observed reduced to three (3) (SW&MI, Do/w&w and Dw/o) and no any ST or ST&MI flow patterns were observed due to increased interfacial disturbance. Also, significant decrease in the region on the map occupied by the oil-dominant flow patterns and a significant increase in the region occupied by the water-dominant flow pattern was observed as a result of the effect of gravitational force on the denser water phase.

- Also, for the Y-type fluid fluid inlet device with a separator plate, only three (3) different flow patterns were identified (ST, SW and SW&MI). The presence of the separator plate minimizes fluid mixing at the inlet and also enhances the formation of stratified flow configuration; hence, dispersed flow patterns were not observed. The SW flow pattern occurred in over 70% of the experimented flow conditions while the ST only occurred at the lowest water cut (WC = 10%) and lowest mixture velocity (U_m = 0.08 m/s).

- Upon increasing the pipe inclination from +1º to +5º, the only significant change observed was an increase in the region occupied by the SW&MI flow pattern as a result of the increased interfacial disturbance.

7.2   Distribution of Oil Volume Fraction (OVF).

- The distribution of the OVF was found to depend on the water cut (WC), mixture velocity (U_m) and the pipe inclination.

- Across all the three types of fluid inlet devices, the OVF was found to decrease on increasing the WC. For the T-type fluid inlet device and at low mixture velocity (U_m = 0.16 m/s), the fluctuation in the measurement of OVF was larger as indicated by the longer sizes of the error bars for all WC which suggests the presence of waves and droplets at the interface (SW&MI flow pattern). But for higher mixture velocity (U_m = 0.4 m/s) and water cut (10% ≤ WC ≤ 40%), the fluctuations in OVF was smaller as

indicated by the smaller sizes of the error bars and this suggest that no interfacial waves were present and the fluctuations was primarily due to the water droplets dispersed in the continuous oil phase (Dw/o&o flow pattern).

- Concerning the axial distribution of OVF as the WC and pipe inclination changes, it was observed that the values of the OVFs measured by the different conductance probes [9.6D (CP1), 19.2D (CP2), 28.8D (CP3) and 56.6D (CP4)] are dependent on the WC. At low WC (10% - 40%), the OVF measured by CP1 and CP2 were significantly higher than that of CP3 and CP4, suggesting a decrease in OVF in the axial direction. This could probably be due to the relatively high inertial force in the oil phase as a result of its high superficial velocity. However, for high WC (50% - 70%), the reverse was the case where the OVF measured by CP1 and CP2 were significantly lower than that of CP3 and CP4 suggesting an increase in the axial distribution of the OVF as a result of the slippage between the oil and water phase.

- The effect of pipe inclination on the axial distribution of OVF was studied. It was observed that at low mixture velocity ($U_m = 0.16$ m/s and $U_m = 0.24$ m/s) and water cut (WC = 10% - 50%), OVF decreases axially to a minimum at +3° and +4° pipe inclination as a result of the overriding influence of the axial component of the gravitational force over the inertial force on the denser water phase. However, for high mixture velocity (Um = 0.32 m/s), the change in pipe inclination did not have a significant effect on the OVF particularly at low water cut (WC = 10%).

7.3 Slippage characteristics

- The slip ratio was found to be a function of the water cut (WC), mixture velocity (U_m) and the pipe inclination.

- For most of the data points, the slip ratio decreases as the WC and U_m increases which agrees with the findings of of Lum et al., (2004), Morgan et al., (2013) and Xu et al., (2016) among others.

- Upon increasing the inclination angle from +1º to +5º, the slip ratio progressively becomes greater than one (S > 1) particularly for mixture velocities (U_m = 0.16 m/s – 0.32 m/s) and water-cuts (10% - 40%). However, for the high mixture velocity (U_m = 0.4 m/s), the change in pipe inclination did not significantly affect the slip ratio and it was noted that for all pipe inclinations and WC, the slip ratio was below one (S < 1), suggesting that the water phase was travelling faster than the oil phase for the given flow conditions. Interestingly, the flow patterns encountered within the range of the given flow conditions are predominantly Dw/o&o flow pattern with water as the dispersed phase.

7.4   Oil-water interfacial behaviour

- Interfacial height measurement using the Double parallel wire probe (DPWP) and the analysis of the flow images using the high-speed camera were used to study the interfacial behaviour.

- There was a good agreement between the interfacial height measured using the DPWP and the one obtained from the analysis of the flow images using Image J software. The mean absolute percent errors (MAPE) are 26.1%, 26.1%, 25.0% and 23.8% for the mixture velocities (U_m) 0.16 m/s, 0.24 m/s, 0.32 m/s and 0.4 m/s respectively. The difference in the two measurements could be as a result of the presence of waves and droplets occurring at the interface that could interfere with the accurate measurement of the interfacial height from the DPWP.

- For a given pipe inclination and mixture velocity, it was observed that the interfacial wave with the largest amplitude appeared at the lowest WC and the wave amplitude was found to progressively decay as the WC increases. For instance, at 10% WC and for $U_m = 0.24$ m/s, the average interfacial wave amplitude are 5.08 mm, 6.41 mm and 8.15 mm for $+1^o$, $+3^o$ and $+5^o$ pipe inclination respectively whereas for the same mixture velocity and pipe inclination with WC = 70%, the average interfacial wave amplitude are 4.84 mm, 6.52 mm and 4.52 mm respectively.

- For a given flow condition, waves of different amplitudes appear along the interface and for ease of analysis, the waves are categorized based on their amplitude into small amplitude waves ($\alpha \leq 2$ mm), intermediate amplitude waves ($2mm \leq \alpha \leq 10$ mm) and large amplitude waves ($\alpha \geq 10$ mm).

- For a given pipe inclination ($+3^o$), it appears that a significant number of the intermediate amplitude and large amplitude waves were observed along the interface at 10% WC and $U_m = 0.24$ m/s based on the analysis of their corresponding number densities compared to similar observations at 70% WC where the appearance of the small amplitude waves was very significant. This implies that for a given pipe inclination and mixture velocity, the interfacial disturbance at 10% WC is more significant with the appearance of large amplitude waves as against similar observation at WC = 70% where there is considerable reduction in interfacial disturbance with the appearance of small amplitude waves. The observation is consistent with the flow images taken at those conditions.

- Upon increasing the pipe inclination from $+3^o$ to $+5^o$ (for both $U_m = 0.24$ m/s, $U_m = 0.4$ m/s and WC = 10%, WC = 70%) there were less appearances of short amplitude waves while there was a significant appearance of both the intermediate amplitude and large

amplitude waves which implies that increasing pipe inclination enhances the interfacial disturbances.

- A direct relationship was found to exist between the mean interfacial wave amplitude and the relative velocity between the oil and water phases particularly at low mixture velocity ($U_m = 0.16$ m/s and $U_m = 0.24$ m/s) and for $+3^{\circ}$ pipe inclination. The higher the relative velocity (which is a form of destabilizing force) between the oil and water phase, the higher the interfacial disturbance and shear along the interface and the larger the interfacial wave amplitude.

- For all the mixture velocities considered ($U_m = 0.16$ m/s – $U_m = 0.4$ m/s) at $+3^{\circ}$ pipe inclination, it was observed that an increase in water-cut leads to a corresponding increase in the wavelength.

- For a given flow condition, the greatest interfacial disturbance occur at the lowest water-cut (WC = 10%) due to the high relative velocity between the water and oil phases which leads to the appearance of larger amplitude waves with shorter wavelengths. Upon increasing the WC, the relative velocity between the phases decreases leading to a decrease in the interfacial disturbance, hence a decrease in the interfacial wave amplitude and a subsequent increase in wavelength.

- The wave aspect ratio which characterizes the growth or decay of interfacial structures was found to decrease asymptotically with the modified Froude number. Experimental data from Castro et al., (2012) and Premanadhan et al., (2019) were plotted along with the current experimental data and all the data follow similar trend and fell within 95% prediction bounds. An empirical correlation between the wave aspect ratio and the modified Froude number was proposed as: $\frac{\lambda_m}{\alpha_m} = 26.55e^{(-2.098Fr_m)} + 14.29$.

- Based on the stability analysis, it was noted that the relative velocities for all the tested flow conditions fell below the stability limit line which suggests that the system is stable

and by implication, it means any disturbance introduced at the inlet will decay with time as the flow traverses in the axial direction. Also, upon tracking the growth or decay of the interfacial wave amplitude across two locations in the axial direction (140 cm and 450 cm from the inlet), it appears that the mean wave amplitude at 140 cm from inlet is higher than the corresponding value at 450 cm from inlet. This decrease in the mean amplitude along the flow direction which is independent of the changes in inclination angle or mixture velocities suggest a dampening of the interfacial waves which potentially could make the system stable.

7.4   Recommendations for future work

The current work attempted to study the flow development and interfacial behaviour for oil-water flow across an upwardly inclined pipe, however for the sake of completeness, future research into similar studies while considering the horizontal, vertical and downwardly inclined pipe will improve the understanding and generate sufficient data to model the behaviour of fluid mixtures in a petroleum pipeline network across an undulating terrain.

Several attempts were made in the current research to measure the pressure drop using a pressure transducer even after re-ranging it but without any success. Future research should consider the measurement of pressure drop which will improve the understanding of flow pattern transition and interfacial behaviour of the oil-water two-phase flow.

Although the phase inversion point was identified in this current research, but a detail study on this very important phenomenon was not carried out due to the operating limit of the oil and water pumps. Hence, higher capacity pumps capable of producing larger throughput that can cause sufficient dispersion of the phases should be considered in future studies.

The introduction of gas into the oil-water two-phase flow will make the system quite complex as a result of multiple deformable interfaces but a successful analysis of such liquid-liquid-gas three-phase system will improve accurate modeling and optimization of oil and gas production and transportation processes, therefore this should be considered in future studies.

In the current study, low viscosity silicone oil (4.7 cP) was used and the effect of change in fluid properties such as viscosity, interfacial tension and density was not investigated. Therefore studies on the effect of surface active agents (surfactants) on the interfacial behaviour of oil-water two-phase should be considered in addition to studying the effects of change in the physical properties of the oils on the flow development.

BIBLIOGRAPHY

Abubakar, A., Al-Wahaibi, Y., Al-Wahaibi, T., Al-Hashmi, A., Al-Ajmi, A., & Eshrati, M. (2015). Effect of low interfacial tension on flow patterns, pressure gradients and holdups of medium-viscosity oil/water flow in horizontal pipe. *Experimental Thermal and Fluid Science*, *68*, 58–67. https://doi.org/10.1016/j.expthermflusci.2015.02.017

Adler, M. N., & Mewes, D. (1997). Flow induced emulsification in the flow of two immiscible liquids in horizontal pipes. In *Int. J. Multiphase Flow* (Vol. 23, Issue 1).

Almutairi, Z.; Al-Alweet, F.M.; Alghamdi, Y.A.; Almisned, O.A.; Alothman, O.Y. (2020). Investigating the Characteristics of Two-Phase Flow Using Electrical Capacitance Tomography (ECT) for Three Pipe Orientations. *Processes*, *8*, 51. https://doi.org/10.3390/pr8010051

Al-Sarkhi, A., Pereyra, E., Mantilla, I., & Avila, C. (2017). Dimensionless oil-water stratified to non-stratified flow pattern transition. *Journal of Petroleum Science and Engineering*, *151*, 284–291. https://doi.org/10.1016/j.petrol.2017.01.016

Al-Sarkhi, A., Sarica, C., & Magrini, K. (2012). Inclination effects on wave characteristics in annular gas-liquid flows. *AIChE Journal*, *58*(4), 1018–1029. https://doi.org/10.1002/aic.12653

Al-Wahaibi, T., & Angeli, P. (2007). Transition between stratified and non-stratified horizontal oil-water flows. Part I: Stability analysis. *Chemical Engineering Science*, *62*(11), 2915–2928. https://doi.org/10.1016/j.ces.2007.01.024

Al-Wahaibi, T., & Angeli, P. (2008). Droplet size and velocity in dual continuous horizontal oil-water flows. *Chemical Engineering Research and Design*, *86*(1 A), 83–93. https://doi.org/10.1016/j.cherd.2007.10.012

Al-Wahaibi, T., & Angeli, P. (2011a). Experimental study on interfacial waves in stratified horizontal oil-water flow. *International Journal of Multiphase Flow*, *37*(8), 930–940. https://doi.org/10.1016/j.ijmultiphaseflow.2011.04.003

Al-Wahaibi, T., & Angeli, P. (2011b). Experimental study on interfacial waves in stratified horizontal oil-water flow. *International Journal of Multiphase Flow*, *37*(8), 930–940. https://doi.org/10.1016/j.ijmultiphaseflow.2011.04.003

Al-Wahaibi, T., & Angeli, P. (2011c). Experimental study on interfacial waves in stratified horizontal oil-water flow. *International Journal of Multiphase Flow*, *37*(8), 930–940. https://doi.org/10.1016/j.ijmultiphaseflow.2011.04.003

Al-Wahaibi, T., Yusuf, N., Al-Wahaibi, Y., & Al-Ajmi, A. (2012). Experimental study on the transition between stratified and non-stratified horizontal oil-water flow. *International Journal of Multiphase Flow*, *38*(1), 126–135. https://doi.org/10.1016/j.ijmultiphaseflow.2011.08.007

Andritsos, N., & Hanratty, T. J. (n.d.). *Influence of Interfacial Waves in Stratified Gas-Liquid Flows*.

Angeli, P., & Hewitt, G. F. (n.d.). *Pressure gradient in horizontal liquid±liquid ⁻ows*.

Angeli, P., & Hewitt, G. F. (2000a). Flow structure in horizontal oil±water ⁻ow. In *International Journal of Multiphase Flow* (Vol. 26). www.elsevier.com/locate/ijmulflow

Angeli, P., & Hewitt, G. F. (2000b). Flow structure in horizontal oil±water ⁻ow. In *International Journal of Multiphase Flow* (Vol. 26). www.elsevier.com/locate/ijmulflow

Arirachakaran, S., Oglesby, K.D., Malinowsky, M.S., Shoham, O., Brill, J.P., 1989. An analysis of oil-water flow phenomena in horizontal pipes. In SPE paper 18836, SPE Prod Operating Sym, Oklahoma, pp. 155-167

Asali,J.C.& Hanratty, T.J.(1993).Ripples generated on a liquid film at high gas velocities.

International Journal of Multiphase Flow. 19 (2). 229-243park

Atmaca, S., Sarica, C., Zhang, H. Q., & Al-Sarkhi, A. S. (2008a). Characterization of oil water flows in inclined pipes. *Proceedings - SPE Annual Technical Conference and Exhibition*, *2*, 1273–1286. https://doi.org/10.2118/115485-ms

Atmaca, S., Sarica, C., Zhang, H. Q., & Al-Sarkhi, A. S. (2008b). Characterization of oil water flows in inclined pipes. *Proceedings - SPE Annual Technical Conference and Exhibition*, *2*, 1273–1286. https://doi.org/10.2118/115485-ms

Atmaca, S., Sarica, C., Zhang, H. Q., & Al-Sarkhi, A. S. (2008c). Characterization of oil water flows in inclined pipes. *Proceedings - SPE Annual Technical Conference and Exhibition*, *2*, 1273–1286. https://doi.org/10.2118/115485-ms

Ayati, A. A. (2018). Experimental characterization of non-linear interfacial wave interaction in stratified gas-liquid pipe flow. *Physics of Fluids*, *30*(6). https://doi.org/10.1063/1.5035082

Bannwart, A. C. (n.d.). *Wavespeed and volumetric fraction in core annular ⁻ow*.

Barral, A. H., & Angeli, P. (2013). Interfacial characteristics of stratified liquid-liquid flows using a conductance probe. *Experiments in Fluids*, *54*(10). https://doi.org/10.1007/s00348-013-1604-5

Bontozoglou, V., & Hanratty, T. J. (1989). Wave height estimation in stratified gas-liquid flows. *AIChE Journal*, *35*(8), 1346–1350. https://doi.org/10.1002/aic.690350813

Brauner, N. (2001.). *The prediction of dispersed flows boundaries in liquid-liquid and gas-liquid systems*. www.elsevier.com/locate/ijmul

Brauner, N., & Maron, D. M. (1991). Analysis of stratified/nonstratified transitional boundaries in horizontal gas-liquid flows. In *Chemical Engrneerrng Science* (Vol. 46, Issue I).

Brauner, N., & Ullmann, A. (n.d.). *Modeling of phase inversion phenomenon in two-phase pipe flows*. www.elsevier.com/locate/ijmulflow

Cai, C., Mudawar, I., Liu, H., & Xi, X. (2021). Assessment of void fraction models and correlations for subcooled boiling in vertical upflow in a circular tube. In *International Journal of Heat and Mass Transfer* (Vol. 171). Elsevier Ltd. https://doi.org/10.1016/j.ijheatmasstransfer.2021.121060

Chakrabarti, D. P., Das, G., & Ray, S. (2005). Pressure drop in liquid-liquid two phase horizontal flow: Experiment and prediction. *Chemical Engineering and Technology*, *28*(9), 1003–1009. https://doi.org/10.1002/ceat.200500143

Chinaud, M., Park, K.H., & Angeli, P. (2017). Flow pattern transition in liquid-liquid flows with a transverse cylinder. *International Journal of Multiphase Flow, 90*, 1-12.

Colombo, L. P. M., Guilizzoni, M., Sotgia, G., Dehkordi, P. B., & Lucchini, A. (2017). Water holdup estimation from pressure drop measurements in oil-water two-phase flows by means of the two-fluid model. *Journal of Physics: Conference Series*, *923*(1). https://doi.org/10.1088/1742-6596/923/1/012012

Colombo, L. P. M., Guilizzoni, M., Sotgia, G. M., Bortolotti, S., & Pavan, L. (2014). Measurement of the oil holdup for a two-phase oil-water flow through a sudden contraction in a horizontal pipe. *Journal of Physics: Conference Series*, *501*(1). https://doi.org/10.1088/1742-6596/501/1/012015

Da Silva, M. J., Dos Santos, E. N., Hampel, U., Rodriguez, I. H., & Rodriguez, O. M. H. (2011). Phase fraction distribution measurement of oil-water flow using a capacitance wire-mesh sensor. In *Measurement Science and Technology* (Vol. 22, Issue 10). Institute of Physics Publishing. https://doi.org/10.1088/0957-0233/22/10/104020

de Castro, M. S., Pereira, C. C., dos Santos, J. N., & Rodriguez, O. M. H. (2011). Geometrical and kinematic properties of interfacial waves in horizontal heavy oil-water stratified flow. *WIT Transactions on Engineering Sciences*, *70*, 227–237. https://doi.org/10.2495/MPF110191

de Castro, M. S., & Rodriguez, O. M. H. (2015). Interfacial waves in stratified viscous oil-water flow. *Experimental Thermal and Fluid Science*, *62*, 85–98. https://doi.org/10.1016/j.expthermflusci.2014.12.003

Du, M., Jin, N. De, Gao, Z. K., Wang, Z. Y., & Zhai, L. S. (2012). Flow pattern and water holdup measurements of vertical upward oil-water two-phase flow in small diameter pipes. *International Journal of Multiphase Flow*, *41*, 91–105. https://doi.org/10.1016/j.ijmultiphaseflow.2012.01.007

Elkow, K.J, & Rezkallah, K.S. "Void Fraction Fluctuations in Two-Phase Flow at 1-G and µ-G." *Proceedings of the ASME 1996 International Mechanical Engineering Congress and Exposition. Heat Transfer: Volume 3 — Experimental Studies in Multiphase Flow; Multiphase Flow in Porous Media; Experimental Multiphase Flows and Numerical Simulation of Two-Phase Flows; Fundamental Aspects of Experimental Methods*. Atlanta, Georgia, USA. November 17–22, 1996. pp. 109-113. ASME. https://doi.org/10.1115/IMECE1996-0100

Elseth G 2001 An experimental study of oil–water flow in horizontal pipes *PhD Thesis* The Norwegian University of Science and Technology, Norway

Fordham,E.J.,Simonian,S.,Ramos, R.T.,Holmes, A.,Huang, S.M and Lenn, C.P (1999). Multi-phase-fluid discrimination with local fibre-optical probes. *Journal of Measurement Science and Technology*.10 (12

Fujii, T., Otha, J., Nakazawa, T., and Morimoto, O. (1994). The Behavior of an Immiscible Equal-Density Liquid-Liquid Two-Phase Flow in a Horizontal Tube. JSME Journal Series B, Fluids and Thermal Engineering, 30(1):22-29.

Flores et al (1999) flow pattern transition modelling.

Ganat, T., Ridha, S., Hairir, M., Arisa, J., & Gholami, R. (2019a). Experimental investigation of high-viscosity oil–water flow in vertical pipes: flow patterns and pressure gradient. *Journal of Petroleum Exploration and Production Technology*, *9*(4), 2911–2918. https://doi.org/10.1007/s13202-019-0677-y

Ganat, T., Ridha, S., Hairir, M., Arisa, J., & Gholami, R. (2019b). Experimental investigation of high-viscosity oil–water flow in vertical pipes: flow patterns and pressure gradient. *Journal of Petroleum Exploration and Production Technology*, *9*(4), 2911–2918. https://doi.org/10.1007/s13202-019-0677-y

Gawas, K., Karami, H., Pereyra, E., Al-Sarkhi, A., & Sarica, C. (2014). Wave characteristics in gas-oil two phase flow and large pipe diameter. *International Journal of Multiphase Flow*, *63*, 93–104. https://doi.org/10.1016/j.ijmultiphaseflow.2014.04.001

Gorelik, D., & Brauner, N. (1999). *The interface con®guration in two-phase strati®ed pipe ¯ows*. www.elsevier.com/locate/ijmulflow

Grassi, B., Strazza, D., & Poesio, P. (2008a). Experimental validation of theoretical models in two-phase high-viscosity ratio liquid-liquid flows in horizontal and slightly inclined pipes. *International Journal of Multiphase Flow*, *34*(10), 950–965. https://doi.org/10.1016/j.ijmultiphaseflow.2008.03.006

Grassi, B., Strazza, D., & Poesio, P. (2008b). Experimental validation of theoretical models in two-phase high-viscosity ratio liquid-liquid flows in horizontal and slightly inclined pipes. *International Journal of Multiphase Flow*, *34*(10), 950–965. https://doi.org/10.1016/j.ijmultiphaseflow.2008.03.006

Grassi, B., Strazza, D., & Poesio, P. (2008c). Experimental validation of theoretical models in two-phase high-viscosity ratio liquid-liquid flows in horizontal and slightly inclined pipes. *International Journal of Multiphase Flow*, *34*(10), 950–965. https://doi.org/10.1016/j.ijmultiphaseflow.2008.03.006

Gui, M., Liu, Z., Liao, B., Wang, T., Wang, Y., Sui, Z., Bi, Q., & Wang, J. (2019). Void fraction measurements of steam–water two-phase flow in vertical rod bundle: Comparison among different techniques. *Experimental Thermal and Fluid Science*, *109*(28). https://doi.org/10.1016/j.expthermflusci.2019.109881

Guo, J., Li, G.-J., & Chen, X.-J. (n.d.). *A linear and non-linear analysis on interfacial instability of gas-liquid two-phase flow through a circular pipe*. www.elsevier.com/locate/ijhmt

Guzhov, A.I.G., Medredev, V.F., Medredeva, O.P., 1973. Emulsion formation during the flow of two immiscible liquids in a pipe. Neft Khoz (in Russian) 8: 58-61

Hamad, F. A., Albarzenji, D., & Ganesan, P. B. (2014). Study of kerosene-water two-phase flow characteristics in vertical and inclined pipes. *Canadian Journal of Chemical Engineering*, *92*(5), 905–917. https://doi.org/10.1002/cjce.21931

Hamad, F. A., He, S., Khan, M. K., & Bruun, H. H. (2013). Development of kerosene-water two-phase up-flow in a vertical pipe downstream of A 90° bend. *Canadian Journal of Chemical Engineering*, *91*(2), 354–367. https://doi.org/10.1002/cjce.21626

Hamad, F. A., Imberton, F., & Bruun, H. H. (1997). An optical probe for measurements in liquid-liquid two-phase flow. In *Meas. Sci. Technol* (Vol. 8).

Hao, H., Fan, Z.,Gao, X & Xu, J. (2023). Void fraction measurement in direct contact heat exchange process using electromagnetic tomography. Chemical Engineering Research and Design. 197. 10.1016/j.cherd.2023.07.035.

Hanafizadeh, P., Hojati, A., & Karimi, A. (2015). Experimental investigation of oil-water two phase flow regime in an inclined pipe. *Journal of Petroleum Science and Engineering*, *136*, 12–22. https://doi.org/10.1016/j.petrol.2016.10.031

Hapanowicz, J. (2008). Slip between the phases in two-phase water-oil flow in a horizontal pipe. *International Journal of Multiphase Flow*, *34*(6), 559–566. https://doi.org/10.1016/j.ijmultiphaseflow.2007.12.002

Hazuku, T., Takamasa, T., & Matsumoto, Y. (2008). Experimental study on axial development of liquid film in vertical upward annular two-phase flow. *International Journal of Multiphase Flow*, *34*(2), 111–127. https://doi.org/10.1016/j.ijmultiphaseflow.2007.10.008

Huang, S. F., Zhang, X. G., Wang, D., & Lin, Z. H. (2007). Water holdup measurement in kerosene-water two-phase flows. *Measurement Science and Technology*, *18*(12), 3784–3794. https://doi.org/10.1088/0957-0233/18/12/013

Hudaya, A. Z., Kuntoro, H. Y., Dinaryanto, O., Deendarlianto, & Indarto. (2016). Experimental investigation on the interfacial characteristics of stratified air-water two-phase flow in a horizontal pipe. *AIP Conference Proceedings*, *1737*. https://doi.org/10.1063/1.4949300

Ibarra, R., Markides, C. N., & Matar, O. K. (2014). A review of liquid-liquid flow patterns in horizontal and slightly inclined pipes. *Multiphase Science and Technology*, *26*(3), 171–198. https://doi.org/10.1615/MultScienTechn.v26.i3.10

Ibarra, R., Matar, O. K., & Markides, C. N. (2021). Experimental investigations of upward-inclined stratified oil-water flows using simultaneous two-line planar laser-induced fluorescence and particle velocimetry. *International Journal of Multiphase Flow*, *135*. https://doi.org/10.1016/j.ijmultiphaseflow.2020.103502

Ibarra, R., Matar, O. K., Markides, C. N., & Zadrazil, I. (n.d.-a). *An experimental study of oil-water flows in horizontal pipes*.

Ibarra, R., Matar, O. K., Markides, C. N., & Zadrazil, I. (n.d.-b). *An experimental study of oil-water flows in horizontal pipes*.

Izwan Ismail, A. S., Ismail, I., Zoveidavianpoor, M., Mohsin, R., Piroozian, A., Misnan, M. S., & Sariman, M. Z. (2015). Experimental investigation of oil-water two-phase flow in horizontal pipes: Pressure losses, liquid holdup and flow patterns. *Journal of Petroleum Science and Engineering*, *127*, 409–420. https://doi.org/10.1016/j.petrol.2015.01.038

Jana, A. K., Das, G., & Das, P. K. (2006a). Flow regime identification of two-phase liquid-liquid upflow through vertical pipe. *Chemical Engineering Science*, *61*(5), 1500–1515. https://doi.org/10.1016/j.ces.2005.09.001

Jana, A. K., Das, G., & Das, P. K. (2006b). Flow regime identification of two-phase liquid-liquid upflow through vertical pipe. *Chemical Engineering Science*, *61*(5), 1500–1515. https://doi.org/10.1016/j.ces.2005.09.001

Jana, A. K., Mandal, T. K., Chakrabarti, D. P., Das, G., & Das, P. K. (2007). An optical probe for liquid-liquid two-phase flows. *Measurement Science and Technology*, *18*(5), 1563–1575. https://doi.org/10.1088/0957-0233/18/5/048

Jin, N. D., Nie, X. B., Ren, Y. Y., & Liu, X. B. (2003). Characterization of oil/water two-phase flow patterns based on nonlinear time series analysis. *Flow Measurement and Instrumentation*, *14*(4–5), 169–175. https://doi.org/10.1016/S0955-5986(03)00022-0

Jin, N. D., Nie, X. B., Wang, J., & Ren, Y. Y. (2003). Flow pattern identification of oil/water two-phase flow based on kinematic wave theory. *Flow Measurement and Instrumentation*, *14*(4–5), 177–182. https://doi.org/10.1016/S0955-5986(03)00023-2

Kumar, K., Fershtman, A., Barnea, D., & Shemer, L. (2021). Evolution of waves in a horizontal pipe propagating on a surface of a liquid film sheared by gas. *Physics of Fluids*, *33*(6). https://doi.org/10.1063/5.0049288

Kumara, W. A. S., Halvorsen, B. M., & Melaaen, M. C. (2010a). Particle image velocimetry for characterizing the flow structure of oil-water flow in horizontal and slightly inclined pipes. *Chemical Engineering Science*, *65*(15), 4332–4349. https://doi.org/10.1016/j.ces.2010.03.045

Kumara, W. A. S., Halvorsen, B. M., & Melaaen, M. C. (2010b). Particle image velocimetry for characterizing the flow structure of oil-water flow in horizontal and slightly inclined pipes. *Chemical Engineering Science*, *65*(15), 4332–4349. https://doi.org/10.1016/j.ces.2010.03.045

Kurban, A. P. A. (1997). *Stratified liquid-liquid flow* (Doctoral dissertation, University of London).

Kwon, G., & Kim, H. (2020). *Void fraction measurement using low energy X-rays*.

Lakis, A. A., & Trinh, N. D. (2016). Void fraction in highly turbulent and large diameter horizontal pipe flow. *European Journal of Engineering and Technology*, *4*(2). www.idpublications.org

Lee, H., Al-Sarkhi, A., Pereyra, E., Sarica, C., Park, C., Kang, J., & Choi, J. (2013). Hydrodynamics model for gas-liquid stratified flow in horizontal pipes using minimum dissipated energy concept. *Journal of Petroleum Science and Engineering*, *108*, 336–341. https://doi.org/10.1016/j.petrol.2013.06.001

Liu, L., Matar, O. K., Lawrence, C. J., & Hewitt, G. F. (2006). Laser-induced fluorescence (LIF) studies of liquid-liquid flows. Part I: Flow structures and phase inversion. *Chemical Engineering Science*, *61*(12), 4007–4021. https://doi.org/10.1016/j.ces.2006.11.047

Loh, W. L., & Premanadhan, V. K. (2016). Experimental investigation of viscous oil-water flows in pipeline. *Journal of Petroleum Science and Engineering*, *147*, 87–97. https://doi.org/10.1016/j.petrol.2016.05.010

Lum, J. Y. L., Al-Wahaibi, T., & Angeli, P. (2006a). Upward and downward inclination oil-water flows. *International Journal of Multiphase Flow*, *32*(4), 413–435. https://doi.org/10.1016/j.ijmultiphaseflow.2006.01.001

Lum, J. Y. L., Al-Wahaibi, T., & Angeli, P. (2006b). Upward and downward inclination oil-water flows. *International Journal of Multiphase Flow*, *32*(4), 413–435. https://doi.org/10.1016/j.ijmultiphaseflow.2006.01.001

Lum, J. Y. L., Lovick, J., & Angeli, P. (2004). Low inclination oil-water flows. *Canadian Journal of Chemical Engineering*, *82*(2), 303–315. https://doi.org/10.1002/cjce.5450820211

Mena, P., Rocha, F.,Teixeira, J., Sechet, P. & Cartellier, A. (2008). Measurement of gas phase characteristics using a monofiber optical probe in a three-phase flow. Chemical Engineering Science. 63. 4100-4115.

Mohamad, E.J.,Rahim, R., Fazalul R., Mohammed H.F.R.,Ameran, H. L.M.,& Muji, S.Z.M., & Marwah, O.M.F.. (2015). Measurement and Analysis of Water/Oil Multiphase Flow Using Electrical Capacitance Tomography Sensor. Flow Measurement and Instrumentation. 47. 10.1016/j.flowmeasinst.2015.12.004.

Oddie, G., Shi, H., Durlofsky, L. J., Aziz, K., Pfeffer, B., & Holmes, J. A. (2003). Experimental study of two and three phase flows in large diameter inclined pipes. *International Journal of Multiphase Flow*, *29*(4), 527–558. https://doi.org/10.1016/S0301-9322(03)00015-6

Oliemans, R.V.A., 1986. The Lubricating-Film Model for Core-Annular Flow, PhD thesis, Delft University, The Netherlands.

Oliemans, R.V.A., Ooms, G., Wu, H.L., Duijvestijn, A., 1987. Core-annular oil/water flow: the turbulent-lubricating film model and measurements in a 5 cm pipe loop. Int J Multiphase Flow 13(1): 23-31

Osundare, O. S., Falcone, G., Lao, L., & Elliott, A. (2020). Liquid-liquid flow pattern prediction using relevant dimensionless parameter groups. *Energies*, *13*(17). https://doi.org/10.3390/en13174355

Pan, Y. X., Zhang, H. B., Hu, Y. J., Liu, X. Bin, & Wang, M. (2021a). Experimental investigation of interfacial wave in stratified low-viscosity-oil and water flow in horizontal and upward pipes. *Energy Sources, Part A: Recovery, Utilization and Environmental Effects*, *43*(6), 738–753. https://doi.org/10.1080/15567036.2019.1632977

Pan, Y. X., Zhang, H. B., Hu, Y. J., Liu, X. Bin, & Wang, M. (2021b). Experimental investigation of interfacial wave in stratified low-viscosity-oil and water flow in horizontal and upward pipes. *Energy Sources, Part A: Recovery, Utilization and Environmental Effects*, *43*(6), 738–753. https://doi.org/10.1080/15567036.2019.1632977

Pan, Y. X., Zhang, H. B., Xie, R. H., Liu, X. Bin, & Wang, M. (2016a). Modeling of low viscosity oil-water annular flow in horizontal and slightly inclined pipes: Experiments and CFD simulations. *Korean Journal of Chemical Engineering*, *33*(10), 2820–2829. https://doi.org/10.1007/s11814-016-0188-1

Pan, Y. X., Zhang, H. B., Xie, R. H., Liu, X. Bin, & Wang, M. (2016b). Modeling of low viscosity oil-water annular flow in horizontal and slightly inclined pipes: Experiments and CFD

simulations. *Korean Journal of Chemical Engineering*, *33*(10), 2820–2829. https://doi.org/10.1007/s11814-016-0188-1

Paras, S.V. & Karabelas, A.J.(1991). Properties of the liquid layer in horizontal annular flow.

International Journal of Multiphase Flow. 17(4). 439 - 454.

Park, K.H.,Chinaud, M. & Angeli, P. (2016). Transition from stratified to non-stratified oil-water flows using a bluff body. Experimental Thermal and Fluid Science. 76. 10.1016/j.expthermflusci.2016.03.017.

Perera, K., Amaratunga, M., & Time, R. W. (2018). Interface detection of oil–water stratified flow. *WIT Transactions on Engineering Sciences*, *120*, 71–82. https://doi.org/10.2495/AFM180081

Perera, K., Kumara, W. A. S., Hansen, F., Mylvaganam, S., & Time, R. W. (2018). Comparison of gamma densitometry and electrical capacitance measurements applied to hold-up prediction of oil-water flow patterns in horizontal and slightly inclined pipes. *Measurement Science and Technology*, *29*(6). https://doi.org/10.1088/1361-6501/aab054

Perera, K., Mylvaganam, S., & Time, R. W. (2018). Characterization of oil-water plug related flow in slightly inclined pipes. *International Journal of Computational Methods and Experimental Measurements*, *6*(2), 373–384. https://doi.org/10.2495/CMEM-V6-N2-373-384

Perera, K., Time, R. W., Pradeep, C., & Kumara, A. S. (2019a). Interfacial wave analysis of low viscous oil-water flow in upwardly inclined pipes. *Chemical Engineering Science*, *196*, 444–462. https://doi.org/10.1016/j.ces.2018.11.014

Perera, K., Time, R. W., Pradeep, C., & Kumara, A. S. (2019b). Interfacial wave analysis of low viscous oil-water flow in upwardly inclined pipes. *Chemical Engineering Science*, *196*, 444–462. https://doi.org/10.1016/j.ces.2018.11.014

Pietrzak, M. (2014a). Flow patterns and volume fractions of phases during liquid-liquid two-phase flow in pipe bends. *Experimental Thermal and Fluid Science*, *54*, 247–258. https://doi.org/10.1016/j.expthermflusci.2013.12.024

Pietrzak, M. (2014b). Flow patterns and volume fractions of phases during liquid-liquid two-phase flow in pipe bends. *Experimental Thermal and Fluid Science*, *54*, 247–258. https://doi.org/10.1016/j.expthermflusci.2013.12.024

Pouraria, H., Seo, J. K., & Paik, J. K. (2016). Numerical modelling of two-phase oil-water flow patterns in a subsea pipeline. *Ocean Engineering*, *115*, 135–148. https://doi.org/10.1016/j.oceaneng.2016.02.007

Premanadhan, V.K., Hernandez-Perez, V.K., Teik, W.T.,Tam, N.D., Bratland, O., & Loh, W.L. (2019). Experimental investigation of interfacial waves in stratified liquid-liquid flows in horizontal pipelines: Characteristics and pressure gradients. *Journal of Petroleum Science and Engineering, 173, 20 - 36*

Qian, J. Y., Li, X. J., Wu, Z., Jin, Z. J., Zhang, J., & Sunden, B. (2019). Slug Formation Analysis of Liquid–Liquid Two-Phase Flow in T-Junction Microchannels. *Journal of Thermal Science and Engineering Applications*, *11*(5). https://doi.org/10.1115/1.4043385

Rodriguez, I. H., Yamaguti, H. K. B., de Castro, M. S., Da Silva, M. J., & Rodriguez, O. M. H. (2011). Slip ratio in dispersed viscous oil-water pipe flow. *Experimental Thermal and Fluid Science*, *35*(1), 11–19. https://doi.org/10.1016/j.expthermflusci.2010.07.017

Rodriguez, O. M. H., & Baldani, L. S. (2012a). Prediction of pressure gradient and holdup in wavy stratified liquid-liquid inclined pipe flow. *Journal of Petroleum Science and Engineering*, *96–97*, 140–151. https://doi.org/10.1016/j.petrol.2012.09.007

Rodriguez, O. M. H., & Baldani, L. S. (2012b). Prediction of pressure gradient and holdup in wavy stratified liquid-liquid inclined pipe flow. *Journal of Petroleum Science and Engineering*, *96–97*, 140–151. https://doi.org/10.1016/j.petrol.2012.09.007

Rodriguez, O. M. H., & Bannwart, A. C. (2006). Experimental study on interfacial waves in vertical core flow. In *Journal of Petroleum Science and Engineering* (Vol. 54, Issues 3–4, pp. 140–148). https://doi.org/10.1016/j.petrol.2006.07.007

Rodriguez, O. M. H., & Castro, M. S. (2014a). Interfacial-tension-force model for the wavy-stratified liquid-liquid flow pattern transition. *International Journal of Multiphase Flow*, *58*, 114–126. https://doi.org/10.1016/j.ijmultiphaseflow.2013.09.003

Rodriguez, O. M. H., & Castro, M. S. (2014b). Interfacial-tension-force model for the wavy-stratified liquid-liquid flow pattern transition. *International Journal of Multiphase Flow*, *58*, 114–126. https://doi.org/10.1016/j.ijmultiphaseflow.2013.09.003

Rodriguez, O. M. H., & Oliemans, R. V. A. (2006a). Experimental study on oil-water flow in horizontal and slightly inclined pipes. *International Journal of Multiphase Flow*, *32*(3), 323–343. https://doi.org/10.1016/j.ijmultiphaseflow.2006.11.001

Rodriguez, O. M. H., & Oliemans, R. V. A. (2006b). Experimental study on oil-water flow in horizontal and slightly inclined pipes. *International Journal of Multiphase Flow*, *32*(3), 323–343. https://doi.org/10.1016/j.ijmultiphaseflow.2006.11.001

Sharma, A., Al-Sarkhi, A., Sarica, C., & Zhang, H. Q. (2011). Modeling of oil-water flow using energy minimization concept. *International Journal of Multiphase Flow*, *37*(4), 326–335. https://doi.org/10.1016/j.ijmultiphaseflow.2010.11.002

Shi, J., Jepson, W.P., Rhyne, L.D, (2003). Segregated modelling of oil–water flows, SPE 84232, in: SPE Annual Technical Conference, Colorado, USA, pp. 1–10

Shi, J., & Yeung, H. (2017a). Characterization of liquid-liquid flows in horizontal pipes. *AIChE Journal*, *63*(3), 1132–1143. https://doi.org/10.1002/aic.15452

Shi, J., & Yeung, H. (2017b). Characterization of liquid-liquid flows in horizontal pipes. *AIChE Journal*, *63*(3), 1132–1143. https://doi.org/10.1002/aic.15452

Shi, J., & Yeung, H. (2017c). Characterization of liquid-liquid flows in horizontal pipes. *AIChE Journal*, *63*(3), 1132–1143. https://doi.org/10.1002/aic.15452

Soto-Cortes, G., Pereyra, E., Sarica, C., Rivera-Trejo, F., & Torres, C. (2019). Effects of high oil viscosity on oil-gas upward flow behavior in deviated pipes. *Experimental Thermal and Fluid Science*, *109*. https://doi.org/10.1016/j.expthermflusci.2019.109896

Spedding, P. L., Murphy, A., Donnelly, G. F., Benard, E., & Doherty, A. P. (2008). Pressure drop in three-phase oil-water-gas horizontal co-current flow: Experimental data and development of prediction models. *Asia-Pacific Journal of Chemical Engineering*, *3*(5), 531–543. https://doi.org/10.1002/apj.165

Taitel, Y., & Dukler, A. E. (1976). A model for predicting flow regime transitions in horizontal and near horizontal gas-liquid flow. *AIChE Journal*, *22*(1), 47–55. https://doi.org/10.1002/aic.690220105

Tan, J., Jing, J., Hu, H., & You, X. (2018a). Experimental study of the factors affecting the flow pattern transition in horizontal oil–water flow. *Experimental Thermal and Fluid Science*, *98*, 534–545. https://doi.org/10.1016/j.expthermflusci.2018.06.020

Tan, J., Jing, J., Hu, H., & You, X. (2018b). Experimental study of the factors affecting the flow pattern transition in horizontal oil–water flow. *Experimental Thermal and Fluid Science*, *98*, 534–545.

Trallero, J.L., 1995. Oil-Water Flow Pattern in Horizontal Pipes. Ph.D. thesis. The University of Tulsa.

Trallero, J. L., Sarica, C., & Brill, J. P. (1997). A Study of Oil/Water Flow Patterns in Horizontal Pipes. In *SPE Production & Facilities*.

Tripathi, S., Tabor, R. F., Singh, R., & Bhattacharya, A. (2017). Characterization of interfacial waves and pressure drop in horizontal oil-water core-annular flows. *Physics of Fluids*, *29*(8).

Valle, A., Utvik, O.H., 1998. Pressure drop, flow pattern and slip for two phase crude oil/water flow: experiments and model predictions. In: Proc Int Symp on Liquid-Liquid Two Phase Flow and Transport Phenomena, Antalya, Turkey, 3-7 Nov: 63-74

Vempati, B., Panchagnula, M. V., Öztekin, A., & Neti, S. (2010). Combined buoyancy and viscous effects in liquid-liquid flows in a vertical pipe. *Acta Mechanica*, *210*(1–2), 1–12.

Vielma, M., Atmaca, S., Sarica, C., and H. Zhang. "Characterization of Oil/Water Flows in Horizontal Pipes." *SPE Proj Fac & Const* 3 (2008): 1–21

Vigneaux, P., Chenais, P., & Hulin, J. P. (1988). Liquid-liquid flows in an inclined pipe. *AIChE Journal*, *34*(5), 781–789. https://doi.org/10.1002/aic.690340508

Voulgaropoulos, V., Jamshidi, R., Mazzei, L., & Angeli, P. (2019). Experimental and numerical studies on the flow characteristics and separation properties of dispersed liquid-liquid flows. *Physics of Fluids*, *31*(7). https://doi.org/10.1063/1.5092720

Wang, W., Cheng, W., Li, K., Lou, C., & Gong, J. (2013). Flow patterns transition law of oil-water two-phase flow under a wide range of oil phase viscosity condition. *Journal of Applied Mathematics*, *2013*. https://doi.org/10.1155/2013/291217

Wang, W., & Gong, J. (2009). Experiment research of phase inversion in mineral oil-water two-phase flow in Horizontal pipe. *Journal of Energy Resources Technology, Transactions of the ASME*, *131*(4), 0430011–0430016. https://doi.org/10.1115/1.4000324

Wang, W., Gong, J., & Angeli, P. (2011). Investigation on heavy crude-water two phase flow and related flow characteristics. *International Journal of Multiphase Flow*, *37*(9), 1156–1164. https://doi.org/10.1016/j.ijmultiphaseflow.2011.05.011

Wongwises, S., Khankaewr', W., & Vetchsupakhun, W. (1998). Prediction of Liquid Holdup in Horizontal Stratified Two-Phase Flow. In *Thammasat Int. J. Sc. Tech* (Vol. 3, Issue 2).

Xinghe,L., Ning-De, J.,Yu, Z.,Meng, D & Lusheng, Z. (2012). The measurement characteristics of parallel-wire conductance probe used in horizontal oil-water two-phase flow, *Proceedings of the 31st Chinese Control Conference*, Hefei, China, 2012, pp. 6888-6893.

Xu, J., Wu, Y., Chang, Y., & Guo, J. (2008). Experimental investigation on the holdup distribution of oil-water two-phase flow in horizontal parallel tubes. *Chemical Engineering and Technology*, *31*(10), 1536–1540. https://doi.org/10.1002/ceat.200800206

Xu, J. yu, Wu, Y. xiang, Feng, F. fei, Chang, Y., & Li, D. hui. (2008). Experimental investigation on the slip between oil and water in horizontal pipes. *Experimental Thermal and Fluid Science*, *33*(1), 178–183. https://doi.org/10.1016/j.expthermflusci.2008.07.011

Xu, X. X. (2007). Study on oil-water two-phase flow in horizontal pipelines. In *Journal of Petroleum Science and Engineering* (Vol. 59, Issues 1–2, pp. 43–58). https://doi.org/10.1016/j.petrol.2007.03.002

Yang, J., Li, P., Zhang, X., Lu, X., Li, Q., & Mi, L. (2021). Experimental investigation of oil–water flow in the horizontal and vertical sections of a continuous transportation pipe. *Scientific Reports*, *11*(1). https://doi.org/10.1038/s41598-021-99660-8

Yang, Y., Hu, H., Wang, K., Wang, S., Liu, M., Zhang, C., & Wang, D. (2021). Area-alterable liquid electrode capacitance sensor for water holdup measurement in oil–water two-phase flow. *Asia-Pacific Journal of Chemical Engineering*, *16*(5). https://doi.org/10.1002/apj.2680

Zhai, L., Qiao, J., Wang, W., & Wang, Y. (2022a). Measurement of Interfacial Characteristics of Horizontal and Inclined Oil–Water Flows by Using Wire-Mesh Sensor. *Energies*, *15*(18). https://doi.org/10.3390/en15186638

Zhai, L., Qiao, J., Wang, W., & Wang, Y. (2022b). Measurement of Interfacial Characteristics of Horizontal and Inclined Oil–Water Flows by Using Wire-Mesh Sensor. *Energies*, *15*(18). https://doi.org/10.3390/en15186638

Zhai, L. S., Jin, N. De, Zong, Y. B., Hao, Q. Y., & Gao, Z. K. (2015). Experimental flow pattern map, slippage and time-frequency representation of oil-water two-phase flow in horizontal small diameter pipes. *International Journal of Multiphase Flow*, *76*, 168–186. https://doi.org/10.1016/j.ijmultiphaseflow.2015.07.007

Zhai, L. S., Jin, N. D., Gao, Z. K., Zhao, A., & Zhu, L. (2014). Cross-correlation velocity measurement of horizontal oil-water two-phase flow by using parallel-wire capacitance probe. *Experimental Thermal and Fluid Science*, *53*, 277–289. https://doi.org/10.1016/j.expthermflusci.2013.12.021

Zhang D, Zhang H, Rui J, et al. (2020) Prediction model for the transition between oil–water two-phase separation and dispersed flows in horizontal and inclined pipes. Journal of Petroleum Science and Engineering. 192: 107161

Zhang, S., Shi, X., Wu, H., & Dong, F. (2021). Oil-gas-water Three-phase Flow Regimes Identification Based on Flow Characterization in Time-frequency Domain. *Chinese Control Conference, CCC*, *2021-July*, 2975–2980. https://doi.org/10.23919/CCC52363.2021.9549430

Zhou, Y., Jin, N., Zhang, H., & Zhai, L. (2020). Method based on parallel-wire conductivity probe for measuring water hold-up in near-horizontal oil–water two-phase flow pipes. *IET Science, Measurement and Technology*, *14*(6), 676–683. https://doi.org/10.1049/iet-smt.2019.0308

Zou, Y., Ye, S. S., Wang, Y. D., & Fei, W. Y. (2016). CFD simulation and PIV measurement of liquid-liquid two-phase flow in pump-mix mixer. *Journal of the Taiwan Institute of Chemical Engineers*, *60*, 15–25. https://doi.org/10.1016/j.jtice.2016.10.007

APPENDIX A

LabView program showing the data acquisition system.